Universitat Autònoma de Barcelona

Doctoral Thesis

Complexity in Slowly-Driven Interaction-Dominated Threshold Systems: the Case of Rainfall

Author:
Anna Deluca Silberberg

Supervisor:
Dr. Álvaro Corral Cano

Tutor:
Dr. Joaquim Bruna Floris

A thesis submitted in fulfilment of the requirements for the degree of Doctor of Philosophy in the

Department of Mathematics UAB and Complex Systems Group CRM

October 2013

Dedicado a
mi Majka y a la Oma.

Acknowledgements

This thesis has been possible only thanks to a very diverse and large scientific and non-scientific community. Interactions with other people really define what we do and what we are, because there is no learning without feeling, there is no memory without emotion. And as we interact in different languages please allow me to switch between them depending to who I refer to.

Primero de todo, quiero agradecerle a Álvaro la oportunidad de hacer la tesis con él. Ya han pasado muchos anos desde aquella entrevista en Física Estadística. Gracias por dirigirme, por animarme a hacer de todo: estancias, escuelas, papers. Gracias, me lo he pasado muy bien. Gracias por aguantarme tanto tiempo. Cómo diria mi santo padre... pobre víctima.

Secondly, I would like to thank to Dr. Ole Peters for giving me the opportunity to start to do research with someone so fantastic, to visit Imperial, to encourage amazing experiences as the Summer School at the Santa Fe Institute. Thank you for teaching me in almost everything! And thanks for sure to Dr. Nicholas Moloney. For being my friend and my colleague, for letting me visit him at the MPI, and in Brazil. For hosting me, for taking care of me, for encouraging me... thanks for all. Thanks also to Prof. Holger Kantz and Prof. Dickman for their kindness. Moltes gràcies Prof. Pere Puig, ha sigut un plaer poder treballar amb tu.

Thanks also to all the great scientists I found on my way across the Complexity world, in Schools, in Conferences, in Workshops. This thesis time would have not been the same without getting to know you all, you are great discoveries of my time as pre-scientist in this complex but small world: Michael, Eugenia, Marina, Michael Sachs, Lydia, Kim, Lucas, Jordi, Annick, Taka...

El CRM ha sigut un lloc humanament fantàstic. Moltes gràcies a tots! Companys de despatx: thanks Mishi for giving me hugs almost without asking for them, gracias Roberto, gràcies Esther, Dani, Rosalba. Gràcies Francesc Primer pel teu bon humor. And thanks Tim for the beers on Friday and thanks Vincent for your help and support in the final moments.

En especial gracias Tomás, por ser mi amigo y por siempre estar allí para un café, una cerveza o para lo que sea. Gracias Pilar, por todas las risas y los cotilleos, el apoyo y los consejos. Francesc Segundo y yo te hemos estado echamos de menos. Gràcies Francesc Segon per ser un gran company de grup i sempre donar-ho tot (sí el tabac també).

I gràcies a tot el personal del CRM. En particular, a ti, Mari Paz, por regalarnos cada día una sonrisa y los buenos días. Gràcies, Oriol per les llargues converses sobre tot

i res, Jordi per les teves piles inacabables, gràcies Àngels pels cigarros al pati. I a la Consol, a la Núria i a tota la resta de gent d administració. Finalment, gràcies també a l equip directiu, al Joaquim per donar-me l oportunitat de fer la tesi al CRM, però molt en especial al Toni Guillamón, per fer quelcom tan tediós com demanar una beca europea un plaer. Gràcies, pel teu suport.

Gràcies a tots els amics, que tot i que els anys vagin passant i les nostres vides es separin seguiu sent els de sempre: Estel, Laura, Elena, Marta, Roger, Guayent, Juanma, Irene... En especial, gracias Ana por todas nuestras comidas, vermuts y cervezas. I a la gent d òptica per el suport final, arigatou Albert, bon viatge.

Gracias mami, por cuidarme, quederme, prepararme comida y estar siempre ahí, por los consejos, por escuchar, por callar, por todo... esta vida no tendría ningún sentido sin ti. Y gracias a toda mi gran familia. A mis hermanos, Martín, Manu, Pau, Lau, Djas y Carol y a todos sus maravillosos hijos, Marcel, Gabi, Maitane, Bruno, Dani, Juli, Luli y Juani. Gracias papá por hacer de todos quienes somos. Gracias también a mi casi familia política: Teresa, Ginés, Víctor, Irene; y en particular a toda la familia de Zaragoza que siempre me recuerdan lo que es realmente importante en la vida.

Dani, les paraules més important són per tu però no les direm pas a ningú! Ja saps que no s em donen bé aquestes coses, de les declaracions amoroses, però potser millor si ens acostumem, així que ho intentarem, que ens casem! Gràcies persona preciosa de la meva vida, gràcies per ajudar-me a ser una miqueta millor cada dia.

Contents

List of Figures

List of Tables

Chapter 1

Introduction

In fact, all epistemological value of the theory of probability
is based on this: The large-scale random phenomena
in their collective action create strict, non-random regularity.
(Gnedenko and Kolmogorov, 1969)

The whole is more than the sum of its parts.
(Aristotle)

The subject of this thesis is to investigate phenomena that occur over a wide range of spatial and temporal scales in systems composed of a large number of interacting units, which present an emergent behaviour. Emergence implies that the collective behaviour of the system cannot be explained by analysing the response of the individual parts that compose it. This often manifests itself as large-scale statistical regularities and coherent structures such as scale-invariant distributions for the coarse-grained observables of the system. Emergent phenomena are a characteristic of *Complex Systems*, whose study demands highly interdisciplinary approaches for developing models with the ability to explain their observed features.

In particular, this research focuses on out-of-equilibrium slowly driven systems with fast (in comparison to the driving) dissipation mechanisms and a dynamical evolution controlled by local threshold-interactions. Many geophysical phenomena, such as atmospheric convection and earthquakes, can be characterized by the aforementioned properties. Theoretical and empirical studies addressing the fundamental mechanisms underlying such processes are required due to the increasing need for improved prediction of natural hazards and forecasting of weather, as well as for climate change projections.

The research presented encompasses empirical analysis of complex systems data, development of statistical methods for model verification and new insights into modelling and prediction of complex systems.

1.1 Format and outline of the Thesis

The thesis format is Thesis by Publication , following the Universitat Autònoma of Barcelona (UAB) required standards: at least two articles published in international peer-reviewed journals or book chapters, an introduction in which a common thematic line is clarified and a summary, discussion and conclusion section. The articles pending publication or preprints have been accepted to be a complementary part of the thesis by the Postgraduate Studies Commission of the UAB. It is a requirement to attach the papers in their original format at the end of the manuscript, apologies for repetition that this constrain may cause.

Chapter 1 corresponds to the introduction and a global summary. A literature overview is provided, placing the scope of the results of the articles in the wider context of the current state-of-the-art. Chapters 2 and 3 correspond to the two published articles that constitute the main part of this thesis. Chapter 4 corresponds to a submitted publication, while Chapter 5 and 6 correspond to preprints of work in progress, which has been already partially published in non-peer-reviewed proceedings (see A). In Chapter 7 we present the general conclusions, synthesizing and combining the results of the previous chapters. In addition, expectations of future research are emphasized.

Finally, in Chapter 8 a copy of the peer-review accepted publications is given. Complementary publications are given, following the requirements of the UAB, in Appendix A that constitute the main part of this thesis.

1.2 Complexity and criticality

The fact that *Complexity* has an ambiguous and non-unique definition has led to scientific controversy due to the overuse of the term. Moreover, in the past few decades the term has been abused due to its perceived marketability. In Complex Systems the term tends to be identified with phenomena occurring in systems with many non-trivially interacting parts which present emergence. The Complexity framework still requires significant theoretical and conceptual refinements, while new appropriate statistical methodologies still need to be developed. Nevertheless, new scientific approaches based on complexity ideas and views have already led to scientific advances, and hold

much promise for understanding and modelling very diverse systems such as biological systems (the brain, insect colonies, ecosystems, cells, *etc.*), social systems (the economy and financial markets, road traffic, language, World Wide Web, *etc.*) and geophysical systems (weather, earthquakes, solar flares, *etc.*) (Newman, 2011, and references therein).

In this context, there are two basic strategies towards gaining scientific understanding regarding a particular system. One strategy is to create highly realistic computer simulations, building on all the interacting parts of the complex system and including all the available details, and then, see if the emergent behaviour of the system is reproduced. This approach is usually based on Monte Carlo simulations, agent-based simulations, molecular dynamics simulations, multiscaling approaches, *etc.* Using this first approach, one can end up creating a new complex system whose behaviour/dynamics is very difficult to grasp. These kind of models can often have a considerable amount of parameters, making their understanding very challenging. Also, the knowledge of the precise interactions may be impossible. The alternative strategy, the one on which this thesis is based, resides in the construction of highly simplified mathematical abstractions capable of capturing the emergent behaviour of the system. These simpler models will be easier to solve mathematically and simulate in a computer than those of the first approach. They are usually based on methodologies and approaches from dynamical systems, information theory, stochastic processes, cellular automata, networks theory, computational complexity, among others. This second strategy presents problems such as oversimplification (the models are too simple and cannot really describe the phenomena) or irresolubility (simple models that are not as simple as initially expected, in the sense that they are not easily mathematically solvable). These kind of models can often be understood as a first step towards a full model: the idea behind this approach is to identify the crucial variables of the system.

Some of the most influential and important ideas in the area of Complex Systems arise from statistical physics and condensed-matter theory. Concepts such as *scale invariance*, *phase transition* and *criticality* have received an enormous attention over the past few decades from the physics and mathematical communities. This has resulted in significant number of research output on their fundamental theory and their applications to real-world problems (Grauwin et al., 2012), including research on mathematical foundations of statistical physics awarded with the Field s Medal (Smirnov, 2001).

Criticality is sometimes understood as a high susceptibility to external perturbations. Even so, in this thesis criticality stands more specifically for the behaviour of a system near a *critical point* of a second order (or continuous) *phase transition*, where the absence

of a characteristic scale *i.e.*, *scale invariance*, manifests itself (Christensen and Moloney, 2005, Stanley, 1999). In the next section a definition for this term is introduced.

1.2.1 Phase transitions and long-range correlations

A system undergoes a *phase transition* when it suffers a qualitative change in some thermodynamic magnitude as a result of the variation of a characteristic parameter of the system so-called *control parameter*. The *order parameter* is an observable of the system that indicates the existence of the phase change. The point of coexistence of both phases is called *critical point*. When the control parameter is continuous but its derivative is not at the critical point the transition is called second order or continuous phase transition.

A classical example of a phase transition is the transition of ferromagnetic to paramagnetic in a magnetic material, which is often modelled by the Ising Model. The Ising Model is a lattice model composed by N sites with a spin at each site i oriented up, $s_i = 1$, or down, $s_i = -1$. The order in the system can be quantified by the *magnetic moment*, which is proportional to the magnetization. It is defined as

$$m(t) = \sum_{k=1}^{N} s_i(t) \tag{1.1}$$

The system is said to be in the magnetic phase if $m > 0$ and in the non-magnetic phase if $m = 0$. One of the control parameter of this system is the temperature (T). For a given critical temperature the magnetization passes from zero to positive.

Around the critical point many interesting properties appear. In particular, the microscopic short-range interactions combine in such a way that correlations are developed over all length scales. The lack of a characteristic scale, also referred to as *scale invariance*, is expressed mathematically by means of *power laws* and *power-law distributions* of certain macroscopic observables of the system.

Away from the critical point the correlations decay exponentially with the distance between two given sites. However, in the proximity of the critical point and taking the thermodynamic limit (size of the system tending to infinity) the spatial correlation decays slowly in space, proportionally to

$$corr(r) \quad \frac{1}{r^{\alpha}} \tag{1.2}$$

In this case, it is said that the system displays *long-range correlations*. Similarly, the temporal correlation function also follows a power law in the proximity of the critical

point. Moreover, the order parameter s susceptibility, which is the degree of change in the order parameter in response to changes in the control parameter, diverges as a power law approaching the critical point. When the system has a finite size, *finite size effects* appear, limiting the power law range. They introduce a *cutoff* on the power-law distributions.

It is only at the *critical point*, with fine tuning of the control or *control parameter*, that second order phase transitions and hence scale-free behaviour (or *scaling*) take place in equilibrium systems. Only at this point, are order and disorder perfectly balanced and emergent behaviour for the coarse grained variables of the system builds on the microscopic short-range interactions.

In a continuous phase transition, the control parameter has to be tuned to a critical value that depends on the microscopic details of the system. However, the critical exponents (exponents of the power laws that emerge) associated with divergent mean variables, such as the correlation function, do not depend on the microscopic details.

For a magnetic system undergoing a ferromagnetic-paramagnetic transition, the order parameter is the net magnetization, as illustrated before for the Ising model, whereas in liquid/gas transitions it is the density difference between the two phases (the transition between the solid and liquid phases is thought always first-order)(Yeomans, 1992).

1.2.2 Universality

Continuous phase transitions have many interesting properties. The phenomena associated with these are often called *critical phenomena*, due to their association with critical points. The most striking fact about phase transitions arising in different systems is that they often share the same set of critical exponents, which characterize them. This phenomenon is a manifestation of what is known as *universality*. For example, the critical exponents at the liquid-gas critical point have been found to be independent of the chemical composition of the fluid (Yeomans, 1992), see there are several *universality classes*, which are sets of systems sharing the same behaviour (in terms of critical exponents and scaling functions). The universality class just depends on the dimensionality of space and the symmetry of the order parameter, for systems in equilibrium and with short-range interactions (Stanley, 1999).

Universality is understood mathematically by means of the renormalization group theory of phase transitions. This theory states that the thermodynamic properties of a system near a critical point of a phase transition depend only on a small number of features, such as dimensionality and symmetries, and are insensitive to the underlying microscopic

properties of the system. This fact was first recognized in 1971 by K. G. Wilson. His seminal work on critical phenomena led to him winning the Nobel Prize for Physics in 1982 (Wilson, 1971).

1.3 The apparent ubiquity of power laws

The existence of a power-law distribution for a coarse-grained variable of a system has been considered as pointing to criticality, and indicative that the models used for understanding and predicting the behaviour of such a system must be non-linear (Newman, 2005). However, there exists linear mechanisms capable to generate power-law distributions, as showed in the next section.

This statistical pattern has been observed in, a priori, a large number of macroscopic variables of different systems. Power-laws distributions have been claimed to be found in diverse range of fields such as sizes of city populations and wars, the frequency of use of words in human languages or surnames in most cultures, the number of written scientific papers and of citations of scientific papers, number of employees in firms, income or wealth, among many others (Newman, 2005, and references therein).

This thesis will focus primarily on geophysical processes. Power-law distributions have been ascertained for earthquakes sizes, rockfalls, landslides, volcanic eruptions, forest fires, rainfall and tropical cyclones, astrophysical phenomena and the times between natural hazards events (see more details and related references in Chapter 2).

Recently there has been an increasing debate about the reliability of the methods used widely in the literature for testing the existence of power laws. The potential relationship between power laws and fashionable terms such as criticality or complexity, has lead to a strong preference for finding power laws. This preference, combined with unreliable methods, has resulted in a strong scepticism about power-law claims (Clauset et al., 2009, Stumpf and Porter, 2012). This is exacerbated by a more general tendency in science and society: we are in the onset of the Big Data era and the so-called Data Science. After the Internet boom we are now facing a data boom, that is expected by many to be a new historical revolution equivalent to the Industrial Revolution, in particular for business models, companies and policy planning. Buzzwords such as real-time customization, improved management, self-regulating processes and reduction of uncertainty, cover non-scientific high-impact journals (for instance, dozens of articles during September 2013 about this topic in Forbes, www.forbes.com). However, all these advances cannot be achieved without mechanistic backing. This also applies to many analyses related to

power-laws distributions. Without models and a theoretical framework supporting the statistical analysis the current state-of-art cannot be advanced.

The importance of proper data analysis cannot be overestimated, and it is ultimately crucial for testing theory against data. Concerning power laws, systematic methods have been developed recently confirming power law behaviour in many relevant systems (Clauset et al., 2009), however, they have been found problematic (Corral et al., 2011).

Next, in Sections 1.3.1 and 1.3.2, a mathematical definition of a power-law distribution, together with the properties associated with it, are given. A more detailed and broader definition, including the so-called truncated power laws, is given in Chapter 2. Section 1.4 will survey different known mechanisms (including the already mentioned criticality) that lead to power-law emergence.

1.3.1 Definition

A continuous random variable X is power-law distributed if its probability density is given by

$$f_X(x) = Cx^{-\alpha} \tag{1.3}$$

where $x \geq x_{min}$, $x_{min} > 0$, $\alpha > 1$ and C is a normalization constant. Power-law distributions are also called Pareto distributions (Evans et al., 2000, Johnson et al., 1994) (or Riemann zeta distributions in the discrete case (Johnson et al., 2005)). Pareto distributions are sometimes associated with slightly different distributions in other contexts (Johnson et al., 1994). For this reason, throughout this thesis only the term power-law distribution will be used.

1.3.2 Properties

The most relevant and unusual statistical properties of power laws are scale invariance and divergence of moments.

As already introduced, scale invariance characterizes power-law distributions due to the fact that a power law is the only function such that it is the same at any scale we look on it. These distributions are invariant under (properly performed) linear rescaling of axes, and therefore have no characteristic scale. Note however that for power-law distributions strict scale-invariance cannot hold, as x_{min} cannot be equal to zero by definition (the distribution would not normalize). In addition, if α (1 2] all the moments diverge (*i.e.* non finite mean, variance, etc.) and the law of large numbers does not hold (Kolmogorov, 1956, p. 65). Hence, the mean of a sequence of realizations of an observable does not

characterize it because it does not converge as the number of realizations increases, but rather tends to infinity (Shiryaev, 1996, p. 393). If α (2 3] the mean exists and is finite, but higher moments diverge and the conditions for the central limit theorem to apply (in its original form) are not satisfied (Bouchaud and Georges, 1990). For higher α s only moments higher than order $\alpha - 1$ are infinite and there is convergence in probability towards the Gaussian law, but very slowly in some cases, depending on the value of α.

A relevant case for many systems analysed in this thesis is when the distribution is a power law with a decay at the tail at least as fast as an exponential function. Such laws obey the central limit theorem but their kurtosis is very large: there is convergence to a Gaussian at the centre of the law, but to a power law at the tails. Moreover the weight in probability of these tails becomes more important as the exponent approaches 2 from above. For exponents smaller than 2, there is no convergence to a Gaussian but to a Lévy Law (Sornette, 2004). In addition, for power laws, there is invariance under aggregation just at the tail of the distribution : power laws are conserved under polynomial transformations (Farmer and Geanakoplos, 2008).

The next section describes different mechanisms for the generation of power laws. Many of them are not related with criticality and then obtaining a power law is just a necessary condition, but not sufficient for criticality.

1.4 Mechanisms for generating power laws

This section overviews several mechanisms that can explain the observed power-law distributions. The one proposed by Bak et al. (1987), Self-Organized Criticality (SOC), will receive a special attention as it is a good candidate for understanding the dynamics of some geophysical systems, as for example the case of rainfall and convection, which we will study in depth in this thesis. More details about this connection will be given in section 1.5.

We do not aim to provide a complete list of mechanisms, but just to give an idea of the variety of possible explanations for power-law behaviour. Some other mechanisms not detailed here include: percolation, fragmentation and other related processes; directed percolation and its universality class of so-called contact processes; crackling noise and avalanches resulting from the competition between frozen disorder and local interactions; and competition between multiplicative noise and birth-death processes. Complete reviews of mechanisms and the corresponding references can be found in Farmer and Geanakoplos (2008), Mitzenmacher (2004), Newman (2005) and Sornette (2004).

Continuous phase transitions, already introduced in section 1.2.1, can be seen also as a mechanism for the power law emergence.

1.4.1 Exponentiation of the Exponential

The first mechanism is one of the most trivial ways of obtaining a power-law distribution. Given a continuous random variable X distributed exponentially, *i.e.*,

$$f_X(x) \quad e^{ax} \tag{1.4}$$

the variable Y defined as the exponential of X, $Y \quad e^{bX}$, will be power-law distributed with distribution

$$f_Y(y) \quad y^{-1+\frac{a}{b}} \tag{1.5}$$

for y greater than a certain value $y_{min} > 0$.

1.4.2 Inverse of random variable

Consider a random variable X. Then the variable $Y = X^{-\frac{1}{\alpha}}$ with $\alpha > 0$ (its inverse variable for $\alpha = 1$) will have distribution

$$f_Y(y) = f_X(x)\left|\frac{dx}{dy}\right| = \alpha\frac{f_X(x)}{y^{1+\alpha}} \tag{1.6}$$

Suppose that $f_X(x(y))$ tends to a constant for $x \quad 0$, then the distribution of Y for large values approaches a power law with exponent $1 + \alpha$. A uniform behaviour of the variable X leads to scale-free behaviour of its inverse power Y.

Jan et al. (1999) show that this argument is relevant for the fractional change of the magnetization between successive measurements for the Ising model at the magnetized phase.

1.4.3 The Yule processes

The Yule Process is a widely used mechanism for power-law emergence, also referred in the literature as cumulative advantage , the richer get richer or preferential attachment . The Yule Process is a stochastic process that consists of discrete elements added randomly to a set of groups. All groups start with k_0 elements and new ones are added at a rate proportional to the number k that they have already, plus a constant $c > -k_0$. New groups can also appear between the appearance of one element and the

next one, at a rate m, and hence the number of groups also grow. Hence, the model has three parameters k_0, c and m. The time in the model is defined as each time one new element is added to a group. It can be demonstrated that the fraction of groups with k elements, when the total number of groups is n, will not depend on n for long times. Thus, the distribution of sizes of the groups for large times goes as

$$p_k = \frac{\mathrm{B}(k\ \ 2+1\ \ m)}{\mathrm{B}(k_0\ \ 2+1\ \ m)} p_{k_0} \tag{1.7}$$

where B is the beta-function (also called first kind Euler integral $\mathrm{B}(x\ \ y) = \int_0^1 t^{x-1}(1-t)^{y-1}dt$) and p_{k_0} is the probability of having k_0 elements in the group. Since the beta-function has a power-law at the tail, the asymptotic exponent will be $\alpha = 2 + \frac{k_0+c}{m}$.

1.4.4 Random walk

Random walks (RW) are very well-studied stochastic processes for which many of their properties associated with their first passage statistics distribute as power laws (Redner, 2001). For example, the first return time to the origin of the RW is power-law distributed for large enough values of t

$$f(t) \quad t^{-3\ \ 2} \text{ if } t \gg 1 \tag{1.8}$$

This is equivalent to considering a random walk with an absorbing boundary at the origin. Also, the areas under the first passage of a random walk present asymptotic power law behaviour for the areas or sizes of the runs.

1.4.5 Branching process

A branching stochastic processes is a process in which an individual (the ancestor) creates a random number of descendants k with probability p_k given by a random variable K_i. The process starts with one individual by definition, Z_1=1. In a given generation t, a total number of individuals Z_t could reproduce following a certain distribution, and then the population at time $t+1$ will be given by $Z_{t+1} = \sum_{i=1}^{Z_t} K_i$.

The average number of first-generation descendants created by an ancestor is the so-called branching ratio, $\sigma = \sum_k kp_k$. Let s consider a simple case in which the number of descendants K_i is distributed following a binomial distribution $Bin(2\ \ p)$, and then K_i can be 0, 1 or 2. If $p > 1\ \ 2$, the branching ratio will be greater than 1 and the process has a certain probability to continue indefinitely. If $p < 1\ \ 2$, the branching ratio will be smaller than 1, and the process will be finish at some point. $p = 1\ \ 2$ corresponds to the

critical case, the branching ratio will be exactly equal to one and the process will finish in a finite time, but the total number of descendants in the process so called size of the process, will follow asymptotically a power-law distribution with exponent 3 2 (Corral and Font-Clos, 2013, Harris, 1989). This is a very simple example of a phase transition. The parameter p can be seen as the control parameter of a phase transition (from finite to infinite size of the total population) with critical point at $p_c = 1\ 2$. In Figure 1.1 a realization of the process for this concrete distribution of descendants is given as an example.

A branching process can be mapped to a random walk (Pruessner, 2012) and to anomalous diffusion process when the distribution of descendants follows a power-law (Saichev et al., 2005). Moreover, branching processes are the mean-field limit of a stochastic SOC model (Zapperi et al., 1995).

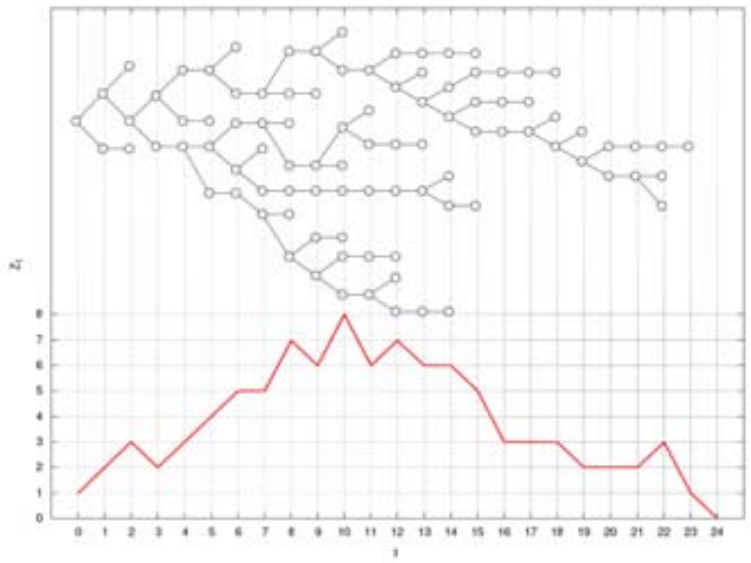

FIGURE 1.1: A realization of a branching processes from the tree point of view (up) and the evolution of descendants for each generation (down). The number of descendants distribution is a binomial distribution $Bin(2\ 1\ 2)$. Reproduced from Corral and Font-Clos (2013).

1.4.6 Self-organized criticality

As highlighted in the previous section, continuous phase transitions present power-law behaviour at the critical point. However, they demand an external adjustment of the *control parameter*, and they cannot explain the power-law behaviour observed in nature.

A mechanism for scale invariance in natural systems was introduced by Bak et al. (1987). They considered non-equilibrium systems of dissipative nature in which the effect of dissipation is compensated by a slow external driving. This creates a flow of energy through the system that leads to a non-equilibrium attractive critical state. The system self-organizes around this scale-invariant critical state. Small local perturbations or instabilities, which appear when some *threshold* is surpassed, can then lead to activity that propagates rapidly through the system. This phenomenon is known as *avalanche* and governs the dynamic evolution of SOC systems. Moreover, as expected in criticality, the distribution of the avalanche sizes and durations are power laws. We will illustrate conceptually these ideas using the metaphor of a *sandpile*.

The sandpile is driven out of equilibrium by a continuous but very slow in comparison to the dissipation rate (grains that leave the pile, usually at the border) addition of grains (*the driving*), one at a time, at random positions. Normally, when the grains land, they find an equilibrium position. Initially, avalanches tend to be very small and localized and the response is simply proportional to the external perturbation. But, if we continue to drop grains, the sandpile grows in size because the pile can maintain a finite slope thanks to the friction between the grains. However, if at some point the pile is too steep, the new grain may be unstable and an avalanche starts at this position. If the slope of the pile becomes too shallow, the addition of grains will tend to increase it, and if the slope becomes too steep, avalanches will tend to decrease it. Therefore, the pile self-organizes into a steady state in which its slope fluctuates around a constant angle of repose (Christensen and Moloney, 2005).

The main characteristic features of SOC systems are:

- a slow external energy input;
- intermediate energy storage;
- a threshold dynamics, *i.e.*, the activity occurs when a threshold is surpassed;
- sudden burst-like energy releases;
- avalanches of all sizes.

In order to emphasize the essential dynamical ingredients in a SOC system, Jensen proposes a new abbreviation of SOC which summarizes them: Slowly driven, interaction-dominated threshold systems, SDIDT (Jensen, 1998, p. 126).

The best candidates to be SOC systems in nature, in the sense that they present SOC characteristics, are given by earthquakes (Gutenberg and Richter, 1944), forest

fires (Malamud et al., 1998), solar flares (Dennis, 1988) or rainfall (Peters and Christensen, 2002, Peters et al., 2010); and with more controversy, the evolution of biological species (Raup, 1986, Sneppen et al., 1995, Solé and Manrubia, 2001), neural networks (Bornholdt and Rohl, 2003) and volcanic activity (Diodati et al., 1991). It is also important to notice that real sandpiles generally do not present such a behaviour (Pruessner, 2012).

SOC is a theory for critical phenomena that occur in natural systems without any tuning necessity and its main goal is to identify which are the main characteristic of such systems. This has been mostly investigated numerically through cellular automata models. The first model, which established the whole topic, is the Bak-Tang-Wiesendfield sandpile model (BTW model) that was introduced by Bak et al. (1987). Since then, many models, deterministic and stochastic, have been proposed and investigated in the literature, see Pruessner (2012, chapters 4 and 5) for a general review.

More than 25 years later, after significant research of the general features of SOC by investigating model properties and their analytical treatment, now the concern is to verify these properties, determine universality classes of the models, as well as to provide a continuous description for the dynamics.

1.4.7 Sweeping the instability

Sornette (1994) presented a robust mechanism for the appearance of a power-law distribution with a complete absence of self-organization that appears as a consequence of some control parameter moving across a critical point, or more generally a global bifurcation. This mechanism is one of the candidates able to explain the array of measures that link criticality and convection and precipitation. Next, in Section 1.5 will summarize them.

1.5 Criticality in convection and precipitation

The atmosphere is a complex system very difficult to analyse, model and understand. But at the same time, it is one of the most accessible and well observed natural systems. Convection and its associated precipitation is a key aspect of the Earth s climate, playing a leading role in the planetary heat, moisture and momentum budgets, particularly in the tropics. A broad range of atmospheric phenomena present scale-free distributions and wide range spatial and temporal variability. In particular, many atmospheric phenomena related to precipitation are associated with many characteristic time and spatial scales,

and have large-scale correlations in time and space, which may result from the coupling between non-linear mechanisms with different temporal and spatial characteristic scales (e.g. Bodenschatz et al., 2010, Vattay and Harnos, 1994, Yano et al., 2003).

In particular, recent high-resolution (of the order of 10 m in the horizontal scale) satellite observation analyses show that projected areas of clouds, together with many of its geometric and radiative properties, follow power-law distributions over more than 5 orders of magnitude (from few to millions of km^2) (Cahalan and Joseph, 1989, Lovejoy, 1982, Peters et al., 2009, Wood and Field, 2011). Modelling convection is then a very challenging problem because computer models cannot simulate explicitly the small convective clouds (which are the most numerous). The simulations performed divide the atmosphere into boxes with typical horizontal sizes of the order of 1-20 km (weather simulations) or of the order of 20-200 km (climate simulations). Figure 1.2 shows the processes related with precipitation and their associated scales, and horizontal resolution scales of different models used in atmospheric sciences: CRMs (Cloud Resolving Models which explicitly model convection) and GCMs (General Circulation Models which do not resolve convection).

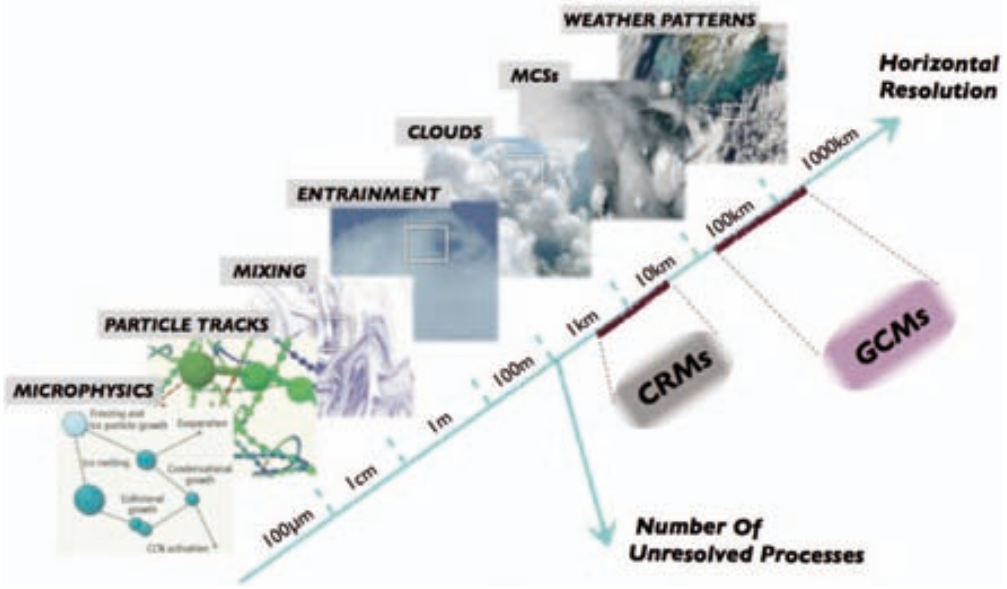

FIGURE 1.2: Processes related with precipitation and their associated scales, and horizontal resolution scales of CRMs and GCMs. MSC states for mesoscale convective clusters, which are organized convective clusters that can be found mostly over tropical oceans. Adaptation from Bodenschatz et al. (2010).

Advances towards higher resolution problems present many challenges, and not just the obvious enormous additional computational costs. For instance, a common simplification is that the effect of the small scales on the resolved scales can be represented as a deterministic function of the large-scale flow. Fluctuations that emerge from small scales are disregarded. However, this is too strong an assumption that breaks down

for grid boxes of order 50 km and smaller (Ball and Plant, 2008): the ensemble size of deep convective elements within a grid box is typically small. Deep convection refers to thermally driven turbulent mixing with vertical motions that take parcels from the lower atmosphere above 500 hPa (The level of 500 hPa is roughly dividing the mass of the atmosphere in two and it lies near 5 km).

Errors in convective parametrizations (models of the unresolved processes as a function of the resolved ones) are related with major issues in climate modelling, in particular with spatially-organized phenomena such as the spatial distribution of tropical rainfall and large uncertainties on whether many regions in the world will get wetter or drier in the future (IPCC4, 2007). On the weather-forecasting timescales, an adequate representation of convection and precipitation in numerical weather prediction (NWP) is important for forecasts of damaging flash-flood events.

Almost all current models of convection used for weather and climate prediction are based on the concept of a collection of convective plumes embedded within a horizontally-homogeneous medium called the environment. Convective quasi-equilibrium (QE) is one of the classical assumptions made and postulates that convection acts to reduce instabilities on a fast time scale as an adjustment to the slow drive arising from the (resolved) large-scale forcing (e.g., radiative and advective cooling of the troposphere and warming and moistening of the boundary layer). The system is self-maintained close to a far-from-equilibrium statistically-stationary state, where driving and dissipation are in balance (Arakawa and Schubert, 1974). Since it was first proposed in 1974, many interpretations and implementations of the QE concept have been suggested. However, QE remains a controversial issue, and both conceptual and practical-implementation problems are still present (Mapes, 1997).

Many contributions have been made for improving parametrizations of deep convection. In recent years, stochastic parametrizations have been proposed in order to represent sub-grid variability stochastically (e.g. Majda and Khouider, 2002, Plant and Craig, 2008). Super-parametrization, which consists of embedding an explicit but very expensive cloud model within each climate model grid box, has also been explored (e.g. Grabowski, 2004). However, although the theoretical framework underlying current operational parametrizations has been much elaborated upon in the details, in its essentials it has remained fundamentally unchanged for more than three decades.

Recent empirical studies across a broad range of observational scales have attempted to characterize aspects of convective phenomena with a view to constraining convective parametrization (modelling of sub-grid processes). The surprising critical properties found empirically connect the convection parametrization problem with Statistical

Physics theories of critical phenomena. This Chapter aims to summarize them and introduce the key concepts that have been used in these analyses. Chapters 3, 4 and 5 will constitute the contribution of this thesis to this research line.

1.5.1 Rainfall seen as relaxation events

SOC ideas have had a significant impact in the geosciences, and in particular for earthquake modelling (Bak, 1996, Sornette and Sornette, 1989). A simplified picture of the rainfall process helps to illustrate SOC characteristics for this particular problem: The Sun continuously radiates electromagnetic energy which translates in the continuous evaporation of water, coming mostly from the oceans. This, together with radiative cooling in the upper atmosphere, translates into an instability that drives convective updrafts. The water vapour carried up by convection is intermediately stored in the atmosphere, and when a saturation threshold is reached in a susceptible environment, condenses and precipitates. However, the coupling mechanisms between nearby regions of the atmosphere is not clear, cold pools or winds associated with rainfall could be candidates (Jordan, 2008).

The key variable from the SOC perspective is the so-called `rain event . Given a precipitation time series in a given location, the rain event is defined as a sequence of non-zero values of rain rate (with units mm/h). The event size s is the integrated rain rate over the event $s = \int_{\text{event}} r(t)dt$ (with units mm). One can also define the inter-event time, as the time between two successive events, or the duration of an event as the time it lasts.

It is important to observe that the application of this concept demands in practice very high temporal-resolution measurements. Conventional rainfall local measurements, which correspond to rainfall accumulation during an hour or a day, are not suitable for this kind of analysis. In general, if the rain rate were known over an area, then the event size could be related with a more physically meaningful variable: the energy released during one event. However, the current available spatial measurements of rainfall are either not continuous in time or too sparse in space.

Andrade et al. (1998) were the first to analyse rainfall time series from this perspective. However the temporal resolution was insufficient for performing a proper analysis and they did not provide a complete description as they did not report results for rain-event sizes, which is the key observable. Later, but independently, Peters et al. (2002) analyzed 1-minute resolution data from a vertical pointing radar situated in mid-latitudes (Baltic coast). Power-law distributions for event sizes and for dry-spells durations over several

orders of magnitude were reported, with exponents $\alpha_s \simeq \alpha_q \simeq 1.4$. For the event-duration distribution the results were unclear, although a power law with an exponent $\alpha_d \simeq 1.6$ was fitted to the data.

1.5.2 Rethinking Quasi-equilibrium

As discussed, an observable distributed as a power law may indicate criticality, but it is not a sufficient condition given that trivial non-critical mechanisms also lead to power laws. Peters and Neelin (2006) showed further evidence using satellite data over tropical oceans: a relationship between satellite estimates of rain rate and water vapour over the tropical oceans compatible with a continuous phase transition. Above a critical value of column water vapour large areas of the troposphere would enter a convectively active phase.

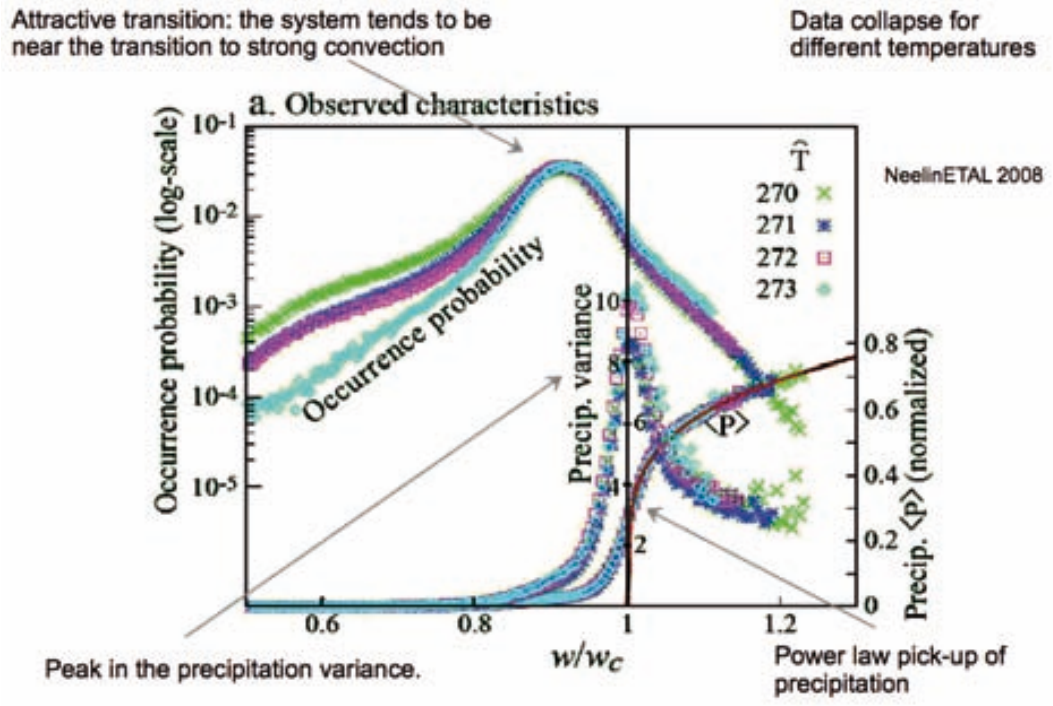

FIGURE 1.3: This figure summarizes the findings by Peters and Neelin (2006) for the East Pacific ocean basin for four different temperature values. It shows the precipitation mean and variance dependence on the amount of water vapour in a given column w normalized by a critical value w_c. The occurrence probability for water vapour conditioned to precipitation occurrence is also shown. Figure from Ref. Neelin et al. (2008)

In addition, they showed that the system tends to be close to the transition point. These results can be interpreted in terms of departures from the point of QE and directly related with a proposed explanation for scale-free behaviour in a variety of real-word systems, self-organized criticality (SOC). However, the data used in this study has been

questioned (Yano and Plant, 2012). When the water vapour is high the measurements of precipitation are highly unreliable and the amount of data is very low. This is still controversial, but some recent studies using high-detailed simulations of clouds and precipitation also suggest the same functional relationship between precipitation and water vapour (Yano et al., 2012). Data from the tropics has also been found to exhibit approximate power-law autocorrelation function decay (Neelin et al., 2008), and mesoscale convective cluster sizes (systems with horizontal dimensions ranging from few kilometers to several hundred kilometers, as illustrated in Fig. 1.2) have been found to follow a power law distribution (Peters et al., 2009, Wood and Field, 2011). Again, these results suggest criticality on the system.

Assuming that the previous functional relationship between precipitation and water vapour is not an artifice of a bad measurement, one of the basic assumptions in which almost all climate and weather-forecast relies can be reformulated: the quasi-convective equilibrium.

1.5.3 Alternative explanations

Although the SOC hypothesis is fully compatible with observational analyses conducted so far, alternative explanations for the observed behaviours are also possible. For example, a closely-related alternative based on a stability threshold for boundary-layer water vapour is able to reproduce some aspects of the observed characteristics (Muller et al., 2009). Moreover, the observations could even be compatible with a complete absence of self-organization: they could for instance arise as a consequence of some control parameter moving across a second-order phase transition, being subject to a sweeping-over mechanism (Sornette, 1994), explained in Section 1.4.7. Or they could result directly from a complex flow field, as was shown in simulations using randomized vortices and passive tracers (Dickman, 2003).

In the previous sections we summarized recent observational studies that have shown strong, although not definitive, evidence in support of criticality in the transition to deep convection. However, the number of studies is still limited and alternative non-critical mechanisms may also explain the observations. Thus, there remains a need to delve further into the observations.

1.5.4 Outline of the contests of the thesis related to this section

The main part of this thesis is devoted to the investigation of an expectation of SOC and criticality: universality of rain event associated exponents. In Chapter 2 a method

for fitting and finding exponents of power-law distributions is presented. In Chapter 3 a study of data from the Atmospheric Radiation Measurement program (ARM) available observational sites is presented. The time series have 1 minute temporal resolution measured with the same optical rain gauge (Peters et al., 2010). The results show unambiguous power-law distributions of event sizes, with apparent universal exponents $\alpha_s = 1\ 17 \pm 0\ 03$, extending the support to the SOC hypothesis in rainfall. Power laws distributions are also found for the dry spell durations, but for event durations the behaviour is unclear.

In Chapter 4 data obtained from a network of 20 rain gauges scattered in a region of the NW Mediterranean coast is analysed. The measurements have 5 minute temporal resolution, but a lower, in comparison to other analyses, threshold of rain rate detection (0.1 mm in 5 minute, while ARM measurements have 0.2 mm in 1 minute).

Finally, in Chapter 5 the ARM analysis is extended to updated and new datasets. New methods for addressing universality are introduced.

Chapter 2

Fitting and Goodness-of-Fit Test of Non-Truncated and Truncated Power-law Distributions

Acta Geophysica 2013

This chapter is corresponds to the contents of the following paper (a copy of the published version can be found in Chapter 8).

Deluca A, Corral A. *Fitting and Goodness-of-Fit Test of Non-Truncated and Truncated Power-law Distributions.* Acta Geophysica 2013; DOI: 10.2478/s11600-013-0154-9.

Abstract Recently, Clauset, Shalizi, and Newman have proposed a systematic method to find over which range (if any) a certain distribution behaves as a power law. However, their method has been found to fail, in the sense that true (simulated) power-law tails are not recognized as such in some instances, and then the power-law hypothesis is rejected. Moreover, the method does not work well when extended to power-law distributions with an upper truncation. We explain in detail a similar but alternative procedure, valid for truncated as well as for non-truncated power-law distributions, based in maximum likelihood estimation, the Kolmogorov-Smirnov goodness-of-fit test, and Monte Carlo simulations. An overview of the main concepts as well as a recipe for their practical implementation is provided. The performance of our method is put to test on several empirical data which were previously analysed with less systematic approaches. We find the functioning of our method very satisfactory.

Keywords power-law distribution estimation, goodness-of-fit tests, binning, seismic-moment distribution, waiting-time distribution, tropical-cyclone energy.

2.1 Introduction

Over the last decades, the importance of power-law distributions has continuously increased, not only in geoscience but elsewhere (Johnson et al., 1994). These are probability distributions defined by a probability density (for a continuous variable x) or by a probability mass function (for a discrete variable x) given by,

$$f(x) \quad \frac{1}{x^{\alpha}} \tag{2.1}$$

for $x \geq a$ and $a > 0$, with a normalization factor (hidden in the proportionality symbol) which depends on whether x is continuous or discrete. In any case, normalization implies $\alpha > 1$. Sometimes power-law distributions are also called Pareto distributions (Evans et al., 2000, Johnson et al., 1994) (or Riemann zeta distributions in the discrete case (Johnson et al., 2005)), although in other contexts the name Pareto is associated to a slightly different distribution (Johnson et al., 1994). So we stick to the clearer term power-law distribution.

These have remarkable, non-usual statistical properties, as are scale invariance and divergence of moments. The first one means that power-law functions (defined between 0 and) are invariant under (properly performed) linear rescaling of axes (both x and f) and therefore have no characteristic scale, and hence cannot be used to define a prototype of the observable represented by x (Christensen and Moloney, 2005, Corral, 2008, Newman, 2005, Takayasu, 1989). For example, no unit of distance can be defined from the gravitational field of a point mass (a power law), whereas a time unit can be defined for radioactive decay (an exponential function). However, as power-law distributions cannot be defined for all $x > 0$ but for $x \geq a > 0$ their scale invariance is not complete or strict.

A second uncommon property is the non-existence of finite moments; for instance, if $\alpha \leq 2$ not a single finite moment exists (no mean, no variance, etc.). This has important consequences, as the law of large numbers does not hold (Kolmogorov, 1956, p. 65), i.e., the mean of a sample does not converge to a finite value as the size of the sample increases; rather, the sample mean tends to infinite (Shiryaev, 1996, p. 393). If $2 < \alpha \leq 3$ the mean exists and is finite, but higher moments are infinite, which means for instance that the central limit theorem, in its classic formulation, does not apply (the mean of a sample is not normally distributed and has infinite standard deviation) (Bouchaud and

Georges, 1990). Higher α s yield higher-order moments infinite, but then the situation is not so critical . Newman reviews other peculiar properties of power-law distributions, such as the 80 20 rule (Newman, 2005).

Although the normal (or Gaussian) distribution gives a non-zero probability that a human being is 10 m or 10 km tall, the definition of the probability density up to infinity is not questionable at all, and the same happens with an exponential distribution and most standard distributions in probability theory. However, one already sees that the power-law distribution is problematic, in particular for $\alpha \leq 2$, as it predicts an infinite mean, and for $2 \leq \alpha < 3$, as the variability of the sample mean is infinite. Of course, there can be variables having an infinite mean (one can easily simulate in a computer processes in which the time between events has an infinite mean), but in other cases, for physical reasons, the mean should be finite. In such situations a simple generalization is the truncation of the tail (Aban et al., 2006, Burroughs and Tebbens, 2001, Carrillo-Menéndez and Suárez, 2012, Johnson et al., 1994), yielding the truncated power-law distribution, defined in the same way as before by $f(x)$ 1 x^{α} but with $a \leq x \leq b$, with b finite, and with normalizing factor depending now on a and b (in some cases it is possible to have $a = 0$, see next section). Obviously, the existence of a finite upper cutoff b automatically leads to well-behaved moments, if the statistics is enough to see the cutoff; on the other hand, a range of scale invariance can persist, if $b \gg a$. What one finds in some practical problems is that the statistics is not enough to decide which is the sample mean and one cannot easily conclude if a pure power law or a truncated power law is the right model for the data.

A well known example of (truncated or not) power-law distribution is the Gutenberg-Richter law for earthquake size (Kagan, 2002, Kanamori and Brodsky, 2004, Utsu, 1999). If by size we understand radiated energy, the Gutenberg-Richter law implies that, in any seismically active region of the world, the sizes of earthquakes follow a power-law distribution, with an exponent $\alpha = 1 + 2B$ 3 and B close to 1. In this case, scale invariance means that if one asks how big (in terms of radiated energy) earthquakes are in a certain region, such a simple question has no possible answer. The non-convergence of the mean energy can easily be checked from data: catastrophic events such as the Sumatra-Andaman mega-earthquake of 2004 contribute to the mean much more than the previous recorded history (Corral and Font-Clos, 2013). Note that for the most common formulation of the Gutenberg-Richter law, in terms of the magnitude, earthquakes are not power-law distributed, but this is due to the fact that magnitude is an (increasing) exponential function of radiated energy, and therefore magnitude turns out to be exponentially distributed. In terms of magnitude, the statistical properties of earthquakes are trivial (well behaved mean, existence of a characteristic magnitude...), but we insist that this is not the case in terms of radiated energy.

Malamud (2004) lists several other natural hazards following power-law distributions in some (physical) measure of size, such as rockfalls, landslides (Hergarten, 2002), volcanic eruptions (Lahaie and Grasso, 1998, McClelland et al., 1989), and forest fires (Malamud et al., 2005), and we can add rainfall (Peters et al., 2002, 2010), tropical cyclones (roughly speaking, hurricanes) (Corral et al., 2010), auroras (Freeman and Watkins, 2002), tsunamis (Burroughs and Tebbens, 2005), etc. In some cases this broad range of responses is triggered simply by a small driving or perturbation (the slow motion of tectonic plates for earthquakes, the continuous pumping of solar radiation in hurricanes, etc.); then, this highly nonlinear relation between input and output can be labelled as crackling noise (Sethna et al., 2001). Notice that this does not apply for tsunamis, for instance, as they are not slowly driven (or at least not directly slowly driven).

Aschwanden (2011) reviews disparate astrophysical phenomena which are distributed according to power laws, some of them related to geoscience: sizes of asteroids, craters in the Moon, solar flares, and energy of cosmic rays. In the field of ecology and close areas, the applicability of power-law distributions has been overviewed by White et al. (2008), mentioning also island and lake sizes. Aban et al. (2006) provides bibliography for power-law and other heavy-tailed distributions in diverse disciplines, including hydrology, and Burroughs and Tebbens (2001) provide interesting geological examples.

A theoretical framework for power-law distributed sizes (and durations) of catastrophic phenomena not only in geoscience but also in condensed matter physics, astrophysics, biological evolution, neuroscience, and even the economy, is provided by the concept of self-organized criticality, and summarized by the sandpile paradigm (Bak, 1996, Christensen and Moloney, 2005, Jensen, 1998, Pruessner, 2012, Sornette, 2004). However, although the ideas of self-organization and criticality are very reasonable in the context of most of the geosystems mentioned above (Corral, 2010, Peters and Christensen, 2006, Peters and Neelin, 2006), one cannot rule out other mechanisms for the emergence of power-law distributions (Czechowski, 2003, Dickman, 2003, Mitzenmacher, 2004, Newman, 2005, Sornette, 2004).

On the other hand, it is interesting to mention that, in addition to sizes and durations, power-law distributions have also been extensively reported in time between the occurrences of natural hazards (waiting times), as for instance in solar flares (Baiesi et al., 2006, Boffetta et al., 1999), earthquakes (Bak et al., 2002, Corral, 2003, 2004a), or solar wind (Wanliss and Weygand, 2007); in other cases the distributions contain a power-law part mixed with other factors (Corral, 2004b, 2009b, Geist and Parsons, 2008, Saichev and Sornette, 2006). Nevertheless, the possible relation with critical phenomena is not direct (Corral, 2005, Paczuski et al., 2005). The distance between events, or jumps, has

received relatively less attention (Corral, 2006, Davidsen and Paczuski, 2005, Felzer and Brodsky, 2006).

The importance of power-law distributions in geoscience is apparent; however, some of the evidence gathered in favour of this paradigm can be considered as anecdotic or tentative, as it is based on rather poor data analysis. A common practice is to find some (naive or not) estimation of the probability density or mass function $f(x)$ and plot $\ln f(x)$ versus $\ln x$ and look for a linear dependence between both variables. Obviously, a power-law distribution should behave in that way, but the opposite is not true: an apparent straight line in a log-log plot of $f(x)$ should not be considered a guarantee of an underlying power-law distribution, or perhaps the exponent obtained from there is clearly biased (Bauke, 2007, Clauset et al., 2009, Goldstein et al., 2004, White et al., 2008). But in order to discriminate between several competing theories or models, as well as in order to extrapolate the available statistics to the most extreme events, it is very important to properly fit power laws and to find the right power-law exponent (if any) (White et al., 2008).

The subject of this paper is a discussion on the most appropriate fitting, testing of the goodness-of-fit, and representation of power-law distributions, both non-truncated and truncated. A consistent and robust method will be checked on several examples in geoscience, including earthquakes, tropical cyclones, and forest fires. The procedure is in some points analogous to that of Clauset et al. (2009), although there are variations is some key steps, in order to correct several drawbacks of the original method (Corral et al., 2011, Peters et al., 2010). The most important difference is in the criterion to select the range over which the power law holds. As the case of most interest in geoscience is that of a continuous random variable, the more involving discrete case will be postponed to a separate publication (Corral et al., 2012).

2.2 Power-law fits and goodness-of-fit tests

2.2.1 Non-truncated and truncated power-law distributions

Let us consider a continuous power-law distribution, defined in the range $a \leq x \leq b$, where b can be finite or infinite and $a \geq 0$. The probability density of x is given by,

$$f(x) = \frac{\alpha - 1}{a^{1-\alpha} - 1 \;\; b^{\alpha-1}} \left(\frac{1}{x}\right)^{\alpha} \tag{2.2}$$

the limit b with $\alpha > 1$ and $a > 0$ provides the non-truncated power-law distribution, also called here pure power law; otherwise, for finite b one has the truncated power

law, for which no restriction exists on α if $a > 0$, but $\alpha < 1$ if $a = 0$ (which is sometimes referred to as the power-function distribution (Evans et al., 2000)); the case $\alpha = 1$ needs a separate treatment, with

$$f(x) = \frac{1}{x \ln(b\ a)} \tag{2.3}$$

We will consider in principle that the distribution has a unique parameter, α, and that a and b are fixed and known values. Remember that, at point x, the probability density function of a random variable is defined as the probability per unit of the variable that the random variable lies in a infinitesimal interval around x, that is,

$$f(x) = \lim_{\Delta x\ 0} \frac{\text{Prob}[x \leq \text{random variable} < x + \Delta x]}{\Delta x} \tag{2.4}$$

and has to verify $f(x) \geq 0$ and $\_\ \ f(x)dx = 1$, see for instance Ross (2002).

Equivalently, the distribution can be also characterized by its (complementary) cumulative distribution function,

$$S(x) = \text{Prob}[\text{random variable} \geq x] = \underset{x}{\ \ f(x\ )dx} \tag{2.5}$$

For a truncated or non-truncated power law this leads to

$$S(x) = \frac{1\ \ x^{\alpha-1} - 1\ \ b^{\alpha-1}}{a^{1-\alpha} - 1\ \ b^{\alpha-1}} \tag{2.6}$$

if $\alpha = 1$ and

$$S(x) = \frac{\ln(b\ \ x)}{\ln(b\ \ a)} \tag{2.7}$$

if $\alpha = 1$. Note that although $f(x)$ always has a power-law shape, $S(x)$ only has it in the non-truncated case (b and $\alpha > 1$); nevertheless, even not being a power law in the truncated case, the distribution is a power law, as it is $f(x)$ and not $S(x)$ which gives the name to the distribution.

2.2.2 Problematic fitting methods

Given a set of data, there are many methods to fit a probability distribution. Goldstein et al. (2004), Bauke (2007), White et al. (2008), and Clauset et al. (2009) check several methods based in the fitting of the estimated probability densities or cumulative distributions in the power-law case. As mentioned in the first section, $\ln f(x)$ is then a linear function of $\ln x$, both for non-truncated and truncated power laws. The same holds for $\ln S(x)$, but only in the non-truncated case. So, one can either estimate $f(x)$ from data, using some binning procedure, or estimate $S(x)$, for which no binning is necessary, and then fit a straight line by the least-squares method. As we find White *et al.* s (2008)

study the most complete, we summarize their results below, although those of the other authors are not very different.

For non-truncated power-law distributions, White et al. (2008) find that the results of the least-squares method using the cumulative distribution are reasonable, although the points in $S(x)$ are not independent and linear regression should yield problems in this case. We stress that this procedure only can work for non-truncated distributions (i.e., with b), truncated ones yield bad results (Burroughs and Tebbens, 2001).

The least-squares method applied to the probability density $f(x)$ has several variations, depending on the way of estimating $f(x)$. Using linear binning one obtains a simple histogram, for which the fitting results are catastrophic (Bauke, 2007, Goldstein et al., 2004, Pueyo and Jovani, 2006, White et al., 2008). This is not unexpected, as linear binning of a heavy-tailed distribution can be considered as a very naive approach. If instead of linear binning one uses logarithmic binning the results improve (when done correctly), and are reasonable in some cases, but they still show some bias, high variance, and bin-size dependence. A fundamental point is to avoid having empty bins, as they are disregarded in logscale, introducing an important bias.

In summary, methods of estimation of probability-distribution parameters based on least-squares fitting can have many problems, and usually the results are biased. Moreover, these methods do not take into account that the quantity to be fitted is a probability distribution (i.e., once the distributions are estimated, the method is the same as for any other kind of function). We are going to see that the method of maximum likelihood is precisely designed for dealing with probability distributions, presenting considerable advantages in front of the other methods just mentioned.

2.2.3 Maximum likelihood estimation

Let us denote a sample of the random variable x with N elements as x_1, x_2, ..., x_N, and let us consider a probability distribution $f(x)$ parameterized by α. The likelihood function $L(\alpha)$ is defined as the joint probability density (or the joint probability mass function if the variable were discrete) evaluated at x_1, x_2, ..., x_N in the case in which the variables were independent, i.e.,

$$L(\alpha) = \prod_{i=1}^{N} f(x_i) \tag{2.8}$$

Note that the sample is considered fixed, and it is the parameter α what is allowed to vary. In practice it is more convenient to work with the log-likelihood, the natural

logarithm of the likelihood (dividing by N also, in our definition),

$$(\alpha) = \frac{1}{N} \ln L(\alpha) = \frac{1}{N} \sum_{i=1}^{N} \ln f(x_i) \tag{2.9}$$

The maximum likelihood (ML) estimator of the parameter α based on the sample is just the maximum of (α) (which coincides with the maximum of $L(\alpha)$, obviously). For a given sample, we will denote the ML estimator as α_e (e is from empirical), but it is important to realize that the ML estimator is indeed a statistic (a quantity calculated from a random sample) and therefore can be considered as a random variable; in this case it is denoted as α. In a formula,

$$\alpha_e = \arg\max_{\alpha} (\alpha) \tag{2.10}$$

where argmax refers to the argument of the function that makes it maximum.

For the truncated or the non-truncated continuous power-law distribution we have, substituting $f(x)$ from Eqs. (2)-(3) and introducing $r = a\ b$, disregarding the case $a = 0$,

$$(\alpha) = \ln \frac{\alpha - 1}{1 - r^{\alpha-1}} - \alpha \ln \frac{g}{a} - \ln a \quad \text{if } \alpha = 1 \tag{2.11}$$

$$(\alpha) = -\ln \ln \frac{1}{r} - \ln g \quad \text{if } \alpha = 1; \tag{2.12}$$

g is the geometric mean of the data, $\ln g = N^{-1} \sum_{1}^{N} \ln x_i$, and the last term in each expression is irrelevant for the maximization of (α). The equation for $\alpha = 1$ is necessary in order to avoid overflows in the numerical implementation of Eq. (2.11). Remember that the distribution is only parameterized by α, whereas a and b (and r) are constant parameters; therefore, (α) is not a function of a and b, but of α.

In order to find the maximum of (α) one can derive with respect α and set the result equal to zero (Aban et al., 2006, Johnson et al., 1994),

$$\left. \frac{d\ (\alpha)}{d\alpha} \right|_{\alpha=\alpha_e} = \frac{1}{\alpha_e - 1} + \frac{r^{\alpha_e - 1} \ln r}{1 - r^{\alpha_e - 1}} - \ln \frac{g}{a} = 0 \tag{2.13}$$

which constitutes the so-called likelihood equation for this problem. For a non-truncated distribution, $r = 0$, and it is clear that there is one and only one solution,

$$\alpha_e = 1 + \frac{1}{\ln(g\ a)} \tag{2.14}$$

which corresponds to a maximum, as

$$L(\alpha) = e^{N\ (\alpha)} = \frac{1}{a^N} (\alpha - 1)^N e^{-N\alpha \ln(g\ a)} \tag{2.15}$$

has indeed a maximum (resembling a gamma probability density, see next subsection). Figure 1 illustrates the log-likelihood function and its derivative, for simulated power-law data.

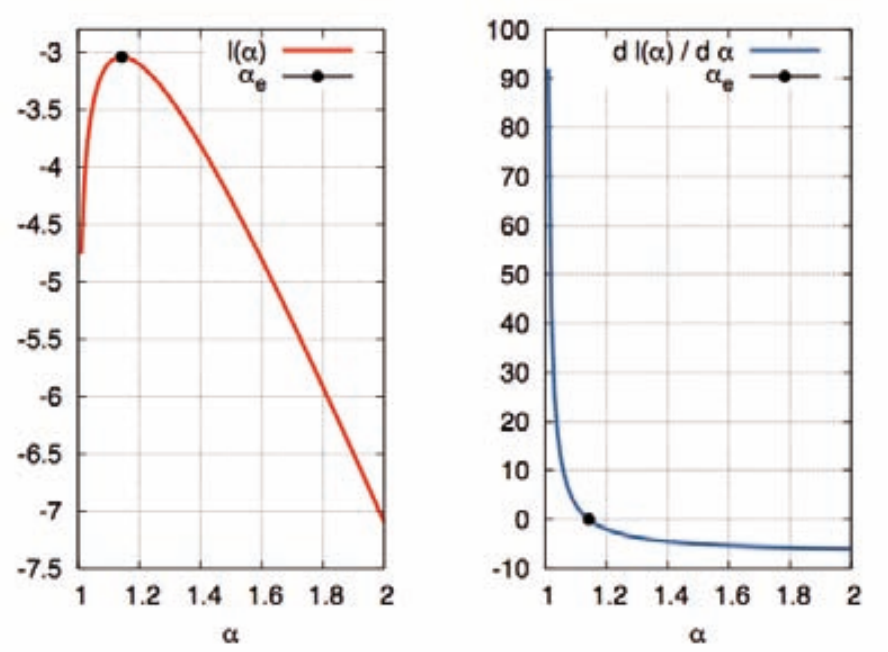

FIGURE 2.1: Log-likelihood $\ell(\alpha)$ and its derivative, for simulated non-truncated power-law data with exponent $\alpha = 1.15$ and $a = 0.001$. The total number of data is $N_{tot} = 1000$. The resulting estimation yields $\alpha_e = 1.143$, which will lead to a confidence interval $\alpha \pm \sigma = 1.143 \pm 0.005$.

In the truncated case it is not obvious that there is a solution to the likelihood equation (Aban et al., 2006); however, one can take advantage of the fact that the power-law distribution, for fixed a and b, can be viewed as belonging to the regular exponential family, for which it is known that the maximum likelihood estimator exists and is unique, see Barndorff-Nielsen (1978, p. 151) or del Castillo (2013). Indeed, in the single-parameter case, the exponential family can be written in the form,

$$f(x) = C^{-1}(\alpha)H(x)e^{\theta(\alpha)\cdot T(x)}, \tag{2.16}$$

where both $\theta(\alpha)$ and $T(x)$ can be vectors, the former containing the parameter α of the family. Then, for $\theta(\alpha) = -\alpha$, $T(x) = \ln x$, and $H(x) = 1$ we obtain the (truncated or not) power-law distribution, which therefore belongs to the regular exponential family, which guarantees the existence of a unique ML solution.

In order to find the ML estimator of the exponent in the truncated case, we proceed by maximizing directly the log-likelihood $\ell(\alpha)$ (rather than by solving the likelihood equation). The reason is a practical one, as our procedure is part of a more general method, valid for arbitrary distributions $f(x)$, for which the derivative of $\ell(\alpha)$ can be

difficult to evaluate. We will use the downhill simplex method, through the routine `amoeba` of Press et al. (2002), although any other simpler maximization procedure should work, as the problem is one-dimensional, in this case. One needs to take care when the value of α gets very close to one in the maximization algorithm, and then replace (α) by its limit at $\alpha = 1$,

$$(\alpha) \quad _{\alpha \ 1} - \ln \ln \frac{1}{r} - \alpha \ln \frac{g}{a} - \ln a \tag{2.17}$$

which is in agreement with the likelihood function for a (truncated) power-law distribution with $\alpha = 1$.

An important property of ML estimators, not present in other fitting methods, is their invariance under re-parameterization. If instead of working with parameter α we use $\nu = h(\alpha)$, then, the ML estimator of ν is in agreement with that of α, i.e., $\nu = h(\alpha)$. Indeed,

$$\frac{d}{d\nu} = \frac{d}{d\alpha}\frac{d\alpha}{d\nu} \tag{2.18}$$

so, the maximum of as a function of ν is attained at the point $h(\alpha)$, provided that the function h is one-to-one . Note that the parameters could be multidimensional as well. Casella and Berger (2002) study this invariance with much more care.

In their comparative study, White *et al.* (2008) conclude that maximum likelihood estimation outperforms the other fitting methods, as always yields the lowest variance and bias of the estimator. This is not unexpected, as the ML estimator is, mathematically, the one with minimum variance among all asymptotically unbiased estimators. This property is called asymptotical efficiency (Bauke, 2007, White et al., 2008).

2.2.4 Standard deviation of the ML estimator

The main result of this subsection is the value of the uncertainty σ of α, represented by the standard deviation of α and given by

$$\sigma = \frac{1}{\overline{N}} \left[\frac{1}{(\alpha_e - 1)^2} - \frac{r^{\alpha_e - 1} \ln^2 r}{(1 - r^{\alpha_e - 1})^2} \right]^{-1 \ 2} \tag{2.19}$$

(Aban et al., 2006). This formula can be used directly, although σ can be computed as well from Monte Carlo simulations, as explained in another subsection. A third option is the use of the jackknife procedure, as done by Peters et al. (2010). The three methods lead to essentially the same results. The rest of this subsection is devoted to the particular derivation of σ for a non-truncated power-law distribution, and therefore can be skipped by readers interested mainly in the practical use of ML estimation.

For the calculation of α (the ML estimator of α) one needs to realize that this is indeed a statistic (a quantity calculated from a random sample) and therefore it can be considered as a random variable. Note that α denotes the true value of the parameter, which is unknown. It is more convenient to work with $\alpha - 1$ (the exponent of the cumulative distribution function); in the non-truncated case ($r = 0$ with $\alpha > 1$) we can easily derive its distribution. First let us consider the geometric mean of the sample, g, rescaled by the minimum value a,

$$\ln \frac{g}{a} = \frac{1}{N} \sum_{i=1}^{N} \ln \frac{x_i}{a} \tag{2.20}$$

As each x_i is power-law distributed (by hypothesis), a simple change of variables shows that $\ln(x_i \ a)$ turns out to be exponentially distributed, with scale parameter $1 \ (\alpha - 1)$; then, the sum will be gamma distributed with the same scale parameter and with shape parameter given by N (this is the key property of the gamma distribution (Durrett, 2010)). Therefore, $\ln(g \ a)$ will follow the same gamma distribution but with scale parameter $N^{-1}(\alpha - 1)^{-1}$.

At this point it is useful to introduce the generalized gamma distribution (Evans et al., 2000, Johnson et al., 1994, Kalbfleisch and Prentice, 2002), with density, for a random variable $y \geq 0$,

$$D(y) = \frac{\delta}{c\Gamma(\gamma \ \delta)} \left(\frac{y}{c}\right)^{\gamma - 1} e^{-(y \ c)^{\delta}} \tag{2.21}$$

where $c > 0$ is the scale parameter and γ and δ are the shape parameters, which have to verify $0 < \gamma \ \delta <$ (so, the only restriction is that they have the same sign, although the previous references only consider $\gamma > 0$ and $\delta > 0$); the case $\delta = 1$ yields the usual gamma distribution and $\delta = \gamma = 1$ is the exponential one. Again, changing variables one can show that the inverse $z = 1 \ y$ of a generalized gamma variable is also a generalized gamma variable, but with transformed parameters,

$$\gamma \ \delta \ c \qquad -\gamma \ -\delta \ \frac{1}{c} \tag{2.22}$$

So, $\alpha - 1 = z = 1 \ \ln(g \ a)$ will have a generalized gamma distribution, with parameters $-N$, -1, and $N(\alpha - 1)$ (keeping the same order as above). Introducing the moments of this distribution (Evans et al., 2000),

$$y^m \ = c^m \frac{\Gamma\left(\frac{\gamma + m}{\delta}\right)}{\Gamma\left(\gamma \ \delta\right)} \tag{2.23}$$

(valid for $m > -\gamma$ if $\gamma > 0$ and for $m < \gamma$ if $\gamma < 0$, and y^m infinite otherwise), we obtain the expected value of $\alpha - 1$,

$$\alpha - 1 \ = \frac{N(\alpha - 1)}{N - 1} \tag{2.24}$$

Note that the ML estimator, α, is biased, as its expected value does not coincide with the right value, α; however, asymptotically, the right value is recovered. An unbiased estimator of α can be obtained for a small sample as $(1 - 1\ N)\alpha_e + 1\ N$, although this will not be of interest to us.

In the same way, the standard deviation of $\alpha - 1$ (and of α) turns out to be

$$\sigma = \quad \overline{(\alpha - 1)^2 \ - \ \alpha - 1\ ^2} = \frac{\alpha - 1}{(1 - 1\ N)\ \overline{N - 2}} \tag{2.25}$$

which leads asymptotically to $(\alpha - 1)\quad \overline{N}$. In practice, we need to replace α by the estimated value α_e; then, this is nothing else than the limit $r = 0$ ($b\qquad$) of the general formula stated above for σ (Aban et al., 2006). The fact that the standard deviation tends to zero asymptotically (together with the fact that the estimator is asymptotically unbiased) implies that any single estimation converges (in probability) to the true value, and therefore the estimator is said to be consistent.

2.2.5 Goodness-of-fit test

One can realize that the maximum likelihood method always yields a ML estimator for α, no matter which data one is using. In the case of power laws, as the data only enters in the likelihood function through its geometric mean, any sample with a given geometric mean yields the same value for the estimation, although the sample can come from a true power law or from any other distribution. So, no quality of the fit is guaranteed and thus, maximum likelihood estimation should be rather called minimum unlikelihood estimation. For this reason a goodness-of-fit test is necessary (although recent works do not take into account this fact (Baró and Vives, 2012, Kagan, 2002, White et al., 2008)).

Following Goldstein et al. (2004) and Clauset et al. (2009) we use the Kolmogorov-Smirnov (KS) test (Chicheportiche and Bouchaud, 2012, Press et al., 2002), based on the calculation of the KS statistic or KS distance d_e between the theoretical probability distribution, represented by $S(x)$, and the empirical one, $S_e(x)$. The latter, which is an unbiased estimator of the cumulative distribution (Chicheportiche and Bouchaud, 2012), is given by the stepwise function

$$S_e(x) = n_e(x)\ N \tag{2.26}$$

where $n_e(x)$ is the number of data in the sample taking a value of the variable larger than or equal to x. The KS statistic is just the maximum difference, in absolute value, between $S(x)$ and $n_e(x)$ N, that is,

$$d_e = \max_{a \le x \le b} S(x) - S_e(x) = \max_{a \le x \le b} \left| \frac{1}{1 - r^{\alpha_e - 1}} \left[\left(\frac{a}{x} \right)^{\alpha_e - 1} - r^{\alpha_e - 1} \right] - \frac{n_e(x)}{N} \right| \qquad (2.27)$$

where the bars denote absolute value. Note that the theoretical cumulative distribution $S(x)$ is parameterized by the value of α obtained from ML, α_e. In practice, the difference only needs to be evaluated around the points x_i of the sample (as the routine `ksone` of Press et al. (2002) does) and not for all x. A more strict mathematical definition uses the supremum instead of the maximum, but in practice the maximum works perfectly. We illustrate the procedure in Fig. 2, with a simulation of a non-truncated power law.

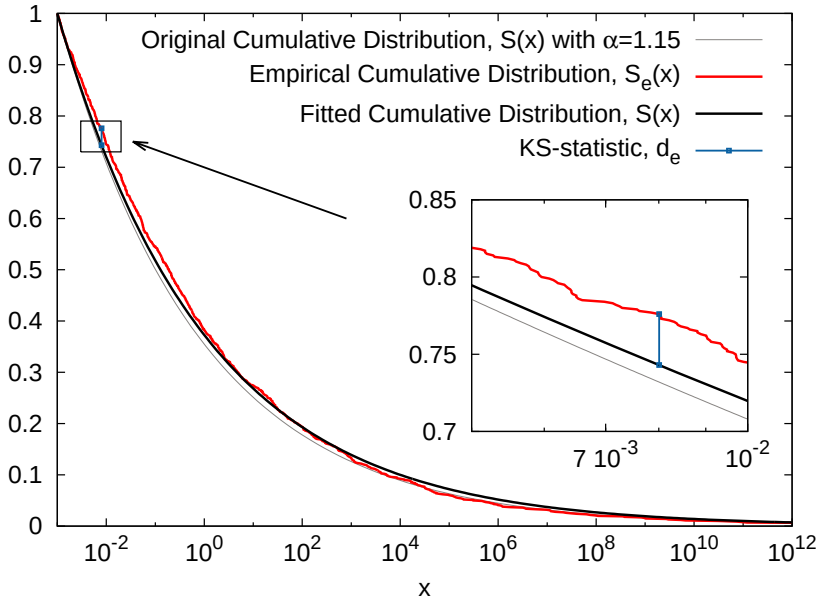

FIGURE 2.2: Empirical (complementary) cumulative distribution for a simulated non-truncated power-law distribution with $\alpha = 1\,15$, $a = 0\,001$, and $N_{tot} = 1000$, together with its corresponding fit, which yields $\alpha_e = 1\,143$. The maximum difference between both curves, $d_e = 0\,033$, is marked as an illustration of the calculation of the KS statistic. The original theoretical distribution, unknown in practice, is also plotted.

Intuitively, if d_e is large the fit is bad, whereas if d_e is small the fit can be considered as good. But the relative scale of d_e is provided by its own probability distribution, through the calculation of a $p-$value. Under the hypothesis that the data follow indeed the theoretical distribution, with the parameter α obtained from our previous estimation (this is the null hypothesis), the $p-$value provides the probability that the KS statistic takes a value larger than the one obtained empirically, i.e.,

$$p = \text{Prob}[\text{KS statistic for power-law data (with } \alpha_e) \text{ is} > d_e]; \qquad (2.28)$$

then, bad fits will have rather small $p-$values.

It turns out that, in principle, the distribution of the KS statistic is known, at least asymptotically, independently of the underlying form of the distribution, so,

$$p_Q = Q(d_e \quad \overline{N} + 0\ 12d_e + 0\ 11d_e \quad \overline{N} = \\ = 2 \sum_{j=1} (-1)^{j-1} \exp[-2j^2(d_e \quad \overline{N} + 0\ 12d_e + 0\ 11d_e \quad \overline{N})^2] \quad (2.29)$$

for which one can use the routine `probks` of Press et al. (2002) (but note their Eq. (14.3.9) is not right). Nevertheless, this formula will not be accurate in our case, and for this reason we use the symbol p_Q instead of p. The reason is that we are optimizing the value of α using the same sample to which we apply the KS test, which yields a bias in the test, i.e., the formula would work for the true value of α, but not for one obtained by ML, which would yield in general a smaller KS statistic and too large $p-$values (because the fit for α_e is better than for the true value α) (Clauset et al., 2009, Goldstein et al., 2004). However, for this very same reason the formula can be useful to reject the goodness of a given fit, i.e., if p_Q obtained in this way is already below 0.05, the true p will be even smaller and the fit is certainly bad. But the opposite is not true. In a formula,

$$\text{if } p_Q < 0\ 05 \qquad \text{reject power law} \quad (2.30)$$

otherwise, no decision can be taken yet. Of course, the significance level 0.05 is arbitrary and can be changed to another value, as usual in statistical tests. As a final comment, perhaps a more powerful test would be to use, instead of the KS statistic, the Kuiper s statistic (Press et al., 2002), which is a refinement of the former one. It is stated by Clauset *et al.* (2009) that both tests lead to very similar fits. In most cases, we have also found no significant differences between both tests.

2.2.6 The Clauset *et al.*'s recipe

Now we are in condition to explain the genuine Clauset *et al.* s (2009) method. This is done in this subsection for completeness, and for the information of the reader, as we are not going to apply this method. The key to fitting a power law is neither the ML estimation of the exponent nor the goodness-of-fit test, but the selection of the interval $[a\ b]$ over which the power law holds. Initially, we have taken a and b as fixed parameters, but in practice this is not the case, and one has to decide where the power law starts and where ends, independently of the total range of the data. In any case, N will be the number of data in the power-law range (and not the total number of data).

The recipe of Clauset *et al.* (2009) applies to non-truncated power-law distributions (b), and considers that a is a variable which needs to be fit from the sample (values of x below a are outside the power-law range). The recipe simply consists in the search of the value of a which yields a minimum of the KS statistic, using as a parameter of the theoretical distribution the one obtained by maximum likelihood, α_e, for the corresponding a (no calculation of a $p-$value is required for each fixed a). In other words,

$$a = \text{the one that yields minimum } d_e \tag{2.31}$$

Next, a global $p-$value is computed by generating synthetic samples by a mixture of parametric bootstrap (similarly to what is explained in the next subsection) and non-parametric bootstrap. Then, the same procedure applied to the empirical data (minimization of the KS distance using ML for fitting) is applied to the synthetic samples in order to fit a and α.

These authors do not provide any explanation of why this should work, although one can argue that, if the data is indeed a power law with the desired exponent, the larger the number of data (the smaller the $a-$value), the smaller the value of d_e, as d_e goes as 1 $\overline{N}$ (for large N, see previous subsection). On the other hand, if for a smaller a the data departs from the power law, this deviation should compensate and overcome the reduction in d_e due to the increase of N, yielding a larger d_e. But there is no reason to justify this overcoming.

Nevertheless, we will not use the Clauset *et al.* s (2009) procedure for two other reasons. First, its extension to truncated power laws, although obvious, and justifiable with the same arguments, yields bad results, as the resulting values of the upper truncation cutoff, b, are highly unstable. Second, even for non-truncated distributions, it has been shown that the method fails to detect the existence of a power law for data simulated with a power-law tail (Corral et al., 2011): the method yields an $a-$value well below the true power-law region, and therefore the resulting p is too small for the power law to become acceptable. We will explain an alternative method that avoids these problems, but first let us come back to the case with a and b fixed.

2.2.7 Monte Carlo simulations

Remember that we are considering a power-law distribution, defined in $a \leq x \leq b$. We already have fit the distribution, by ML, and we are testing the goodness of the fit by means of the KS statistic. In order to obtain a reliable $p-$value for this test we will perform Monte Carlo simulations of the whole process. A synthetic sample power-law distributed and with N elements can be obtained in a straightforward way, from the

inversion or transformation method (Devroye, 1986, Press et al., 2002, Ross, 2002),

$$x_i = \frac{a}{[1-(1-r^{\alpha_e-1})u_i]^{1\ (\alpha_e-1)}} \tag{2.32}$$

where u_i represents a uniform random number in $[0\ \ 1)$. One can use any random number generator for it. Our results arise from `ran3` of Press et al. (2002).

2.2.8 Application of the complete procedure to many synthetic samples and calculation of $p-$value

The previous fitting and testing procedure is applied in exactly the same way to the synthetic sample, yielding a ML exponent α_s (where the subindex s stands from synthetic or simulated), and then a KS statistic d_s, computed as the difference between the theoretical cumulative distribution, with parameter α_s, and the simulated one, $n_s(x)\ \ N$ (obtained from simulations with α_e, as described in the previous subsection), i.e.,

$$d_s = \max_{a\le x\le b}\left|\frac{1}{1-r^{\alpha_s-1}}\left[\left(\frac{a}{x}\right)^{\alpha_s-1} - r^{\alpha_s-1}\right] - \frac{n_s(x)}{N}\right| \tag{2.33}$$

Both values of the exponent, α_e and α_s, should be close to each other, but they will not be necessarily the same. Note that we are not parametrizing $S(x)$ by the empirical value α_e, but with a new fitted value α_s. This is in order to avoid biases, as a parametrization with α_e would lead to worse fits (as the best one would be with α_s) and therefore to larger values of the resulting KS statistic and to artificially larger $p-$values. So, although the null hypothesis of the test is that the exponent of the power law is α_e, and synthetic samples are obtained with this value, no further knowledge of this value is used in the test. This is the procedure used by Clauset et al. (2009) and Malmgren et al. (2008), but it is not clear if it is the one of Goldstein et al. (2004).

In fact, one single synthetic sample is not enough to do a proper comparison with the empirical sample, and we repeat the simulation many times. The most important outcome is the set of values of the KS statistic, d_s, which allows to estimate its distribution. The $p-$value is simply calculated as

$$p = \frac{\text{number of simulations with } d_s \ge d_e}{N_s} \tag{2.34}$$

where N_s is the number of simulations. Figure 3 shows an example of the distribution of the KS statistic for simulated data, which can be used as a table of critical values when the number of data and the exponent are the same as in the example (Goldstein et al., 2004).

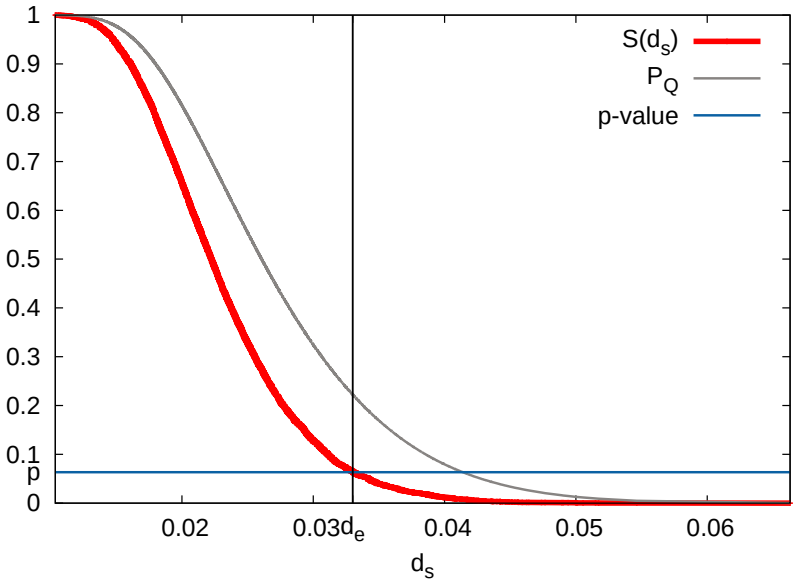

FIGURE 2.3: Cumulative (complementary) distribution of the Kolmogorov-Smirnov statistic for simulated non-truncated power-law distributions with $\alpha = \alpha_e = 1\ 143$, $a = 0\ 001$, and $N_{tot} = 1000$. The original empirical value $d_e = 0\ 033$ is also shown. The resulting $p-$value turns our to be $p = 0\ 060 \pm 0\ 008$. The false $p-$value, p_Q, arising from the KS formula, leads to higher values for the same d_e, in concrete, $p_Q = 0\ 22$.

The standard deviation of the $p-$value can be calculated just using that the number of simulations with $d_s \geq d_e$ is binomially distributed, with standard deviation $\sqrt{N_s p(1-p)}$ and therefore the standard deviation of p is the same divided by N_s,

$$\sigma_p = \sqrt{\frac{p(1-p)}{N_s}} \tag{2.35}$$

In fact, the $p-$value in this formula should be the ideal one (the one of the whole population) but we need to replace it by the estimated value; further, when doing estimation from data, N_s should be $N_s - 1$, but we have disregarded this bias correction. It will be also useful to consider the relative uncertainty of p, which is the same as the relative uncertainty of the number of simulations with $d_s \geq d_e$ (as both are proportional). Dividing the standard deviation of p by its mean (which is p), we obtain

$$CV_p = \sqrt{\frac{1-p}{pN_s}} \qquad \sqrt{\frac{1-p}{\text{number of simulations with } d_s \geq d_e}} \tag{2.36}$$

(we will recover this formula for the error of the estimation of the probability density).

In this way, small $p-$values are associated to large values of d_e, and therefore to bad fits. However, note that if we put the threshold of rejection in, let us say, $p \leq 0\ 05$, even true power-law distributed data, with exponent α_e, yield bad fits in one out of 20 samples (on average). So we are rejecting true power laws in 5 % of the cases (type I error).

On the other hand, lowering the threshold of rejection would reduce this problem, but would increase the probability of accepting false power laws (type II error). In this type of tests a compromise between both types of errors is always necessary, and depends on the relative costs of rejecting a true hypothesis or accepting a false one.

In addition, we can obtain from the Monte Carlo simulations the uncertainty of the ML estimator, just computing $\bar{\alpha}_s$, the average value of α_s, and from here its standard deviation,

$$\sigma = \sqrt{\overline{(\alpha_s - \bar{\alpha}_s)^2}} \tag{2.37}$$

where the bars indicate average over the N_s Monte Carlo simulations. This procedure yields good agreement with the analytical formula of Aban et al. (2006), but can be much more useful in the discrete power-law case.

2.2.9 Alternative method to the one by Clauset *et al.*

At this point, for given values of the truncation points, a and b, we are able to obtain the corresponding ML estimation of the power-law exponent as well as the goodness of the fit, by means of the $p-$value. Now we face the same problem Clauset *et al.* (2009) tried to solve: how to select the fitting range? In our case, how to find not only the value of a but also of b? We adopt the simple method proposed by Peters et al. (2010): sweeping many different values of a and b we should find, if the null hypothesis is true (i.e., if the sample is power-law distributed), that many sets of intervals yield acceptable fits (high enough $p-$values), so we need to find the best of such intervals. And which one is the best? For a non-truncated power law the answer is easy, we select the largest interval, i.e., the one with the smaller a, provided that the $p-$value is above some fixed significance level p_c. All the other acceptable intervals will be inside this one.

But if the power law is truncated the situation is not so clear, as there can be several non-overlapping intervals. In fact, many true truncated power laws can be contained in the data, at least there are well know examples of stochastic processes with double power-law distributions (Boguná and Corral, 1997, Corral, 2003, 2009a, Klafter et al., 1996). At this point any selection can be reasonable, but if one insists in having an automatic, blind procedure, a possibility is to select either the interval which contains the larger number of data, N (Peters et al., 2010), or the one which has the larger log-range, b a. For double power-law distributions, in which the exponent for small x is smaller than the one for large x, the former recipe has a tendency to select the first (small x) power-law regime, whereas the second procedure changes this tendency in some cases.

In summary, the final step of the method for truncated power-law distributions is contained in the formula

$$[a\ b] = \text{the one that yields higher} \begin{matrix} N \\ \text{or} \\ b\ a \end{matrix} \text{provided that } p > p_c \tag{2.38}$$

which contains in fact two procedures, one maximizing N and the other maximizing $b\ a$. We will test both in this paper. For non-truncated power-law distributions the two procedures are equivalent.

One might be tempted to choose $p_c = 0\ 05$, however, it is safer to consider a larger value, as for instance $p_c = 0\ 20$. Note that the $p-$value we are using is the one for fixed a and b, and then the $p-$value of the whole procedure should be different, but at this point it is not necessary to obtain such a $p-$value, as we should have already come out with a reasonable fit. Figure 4 shows the results of the method for true power-law data.

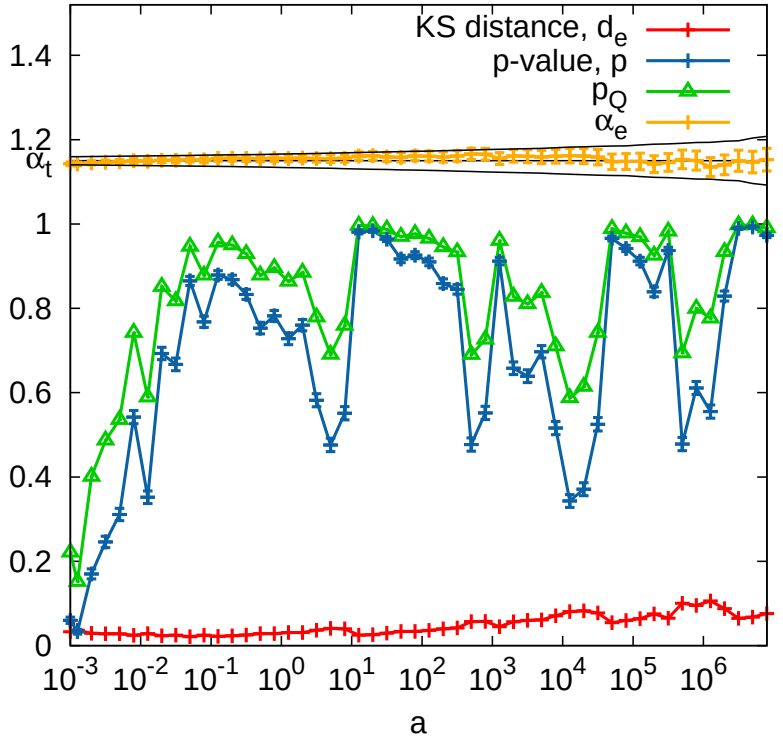

FIGURE 2.4: Evolution as a function of a of the KS statistic, the false $p-$value p_Q, the true $p-$ value (for fixed a), and the estimated exponent. The true exponent, here called α_t and equal to 1.15, is displayed as a thin black line, together with a 2σ interval.

2.2.10 Truncated or non-truncated power-law distribution?

For broadly distributed data, the simplest choice is to try to fit first a non-truncated

power-law distribution. If an acceptable fit is found, it is expected that a truncated power law, with $b \geq x_{max}$ (where x_{max} is the largest value of x) would yield also a good fit. In fact, if b is not considered as a fixed value but as a parameter to fit, its maximum likelihood estimator when the number of data is fixed, i.e., when b is in the range $b \geq x_{max}$, is $b_e = x_{max}$. This is easy to see (Aban et al., 2006), just looking at the equations for (α), (11) and (12), which show that (α) increases as b approaches x_{max}. (In the same way, the ML estimator of a, for fixed number of data, would be $a_e = x_{min}$, but we are not interested in such a case now.) On the other hand, it is reasonable that a truncated power law yields a better fit than a non-truncated one, as the former has two parameters and the latter only one (assuming that a is fixed, in any case).

In order to do a proper comparison, in such situations the so-called Akaike information criterion (AIC) can be used. This is defined simply as the difference between twice the number of parameters and twice the maximum of the log-likelihood multiplied by the number of data, i.e.,

$$AIC = 2 \times (\text{number of parameters}) - 2N \ (\alpha_e) \tag{2.39}$$

In general, having more parameters leads to better fits, and to higher likelihood, so, the first term compensates this fact. Therefore, given two models, the one with smaller AIC is preferred. Note that, in order that the comparison based on the AIC makes sense, the fits that are compared have to be performed exactly over the same data. So, in our case this can only be done for non-truncated power laws and for truncated power laws with $b \geq x_{max}$. Nevertheless, due to the limitations of this paper we have not performed the comparison.

2.3 Estimation of probability densities and cumulative distribution functions

The method of maximum likelihood does not rely on the estimation of the probability distributions, in contrast to other methods. Nevertheless, in order to present the results, it is useful to display some representation of the distribution, together with its fit. This procedure has no statistical value (it cannot provide a substitution of a goodness-of-fit test) but is very helpful as a visual guide, specially in order to detect bugs in the algorithms.

2.3.1 Estimation of the probability density

In the definition of the probability density,

$$f(x) = \lim_{\Delta x \to 0} \frac{\text{Prob}[x \leq \text{random variable} < x + \Delta x]}{\Delta x} \tag{2.40}$$

a fundamental issue is that the width of the interval Δx has to tend to zero. In practice Δx cannot tend to zero (there would be no statistics in such case), and one has to take a non-zero value of the width. The most usual procedure is to draw a histogram using linear binning (bins of constant width); however, there is no reason why the width of the distribution should be fixed (some authors even take $\Delta x = 1$ as the only possible choice). In fact, Δx should be chosen in order to balance the necessity of having enough statistics (large Δx) with that of having a good sampling of the function (small Δx). For power-law distributions and other fat-tailed distributions, which take values across many different scales, the right choice depends of the scale of x. In this cases it is very convenient to use the so-called logarithmic binning (Hergarten, 2002, Pruessner, 2012). This uses bins that appear as constant in logarithmic scale, but that in fact grow exponentially (for which the method is sometimes called exponential binning instead). Curiously, this useful method is not considered by classic texts on density estimation (Silverman, 1986).

Let us consider the semi-open intervals $[a_0\ b_0)\ [a_1\ b_1)\ \ \ [a_k\ b_k)\ \ \ $, also called bins, with $a_{k+1} = b_k$ and $b_k = Ba_k$ (this constant B has nothing to do with the one in the Gutenberg-Richter law, Sec. 2.1). For instance, if $B = \sqrt[5]{10}$ this yields 5 intervals for each order of magnitude. Notice that the width of every bin grows linearly with a_k, but exponentially with k, as $b_k - a_k = (B-1)a_k = a_0(B-1)B^k$. The value of B should be chosen in order to avoid low populated bins, otherwise, a spurious exponent equal to one appears (Pruessner, 2012).

We simply will count the number of occurrences of the variable in each bin. For each value of the random variable x_i, the corresponding bin is found as

$$k = \text{int}\left(\frac{\ln(x_i\ a_0)}{\ln B}\right) \tag{2.41}$$

where the function int denotes the integer part of its argument. Of course, a_0 has to be smaller than any possible value of x. For a continuous variable the concrete value of a_0 should be irrelevant (if it is small enough), but in practice one has to avoid that the resulting values of a_k coincide with round values of the variable (Corral et al., 2011).

So, with this logarithmic binning, the probability density can be estimated (following its definition) as the relative frequency of occurrences in a given bin divided by its width,

i.e.,

$$f_e(x_k^*) = \frac{\text{number of occurrences in bin } k}{(b_k - a_k) \times \text{number of occurrences}} \tag{2.42}$$

where the estimation of the density is associated to a value of x represented by x_k^*. The most practical solution is to take it in the middle of the interval in logscale, so $x_k^* = \overline{a_k b_k}$. However, for sparse data covering many orders of magnitude it is necessary to be more careful. In fact, what we are looking for is the point x_k^* whose value of the density coincides with the probability of being between a_k and b_k divided by the width of the interval. This is the solution of

$$f(x_k^*) = \frac{1}{b_k - a_k} \int_{a_k}^{b_k} f(x)dx = \frac{S(a_k) - S(b_k)}{b_k - a_k} \tag{2.43}$$

where f and S are the theoretical distributions. When the distribution and its parameters are known, the equation can be solved either analytically or numerically. It is easy to see that for a power-law distribution (truncated or not) the solution can be written

$$x_k^* = \overline{a_k b_k} \left(\alpha - 1\right) \frac{B^{\alpha\ 2-1}(B-1)}{B^{\alpha-1} - 1}^{\ 1\ \alpha} \tag{2.44}$$

where we have used that $B = b_k\ a_k$ (if we were not using logarithmic binning we would have to write a bin-dependent B_k). Note that for constant (bin-independent) B, i.e., for logarithmic binning, the solution is proportional but not equal to the geometric mean of the extremes of the bin. Nevertheless, the omission of the proportionality factor does not alter the power-law behavior, just shifts (in logarithmic scale) the curve. But for a different binning procedure this is no longer true. Moreover, for usual values of B the factor is very close to one (Hergarten, 2002), although large values of B (Corral et al., 2011) yield noticeable deviations if the factor in brackets is not included, see also our treatment of the radionuclide half-lives in Sec. 2.3, with $B = 10$. Once the value of B is fixed (usually in this paper to $\sqrt[5]{10}$), in order to avoid empty bins we merge consecutive bins until the resulting merged bins are not empty. This leads to a change in the effective value of B for merged bins, but the method is still perfectly valid.

The uncertainty of $f_e(x)$ can be obtained from its standard deviation (the standard deviation of the estimation of the density, f_e, not of the original random variable x). Indeed, assuming independence in the sample (which is already implicit in order to apply maximum likelihood estimation), the number of occurrences of the variable in bin k is a binomial random variable (in the same way as for the $p-$value). As the number of occurrences is proportional to $f_e(x)$, the ratio between the standard deviation and the

mean for the number of occurrences will be the same as for $f_e(x)$, which is,

$$\frac{\sigma_f(x)}{f_e(x)} = \frac{\sqrt{\dfrac{q}{\text{mean number of occurrences in } k}}}{\dfrac{1}{\text{occurrences in } k}} \tag{2.45}$$

where we replace the mean number of occurrences in bin k (not available from a finite sample) by the actual value, and q, the probability that the occurrences are not in bin k, by one. This estimation of $\sigma_f(x)$ fails when the number of counts in the bin is too low, in particular if it is one.

One final consideration is that the fitted distributions are normalized between a and b, with N number of data, whereas the empirical distributions include all data, with N_{tot} of them, $N_{tot} \geq N$. Therefore, in order to compare the fits with the empirical distributions, we will plot $Nf(x)\ N_{tot}$ together with $f_e(x_k^*)$.

2.3.2 Estimation of the cumulative distribution

The estimation of the (complementary) cumulative distribution is much simpler, as bins are not involved. One just needs to sort the data, in ascending order, $x_{(1)} \leq x_{(2)} \leq \cdots \leq x_{(N_{tot}-1)} \leq x_{(N_{tot})}$; then, the estimated cumulative distribution is

$$S_e(x_{(i)}) = \frac{n_e(x_{(i)})}{N_{tot}} = \frac{N_{tot} - i + 1}{N_{tot}} \tag{2.46}$$

for the data points, $S_e(x)$ =constant below these data points, and $S_e(x) = 0$ for $x > x_{(N_{tot})}$; $n_e(x_{(i)})$ is the number of data with $x \geq x_{(i)}$ in the empirical sample. The formula relating $n_e(x_{(i)})$ with i assumes that repeated values of the variable are not possible, so it would not be valid for a discrete x. We use the case of empirical data as an example, but it is of course the same for simulated data. For the comparison of the empirical distribution with the theoretical fit we need to correct the different number of data in both cases. So, we plot both $[NS(x) + n_e(b)]\ N_{tot}$ and $S_e(x)$, in order to check the accuracy of the fit.

2.4 Data Analyzed and Results

We have explained how, in order to certify that a dataset is compatible with a simple power-law distribution, many mathematical formulas are required, leading to an astonishingly large number of calculations. Now we check the performance of our method with diverse geophysical data, which were previously analyzed with different, less rigorous or worse-functioning methods. For the peculiarities and challenges of the dataset, we

also include the half-lives of unstable nuclides. The parameters of the method are fixed to $N_s = 1000$ Monte Carlo simulations and the values of a and b are found sweeping a fixed number of points per order of magnitude, equally spaced in logarithmic scale. This number is 10 for non-truncated power laws (in which b is fixed to infinity) and 5 for truncated power laws. Three values of p_c are considered: 0.1, 0.2, and 0.5, in order to compare the dependence of the results on this parameter. The results are reported using the Kolmogorov-Smirnov test for goodness-of-fit. If, instead, the Kuiper s test is used, the outcome is not significantly different in most of the cases. In a few cases the fitting range, and therefore the exponent, changes, but without a clear trend, i.e., the fitting range can become smaller or increase. These cases deserve a more in-depth investigation.

2.4.1 Half-lives of the radioactive elements

Corral et al. (2011) studied the statistics of the half-lives of radionuclides (comprising both nuclei in the fundamental and in excited states). Any radionuclide has a constant probability of disintegration per unit time, the decay constant, let us call it λ (Krane, 1988). If M is the total amount of radioactive material at time t, this means that

$$-\frac{1}{M}\frac{dM}{dt} = \lambda \tag{2.47}$$

This leads to an exponential decay, for which a half-life $t_{1\ 2}$ or a lifetime θ can be defined, as

$$t_{1\ 2} = \theta \ln 2 = \frac{\ln 2}{\lambda} \tag{2.48}$$

It is well known that the half-lives take disparate values, for example, that of ^{238}U is 4.47 (American) billions of years, whereas for other nuclides it is a very tiny fraction of a second.

It has been recently claimed that these half-lives are power-law distributed (Corral et al., 2011). In fact, three power-law regions were identified in the probability density of $t_{1\ 2}$, roughly,

$$f(t_{1\ 2}) \qquad \begin{array}{ll} 1\ t_{1\ 2}^{0\ 65} & \text{for } 10^{-6}s \leq t_{1\ 2} \leq 0\ 1s \\ 1\ t_{1\ 2}^{1\ 19} & \text{for } 100s \leq t_{1\ 2} \leq 10^{10}s \\ 1\ t_{1\ 2}^{1\ 09} & \text{for } t_{1\ 2} \geq 10^{8}s \end{array} \tag{2.49}$$

Notice that there is some overlap between two of the intervals, as reported in the original reference, due to problems in delimiting the transition region. The study used variations of the Clauset *et al.* s (2009) method of minimization of the KS statistic, introducing and upper cutoff and additional conditions to escape from the global minimum of the KS statistic, which yielded the rejection ($p = 0\ 000$) of the power-law hypothesis. These

additional conditions were of the type of taking either a or b a greater than a fixed amount.

For comparison, we will apply the method explained in the previous section to this problem. Obviously, our random variable will be $x = t_{1\ 2}$. The data is exactly the same as in the original reference, coming from the Lund/LBNL Nuclear Data Search web page (Chu et al., version 2.0, February 1999). Elements whose half-life is only either bounded from below or from above are discarded for the study, which leads to 3002 radionuclides with well-defined half-lives; 2279 of them are in their ground state and the remaining 723 in an exited state. The minimum and maximum half-lives in the dataset are 3×10^{-22} s and 7×10^{31} s, respectively, yielding more than 53 orders of magnitude of logarithmic range. Further details are in Corral et al. (2011).

The results of our fitting and testing method are shown in Table 2.1 and in Fig. 2.5. The fitting of a non-truncated power law yields results in agreement with Corral et al. (2011), with $\alpha = 1\ 09 \pm 0\ 01$ and $a = 3 \times 10^7$ s, for the three values of p_c analyzed (0.1, 0.2, and 0.5). When fitting a truncated power law, the maximization of the log-range, $b\ a$, yields essentially the same results as for a non-truncated power law, with slightly smaller exponents α due to the finiteness of b (results not shown). In contrast, the maximization of the number of data N yields an exponent $\alpha\ \ 0\ 95$ between $a\ \ 0\ 1$ s and $b\ \ 400$ s (with some variations depending on p_c). This result is in disagreement with Corral et al. (2011), which yielded a smaller exponent for smaller values of a and b. In fact, as the intervals do not overlap both results are compatible, but it is also likely that a different function would lead to a better fit; for instance, a lognormal between 0.01 s and 10^5 s was proposed by Corral et al. (2011), although the fitting procedure there was not totally reliable. Finally, the intermediate power-law range reported in the original paper (the one with $\alpha = 1\ 19$) is not found by any of our algorithms working on the entire dataset. It is necessary to cut the dataset, removing data below, for instance, 100 s (which is equivalent to impose $a > 100$ s), in order that the algorithm converges to that solution. So, caution must be taken when applying the algorithm blindly, as important power-law regimes may be hidden by others having either larger N or larger log-range.

2.4.2 Seismic moment of earthquakes

The statistics of the sizes of earthquakes (Gutenberg and Richter, 1944) has been investigated not only since the introduction of the first magnitude scale, by Richter, but even before, in the 1930 s, by Wadati (Utsu, 1999). From a modern perspective, the most reliable measure of earthquake size is given by the (scalar) seismic moment M, which is

TABLE 2.1: Results of the fits for the $N_{tot} = 3002$ nuclide half-lives data, for different values of p_c. We show the cases of a pure or non-truncated power law (with $b =$, fixed) and truncated power law (with b finite, estimated from data), maximizing N. The latter is splitted into two subcases: exploring the whole range of a (rows 4, 5, and 6) and restricting a to $a > 100$ s (rows 7, 8, and 9).

N	a (s)	b (s)	b a	$\alpha \pm \sigma$	p_c
143	0.316×10^{8}			1.089± 0.007	0.10
143	0.316×10^{8}			1.089± 0.007	0.20
143	0.316×10^{8}			1.089± 0.008	0.50
1596	0.0794	501	6310	0.952± 0.010	0.10
1539	0.1259	501	3981	0.959± 0.011	0.20
1458	0.1259	316	2512	0.950± 0.011	0.50
1311	125.9	0.501×10^{23}	0.398×10^{21}	1.172± 0.005	0.10
1309	125.9	0.316×10^{22}	0.251×10^{20}	1.175± 0.005	0.20
1303	125.9	0.794×10^{18}	0.631×10^{16}	1.177± 0.005	0.50

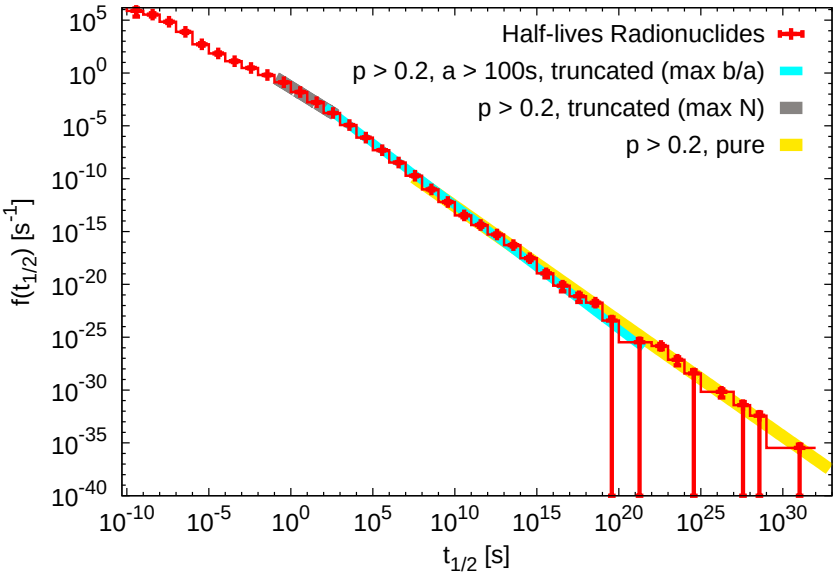

FIGURE 2.5: Estimated probability density of the half-lives of the radionuclides, together with the power-law fits explained in the text. The number of log-bins per order of magnitude is one, which poses a challenge in the correct estimation of the density, as explained in Sec. 2.3. Data below 10^{-10} s are not shown.

the product of the mean final slip, the rupture area, and the rigidity of the fault material (Ben-Zion, 2008). It is usually assumed that the energy radiated by an earthquake is proportional to the seismic moment (Kanamori and Brodsky, 2004), so, a power-law distribution of the seismic moment implies a power-law distribution of energies, with the same exponent.

The most relevant results for the distribution of seismic moment are those of Kagan for worldwide seismicity (Kagan, 2002), who showed that its probability density has a power-law body, with a universal exponent in agreement with $\alpha = 1\ 63 \quad 5\ 3$, but with

an extra, non-universal exponential decay (at least in terms of the complementary cumulative distribution). However, Kagan s (2002) analysis, ending in 2000, refers to a period of global seismic quiescence ; in particular, the large Sumatra-Andaman earthquake of 2004 and the subsequent global increase of seismic activity are not included. Much recently, Main et al. (2008) have shown, using a Bayesian information criterion, that the inclusion of the new events leads to the preference of the non-truncated power-law distribution in front of models with a faster large-M decay.

We take the Centroid Moment Tensor (CMT) worldwide catalog analyzed by Kagan (2002) and by Main *et al.* (2008), including now data from January 1977 to December 2010, and apply our statistical method to it. Although the statistical analysis of Kagan is rather complete, his procedure is different to ours. Note also that the dataset does not comprise the recent (2011) Tohoku earthquake in Japan, nevertheless, the qualitative change in the data with respect to Kagan s period of analysis is very remarkable. Following this author, we separate the events by their depth: shallow for depth ≤ 70 km, intermediate for 70 km $<$ depth ≤ 300 km, and deep for depth > 300 km. The number of earthquakes in each category is 26824, 5281, and 1659, respectively.

Second, we also consider the Southern California s Waveform Relocated Earthquake Catalog, from January 1st, 1981 to June 30th, 2011, covering a rectangular box of coordinates (122°W,30°N), (113°W,37 5°N) (Hauksson et al., Shearer et al., 2005). This catalog contains 111981 events with $m \geq 2$. As, in contrast with the CMT catalog, this one does not report the seismic moment M, the magnitudes m there are converted into seismic moments, using the formula

$$\log_{10} M = \frac{3}{2}(m + 6\ 07) \tag{2.50}$$

where M comes in units of Nm (Newtons times meters); however, this formula is a very rough estimation of seismic moment, as it is only accurate (and exact) when m is the so-called moment magnitude (Kanamori and Brodsky, 2004), whereas the magnitudes recorded in the catalog are not moment magnitudes. In any case, our procedure here is equivalent to fit an exponential distribution to the magnitudes reported in the catalog.

Tables 2.2 and 2.3 and Fig. 6 summarize the results of analyzing these data with our method, taking $x = M$ as the random variable. Starting with the non-truncated power-law distribution, we always obtain an acceptable (in the sense of non-rejectable) power-law fit, valid for several orders of magnitude. In all cases the exponent α is between 1.61 and 1.71, but for Southern California it is always very close to 1.66. For the worldwide CMT data the largest value of a is 3×10^{18} Nm, corresponding to a magnitude $m = 6\ 25$ (for shallow depth), and the smallest is $a = 8 \times 10^{16}$ Nm, corresponding to $m = 5\ 2$ (intermediate depth). If the events are not separated in terms of their depth (not

TABLE 2.2: Results of the non-truncated power-law fit ($b =$) applied to the seismic moment of earthquakes in CMT worldwide catalog (separating by depth) and to the Southern California catalog, for different p_c.

Catalog	N	a (Nm)	$\alpha \pm \sigma$	p_c
CMT deep	1216	0.1259×10^{18}	1.622± 0.019	0.10
intermediate	3701	0.7943×10^{17}	1.654± 0.011	0.10
shallow	5799	0.5012×10^{18}	1.681± 0.009	0.10
CMT deep	898	0.1995×10^{18}	1.608± 0.020	0.20
intermediate	3701	0.7943×10^{17}	1.654± 0.011	0.20
shallow	5799	0.5012×10^{18}	1.681± 0.009	0.20
CMT deep	898	0.1995×10^{18}	1.608± 0.021	0.50
intermediate	3701	0.7943×10^{17}	1.654± 0.011	0.50
shallow	1689	0.3162×10^{19}	1.706± 0.018	0.50
S. California	1327	0.1000×10^{16}	1.660± 0.018	0.10
S. California	1327	0.1000×10^{16}	1.660± 0.018	0.20
S. California	972	0.1585×10^{16}	1.654± 0.021	0.50

shown), the results are dominated by the shallow case, except for $p_c = 0\ 5$, which leads to very large values of a and α ($a = 5 \times 10^{20}$ Nm and α 2). The reason is probably the mixture of the different populations, in terms of depth, which is not recommended by Kagan (2002). This is an indication that the inclusion of an upper limit b to the power law may be appropriate, with each depth corresponding to different b s. For Southern California, the largest a found (for $p_c = 0\ 5$) is $1\ 6 \times 10^{15}$ Nm, giving $m = 4$. This value is somewhat higher, in comparison with the completeness magnitude of the catalog; perhaps the reason that the power-law fit is rejected for smaller magnitudes is due to the fact that these magnitudes are not true moment magnitudes, but come from a mixture of different magnitude definitions. If the value of a is increased, the number of data N is decreased and the power-law hypothesis is more difficult to reject, due simply to poorer statistics. When a truncated power law is fitted, using the method of maximizing the number of data leads to similar values of the exponents, although the range of the fit is in some cases moved to smaller values (smaller a, and b smaller than the maximum M on the dataset). The method of maximizing b a leads to results that are very close to the non-truncated power law.

TABLE 2.3: Same as the previous table, but fitting a truncated power-law distribution, by maximizing the number of data. Except for global shallow seismicity (and for the global deep case with $p_c = 0\,20$) the selected b is larger than the maximum value of the variable.

Catalog	N	a (Nm)	b (Nm)	$b\ a$	$\alpha \pm \sigma$	p_c
CMT deep	1216	0.1259×10^{18}	0.3162×10^{23}	0.2512×10^{6}	1.621± 0.019	0.10
intermediate	3701	0.7943×10^{17}	0.7943×10^{22}	0.1000×10^{6}	1.655± 0.011	0.10
shallow	13740	0.1259×10^{18}	0.5012×10^{20}	0.3981×10^{3}	1.642± 0.007	0.10
CMT deep	1076	0.1259×10^{18}	0.5012×10^{19}	0.3981×10^{2}	1.674± 0.033	0.20
intermediate	3701	0.7943×10^{17}	0.7943×10^{22}	0.1000×10^{6}	1.655± 0.011	0.20
shallow	13518	0.1259×10^{18}	0.1995×10^{20}	0.1585×10^{3}	1.636± 0.008	0.20
CMT deep	898	0.1995×10^{18}	0.3162×10^{23}	0.1585×10^{6}	1.604± 0.021	0.50
intermediate	3701	0.7943×10^{17}	0.7943×10^{22}	0.1000×10^{6}	1.655± 0.011	0.50
shallow	11727	0.1259×10^{18}	0.1995×10^{19}	0.1585×10^{2}	1.608± 0.012	0.50
S. California	1146	0.1259×10^{16}	0.1259×10^{22}	0.1000×10^{7}	1.663± 0.020	0.10
S. California	1146	0.1259×10^{16}	0.1259×10^{22}	0.1000×10^{7}	1.663± 0.020	0.20
S. California	344	0.7943×10^{16}	0.1259×10^{22}	0.1585×10^{6}	1.664± 0.036	0.50

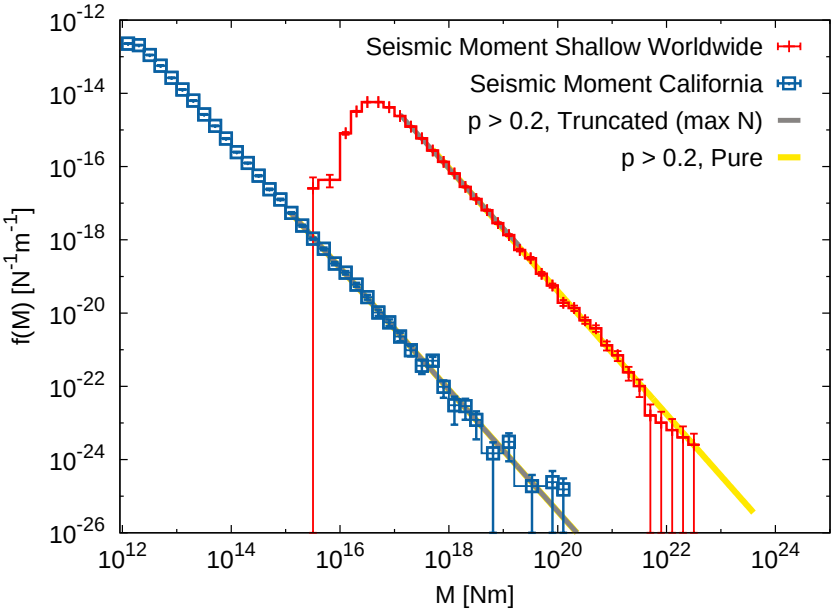

FIGURE 2.6: Estimated probability densities and corresponding power-law fits of the seismic moment M of shallow earthquakes in the worldwide CMT catalog and of the estimated M in the Southern California catalog.

2.4.3 Energy of tropical cyclones

Tropical cyclones are devastating atmospheric-oceanic phenomena comprising tropical depressions, tropical storms, and hurricanes or typhoons (Emanuel, 2005a). Although the counts of events every year have been monitored for a long time, and other measurements to evaluate annual activity have been introduced (see Corral and Turiel (2012) for an overview), little attention has been paid to the statistics of individual tropical cyclones.

In 2005, Emanuel introduced the power-dissipation index (PDI) as a simple way to obtain a rough estimation of the total energy dissipated by all tropical cyclones in a given season and some ocean basin (Emanuel, 2005b). But the PDI can also be used to characterize individual events as well, as it was done later by Corral et al. (2010). Indeed, the PDI is defined as the sum for all the discrete times t (that comprise the lifetime of a tropical cyclone) of the cube of the maximum sustained wind speed multiplied by the time interval of sampling, Δt. In a formula,

$$PDI = \sum_t v_t^3 \Delta t \tag{2.51}$$

where v_t is the maximum sustained wind speed. In the so-called best-track records, $\Delta t = 6$ hours; this factor would only be necessary in order to compare with other data with different Δt (but caution should be present in this case for the possible fractal nature

of the speed signal). Although the speeds are reported in knots, they are converted to m/s (using that 1 knot=0.514 m/s), and then we report the PDI in m^3/s^2.

Corral et al. (2010) studied the statistics of the PDI (defined for individual events, in contrast to Emanuel s (2005b) work) in 4 different ocean basins for several time periods. The results showed a rapid, perhaps exponential, decay at the tail, but a body of the distribution compatible with a power law, for 1 or 2 orders of magnitude, with exponents close to one. The connection with SOC phenomena was discussed by Corral (2010). The method used was again a variation of the Clauset *et al.* s (2009) one, introducing an upper cutoff and additional restrictions to the variations of the parameters. Here we revisit this problem, trying to use updated data (whenever it has been possible), and applying the method which is the subject of this paper to $x = PDI$.

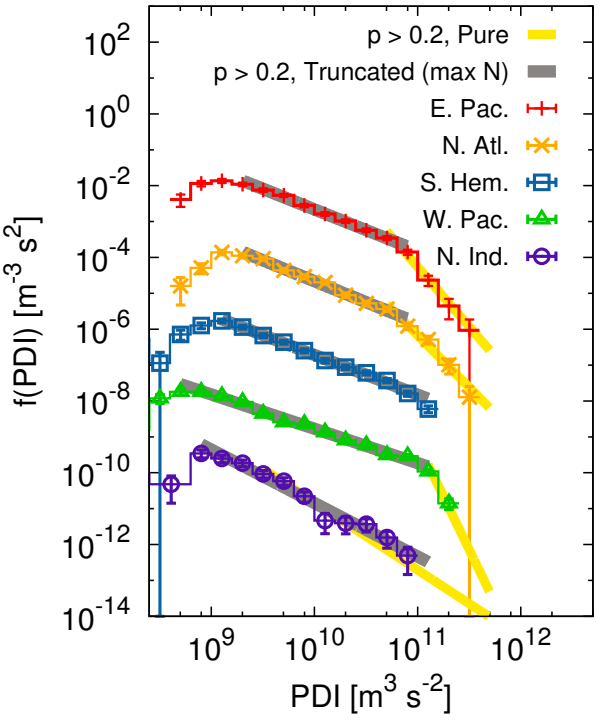

FIGURE 2.7: Estimated probability densities of the PDI of tropical cyclones in 5 ocean basins, together with their power-law fits. The values of the densities are multiplied by 1, 10^2, 10^4, 10^6, and 10^8, for clarity sake. The fits for the non-truncated case are akso displayed, although they are not tabulated.

The data has been downloaded from the National Hurricane Center (NHC) of NOAA, for the North Atlantic and the Northeastern Pacific (Jarvinen et al., 1988, National Hurricane Center) and from the Joint Typhoon Warning Center (JTWC) of the US Navy (Chu et al., 2002, Joint Typhoon Warning Center, Annual Tropical Cyclone Reports) for the Northwestern Pacific, the Southern Hemisphere (comprising the Southern Indian and the Southwestern Pacific), and the Northern Indian Ocean. The abbreviation, time

span, and number of events for each basin are: NAtl, 1966 2011, 532; EPac, 1966 2011, 728; WPac, 1986 2011, 690; SHem, 1986 2007 (up to May), 523; NInd, 1986 2007, 110. The latter case was not studied in any of the previous works.

The results for a truncated power law maximizing N, shown in Table 2.4 and Fig. 2.7, are in agreement with those of Corral et al. (2010). In general, exponents are close but above 1, except for the Northwestern Pacific, where α 0 96, and for the North Indian, where α is substantially higher than one. We consider that this method performs rather well. It would be interesting to test if universality can nevertheless hold (the high value for the North Indian Ocean is based in much less data than for the rest of basins), or if there is some systematic bias in the value of the exponents (the protocols of the NHC and the JTWC are different, and the satellite coverage of each basin is also different).

If a non-truncated power law is fit to the data, the fits turn out to be rather short, with a high exponent (up to 6) describing the tail of the distribution (except for the Southern Hemisphere, where no such tail is apparent). We do not give any relevance to these results, as other alternatives, as for instance a simple exponential tail, have to be considered (Corral and Turiel, 2012, del Castillo et al., 2012). Coming back to a truncated power law, but maximizing the log-range, the algorithm sometimes fits the power law in the body of the distribution (with exponent close to 1) and for some other times the algorithm goes to the fast-decaying tail. So the method of maximizing b a is not useful for this data.

TABLE 2.4: Results of the truncated power-law fits, maximizing N, for the PDI in the 5 ocean basins with tropical-cyclone activity, for different values of p_c.

basin	N	a (m^3 s^2)	b (m^3 s^2)	b a	$\alpha \pm \sigma$	p_c
EPac	637	0.1259×10^{10}	0.7943×10^{11}	63	1.094± 0.033	0.10
NAtl	417	0.1995×10^{10}	0.7943×10^{11}	40	1.168± 0.047	0.10
SHem	523	0.1259×10^{10}	0.1259×10^{12}	100	1.108± 0.034	0.10
WPac	637	0.5012×10^{9}	0.1259×10^{12}	251	0.957± 0.025	0.10
NInd	102	0.7943×10^{9}	0.1995×10^{12}	251	1.520± 0.077	0.10
EPac	571	0.1995×10^{10}	0.7943×10^{11}	40	1.149± 0.039	0.20
NAtl	417	0.1995×10^{10}	0.7943×10^{11}	40	1.168± 0.047	0.20
SHem	523	0.1259×10^{10}	0.1259×10^{12}	100	1.108± 0.033	0.20
WPac	637	0.5012×10^{9}	0.1259×10^{12}	251	0.957± 0.025	0.20
NInd	102	0.7943×10^{9}	0.1259×10^{12}	158	1.490± 0.077	0.20
EPac	571	0.1995×10^{10}	0.7943×10^{11}	40	1.149± 0.040	0.50
NAtl	417	0.1995×10^{10}	0.7943×10^{11}	40	1.168± 0.045	0.50
SHem	465	0.1995×10^{10}	0.1259×10^{12}	63	1.132± 0.040	0.50
WPac	637	0.5012×10^{9}	0.1259×10^{12}	251	0.957± 0.024	0.50
NInd	86	0.7943×10^{9}	0.1259×10^{11}	16	1.323± 0.139	0.50

2.4.4 Area of forest fires

The statistics of the size of forest fires was an intense topic of research since the introduction of the concept of SOC, at the end of the 1980 s, but only from the point of view of cellular-automaton models. Real data analysis had to wait several years (Malamud et al., 1998, 2005), leading to power-law distributions, more or less in agreement with the models. Here we are particularly interested in a dataset from Italy, for which a power-law distribution of sizes was ruled out (Corral et al., 2008). Instead, a lognormal tail was proposed for the fire-size probability density.

The data considered by (Corral et al., 2008), and reanalyzed in this study, comes from the Archivio Incendi Boschivi (AIB) fire catalog compiled by the (Italian) (http://www.corpoforestale.it). The subcatalog to which we restrict covers all Italy and spans the 5-year period 1998-2002, containing 36 748 fires. The size of each fire is measured by the burned area A, in hectares, with 1 ha=10^4 m^2. In this subsection we analyze the case of $x = A$.

The results in Table 2.5 and Fig. 2.8 show that a pure (non-truncated) power law is only acceptable (in the sense of non-rejectable) for the rightmost part of the tail of the distribution, comprising less than one order of magnitude. It is very indicative that only 51 data are in the possible power-law tail. Therefore, we disregard this power-law behavior as spurious and expect that other distributions can yield a much better fit (not in order of the quality of the fit but regarding the number of data it spans). This seems in agreement with other analyses of forest-fire data (Clauset et al., 2009, Newman, 2005). If a truncated power-law is considered, fitted by maximizing the number of data, the results are not clearly better, as seen in the table. Moreover, there is considerable variation with the value of p_c. So, we do not give any relevance to such power-law fits. Finally, the method of maximizing b a yields the same results as for the non-truncated power law (except by the fact that the exponents are slightly smaller, not shown). In order to provide some evidence for the better adequacy of the lognormal tail in front of the power-law tail for these data, it would be interesting to apply an adaptation of the test explained by del Castillo and Puig (1999).

2.4.5 Waiting time between earthquakes

The temporal properties of earthquakes has been a subject relatively little studied (at least in comparison with the size of earthquakes). It is true that the Omori law has been known for more than 100 years (Utsu, 2002, Utsu et al., 1995), and that this is a law extremely important in order to assess the hazard of aftershocks after a big event, but

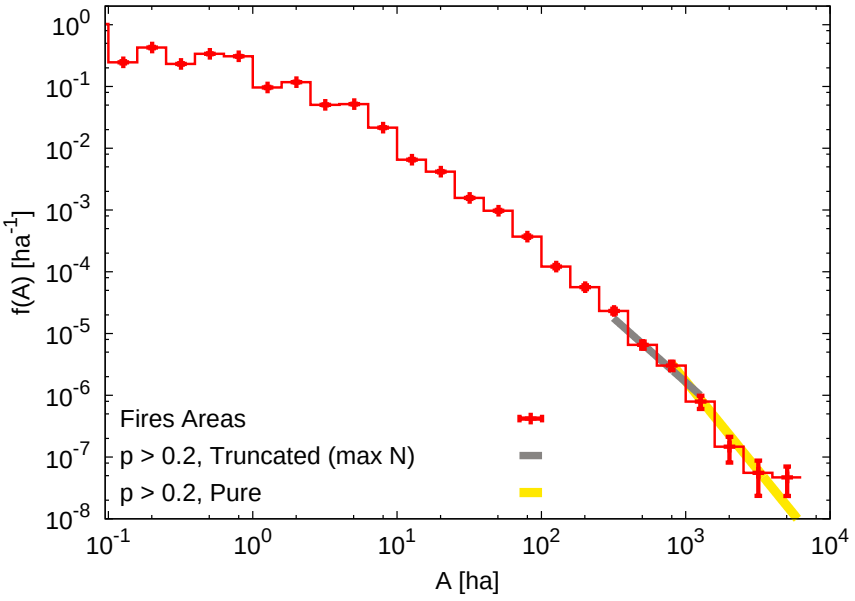

FIGURE 2.8: Estimated probability density of the area of fires in the Italian catalog, together with the power-law fits. In contrast to the previous datasets analyzed, we consider these power-law fits as irrelevant.

TABLE 2.5: Results of the fits for the burned area of the $N_{tot} = 36\ 748$ fires recorded in the Italian catalog, for different p_c. The cases of a non-truncated power law and a truncated power law, maximizing N, are shown. In the latter case, for $p_c = 0\ 10$ and $0\ 50$ the value of b is larger than the maximun value of the variable.

N	a (ha)	b (ha)	$b\ a$	$\alpha \pm \sigma$	p_c
51	794			2.880± 0.276	0.10
51	794			2.880± 0.277	0.20
51	794			2.880± 0.277	0.50
168	316	7943	25	2.353± 0.117	0.10
148	316	1259	4	2.075± 0.213	0.20
51	794	79430	100	2.870± 0.281	0.50

the Omori law looks at time properties in a very coarse-grained way, as it only provides the number of events in relatively large time windows. Thus, no information on the fine time structure of seismicity is provided, at least directly.

The situation has changed in the last decade, since the seminal study of Bak et al. (2002), who found a unified scaling law for earthquake waiting-time distributions. They took Southern California and divided it in different areas, and computed the time between consecutive earthquakes for each area. So, if t_i^j denotes the time of occurrence of the $i-$th earthquake in area j, the corresponding waiting time θ_i^j is

$$\theta_i^j = t_i^j - t_{i-1}^j \tag{2.52}$$

The key point is that all the resulting waiting times were added to the same distribution

(and not to a different distribution j for each area). Subsequently, the unified scaling law was found to be valid for other regions of the world (Corral, 2004a). The shape of the resulting probability density corresponds to a double power law, one for small waiting times, associated to a mixture of scales of waiting times due to the Omori law, and another for large waiting times, due to spatial heterogeneity arising from the mixture of different areas with different seismic rates (Bak et al., 2002, Corral, 2003, 2004a, Corral and Christensen, 2006). The first exponent was found to be close to 1, whereas the second one was about 2.2; the fits were done by means of the nonlinear least-squares Marquardt-Levenberg algorithm from `gnuplot`, applied to the logarithm of the log-binned empirical density. Here we apply our more sophisticated method to updated data for Southern California seismicity, with $x = \theta$.

We use again the relocated Southern California catalog of Hauksson et al., see also Shearer et al. (2005), but starting in 1984 and ending in June 30th, 2011. This is to avoid some holes in the catalog for the preceding years. As for earthquake sizes, the occurrence takes place in a rectangle of coordinates (122°W,30°N), (113°W,37 5°N). This rectangle is divided into equal parts both in the West-East axis and in the South-North axis, in such a way that we consider a number of subdivisions of 4×4, 8×8, 16×16, and 32×32. The waiting times for events of magnitude $m \geq 2$ in each of these subdivisions are computed as explained above, resulting in a number of data between 103000 and 104000 in all cases.

For a non-truncated power law, the results are only coherent with the previous reported ones (exponent around 2.2) for the intermediate cases, i.e., 8×8 and 16×16, see Table 2.6 and Fig. 2.9. The disagreement for the other cases can easily be explained. For 4×4, the number of resulting subdivisions, 16, seems rather small. As mentioned, in Corral and Christensen (2006) the power-law tail was explained in terms of a power-law mixture of exponentials; so, with only 16 regions is possible that the asymptotic behavior is still not reached. On the other hand, the effect of the finite duration of the catalog is visible in the 32×32 data. Due to the scaling behavior of the distributions (Corral, 2003, 2004a), the possible power-law tail in this case is displaced to larger waiting times; but the time span of the catalog, about 10^{10} s, clearly alters this power law, which starts to bend at about 10^9 s. Thus, we conclude that a power-law exponent of about α 2 2 or 2.3 indeed exists, provided that the number of spatial subdivisions is high enough and the temporal extension of the catalog is large enough.

When a truncated power-law is fitted, using the method of maximizing the number of data N, the other power law emerges, but for a range shorter than what the plot of the densities suggests. The exponent is in a range from 0.95 to 1.04 (except for the 4×4 cases, in which it is a bit smaller). The largest log-range is 100, i.e., two decades.

TABLE 2.6: Results of the fits with a non-truncated power law and a truncated power law, maximizing N, for earthquake waiting times calculated for different subdivisions of Southern California. Different minimum $p-$values are shown. The total number of data is above 103000 in any case.

Subdivisions	N	a (s)	b (s)	b a	$\alpha \pm \sigma$	p_c
4×4	124	0.5012×10^7			1.921± 0.085	0.10
8×8	1671	0.3162×10^7			2.198± 0.031	0.10
16×16	542	0.3162×10^8			2.324± 0.056	0.10
32×32	67	0.3162×10^9			4.404± 0.405	0.10
4×4	124	0.5012×10^7			1.921± 0.085	0.20
8×8	1671	0.3162×10^7			2.198± 0.031	0.20
16×16	542	0.3162×10^8			2.324± 0.056	0.20
32×32	67	0.3162×10^9			4.404± 0.403	0.20
4×4	77	0.7943×10^7			1.856± 0.098	0.50
8×8	322	0.1259×10^8			2.231± 0.070	0.50
16×16	24	0.3162×10^9			4.106± 0.703	0.50
32×32	67	0.3162×10^9			4.404± 0.449	0.50
4×4	38765	1995	0.5012×10^5	25	0.867± 0.006	0.10
8×8	39851	316	0.1995×10^5	63	0.987± 0.004	0.10
16×16	44178	7943	0.7943×10^6	100	0.956± 0.004	0.10
32×32	43512	1259	0.1995×10^6	158	1.029± 0.003	0.10
4×4	38765	1995	0.5012×10^5	25	0.867± 0.006	0.20
8×8	39851	316	0.1995×10^5	63	0.987± 0.004	0.20
16×16	39481	7943	0.5012×10^6	63	0.950± 0.005	0.20
32×32	39654	1259	0.1259×10^6	100	1.033± 0.004	0.20
4×4	34113	3162	0.5012×10^5	16	0.864± 0.007	0.50
8×8	39851	316	0.1995×10^5	63	0.987± 0.004	0.50
16×16	39481	7943	0.5012×10^6	63	0.950± 0.005	0.50
32×32	39654	1259	0.1259×10^6	100	1.033± 0.004	0.50

The graphical representation of the density seems to indicate that the possible power law is influenced by the effect of two crossovers, one for large waiting times, associated to a change in exponent, and another one for smaller times, where the distribution becomes flat. Finally, the method of fitting which maximizes the log-range leads to results that are similar to the non-truncated power-law case, although sometimes intervals corresponding to very small times are selected. The latter results have no physical meaning, as correspond to times below 1 s, i.e., below the error in the determination of the occurrence time.

2.5 Conclusions

For power-law distributions, the fitting and the testing of the goodness of the fit is a difficult but very relevant problem in complex-systems science, in general, and in geoscience in particular. The most critical step is to select, automatically (without

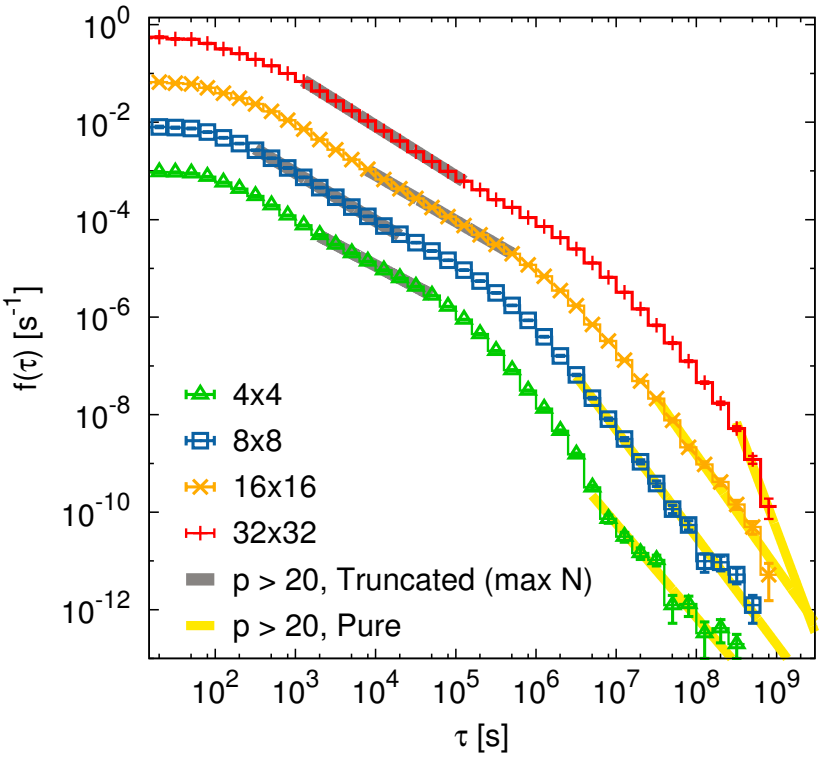

FIGURE 2.9: Estimated probability densities and corresponding power-law fits for the waiting times of $m \geq 2$ in the Southern California catalog, for different spatial subdivisions. The values of the density are multiplied by factors 1, 10, 100, and 1000, for clarity sake.

introducing any subjective bias), where the power-law regime starts and where it ends. We have explained in detail a conceptually simple but somewhat laborious procedure in order to overcome some difficulties previously found in the method introduced by Clauset *et al.* (2009), see Corral et al. (2011). Our method is summarized in fitting by maximum likelihood estimation and testing the goodness of fit by the Kolmogorov-Smirnov statistic, using Monte Carlo simulations. Although these steps are in common with the Clauset *et al.* s (2009) recipe, the key difference is in the criterion of selection of the power-law range. Despite the many steps of these procedures, ours can be easily implemented, and the resulting algorithms run very fast in current computers. We also have explained how to estimate properly the probability density of a random variable which has a power law or a fat-tail distribution. This is important to draw graphical representations of the results of the fitting (specially in Fig. 5) but it is not required to perform neither the fits nor the goodness-of-fit tests.

The performance of the method is quite good, as checked in synthetic power-law datasets, and the results of the analysis of previously reported power laws are very consistent. We confirm a very broad power-law tail in the distribution of the half-lives of the radionuclides, with exponent $\alpha = 1\ 09$, as well as other power-law regimes in the body of the

distribution. The results for the power-law exponent of the distribution of seismic moments worldwide and in Southern California are in agreement with previous estimates, but in addition our method provides a reliable way to determining the minimum seismic-moment value for which the Gutenberg-Richter law holds. This can be useful to check systematically for the completeness thresholds of seismic catalogs. For the energy dissipated by tropical cyclones, measured roughly through the PDI, we confirm the power-law behavior in the body of the distribution previously reported, with exponents close to one. We also survey new results for the Southern Indian Ocean, but with a higher power-law exponent. In contrast, for the case of the area affected by forest fires in an Italian catalog, we obtain power-law-distributed behavior only for rather small windows of the burnt area, containing a very few number of fires. Finally, for the waiting times between earthquakes in different subdivisions of Southern California we conclude that the power-law behavior of the tail is very delicate, affected either by a small number of subdivisions, when the size of those is large, or by the finite duration of the record, which introduces a sharp decay of the distribution when the number of subdivisions is high. For the body of the distribution another power law is found, but the range is limited by crossovers below and above it. We conclude that, in general, the method for truncated power laws works better when the number of data in the power-law range is maximized. When the quantity that is maximized is the logarithmic range ($b\ a$) the fitting range can jump between different regimes. Also, the selection of a $p-$value above 0.50 seems too strict sometimes, and values about 0.10 or 0.20 are more useful. Naturally, the methods studied in this paper can be directly applied to the overwhelming number of fat-tailed distributions reported during the last decades in geoscience.

Chapter 3

Universality of rain event size distributions

Journal of Statistical Mechanics: Theory and Experiment. P11030 (2010)

This chapter contains the following paper (a copy of the published version can be found in Chapter 8).

Peters O, Deluca A, Corral A, Neelin JD, Holloway C E. *Universality of rain event size distributions.* Journal of Statistical Mechanics: Theory and Experiment. P11030 (2010). DOI: 10.1007/s10955-010-0039-0.

Abstract We compare rain event size distributions derived from measurements in climatically different regions, which we find to be well approximated by power laws of similar exponents over broad ranges. Differences can be seen in the large-scale cutoffs of the distributions. Event duration distributions suggest that the scale-free aspects are related to the absence of characteristic scales in the meteorological

PACS 05.65.+b, 05.70.Jk, 64.60.Ht

3.1 Introduction

Atmospheric convection and precipitation have been hypothesised to be a real-world realization of self-organized criticality (SOC). This idea is supported by observations of avalanche-like rainfall events (Andrade et al., 1998, Peters et al., 2002) and by the

nature of the transition to convection in the atmosphere (Neelin et al., 2009, Peters and Neelin, 2006). Many questions remain open, however, as summarized below. Here we ask whether the observation of scale-free avalanche size distributions is reproducible using data from different locations and whether the associated fitted exponents show any sign of universality.

Many atmospheric processes are characterized by long-range spatial and temporal correlation, and by corresponding structure on a wide range of scales. There are two complementary explanations why this is so, and both are valid in their respective regimes: structure on many scales can be the result of different processes producing *many* characteristic scales (Bodenschatz et al., 2010, Klein, 2010); it can also be the result of an *absence* of characteristic scales over some range, such that all intermediate scales are equally significant (Barenblatt, 1996). The latter perspective is relevant, for instance, in critical phenomena and in the inertial subrange of fully developed turbulence.

Processes relevant for precipitation are associated with many different characteristic time and spatial scales, see *e.g.* Ref. (Bodenschatz et al., 2010). The list of these scales has a gap, however, from a few km (a few minutes) to 1,000 km (a few days), spanning the so-called mesoscale, and it is in this gap that the following arguments are most likely to be relevant.

The atmosphere is slowly driven by incident solar radiation, about half of which is absorbed by the planet s surface, heating and moistening the atmospheric boundary layer; combined with radiative cooling at the top of the troposphere this creates an instability. This instability drives convection, which in the simplest case is dry. More frequently, however, moisture and precipitation play a key role. Water condenses in moist rising air, heating the environment and reinforcing the rising motion, and often, the result of this process is rainfall. The statistics of rainfall thus contain information about the process of convection and the decay towards stability in the troposphere. A common situation is conditional instability, where saturated air is convectively unstable, whereas dry air is stable. Under-saturated air masses then become unstable to convection if lifted by a certain amount, meaning that relatively small perturbations can trigger large responses.

Since driving processes are generally slow compared to convection, it has been argued that the system as a whole should typically be in a far-from equilibrium statistically stationary state close to the onset of instability. In the parlance of the field this idealized state, where drive and dissipation are in balance, is referred to as Quasi-Equilibrium (QE) (Arakawa and Schubert, 1974). In Ref. (Peters and Neelin, 2006), using satellite data over tropical oceans, it was found that departures from the point of QE into the unstable regime can be described as triggering a phase transition whereby large parts

of the troposphere enter into a convectively active phase. Assuming that the phase transition is continuous, the attractive QE state would be a case of SOC a critical point of a continuous phase transition acting as an attractor in the phase space of a system (Dickman et al., 1998, Tang and Bak, 1988).

The link between SOC and precipitation processes has also been made by investigating event size distributions in a study using data from a mid-latitude location (Peters et al., 2002). Both the tropical data in Ref. (Peters and Neelin, 2006) and the mid-latitude data in Ref. (Peters et al., 2002) support some notion of SOC in precipitation processes, but the climatologies in these regions are very different. Rainfall in the mid-latitudes is often generated in frontal systems, whereas in the tropics, much of the precipitation is convective, supporting high rain rates. It is not *a priori* clear whether these differences are relevant to the SOC analogy, or whether they are outweighed by the robust similarities between the systems. For instance, drive and dissipation time scales are well separated also in the mid-latitudes. In time series from Sweden the average duration of precipitation events was found to be three orders of magnitude smaller than the average duration of dry spells (Olsson et al., 1993). It is therefore desirable to compare identical observables from different locations.

Scale-free event size distributions suggest long-range correlation in the system, which in turn hints at a continuous transition to precipitation. Similar effects, however, can also result directly from a complex flow field, as was shown in simulations using randomized vortices and passive tracers (Dickman, 2003). Since the fluid dynamics is complex enough to generate apparent long-range correlation, and it is difficult from direct observation to judge whether the transition is continuous, we cannot rule out a discontinuous jump.

This uncertainty is mirrored in parameterizations of convection. The spatial resolution of general circulation models is limited by constraints in computing power to about 100 km in the horizontal. Dynamically there is nothing special about this scale, and the approach in climate modeling for representing physical processes whose relevant spatial scales are smaller is to describe their phenomenology in parameterizations. Parameterizations of convection and precipitation processes often contain both continuous and discontinuous elements. For instance, the intensity of convection and precipitation typically depends continuously on a measure of convective plume buoyancy (such as convective available potential energy) and water vapor content (Arakawa and Schubert, 1974, Betts and Miller, 1986), but sometimes a discontinuous threshold condition is introduced to decide whether convection occurs at all (Neelin et al., 2008).

3.2 Data sets

We study rain data from all 10 available sites of the Atmospheric Radiation Measurement (ARM) Program, see www.arm.gov, over periods from about 8 months to 4 years, see Table 1. Precipitation rates were recorded at one-minute resolution, with an optical rain gauge, Model ORG-815-DA MiniOrg (Optical Scientific, Inc.) (Ritsche). Data were corrected using the ARM Data Quality Reports (Program), and rates below 0.2 mm/h were treated as zero measurements, as recommended by the ARM Handbook (Ritsche), see Figure 3.1.

The measurements are from climatically different regions using a standardized technique, making them ideal for our purpose. Three sites are located in the Tropical Western Pacific (Manus, Nauru and Darwin), known for strong convective activity. Niamey is subject to strong monsoons, with a pronounced dry season. Heselbach is a mid-latitude site with an anomalously large amount of rainfall due to orographic effects. Rainfall in Shouxian is mostly convective in the summer months, which constitute most of the data set. Graciosa Island in the Azores archipelago is a sub-tropical site, chosen for the ARM program to study precipitation in low clouds of the marine boundary layer.

Three data are less straight-forward: The Point Reyes measurements specifically target Marine Stratus clouds, which dominate the measurement period and are known to produce drizzle in warm-cloud conditions (without ice phase). Unfortunately the measurements only cover six months, and it is unclear whether observed differences are due to the different physics or to the small sample size. The Southern Great Plains (SGP) measurements suffer from a malfunction that led to apparent rain rates of about 0.1 mm/h over much of the observation period. The problem seems to be present in most other data sets but is far less pronounced there, see Figure 3.1. Measurements at temperatures below 3°C were discarded as these can contain snow from which it is difficult to infer equivalent rates of liquid water precipitation. The North Slope of Alaska (NSA) data set contains mostly snow; it is included only for completeness.

None of the data sets showed significant seasonal variations in the scaling exponents. In the Point Reyes, SGP and NSA data we found slight variations but could not convince ourselves that these were significant. Data from all seasons are used.

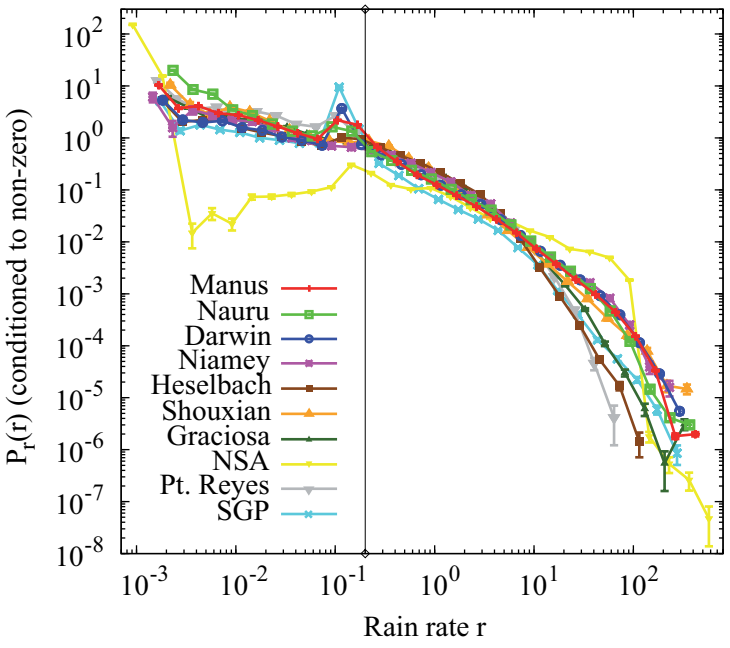

FIGURE 3.1: Probability (relative frequency) density of precipitation rate, r in mm/h. The vertical line indicates the lower intensity cutoff at 0.2 mm/h. Smaller rain rates are treated as zero. The peak around 0.1 mm/h, most pronounced in the Southern Great Plains data, is due to a malfunction of the instrument. The Alaska data set contains mostly snow and is included only for completeness.

TABLE 3.1: Observation sites with corresponding time periods, number of observed precipitation events N, estimated annual precipitation in mm, and location.

Site	From	Until	N	Precip./yr	Location
Manus Island, Papua New Guinea	02/15/2005	08/27/2009	11981	5883.29	2.116° S, 147.425° E
Nauru Island, Republic of Nauru	02/15/2005	08/27/2009	5134	1860.87	0.521° S, 166.916° E
Darwin, Australia	02/15/2005	08/27/2009	2883	1517.09	12.425° S, 130.892° E
Niamey, Niger	12/26/2005	12/08/2006	262	608.37	13.522° N, 2.632° E
Heselbach, Germany	04/01/2007	01/01/2008	2439	2187.85	48.450° N, 8.397° E
Shouxian, China	05/09/2008	12/28/2008	480	1221.20	32.558° N, 116.482° E
Graciosa Island, Azores	04/14/2009	07/10/2010	3066	702.35	39.091° N, 28.029° E
NSA, USA	04/01/2001	10/13/2003	9097	23516.16	71.323° N, 156.616° E
Point Reyes, USA	02/01/2005	09/15/2005	579	797.85	38.091° N, 122.957° E
SGP, USA	11/06/2007	08/24/2009	1624	968.95	36.605° S, 97.485° E

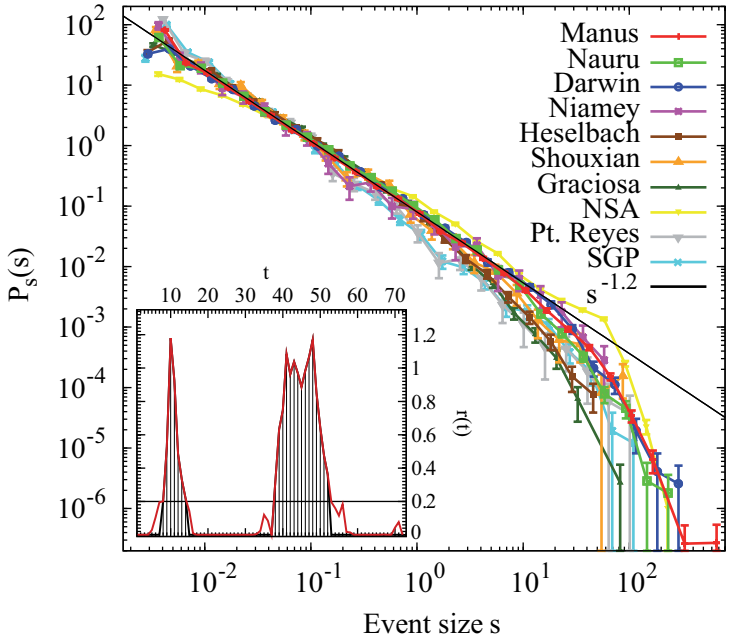

FIGURE 3.2: Probability densities of event sizes, s in mm, and a power-law fit (black straight line).
Inset: Precipitation rates from Niamey, including two rain events lasting 7 and 15 minutes respectively. Interpreting reported rain rates of less than 0.2 mm/h as zero, the shaded areas are the corresponding event sizes.

3.3 Event sizes

The data used here are (0+1)-dimensional time series, whereas the atmosphere is a (3+1)-dimensional system. We leave the question unanswered which spatial dimensions are most relevant the system becomes vertically unstable, but it also communicates in the two horizontal dimensions through various processes (Neelin et al., 2009).

Following Ref. (Peters et al., 2002), we define an event as a sequence of non-zero measurements of the rain rate, see inset in Figure 3.2. The event size s is the rain rate, $r(t)$, integrated over the event, $s = \int_{\text{event}} dt\ r(t)$. The dimension of this object is $[s]$ =mm, specifying the depth of the layer of water left on the ground during the event. One mm corresponds to an energy density of some 2500 kJ/m^2 released latent heat of condensation. If the rain rate were known over the area covered by the event, then the event size could be defined precisely as the energy released during one event. Since spatial information is not available, it is ignored in our study.

For each data set, the probability density function $P_s(s)$ in a particular size interval $[s\ \ s + \Delta s)$ is estimated as $P_s(s) \approx n(s)\ \ (N\Delta s)$, where $n(s)$ is the number of events in the interval and N the total number of events. We use $(s + \Delta s)\ \ s = 10^{1\ 5} \approx 1\ 58$, *i.e.* 5 bins per order of magnitude in s. Standard errors are shown, for $P_s(s)$: assuming

Poissonian arrivals of events in any given bin, the error in $n(s)$ is approximated by $\overline{n(s)}$.

3.4 SOC scaling

Studies of simple SOC models that approach the critical point of a continuous phase transition focus on avalanche size distributions, which we liken to rain event sizes. Critical exponents are derived from finite-size scaling, that is, the scaling of observables with system size (as opposed to critical scaling, the scaling of observables with the distance from criticality). In SOC models, moments of the avalanche size distribution scale with system size L like

$$s^k \qquad L^{D(1+k-\tau_s)} \text{ for } k > \theta_s - 1 \tag{3.1}$$

defining the exponent D, sometimes called the avalanche dimension, and the exponent θ_s, which we call the avalanche size exponent. Equation 3.1 is consistent with probability density functions $P_s(s)$ of the form

$$P_s(s) = s^{-\tau_s} \mathcal{G}_s(s \;\; s_\xi) \text{ for } s > s_l \tag{3.2}$$

where $s_\xi = L^D$, and the scaling function $\mathcal{G}_s(s \;\; s_\xi)$ falls off very fast for large arguments, $s \;\; s_\xi > 1$, and is constant for small arguments, $s \;\; s_\xi \ll 1$, down to a lower cutoff, $s = s_l$, where non-universal microscopic effects (*e.g.* discreteness of the system) become important.

Assuming that we have observations from an SOC system, and that a significant part of the observed avalanche sizes are in the region $s_l < s \ll s_\xi$, we expect to find a range of scales where the power law

$$P_s(s) = \mathcal{G}_s(0) s^{-\tau_s} \tag{3.3}$$

holds. Under sufficiently slow drive the exponent θ_s is believed to be robust in SOC models (Alava et al., 2008, Pruessner and Peters, 2008). We infer event size distributions like in Ref. (Peters et al., 2002) from measurements in different locations and compare values for the apparent avalanche size exponent θ_s. As a first step to assess the validity of Equation 3.3 we produce log-log plots of $P_s(s)$ vs. s and look for a linear regime, Figure 3.2. Since the study of critical phenomena is a study of limits that cannot be reached in physical systems, the field is notorious for debates regarding the significance of experimental work, which is especially true for SOC. While an element of interpretation necessarily remains, we devise methods to maximize the objectivity of our analysis.

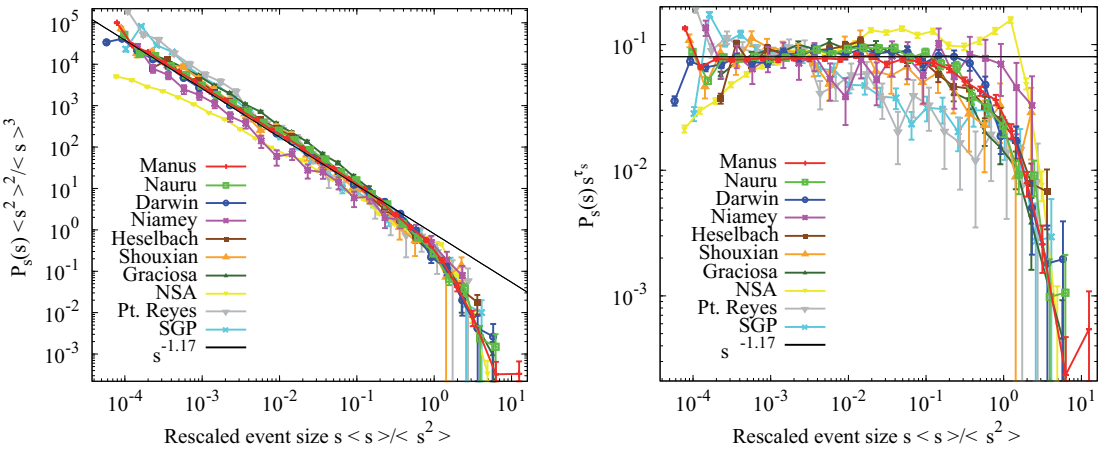

FIGURE 3.3: (a) Event size distributions shifted along the supposed power laws to collapse the loci of the cutoffs. (b) Inferred scaling function $\mathcal{G}_s$, using $\theta_s = 1\ 17$ for all data sets. By far the largest deviations from a common scaling function are observed for the unreliable data sets, Alaska (NSA) and Southern Great Plains (SGP).

In our data sets, time series of rain rates from different locations, we interpret the upper limit s_ξ of the scale-free range as an effective system size. We cannot control this size; nonetheless the scaling hypothesis, Equation 3.2, can be tested using appropriate moment ratios (Rosso et al., 2009). For instance, $s_\xi \quad \langle s^2 \rangle \quad s$, provided $s_l \ll s_\xi$. Hence, to account for changes in effective system sizes the s-axis in Figure 3.2 can be rescaled to $s \ s \quad \langle s^2 \rangle$, see Figure 3.3(a). This collapses the loci of the large-scale cutoffs. The $P_s(s)$-axis is rescaled by $\langle s^2 \rangle^2 \quad s^{\ 3} \quad s_\xi^\tau$, so that Figure 3.3(a) shows the curves of Figure 3.2 shifted along their supposed power-laws, without having to estimate any parameters. The curves are neither normalized nor do they collapse vertically the degree of vertical collapse is comparable to that in Figure 3.2. Plotting $P_s(s)s^{\tau_s}$ against the rescaled variable $s \ s \quad \langle s^2 \rangle$ produces Figure 3.3(b) of the scaling function $\mathcal{G}_s(s \ (as_\xi))$, where a is the proportionality constant relating s_ξ to the moment ratio. This has the advantage of reducing the logarithmic vertical range, which makes it possible to see differences in the distributions that would otherwise be concealed visually. Figure 3.3(a) covers 9 orders of magnitude vertically, whereas 3.3(b) covers little more than 2.

3.5 Exponent estimation and goodness of fit

For a detailed discussion, see 3.9. We apply a form of Kolmogorov-Smirnov (KS) test (Press et al., 2002) similar to that in Ref. (Clauset et al., 2009). First, a fitting range $[s_{\min} \ s_{\max}]$ is selected. In this range the maximum-likelihood value for θ_s in Equation 3.3 is found. Next, the maximum difference between the empirical cumulative distribution in this range and the cumulative distribution corresponding to the best-fit power law is

found. The same measure is applied to synthetic samples of data (each with the same number of instances), generated from the best-fit power-law distribution. This yields the p -value, *i.e.* the fraction of samples generated from the tested model (the best-fit power law) where at least such a difference is observed. We stress that each synthetic data set is compared to its own maximum-likelihood power-law distribution, *i.e.* an exponent has to be fitted for each sample, so that no bias be introduced.

We keep a record of the triplet ($s_{\min}$ $s_{\max}$ θ_s) if the $p-$value is greater than 10% (our arbitrarily chosen threshold). After trying all possible fitting ranges with $s_{\min}$ and $s_{\max}$ increasing by factors of $10^{0\ 01}$, we select the triplet which maximizes the number $\bar{N}$ of data between $s_{\min}$ and $s_{\max}$.

The distributions in Figure 3.2 are visually compatible with a power law (black straight line) over most of their ranges. The procedure consisting of maximum-likelihood estimation plus a goodness-of-fit test confirms this result: over ranges between 2 and 4 orders of magnitude, all data sets are consistent with a power-law distribution and the estimates of the apparent exponents are in agreement with the hypothesis of a single exponent $\theta_s = 1\ 17(3)$, brackets indicating the uncertainty in the last digit, except for the three problematic data sets from Point Reyes, the Southern Great Plains and Alaska. The complete results are collected in Table 3.2. While the best-fit exponents in this table are surprisingly similar (given the climatic differences between the measuring sites), the error estimates are unrealistically small. Taking the statistical results literally, we would have to conclude that the exponents are very similar but mutually incompatible (*e.g.* ${\theta_s}^{\text{Manus}} = 1\ 18(1)$ and ${\theta_s}^{\text{Nauru}} = 1\ 14(1)$) suggesting that θ_s is not universal. On physical grounds we do not believe this conclusion because systematic errors arising from the measurement process, the introduction of the sensitivity threshold, binning during data recording *etc.*, are likely to be much larger than the purely statistical errors quoted here. For example, Ref. (Peters et al., 2002) used a different type of measurement with a smaller sensitivity threshold and led to a best estimate for the exponent of 1.36. Furthermore, the apparent exponent can only be seen as a rough estimate of any true underlying exponent. We tested that, fixing $\theta_s = 1\ 17$, all data sets yield $p > 10\%$ over a range larger than two and a half orders of magnitude, except for the three problematic data sets. A two-sample Kolmogorov-Smirnov test for all pairs of datasets further confirms the similarity of the distributions for the different sites, 3.10.

In Figure 3.4(a) we show a color plot of all triplets ($s_{\min}$ $s_{\max}$ θ_s), corresponding to the Manus dataset. There is a large plateau where $\theta_s \approx 1\ 17$, indicating that this value is the best estimate for many intervals. Figure 3.4(b) is an analogous plot for the $p-$value, showing that the goodness of the fit is best in the region of the plateau.

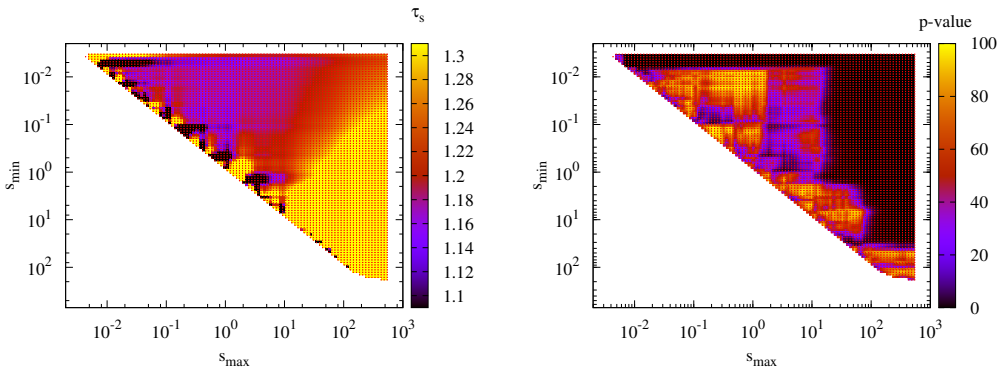

(a) (b)

FIGURE 3.4: (a) Color map showing the best-fit value for the exponent θ_s for all pairs of $s_{\min}$ and $s_{\max}$, (lower and upper ends of the chosen fitting range in mm) for the Manus dataset. The large plateau corresponds to $\theta_s \approx 1\,17$. (b) Analogous plot for the $p-$value.

TABLE 3.2: Avalanche size exponent θ_s for all sites (last column). Lower and upper end of fitting range (in mm), logarithmic range $s_{\max}\ s_{\min}$, number of events N, number of events in fitting range $\bar{N}$, and a moment ratio proportional to the cutoff s_ξ are shown. Brackets () denote errors in the last digit, determined by jackknife (Efron, 1982).

Site	$s_{\min}$	$s_{\max}$	$s_{\max}\ s_{\min}$	N	$\overline{N}$	$\langle s^2\rangle\ \ s\ (er)$	$\theta_s(er)$
Manus	0.0069	18.7	2719.	11981	9320	53.(1)	1.19(1)
Nauru	0.0066	4.7	704.	5134	3996	37.(1)	1.14(1)
Darwin	0.0067	21.6	3230.	2883	2410	50.(1)	1.16(1)
Niamey	0.0041	55.0	13500.	262	232	25.(2)	1.19(3)
Heselbach	0.0072	1.4	195.	2439	1764	13.(1)	1.18(2)
Shouxian	0.0037	2.5	677.	480	406	39.(2)	1.19(3)
Graciosa	0.0069	1.0	148.	3066	2260	14.4(3)	1.16(1)
NSA	0.0205	5.9	288.	9097	6030	47.(1)	1.01(1)
Pt. Reyes	0.0062	66.7	10796.	579	427	37.(2)	1.40(2)
SGP	0.0062	58.8	9463.	1624	1196	27.(1)	1.40(2)

Climatic differences between regions are scarcely detectable in event size distributions, which may be surprising on the grounds of climatological considerations. However, the cutoff s_ξ, representing the capacity of the climatic region around a measuring site to generate rain events, changes significantly from region to region, confirming meteorological intuition. This is difficult to see in the logarithmic scales of Figure 3.2 but is easily extracted from the moments of the distributions, Table 3.2. Thus, the smallest cutoff (and likely maximum event size) in the ARM data is found in Heselbach (mid-latitudes), whereas the largest is in Manus (Western Pacific warm pool). We note that $\langle s^2\rangle\ \ s$ is only proportional to the actual cutoff s_ξ. Assuming a box function for the scaling function and using the value $\theta_s = 1\,17$, we can estimate the proportionality constant and find $s_\xi \approx 2\,2\,\langle s^2\rangle\ \ s$. With this estimate, none of the fitting ranges extends beyond

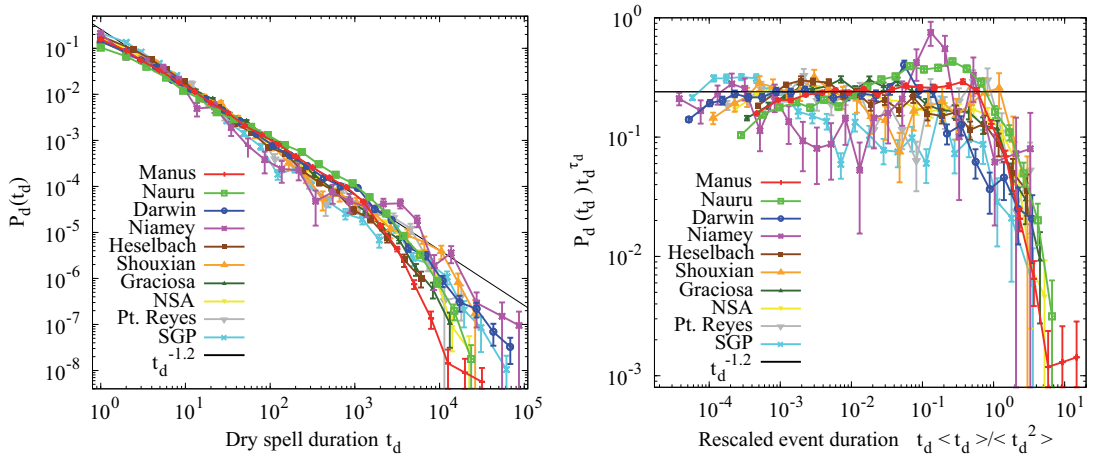

(a) (b)

FIGURE 3.5: (a) Probability densities for dry spell durations (in min). The diurnal cycle is most pronounced in Niamey, otherwise the distributions are similar. (b) Distributions collapsed onto their scaling function, similar to Figure 3.3(b).

the cutoff.

3.6 Dry spells

The durations of precipitation-free intervals have also been reported to follow an approximate power law (Lavergnat and Golé, 1998, Peters et al., 2002). We therefore repeat for dry-spell durations the same analysis as for the event sizes. Figure 3.5(a) shows the distributions, with a collapse corresponding to Figure 3.3(b) in Figure 3.5(b). We notice the different strengths of the diurnal cycle, here visible as a relative peak near 1 day dry spell duration. Exponents fitted to the distributions are similar, see Table 3.3. They also agree with the analyses in Ref. (Lavergnat and Golé, 1998), where a double-power-law fit was performed. For dry spell durations between a few seconds and a few hours the authors found an exponent value of 1.35. The second, smaller, exponent for longer dry spells found in that study may reflect the signal from the diurnal cycle. This signal is strong in Ref. (Peters et al., 2002), where a single-power-law fit yielded an exponent estimate of 1.42.

3.7 Event durations

Precipitation event duration distributions are broad for all locations. Durations provide a link to studies of geometric properties of precipitation fields. Numerous studies of tropical deep convective rain fields (Peters et al., 2009), shallow convection fields (Trivej

and Stevens, 2010), clouds (Benner and Curry, 1998, Cahalan and Joseph, 1989, Mapes and Jr., 1993), and model data from large eddy simulations (Neggers et al., 2003) have reported the distributions of ground covered by events (in radar snap shots etc.) to be well approximated by power laws. We note that in the clustering null model of critical two-dimensional percolation, clusters defined in one-dimensional cuts, akin to durations, do not scale, whereas two-dimensional clusters, akin to cloud-projections, do.

Applying to the durations the methods we used for the event sizes, we find comparatively short power-law ranges, see Table 3.4. The scaling range, if it exists, is expected to be smaller than for event sizes as the size distribution is a complicated convolution of the event duration and precipitation rate distributions, Figure 3.1, whose product covers a broader range than either of the distributions alone. The event size distribution is broader than the duration distribution also because long events tend to be more intense (not shown).

3.8 Conclusions

We find that the apparent avalanche size exponents, measured with identical instruments in different locations, are consistent with a single value of $\theta_s = 1\,17(3)$ for all reliable data sets. We note that the data sets from Point Reyes and from the Southern Great Plains are similar in many respects, despite the different reasons for treating them with suspicion.

TABLE 3.3: Dry spell exponent (last column). Lower and upper end of fitting range (in min), logarithmic range $t_{d\max}\ t_{d\min}$, number of dry spells in data set, N, and number of dry spells in the fitting range $\bar{N}$, and a moment ratio proportional to the cutoff are shown are shown. Brackets () denote errors in the last digit, determined by jackknife. The number of dry spells need not be within ± 1 of the number of events, as our definition of an event (and a dry spell) implies that it can be split in two if it contains an erroneous measurement. Note the magnitude of this effect in the NSA data set.

Site	$t_{d\min}$	$t_{d\max}$	$t_{d\max}\ t_{d\min}$	N	$\overline{N}$	$\langle {t_d}^2 \rangle \quad t_d \ (er)$	$\theta_d(er)$
Manus	24.4	1363.1	55.8	11992	4505	2149.(20)	1.16(2)
Nauru	7.5	1027.5	137.7	5126	2912	3557.(50)	0.99(2)
Darwin	8.5	3660.6	432.6	2892	1595	19477.(368)	1.17(1)
Niamey	2.4	1774.0	726.1	262	135	26386.(1699)	1.33(5)
Heselbach	9.5	5748.0	605.4	2441	1035	2043.(34)	1.37(2)
Shouxian	2.7	13488.5	4957.1	478	365	8776.(404)	1.27(3)
Graciosa	14.6	415.2	28.5	3068	1185	2943.(49)	1.28(3)
NSA	12.2	9033.2	739.7	3440	1531	4293.(73)	1.3(2)
Pt. Reyes	3.6	17141.0	4826.3	579	379	5513.(233)	1.27(2)
SGP	8.4	2248.7	268.5	1625	523	17243.(463)	1.46(3)

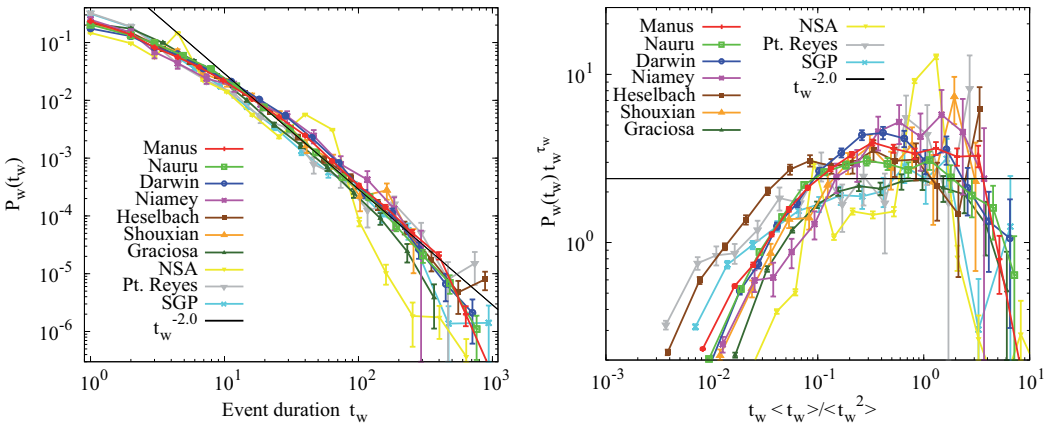

(a) (b)

FIGURE 3.6: (a) Probability densities for event durations (in min) are broad for all data sets. From a few min up to a few hundred min a power law with an exponent $\theta_m \approx 2\ 0$ roughly describes the data. (b) Collapsed distributions, similar to Figure 3.3(b).

TABLE 3.4: Duration exponent (last column). Lower and upper end of fitting range (in min), logarithmic range $t_{w\max}\ t_{w\min}$, number of events in data set, N, and number of events in the fitting range $\bar{N}$ are shown. Brackets () denote errors in the last digit, determined by jackknife.

Site	$t_{w\min}$	$t_{w\max}$	$t_{w\max}\ t_{w\min}$	N	$\overline{N}$	$\langle t_w{}^2 \rangle\ t_w$	$\theta_w(er)$
Manus	34.4	641.9	18.7	11981	1200	122.(1)	2.12(4)
Nauru	25.4	437.5	17.2	5134	540	106.(1)	2.09(6)
Darwin	17.87	89.30	5.00	2883	554	109.(2)	2.0(1)
Niamey	2.7	211.8	78.4	262	157	79.(5)	1.39(7)
Heselbach	18.2	1005.0	55.1	2439	388	261.(5)	1.97(6)
Shouxian	7.7	197.5	25.5	480	172	84.(4)	1.73(9)
Graciosa	12.7	424.0	33.4	3066	512	60.(1)	2.12(6)
NSA	75.2	103.3	1.4	9097	16	49.(1)	6.(3)
Pt. Reyes	5.7	784.0	138.6	579	178	272.(1)	1.71(7)
SGP	9.4	278.2	29.7	1624	303	143.(4)	1.74(7)

The statistical error in this estimate is surprisingly small, but neither the value itself nor the error change much using different fitting techniques or introducing different sensitivity thresholds (not shown). Nonetheless we believe systematic errors to be larger. Thus, the analysis gives an impression of the universality of the result but not necessarily the physical true value of the exponent. This does not contradict the climatological situation tropical regions, for instance, are expected to support larger events than mid-latitude locations, which could be realized as a smaller exponent value θ_s. While the exponents are not significantly different, the larger tropical events are reflected in the greater large-scale cutoff of the tropical distributions. Similarly, the dry-spell durations seem to follow another power law with $\theta_d = 1\ 2(1)$, and regional differences can be seen in the strength of the diurnal cycle and the cutoff dry spell duration. The broad range of event durations, Figure 3.6, suggests a link to the lack of characteristic

scales in the mesoscale regime, where approximately scale-free distributions of clusters of convective activity, for example cloud or precipitation, have been observed to span areas between $\mathcal{O}(1\ \mathrm{km}^2)$ and $\mathcal{O}(10^6\ \mathrm{km}^2)$ (Benner and Curry, 1998, Cahalan and Joseph, 1989, Neggers et al., 2003, Peters et al., 2009, Trivej and Stevens, 2010). The observation of scale-free rainfall event sizes suggests long-range correlation in the pertinent fields, a possible indication of critical behaviour near the transition to convective activity. Direct measurements of the behaviour of the correlation function for the precipitation field under changes of the (much more slowly varying) background fields of water vapour and temperature are desirable to clarify whether the long range correlation is a consequence of the flow field, of the proximity to a critical point, or of a combination of both.

3.9 Appendix: Fitting procedure

In order to obtain reliable values of, for example, the exponent θ_s, independent of the binning procedure used for the plots of $P_s(s)$, we use maximum likelihood estimation. We assume a power-law distribution $P_s(s) = a_{\tau_s} s^{-\tau_s}$, with support $[s_{\min}\ s_{\max}]$. Normalization yields $a_{\tau_s} = (1-\theta_s)\ (s_{\max}^{1-\tau_s} - s_{\min}^{1-\tau_s})$ for a given value of θ_s.

We compute the log-likelihood function,

$$\mathcal{L} := \ln \prod_{i=1}^{\bar{N}} P_s(s_i) = \sum_{i=1}^{\bar{N}} \ln \left(a_{\tau_s} {s_i}^{-\tau_s} \right) \tag{3.4}$$

where the index i runs over all $\bar{N}$ events whose size s_i is between $s_{\min}$ and $s_{\max}$. Holding $s_{\min}$ and $s_{\max}$ fixed, the value of θ_s which maximizes $\mathcal{L}$ is the maximum likelihood estimate of the exponent. Uncertainties in θ_s are determined using the jackknife method.

The goodness of the fit is assessed by a Kolmogorov-Smirnov (KS) test (Press et al., 2002). The KS statistic, or KS distance, d, is defined as

$$d := \max_{s_{\min} \le s \le s_{\max}} S_{\bar{N}}(s) - F_s(s) \tag{3.5}$$

where $S_{\bar{N}}(s)$ denotes the empirical cumulative distribution, defined as the fraction of observed events with a size smaller than s, in the interval $[s_{\min}\ s_{\max}]$. Thus, ordering the observed values by size, $s_1 \le \cdots \le s_i \le s_{i+1} \cdots \le s_{\bar{N}}$, we have $S_{\bar{N}}(s) = i\ \bar{N}$ if $s_i < s \le s_{i+1}$; F_s denotes the cumulative distribution of the maximum-likelihood distribution, $F_s(s) := \int_{s_{\min}}^{s} P_s(t)dt$.

The KS distance translates into the $p-$value. The $p-$value is the probability that synthetic data, here drawn from a power law distribution with exponent θ_s, result in a

KS-distance of at least d. For instance, $p = 10\%$ means that for power-law distributed data with exponent θ_s there is a probability of 0.90 that the KS distance takes a value smaller than d. Thus, if the data really are generated by a power law and we decide to reject the power law as a model if $p < 10\%$, we will reject the correct model in 10% of our tests. Conversely, decreasing the limit of rejection in the $p-$value implies that we accept more false models.

In our implementation of the KS test the distribution to be tested, $P_s(s)$, is not independent of the empirical data. This is because the exponent θ_s is obtained from the data that are later used to test the distribution. We therefore cannot use the standard analytic expression for $p(d)$, see Ref. (Press et al., 2002), Ch. 15. Instead, we determine the distribution of the KS distance and therefore the $p-$value by means of Monte Carlo simulations: we generate synthetic power-law-distributed data sets between $s_{\min}$ and $s_{\max}$ with exponent θ_s and number of data $\bar{N}$ (see Table 3.2), and proceed exactly in the same way as for the empirical data, first obtaining a maximum likelihood estimate of the exponent θ_s and then computing the KS distance between the empirical distribution of the simulated data and the fitted distribution containing the estimated value of θ_s. The $p-$value is obtained as the fraction of synthetic data sets for which the KS statistic is larger than the value obtained for the empirical data.

The final step is to compare results for different ranges $[s_{\min}\ s_{\max}]$. We try all possible fitting ranges with $s_{\min}$ and $s_{\max}$ increasing by factors of $10^{0\,01} \approx 1\,023$. We choose to report those intervals $[s_{\min}\ s_{\max}]$ that contain the largest number of events $\bar{N}$ with a corresponding $p-$value larger than 10%.

3.10 Appendix: Two-sample Kolmogorov-Smirnov Tests

A two-sample Kolmogorov-Smirnov test was performed for each pair of data sets, $i\ j$ to test whether the two underlying event size probability distributions differ. This test does not assume any functional form for the probability distributions (Press et al., 2002). As in the fitting of the exponent, we vary the testing ranges $[s_{\min}\ s_{\max}]$, keeping those which yield $p > 10\%$. We report the range with the maximum effective number of data, $\bar{N}_{\text{eff}} \equiv \bar{N}_i \bar{N}_j\ (\bar{N}_i + \bar{N}_j)$. The results, shown in Table 3.5, confirm that the pairs of distributions from the reliable data sets are similar over broad ranges.

TABLE 3.5: Maximum range $s_{\max}$ $s_{\min}$ over which the p-value of of a two-sample KS test is greater than 10%.

	Nauru	Darwin	Niamey	Heselbach	Shouxian	Graciosa	NSA	Pt. Reyes	SGP
Manus	5386.	16257.	16386.	679.	6355.	638.	14.	32.	8.
Nauru	-	6753.	13495.	236.	221.	342.	27.	19.	7.
Darwin	-	-	12247.	236.	271.	575.	27.	16.	5.
Niamey	-	-	-	3466.	16420.	2358.	1599.	668.	253.
Heselbach	-	-	-	-	14600.	13265.	18.	20.	5.
Shouxian	-	-	-	-	-	26440.	13.	65.	39.
Graciosa	-	-	-	-	-	-	11.	17.	589.
NSA	-	-	-	-	-	-	-	10.	3.
Pt. Reyes	-	-	-	-	-	-	-	-	19916.

Chapter 4

Scale Invariant Events and Dry Spells for Medium Resolution Local Rain Data

Submitted to Nonlinear Processes in Geophysics

Abstract We analyze distributions of rain-event sizes, rain-event durations, and dry-spell durations for data obtained from a network of 20 rain gauges scattered in a region of the NW Mediterranean coast. While power-law distributions model the dry-spell durations with a common exponent $1\ 50 \pm 0\ 05$, density analysis is inconclusive for event sizes and event durations, due to finite size effects. However, we present alternative evidence of the existence of scale invariance in these distributions by means of different data collapses of the distributions. These results are in agreement with the expectations from the Self-Organized Criticality paradigm, and demonstrate that scaling properties of rain events and dry spells can also be observed for medium resolution rain data.

4.1 Introduction

The complex atmospheric processes related to precipitation and convection arise from the cooperation of diverse non-linear mechanisms with different temporal and spatial characteristic scales. Precipitation combines, for instance, the $O(100\mu m)$ microphysics effects as evaporation with $O(1000km)$ planetary circulation of masses and moisture. Rain fields also presents high spatial and temporal intermittency as well as extreme

variability, in such a way that their intensity cannot be characterized by its mean value (Bodenschatz et al., 2010). Despite the complexity of the processes involved, surprising statistical regularities have been found: numerous geometric and radiative properties of clouds present clear scaling or multiscaling behavior (Cahalan and Joseph, 1989, Lovejoy, 1982, Peters et al., 2009, Wood and Field, 2011); also, raindrop arrival times and raindrop sizes, are well characterized by power-law distributions over several of orders of magnitude (Lavergnat and Golé, 2006, Olsson et al., 1993).

The concept of self-organized criticality (SOC) aims for explaining the origin of the emergence of structures across many different spatial and temporal scales in a broad variety of systems (Bak, 1996, Christensen and Moloney, 2005, Jensen, 1998, Sornette, 2004). Indeed, it has been found that for diverse phenomena that take place intermittently, in terms of bursts of activity interrupting larger quiet periods, the size s of these bursty events or avalanches follows a power-law distribution,

$$P(s) \quad \frac{1}{s^{\tau_s}} \tag{4.1}$$

over a certain range of s, with $P(s)$ the probability density of the event size and θ_s its exponent (and the sign indicating proportionality). The size s can be understood as a measure of energy dissipation. If durations of events are measured, a power-law distribution also holds. These power-law distributions provide an unambiguous proof of the absence of characteristic scales within the avalanches, as power laws are the only fully scale-invariant functions (Christensen and Moloney, 2005).

The main idea behind SOC is the recognition that such scale invariance is achieved because of the existence of a non-equilibrium continuous phase transition whose critical point is an attractor of the dynamics (Dickman et al., 1998, 2000, Tang and Bak, 1988). When the system settles at the critical point, scale invariance and power-law behavior are ensured, as these peculiarities are the defining characteristics of critical phenomena (Christensen and Moloney, 2005). Although sometimes SOC is understood in a broader sense, as the spontaneous emergence of scale invariance, we will follow the previous less-ambiguous definition. The concept of SOC has had big impact in the geosciences, in particular earthquakes (Bak, 1996, Sornette and Sornette, 1989), landslides and rock avalanches (Malamud, 2004), or forest fires (Malamud et al., 1998). Due to the existence of power-law distributed events in them, these systems have been proposed as realizations of SOC in the natural world.

The SOC perspective has also been applied to rainfall, looking at precipitation as an avalanche process, and paying attention to the properties of these avalanches, called rain events. The first works following this approach are those of Andrade et al. (1998) and Peters *et al.* (2002; Peters and Christensen 2002, 2006). These authors defined,

independently, a rain event as the sequence of rain occurrence with rain rate (i.e., the activity) always greater than zero. Then, the focus of the SOC approach is not on the total amount of rain recorded in a fixed time period (for instance, one hour, one day, or one month), but on the rain event, which is what defines in each case the time period of rain-amount integration. In this way, the event size is the total amount of rain collected during the duration of the event.

Andrade *et al.* studied long-term daily local (i.e., zero-dimensional) rain records from weather stations in Brazil, India, Europe, and Australia, with observation times ranging from a decade to a century approximately, with detection threshold 0.1 mm/day. Although the dry spells (the times between rain events) seemed to follow in some case a steep power-law distribution, the rain-event size distributions were not reported, and therefore the connection between SOC and rainfall could not really be checked. Later, Peters *et al.* analyzed high resolution rain data from a vertically pointing Doppler radar situated in the Baltic coast, which provided rates at an altitude between 250 m and 300 m above sea level, covering an area of 70 m^2, with detection threshold 0.0005 mm/hour and temporal resolution of 1 minute. Power-law distributions for event sizes and for dry-spells durations over several orders of magnitude were reported, with exponents θ_s θ_q 1 4. For the event-duration distribution the results were unclear, although a power law with an exponent θ_d 1 6 was fit to the data.

More recently, a study covering 10 sites across different climates has checked the universality of rain-event statistics using rain data from optical gauges (Peters et al., 2010). The data had a resolution of 0 2 mm/hr, collected at intervals of 1 minute. The results showed unambiguous power-law distributions of event sizes, with apparent universal exponents $\theta_s = 1\ 17 \pm 0\ 03$, extending the support to the SOC hypothesis in rainfall. Power laws distributions were also found for the dry spell durations, but for event durations the behavior was not so clear.

Nevertheless, scale-free distributions of the observables are insufficient evidence for SOC dynamics, as there are many alternative mechanisms of power-law genesis (Dickman, 2003, Sornette, 2004). In other words, SOC implies power laws, but the reciprocal is not true, power laws are not a guarantee of SOC. In particular, the multifractal approach can also reproduce scale invariance, but using different observables. When applied to rainfall, this approach focus on the rain rate field, which is hypothesized to have multifractal support as a result from a multiplicative cascade process. From this point of view, alternative statistical models new forecasting and downscaling methods have emerged (Deidda et al., 2000, Lovejoy and Schertzer, 1995, Veneziano and Lepore, 2012).

In general, one can distinguish between continuous and within-storm multifractal analysis. The first one considers the whole rain rate time series (including dry spells), while the second one analyzes just rain rate time series within storms. This requires a storm definition, which usually contains dry periods too, but with duration smaller than a certain threshold. The connections between SOC and the multifractal approach are still an open question, despite some seminal works (Hooge et al., 1994, Olami and Christensen, 1992, Schertzer and Lovejoy, 1994). We expect that these connections could be developed more in depth from the within-storm multifractal approach, which presents more similarities with the SOC one; however, such an ambitious goal is beyond the scope of this article.

Coming back to the problem of SOC in rainfall, a more direct approach was undertaken by Peters and Neelin (2006). They analyzed satellite estimates of rain rate and vertically integrated (i.e., column) water vapour content in grid points covering the tropical oceans (with a 0 25° spatial resolution in latitude and longitude) from the Tropical Rainfall Measuring Mission, and they found a sharp increase of the rain rate when a threshold value of the water vapor was reached, in the same way as in critical phase transitions. Moreover, these authors showed that most of the time the state of the system was close to the transition point (i.e., most of the measurements of the water vapor correspond to values near the critical one), providing convincing observational support of the validity of SOC theory in rainfall. Further, they connected these ideas with the classical concept of quasi-equilibrium for atmospheric convection (Arakawa and Schubert, 1974), allowing the application of the SOC ideas in cloud resolving model development (Stechmann and Neelin, 2011). Remarkably, as far as we know, an analogous result has not been found in other claimed SOC natural systems, as earthquakes or forest fires; this would imply that the result of Peters and Neelin is the first unambiguous proof of SOC in these systems.

In any case, the existence of SOC in rainfall posses many questions. As we have seen, the number of studies addressing this is rather limited, mostly due to the supposed requirement that the data has to be of very high time and rate resolution. Moreover, testing further the critical dependence of rain rate on column water vapor (CWV), as seen in Peters and Neelin (2006), is nonviable for local data due to current problems of the microwave radiometers at hight CWV values (Holloway and Neelin, 2010). Finally, the kind of data analyzed by Peters and Neelin is completely different to the data employed in the studies yielding power-law distributed events (Peters et al., 2002, 2010), so, direct comparison between both kinds of approaches is not possible.

The goal of this paper is to extend the evidence for SOC in rainfall, studying the applicability of this paradigm when the rain data available is not of high resolution. With

this purpose, we perform an in-depth analysis of local rainfall records in a representative region of the Northwestern Mediterranean. For this lower (in comparison with previous studies) resolution, the range in which the power-law holds can be substantially decreased. This may require the application of more refined fitting techniques and scaling methods. Thus, as a by-product, we explore different scaling forms and develop a collapse method based on minimizing the distance between distributions that also gives an estimation of the power-law exponent. With these tools will be able to establish the existence of scale-invariant behavior in the medium resolution rain data analyzed.

We proceed as follows: Section 2 describes the data used in the present analysis and defines the rain event, its size and duration, and the dry spell. Section 3 shows the corresponding probability densities and describes and applies an accurate fitting technique for evaluating the power-law existence. Section 4 introduces two collapse methods (parametric and non-parametric) in order to establish the fulfillment of scaling, independently of power-law fitting. Discussion and conclusions are presented in section 5.

4.2 Data and definitions

4.2.1 Data

We have analyzed 20 stations in Catalonia (NE Spain) from the database maintained by the Agència Catalana de l Aigua (ACA, `http://aca-web.gencat.cat/aca`). These data come from a network of rain gauges, called SICAT (Sistema Integral del Cicle de l Aigua al Territori, formerly SAIH, Sistema Automàtic d Informació Hidrològica), used to monitor the state of the drainage basins of the rivers that are born and die in the Catalan territory. The corresponding sites are listed in Table 4.1 and have longitudes and latitudes ranging from 1° 10 51 to 3° 7 35 E and from 41° 12 53 to 43° 25 40 N. All datasets cover a time period starting on January 1st, 2000, at 0:00, and ending either on June 30th or on July 1st, 2009 (spanning roughly 9.5 years), except the Cap de Creus one, which ends on June 19th, 2009.

TABLE 4.1: Characteristics of all the sites for the 9-year period 2000-2008. Every site is named by the corresponding river basin or subbasin (the municipality is included in ambiguous cases); Ll. stands for Llobregat river. f_M is the fraction (in %) of missing records (time missing divided by total time); f_D is the fraction (in %) of discarded times; f_r is the fraction (in %) of rainy time (time with $r > 0$ divided by total undiscarded time, for a time resolution $\Delta t = 5$ min); a. rate is the annual rain rate in mm/yr, calculated only over undiscarded times; c. rate is the rain rate in mm/hr conditioned to rain, i.e., calculated over the (undiscarded) rainy time; N_s is the number of rain events and N_q the number of dry spells (the differences between N_s and N_q are due to the missing records); the rest of symbols are explained in the text. s is measured in mm, and d and q in min. Sites are ordered by increasing annual rate. The table shows a positive correlation between f_r, the annual rate, N_s and N_q, and that these variables are negatively correlated with q . In contrast, the rate conditioned to rain is roughly constant, taking values between 3.3 and 3.8 mm/hr.

Site	f_M	f_D	f_r	a. rate	c. rate	N_s	N_q	s	d	q
1 Gaià	0.08	3.71	1.6	470.9	3.3	5021	5014	0.81	14.9	894.
2 Foix	0.07	3.38	1.6	500.6	3.6	4850	4844	0.90	15.0	929.
3 Baix Ll. S.J. Despí	0.07	2.28	1.7	505.8	3.3	5374	5369	0.83	15.0	847.
4 Garraf	0.09	3.30	1.6	507.8	3.7	4722	4716	0.94	15.2	956.
5 Baix Ll. Castellbell	0.06	2.81	1.7	510.7	3.4	4950	4947	0.90	15.8	914.
6 Francolí	0.44	13.37	1.8	528.2	3.4	4539	4540	0.91	16.1	887.
7 Besòs Barcelona	0.15	4.17	1.7	531.8	3.5	4808	4803	0.95	16.2	928.
8 Riera de La Bisbal	0.07	3.66	1.6	540.0	3.8	4730	4724	0.99	15.8	950.
9 Besòs Castellar	4.34	13.59	2.0	633.3	3.6	4918	4970	1.00	16.9	806.
10 Ll. Cardener	0.07	3.33	2.1	652.4	3.5	6204	6197	0.92	15.7	723.
11 Ridaura	0.12	2.41	2.0	674.2	3.8	5780	5774	1.02	16.1	784.
12 Daró	0.06	2.09	2.2	684.5	3.6	5553	5547	1.09	18.0	818.
13 Tordera	0.08	2.04	2.3	688.8	3.4	7980	7977	0.76	13.6	568.
14 Baix Ter	0.07	2.71	2.3	710.2	3.6	6042	6036	1.03	17.4	746.
15 Cap de Creus	0.07	2.92	2.3	741.5	3.7	5962	5955	1.09	17.7	754.
16 Alt Llobregat	3.12	5.82	2.6	742.8	3.3	6970	6988	0.90	16.7	621.
17 Muga	0.06	2.56	2.4	749.3	3.6	6462	6457	1.02	16.9	698.
18 Alt Ter Sau	0.08	2.43	2.5	772.1	3.6	6966	6961	0.97	16.3	647.
19 Fluvià	3.09	4.74	2.3	772.4	3.8	6287	6319	1.05	16.7	697.
20 Alt Ter S. Joan	0.07	1.98	2.8	795.1	3.3	8333	8327	0.84	15.5	452.

In all the stations, rain is measured by the same weighing precipitation gauge, the device called *Pluvio* from OTT (`http://www.ott-hydrometry.de`), either with a capacity of 250 or 1000 mm and working through the balance principle. It measures both liquid or/and solid precipitation. The precipitation rate is recorded in intervals of $\Delta t = 5$ min, with a resolution of 1 2 mm/hr (which corresponds to 0.1 mm in 5 min). This precipitation rate can be converted into an energy flux through the latent heat of condensation of water, which yields 1 mm/hr 690 W/m^2, nevertheless, we have not performed such conversion. Figure 4.1(a) shows a subset of the time series for site 17 (Muga).

In order to make the files more manageable, the database reports zero-rain rates only every hour; then we consider time voids larger than 1 hour as operational errors. The ratio of these missing times to the total time covered in the record is denoted as f_M in Table 4.1, where it can be seen that this is usually below 0.1 %. However, there are 3 cases in which its value is around 3 or 4 %. Other quantities reported in the table are the fraction of time corresponding to rain (or wet fraction), f_r, the annual mean rate, and the mean rate conditioned to rain periods. Nevertheless, note that for a fractal point process a quantity as f_r depends on the time resolution, so, f_r only makes sense for a concrete time division, in our case, $\Delta t = 5$ min.

4.2.2 Rain event sizes, rain event durations, and dry spell durations

Following Andrade et al. (1998) and Peters et al. (2002), we define a rain event as a sequence of consecutive rain rates bigger than zero delimited by zero rates, i.e., $r(t_n)$ $r(t_{n+1})$ $r(t_m)$, such that $r(t_i) > 0$ for $i = n$ $n+1$ m with $r(t_{n-1}) = r(t_{m+1}) = 0$. Due to the resolution of the record, this is equivalent to take a threshold with a value below 1.2 mm/hour. It is worth mentioning that this simple definition of rain events may be in conflict with those used by the hydrologists community, so caution is required in order to make comparisons between the different approaches (Molini et al., 2011).

The first observable to consider is the duration d of the event, which is the time that the event lasts (a multiple of 5 min, in our case). The size of the event is defined as the total rain during the event, i.e., the rate integrated over the event duration,

$$s \equiv \sum_{i=n}^{m} r(t_i)\Delta t \qquad \int_{t_n}^{t_m} r(t)dt$$

measured in mm (and multiple of 0.1 mm in our case, 1.2 mm/hr $\times$ 5 min). Notice that this event size is not the same as the usual rain depth, due to the different definition of the rain event in each case. Figure 4.1(b) shows as an illustration the evolution of

the rate for the largest event in the record, which happens at the Muga site, whereas Figure 4.1(c) displays the sequence of all event sizes in the same site for the year 2002. It is important to realize that this quantity is different to the one at Fig. 4.1(b). Regarding event durations, the time series have a certain resemblance to Fig. 1c, as usually they are (nonlinearly) correlated with event sizes (Telesca et al., 2007). Further, the dry spells are the periods between consecutive rain events (then, they verify $r(t) = 0$); we denote their durations by q. When a rain event, or a dry spell, is interrupted due to missing data, we discard that event or dry spell, and count the recorded duration as discarded time; the fraction of these times in the record appears in Table 4.1, under the symbol f_D. Although in some cases the duration of the interrupted event or dry spell can be bounded from below or from above (as in censored data), we have not attempted to use that partial information.

4.3 Power-law distributions

4.3.1 Probability densities

Due to the enormous variability of the 3 quantities just defined, the most informative approach is to work with their probability distributions. Taking the size as an example, its probability density $P(s)$ is defined as the probability that the size is between s and $s + ds$ divided by ds, with $ds \to 0$. Then, $\int_0 P(s)ds = 1$. This implicitly assumes that s is considered as a continuous variable (but this will be corrected later, see more details on Appendix 4.6). In general, we illustrate all quantities with the event size s, the analogous for d and q are obtained by replacing s with the symbol of each observable. The corresponding probability densities are denoted as $P(d)$ and $P(q)$, with the implicit understanding that their functional forms may be different. Note that the annual number densities (Peters and Christensen, 2002, 2006, Peters et al., 2002) are trivially recovered multiplying the probability densities by the total number of events or dry spells and dividing by total time.

The results for the probability densities $P(s)$, $P(d)$, and $P(q)$ of all the sites under study are shown in Figs. 4.2(a), 4.2(b), and 4.2(c), respectively. In all cases the distributions show a very clear behavior, monotonically decreasing and covering a broad range of values. However, to the naked eye, a power-law range is only apparent for the distributions of dry spells, $P(q)$ (remember that a power law turns into a straight line in a log-log plot). Moreover, the $P(q)$ are the broadest distributions, covering a range of more than 4 orders of magnitude (from 5 min to about a couple of months), and present in some cases a modest daily peak (in comparison to Peters et al. (2002), with 1 day = 1440

min). In the opposite side we find the distributions of durations, $P(d)$, whose range is the shortest, from 5 min to about 1 day (two and a half orders of magnitude), and for which no straight line is visible in the plot; rather, the distributions appear as convex. The size distributions, $P(s)$, defined for about 3 orders of magnitude (from 0.1 to 200 mm roughly), can be considered in between the other two cases, with a visually shorter range of power-law behavior.

4.3.2 Fitting and testing power laws

A quantitative method can put more rigor into these observations. The idea is based on the recipe proposed by Clauset et al. (2009) see also Corral et al. (2011) but improved and generalized to our problem. Essentially, an objective procedure is required in order to find the optimum range in which a power law may hold. Taking again the event size for illustration, we report the power-law exponent fit between the values of $s_{\min}$ and $s_{\max}$ which yield the maximum number of data in that range but with a $p-$value greater than 10%. The method is described in detail in Peters et al. (2010), but we summarize it in the next paragraphs.

For a given value of the pair $s_{\min}$ and $s_{\max}$, the maximum-likelihood (ML) power-law exponent is estimated for the events whose size lies in that range. This exponent yields a fit of the distribution, and the goodness of such a fit is evaluated by means of the Kolmogorov-Smirnov (KS) test (Press et al., 2002). The purpose is to get a $p-$value, which is the probability that the KS test gives a distance between true power-law data and its fit larger than the distance obtained between the empirical data and its fit.

For instance, $p = 20\%$ would mean that truly power-law distributed data were closer than the empirical data to their respective fits in 80% of the cases, but in the rest 20% of the cases a true power law were at a larger distance than the empirical data. So, in such a case the KS distance turns out to be somewhat large, but not large enough to reject that the data follow a power law with the ML exponent.

As in the case in which some parameter is estimated from the data there is no closed formula to calculate the $p-$value, we perform Monte Carlo simulations in order to compute the statistics of the Kolmogorov-Smirnov distance and from there the $p-$value. In this way, for each $s_{\min}$ and $s_{\max}$ we get a number of data $\bar{N}_s$ in that range and, repeating the procedure many times, a $p-$value. We look for the values of the extremes ($s_{\min}$ and $s_{\max}$) which maximize the number of data in between but with the restriction that the $p-$value has to be greater than 10% (this threshold is arbitrary, but the conclusions do not change if it is moved). The maximization is performed sweeping 100 values of $s_{\min}$ and 100 values of $s_{\max}$, in log-scale, in such a way that all possible ranges (within this

log-resolution) are taken into account. We have to remark that, in contrast with Peters et al. (2010), we have considered always discrete probability distributions, both in the ML fit and in the simulations. Of course, it is a matter of discussion which approach (continuous or discrete) is more appropriate for discrete data that represent a continuous process. In any case, the differences in the outcomes are rather small. Notice also that the method is not based on the estimation of the probability densities shown in the previous subsections, what would be inherently more arbitrary (Clauset et al., 2009).

The results of this method are in agreement with the visual conclusions obtained in the previous subsection, as can be seen in Table 4.2. Starting with the size statistics, 13 out of the 20 sites yield reasonable results, with an exponent θ_s between 1.43 and 1.54 over a logarithmic range $s_{\max}\ s_{\min}$ from 12 to more than 200. For the rest of the sites, the range is too short, less than one decade (a decade is understood from now as an order of magnitude). In the application of the algorithm, it has been necessary to restrict the value of $s_{\min}$ to be $s_{\min} \geq 0\,2$ mm; otherwise, as the distributions have a concave shape (in logscale) close to the origin (which means that there are many more events in that scale than at larger scales), the algorithm (which maximizes the number of data in a given range) prefers a short range with many data close to the origin than a larger range with less data away from the origin. It is possible that a variation of the algorithm in which the quantity that is maximized were different (for instance related with the range), would not need the restriction in the minimum size.

For the distribution of durations the resulting power laws turn out to be very limited in range; only 4 sites give not too short power laws, with $d_{max}\ d_{min}$ from 6 to 12 and θ_d from 1.66 to 1.74. The other sites yield extremely short ranges for the power law be of any relevance. The situation is analogous to the case of the distribution of sizes, but the resulting ranges are much shorter here (Peters et al., 2010). Notice that the excess of events with $d = 5$ min, eliminated from the fits imposing $d_{min} \geq 10$ min, has no counterpart in the value of the smallest rate (not shown), and therefore, we conclude that this extra number of events is due to problems in the time resolution of the data.

Considerably more satisfactory are the results for the dry spells. 16 sites give consistent results, with θ_q from 1.45 to 1.55 in a range $q_{max}\ q_{min}$ from 30 to almost 300. It is noticeable that in these cases q_{max} is always below 1 day. The removal by hand of dry spells around that value should enlarge a little the power-law range. In the rest of sites, either the range is comparatively too short (for example, for the Gaià site, the power-law behavior of $P(q)$ is interrupted at around $q = 100$ min), or the algorithm has a tendency to include the bump the distributions show between the daily peak (q beyond 1000 min) and the tail. This makes the value of the exponent smaller (around 1.25). Nevertheless, the value of the exponent is much higher than the one obtained

for the equivalent problem of earthquake waiting times, where the Omori law leads to values around one, or less. This points to a fundamental differencesbetween both kind of processes (from a statistical point of view).

In summary, the power laws for the distributions of durations are too short to be relevant, and the fits for the sizes are in the limit of what is acceptable (some cases are clear and some other not). Only the distributions of dry spells give really good power laws, with $\theta_q = 1\ 50 \pm 0\ 05$, and for more than two decades in 6 sites.

4.4 Scaling

4.4.1 Non-parametric scaling

However, the fact that a power-law behaviour does not exist over a broad range of values does not rule out the existence of SOC (Christensen and Moloney, 2005). In fact, the fulfilment of a power-law distribution in the form of Eq. (4.1) is only valid when finite-size effects are small , which only happens for large enough systems. In general, when these effects are taken into account, SOC behaviour leads to distributions of the form (Christensen and Moloney, 2005, Peters et al., 2010),

$$P(s) = s^{-\tau_s} \mathcal{G}_s(s \ s_\xi) \quad \text{for} \ \ s > s_l \tag{4.2}$$

where $\mathcal{G}_s(x)$ is a scaling function that is essentially constant for $x \ll 1$ and decays fast for $x \gg 1$, accounting in this way for the finite-size effects when s is above the crossover value s_ξ; the size s_l is just a lower cutoff limiting the validity of this description. The pure power law only emerges for s_ξ , nevertheless, a truncated power law holds over an appreciable range if the scales given by s_l and s_ξ are well separated, i.e., $s_l \ll s_\xi$. As s_ξ increases with system size, typically as $s_\xi \quad L^{D_s}$ (with D_s the so-called avalanche dimension, or event-size dimension), the power-law condition (4.1) can only be fulfilled for large enough system sizes.

Note that, in the case of a too short power-law range or a non-conclusive fit, we still could check the existence of scaling using Eq. (4.2) if we knew s_ξ or L. However, s_ξ is difficult to measure, needing a parameterization of the scaling function, and it is not clear what the system size L is for rainfall. It could be the vertical extension of the clouds, or the depth of the troposphere. Nevertheless, it is important to realize that the scaling ansatz (3.2) still can be checked from data without knowledge of L or s_ξ. First, notice that the ansatz implies that the $k-$order moment of s scales with L as

$$s^k \quad L^{D_s(k+1-\tau_s)} \quad \text{for} \ \ 1 < \theta_s < k+1 \tag{4.3}$$

if $s_l \ll s_\xi$, see Christensen and Moloney (2005). Second, Eq. (3.2) can be written in a slightly different form, as a scaling law,

$$P(s) = L^{-D_s\tau_s}\mathcal{F}_s(s\ L^{D_s}) \quad \text{for } s > s_l \tag{4.4}$$

where the new scaling function $\mathcal{F}_s(x)$ is defined as $\mathcal{F}_s(x) \equiv x^{-\tau_s}\mathcal{G}_s(x\ a)$ (a is the constant of proportionality between s_ξ and L^{D_s}). This form of $P(s)$ (in fact, $P(s\ L)$), with an arbitrary $\mathcal{F}$, is the well-known scale-invariance condition for functions with two variables (Christensen and Moloney, 2005). Changes of scale (linear transformations) in s and L may leave the shape of the function $P(s\ L)$ unchanged (this is what scale invariance really means, power laws are just a particular case in one dimension).

Substituting L^{D_s} $\langle s^2\rangle$ s and $L^{D_s\tau_s}$ L^{2D_s} s $\langle s^2\rangle^2$ $s^{\ 3}$ (from the scaling of $\langle s^k\rangle$, assuming $\theta_s < 2$) into Eq. (4.4) leads to

$$P(s) = s^{\ 3}\langle s^2\rangle^{-2}\mathcal{F}_s(s\ s\ \langle s^2\rangle) \tag{4.5}$$

where $\mathcal{F}_s(x)$ is essentially the scaling function $\mathcal{F}_s(x)$, absorbing the proportionality constants. Therefore, if scaling holds, a plot of $\langle s^2\rangle^2 P(s)$ $s^{\ 3}$ versus s s $\langle s^2\rangle$ for all the sites has to yield a collapse of the distributions into a single curve, which draws $\mathcal{F}_s(x)$ (a similar procedure is outlined in Rosso et al. (2009)). In order to proceed, the mean and the quadratic mean, s and $\langle s^2\rangle$, can be easily estimated from data. Since no estimation of parameters is involved for this procedure, we call it non-parametric scaling.

The outcome for $P(s)$, $P(d)$, and $P(q)$ is shown in Figs. 4.3(a), 4.3(b), and 4.3(c), with reasonable results, especially for the distribution of dry spells. The plot suggests that the scaling function $\mathcal{G}_q$ of the dry-spell distribution has a maximum around x 1, but this does not in disagreement with our approach, which only assumed a constant scaling function for small x and a fast decay for large x.

Note that the quotient $\langle s^2\rangle$ s gives the scale for the crossover value s_ξ (as s_ξ $\langle s^2\rangle$ s , with a constant of proportionality that depends on the scaling function $\mathcal{G}_s$ and on s_l s_ξ), and therefore it is the ratio of the second moment to the mean and not the mean which describes the scaling behaviour of the distribution. This can have important implications for extreme events: an increase in the value of the mean is not proportional to an increase of the most extreme events, represented by s_ξ. For the case of event sizes, we get values of $\langle s^2\rangle$ s between 10 and 30 mm (which is a variability much higher than that of s), and therefore the condition $s_l \ll s_\xi$ is very well fulfilled (assuming that the moment ratio $\langle s^2\rangle$ s is of the same order as s_ξ, and with s_l s_{min}), which is a test for the consistency of our approach. For dry spells $\langle q^2\rangle$ q is between 5 and 13

days, which is even better for the applicability of the scaling analysis. The case of the event durations is somewhat critical , with $\langle d^2 \rangle$ d between 70 and 120 min, which yields d_ξ d_l in the range from 14 to 24. Nevertheless, we observe that the condition $s_l \ll s_\xi$ for the power law to show up is stronger than the same condition for the scaling analysis to be valid.

4.4.2 Parametric scaling

Further, a scaling ansatz as Eq. (3.2) or (4.4) allows an estimation of the exponent θ_s, even in the case in which a power law cannot be fit to the data. From the scaling of the moments of s we get, taking $k = 1$, L^{D_s} $s^{1\ (2-\tau_s)}$ and $L^{D_s\tau_s}$ $s^{\tau_s\ (2-\tau_s)}$ (again with $\theta_s < 2$); so, substituting into Eq. (4.4),

$$P(s) = s^{-\tau_s\ (2-\tau_s)} \mathcal{F}_s(s\ \ s^{1\ (2-\tau_s)}) \tag{4.6}$$

One only needs to find the value of θ_s that optimizes the collapse of all the distributions, i.e., that makes the previous equation valid, or at least as close to validity as possible. As the scaling depends on the parameter θ_s, we refer to this procedure as parametric scaling.

We therefore need a measurement to quantify distance between rescaled distributions. In order to do that, we have chosen to work with the cumulative distribution function, $S(s) \equiv \int_s P(s')ds'$, rather than with the density (to be rigorous, $S(s)$ is the complementary of the cumulative distribution function, and is called survivor function or reliability function in some contexts). Although in practice both $P(s)$ and $S(s)$ contain the same probabilistic information, the reason to work with $S(s)$ is double: the estimation of the cumulative distribution function does not depend of an arbitrarily selected bin width ds (Press et al., 2002), and it does not give equal weight to all scales in the representation of the function (i.e., in the number of points that constitute the function). The scaling laws (4.4) and (4.6) turn out to be, then,

$$S(s) = L^{-D_s(\tau_s-1)}\mathcal{H}_s(s\ \ L^{D_s}) \tag{4.7}$$

$$S(s) = s^{-(\tau_s-1)\ (2-\tau_s)}\mathcal{H}_s(s\ \ s^{1\ (2-\tau_s)}) \tag{4.8}$$

with $\mathcal{H}_s(x)$ and $\mathcal{H}_s(x)$ the corresponding scaling functions.

The first step of the method of collapse is to merge all the pairs $s\ S(s)_i$ into a unique rescaled function $x\ y$. If $i = 1$ 20 runs for all sites, and $j = 1$ $M_s(i)$ for all the different values that the size of events takes on site i (note that $M_s(i) \leq N_s(i)$),

then,

$$x\ (\theta) \equiv \log(s_{ji} \quad s_{\ i}^{\ 1\ (2-\tau)})$$

$$y\ (\theta) \equiv \log(S_i(s_{ji})\ \ s_{\ i}^{(\tau-1)\ (2-\tau)})$$

with s_{ji} the j-th value of the size in site i, $s_{\ i}$ the mean on s in i, $S_i(s_{ji})$ the cumulative distribution function in i, and θ a possible value of the exponent θ_s. The index $\quad$ labels the new function, from 1 to $\quad_i M_s(i)$, in such a way that $x\ (\theta) \leq x\ _{+1}(\theta)$; i.e., the pairs $x\ (\theta)\ y\ (\theta)$ are sorted by increasing x.

Then, we just compute

$$D(\theta) \equiv \quad \left([x\ (\theta) - x\ _{+1}(\theta)]^2 + [y\ (\theta) - y\ _{+1}(\theta)]^2\right) \tag{4.9}$$

which represents the sum of all Euclidean distances between the neighbouring points in a (tentative) collapse plot in logarithmic scale. The value of θ which minimizes this function is identified with the exponent θ_s in Eq. (3.2). We have tested the algorithm applying it to SOC models whose exponents are well known (not shown).

The results of this method applied to our datasets, not only for the size distributions but also to the distributions of d, are highly satisfactory. There is only one requirement: the removal of the first point in each distribution ($s = 0\,1$ mm and $d = 5$ min), as with the ML fits. The exponents we find are $\theta_s = 1\ 52 \pm 0\ 12$ and $\theta_d = 1\ 69 \pm 0\ 01$, in agreement with the ones obtained by the power-law fitting method presented above; the corresponding rescaled plots are shown in Figure 4.4. Although the visual display does not allow to evaluate properly the quality of the collapse, the reduction in the value of the function $D(\theta)$ is notable. Then, the performance of the method is noteworthy, taking into account that the mean values of the distributions show little variation in most cases. In addition, the shape of the scaling function $\mathcal{G}_s$ can be obtained by plotting, as suggested by Eq. (3.2), $s^{\tau_s}P(s)$ versus $s \quad s^{\ 1\ (2-\tau_s)}$, and the same for the other variable, d. Fig. 4.5 displays what is obtained for each distribution. In contrast, the application of this method to $P(q)$ does not yield consistent results, as θ_q turns out to be rather small (1.24). Notice that the existence of a daily peak in the distributions is an obstacle to a data collapse, as the peak prevents a good scaling.

4.5 Discussion and conclusions

We have performed an in-depth study of the properties of SOC related observables in rainfall in the Mediterranean region in order to check if this framework can be useful for modeling rain events and dry spells. The results support this hypothesis, which

had not been checked before in this region or for this kind of data resolution. For the distributions of rain-event sizes we get power-law exponents valid for one or two decades in the majority of sites, with exponent values θ_s 1 50 $\pm$ 0 05. For the distributions of event durations, the fitting ranges are shorter, reaching in the best case one decade, with exponents θ_d 1 70 $\pm$ 0 05. This range is expected to be shorter than for event sizes, given that these combine the event duration distribution with the rain rate (Peters et al., 2010). And finally, the dry spell distributions yield the more notable power law fits, with exponents in the range θ_q 1 50$\pm$0 05, in some cases for more than 2 decades.

These results are compatible with the ones obtained for the Baltic sea by Peters et al. (2002), which yielded θ_s θ_q 1 4 and θ_d 1 6. The agreement is remarkable, taking into account the different nature of the data analyzed and the disparate fitting procedures. However, the concordance with the more recent results of Peters et al. (2010) is not very good, quantitatively. That previous study, with a minimum detection rate of 0.2 mm/hr and a time resolution $\Delta t = 1$ min, found θ_s 1 18 for several sites across different climates, using essentially the same statistical techniques as in the present study. Exponents were found not universal for durations of events and dry-spells, but for the latter they were close in many cases to θ_d 1 3. The difference between the size and dry-spell duration exponents may be due to data resolution. Changes in the detection threshold have a non-trivial repercussion in the size and duration of the events and the dry spells (an increase in the threshold can split one single event into two or more separate ones but also can remove events). Further, better time resolution and lower detection threshold allow the detection of smaller events, enlarging the power law range and reducing the weight from the part close to the crossover point (where the distribution becomes steeper); this trivially leads to smaller values of the exponent. In the dry spells case, the power-law range in this study is enough to guarantee that our estimation of the exponents are robust, so the discrepancy with Peters et al. (2010) may be due to the non-trivial effect of the change in the detection thresholds or differences on the measurement devices.

On the other hand, finite size effects can explain the limited power-law range obtained for s and d observables, as it occurs in other (self-organized and non-self-organized) critical phenomena. The finite-size analysis performed, in terms of combinations of powers of the moments of the distributions, supports this conclusion. The collapse of the distributions is a clear signature of scale-invariance: different sites share a common shape of the rain-event and dry-spell distributions, with differences in the scale of those distributions, depending on system size. Then, in the ideal case of an infinite system, the power laws would lack an upper cutoff. Moreover, the collapse of the distributions allows an independent estimate of the power-law exponents, which, for event durations and sizes,

are in surprising agreement with the values obtained by the maximum-likelihood fit. For dry spell durations, a daily peak in the distributions hinders their collapse.

Nevertheless, future work should consider spatially extended events. Our measurements are taken in a point of the system which reflects information on the vertical scale, then, the results could be affected by this. Another important issue are the implications of the results for hazard assessment. If there is not a characteristic rain-event size, then there is neither a definite separation nor a fundamental difference between the smallest harmless rains and the most hazardous storms. Further, it is generally believed that the critical evolution of events in SOC systems implies that, at a given instant, it is equally likely that the event intensifies or weakens, which would make detailed prediction unattainable. However, this view has been recently proved wrong, as it has been reported that a critical evolution describes the dynamics of some SOC systems only on average; further, the existence of finite size effects can be used for prediction (Garber et al., 2009, Martin et al., 2010). Interestingly, in the case of rain, it has been recently shown by Molini et al. (2011) that knowledge of internal variables of the system allows some degree of prediction for the duration of the events, related also to the departure of the system from quasi-equilibrium conditions. Finally, we urge studies which explore the effects of resolution and detection-threshold value in high-resolution rain data. A common SOC misbelief is that avalanches happen following a memoryless process, leading therefore to exponential distributions for the waiting times (Corral, 2005). This has been proved wrong if a threshold on the intensity is present (Paczuski et al., 2005). In this case, times between avalanches follow a power-law distribution, as we find for dry spells.

In summary, we conclude that the statistics of rainfall events in the NW Mediterranean area studied are in agreement with the SOC paradigm expectations. This is the first time this study is realized for this region and it is a confirmation of what has been found for other places of the world, but using in ourcase data with lower resolution. If a representative universal exponent existed, this would mean that just one parameter is enough for characterizing the distributions. This would indicate that the rain event observable cannot detect climatic differences between regions, but would shed light on universal properties and mechanisms of rainfall generation.

4.6 Appendix: Details on the estimation of the probability density

In practice, the estimation of the density from data is performed taking a value of ds large enough to guarantee statistical significance, and then compute $P(s)$ as $n(s)$ $(N_s\Delta)$,

where $n(s)$ is the number of events with size in the range between s and $s + ds$, N_s the total number of events, and Δ is defined as

$$\Delta = R_s(\ (s + ds)\ R_s\ -\ s\ R_s\ )$$

with x the integer part of x and R_s the resolution of s, i.e. $R_s = 0\ 1$ mm (but note that high resolution means low R_s). So, $\Delta\ R_s$ is the number of possible different values of the variable in the interval considered. Notice that using Δ instead of ds in the denominator of the estimation of $P(s)$ allows one to take into account the discreteness of s. If R_s tended to zero, then Δ ds and the discreteness effects would become irrelevant.

How large does ds have to be to guarantee the statistical significance of the estimation of $P(s)$? Working with long-tailed distributions (where the variable covers a broad range of scales) a very useful procedure is to take a width of the interval ds that is not the same for all s, but that is proportional to the scale, as $[s\ \ s + ds) = [s_o\ \ bs_o)$, $[bs_o\ \ b^2 s_o)$, $[b^k s_o\ \ b^{k+1} s_o)$, i.e., $ds = (b-1)s$ (with $b > 1$). Given a value of s, the corresponding value of k that associates s with its bin is given by $k = \log_b(s\ \ s_o)$. Correspondingly, the optimum choice to assign a point to the interval $[s\ \ s + ds)$ is given by the value $\bar{b}s$. This procedure is referred to as logarithmic binning, because the intervals appear with fixed width in logarithmic scale (Hergarten, 2002). In this paper we have generally taken b 1 58, in such a way that $b^5 = 10$, providing 5 bins per order of magnitude.

As the distributions are estimated from a finite number of data, they display statistical fluctuations. The uncertainty characterizing these fluctuations is simply related to the density by

$$\frac{\sigma_P(s)}{P(s)} \quad \frac{1}{\overline{n(s)}}$$

where $\sigma_P(s)$ is the standard deviation of $P(s)$ (do not confound with the standard deviation of s). This is so because $n(s)$ can be considered a binomial variable (von Mises, 1964), and then, the ratio between its standard deviation and mean fulfills $\sigma_n(s)\ \ n(s)$ 1 $\overline{n(s)}$, with $n(s)\ N_s \ll 1$. As $P(s)$ is proportional to $n(s)$, the same relation holds for its relative uncertainty.

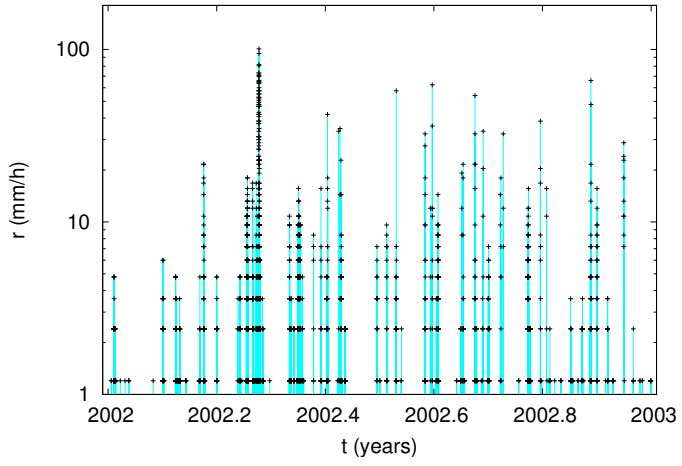

(a)

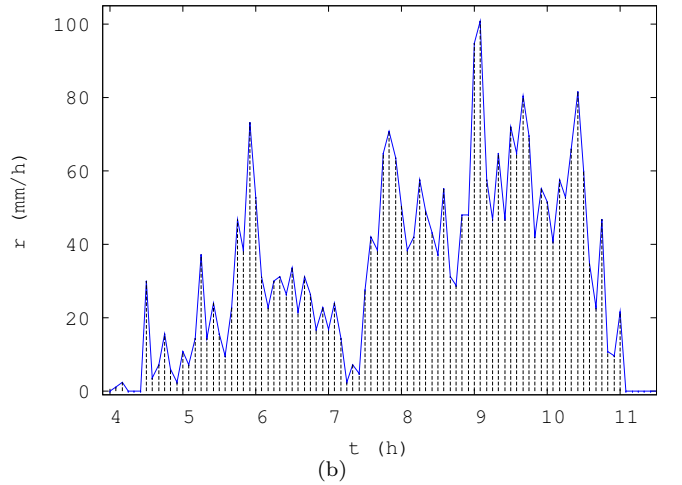

(b)

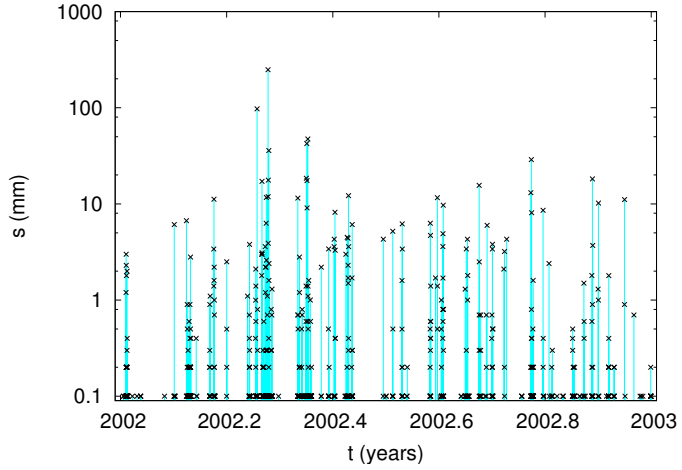

(c)

FIGURE 4.1: (a) Subset of the rain rate time series for site 17 (Muga) for year 2002. (b) More reduced subset of the rain rate time series for the same site, corresponding to the largest rain event on the record, with $s = 248\ 7$ mm, on April 11, 2002. Time refers to hours since midnight. A very small rain event is also present at the beginning, with $s = 0\ 3$ mm and separated to the main event by a dry spell of duration $q = 15$ min. (c) Corresponding event-size time series for the same site, for year 2002.

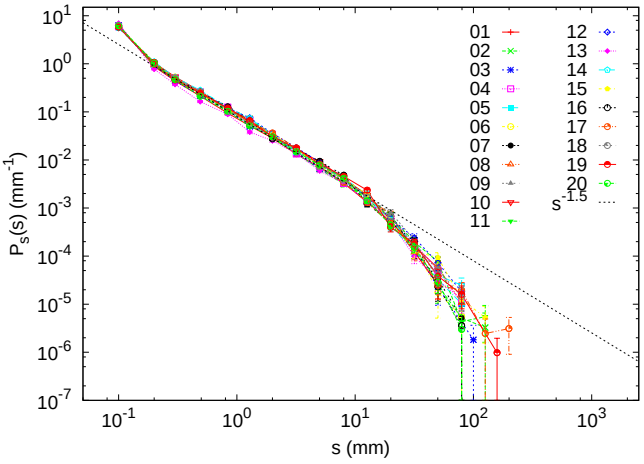

(a)

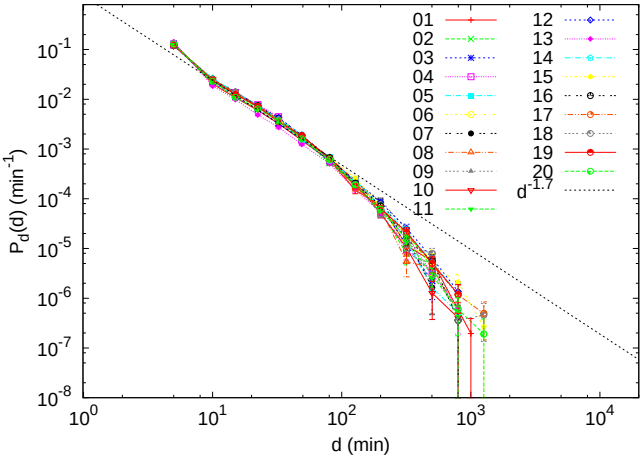

(b)

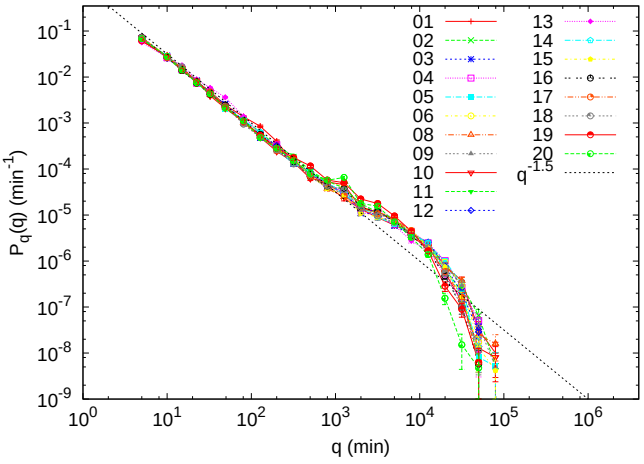

(c)

FIGURE 4.2: Probability densities for all the sites for the whole time covered by the record of: (a) Event sizes, (b) Event durations, and (c) Dry spells.

TABLE 4.2: Results of the power-law fitting and goodness-of-fit tests applied to event sizes, event durations, and dry-spell durations (in mm or in min), for the period of 9 and a half years specified in the main text. The table displays the minimum of the fitting range, s_{min}, and the ratio between the maximum and the minimum of the fitting range (logarithmic range, s_{max} s_{min}), total number of events, number of events in fitting range ($\bar{N}_s$, $\bar{N}_d$, and $\bar{N}_q$, for s, d, and q, respectively), and the power-law exponent with its uncertainty (one standard deviation) calculated as stated by Bauke (2007) and displayed between parenthesis as the variation of the last digit.

Site	s_{min}	$\frac{s_{max}}{s_{min}}$	N_s	$\bar{N}_s$	θ_s	d_{min}	$\frac{d_{max}}{d_{min}}$	$\bar{N}_d$	θ_d	q_{min}	$\frac{q_{max}}{q_{min}}$	N_q	$\bar{N}_q$	θ_q
1	0.2	180.5	5393	1886	1.54(2)	10	10.0	1668	1.67(4)	95	7.8	5387	743	1.75(7)
2	0.2	4.5	5236	1323	1.64(6)	10	4.0	1581	1.60(6)	5	273.0	5231	4729	1.46(1)
3	0.2	155.5	5749	2111	1.53(2)	10	6.0	1726	1.66(5)	10	80.0	5745	3207	1.53(2)
4	0.2	12.0	5108	1745	1.43(3)	10	3.5	1564	1.41(7)	5	196.0	5103	4520	1.47(1)
5	0.2	140.0	5289	2106	1.52(2)	10	3.5	1530	1.58(7)	20	47.3	5287	1706	1.45(2)
6	0.2	68.0	4924	1969	1.49(2)	10	3.5	1441	1.59(7)	20	31.3	4926	1537	1.47(3)
7	0.2	105.5	5219	2234	1.51(2)	10	3.5	1621	1.51(7)	5	256.0	5215	4734	1.51(1)
8	0.2	213.0	5112	2047	1.53(2)	10	4.0	1567	1.55(6)	15	65.0	5107	2098	1.50(2)
9	0.2	5.0	5366	1459	1.53(5)	10	4.0	1658	1.51(6)	10	90.0	5419	2889	1.55(2)
10	0.2	19.0	6691	2452	1.51(2)	10	3.5	2066	1.57(6)	25	33.0	6685	1758	1.48(3)
11	0.2	65.0	6224	2373	1.49(2)	10	5.0	1932	1.56(5)	45	468.3	6219	2005	1.24(1)
12	0.2	4.0	5967	1500	1.53(6)	10	4.0	1889	1.49(6)	5	235.0	5961	5376	1.47(1)
13	0.3	66.7	8330	1853	1.45(2)	10	12.5	2288	1.74(3)	130	158.5	8328	1501	1.27(2)
14	0.2	3.5	6525	1711	1.56(6)	10	5.0	2299	1.62(4)	5	215.0	6520	5906	1.47(1)
15	0.3	3.7	6485	1102	1.39(7)	10	5.0	2095	1.64(5)	15	49.7	6479	2560	1.51(2)
16	0.2	3.5	7491	1852	1.59(5)	10	4.0	2385	1.59(5)	5	214.0	7510	6789	1.50(1)
17	0.2	80.5	6962	2853	1.52(2)	10	3.5	2087	1.60(6)	10	68.5	6958	3719	1.52(1)
18	0.2	41.5	7511	2847	1.51(2)	10	3.5	2238	1.57(6)	20	31.0	7507	2302	1.53(2)
19	0.2	99.5	6767	2742	1.47(2)	10	3.5	1958	1.60(6)	50	21.7	6800	1378	1.26(3)
20	0.2	3.5	9012	2047	1.69(5)	10	8.5	2972	1.66(3)	15	34.3	9007	3367	1.50(2)

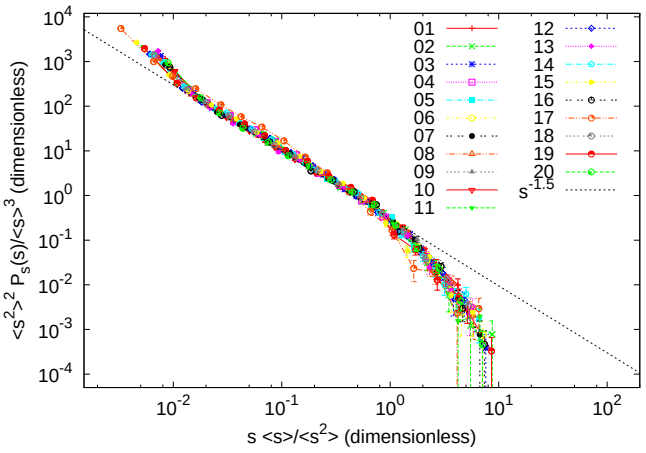

(a)

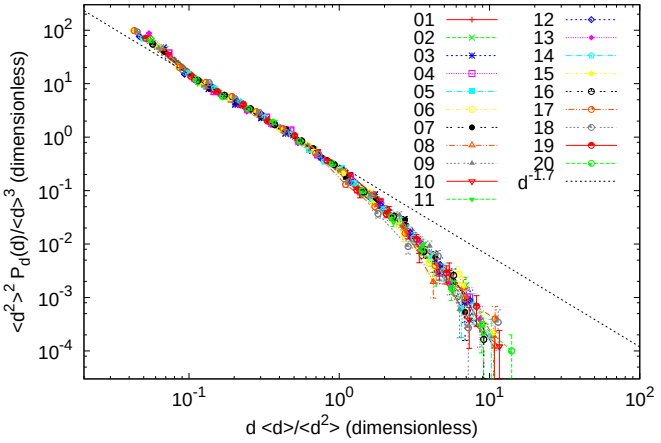

(b)

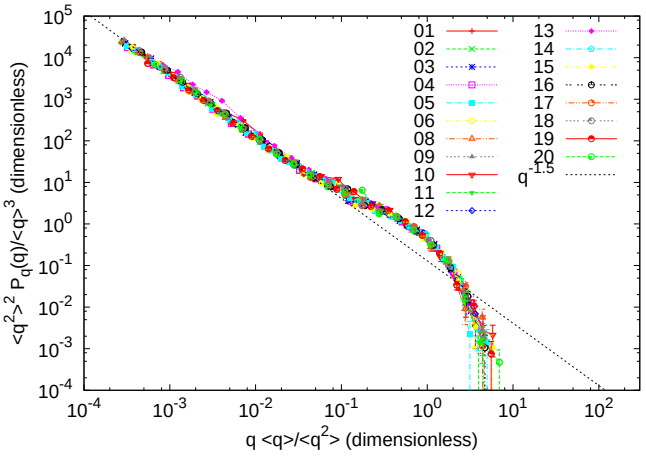

(c)

FIGURE 4.3: Collapse of the probability densities for all the sites for the whole time covered by the record of: (a) Event sizes, (b) Event durations, and (c) Dry spells. Rescaling is performed using the first and second moment of each distribution, following Eq. (4.5).

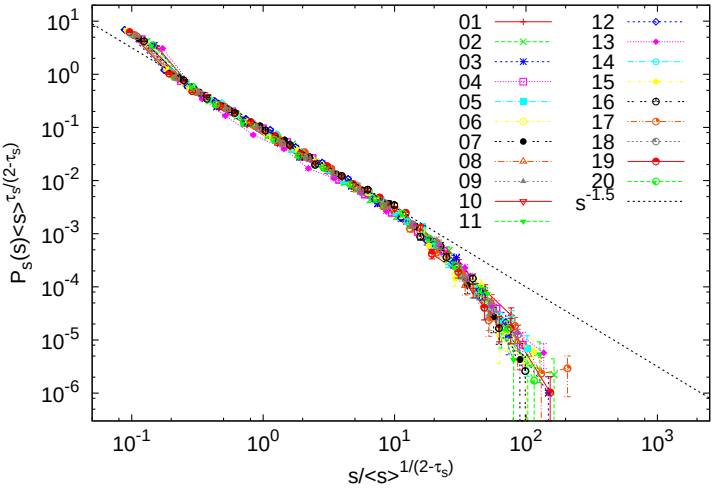

(a)

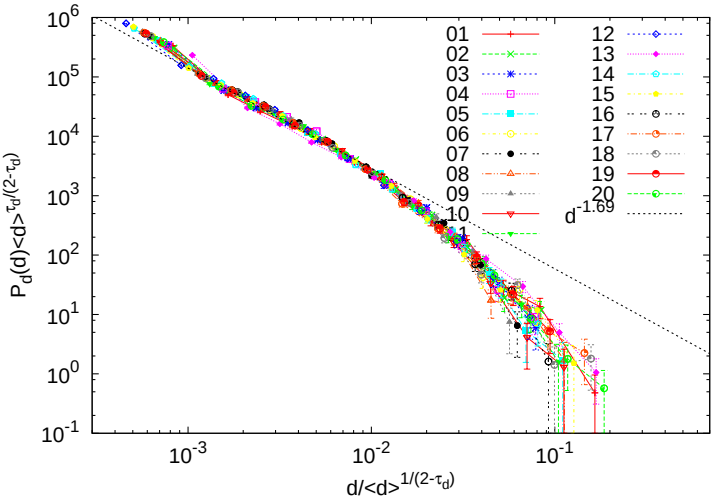

(b)

FIGURE 4.4: Collapse of the probability densities for all the sites for the whole time covered by the record of: (a) Event sizes and (b) Event durations; rescaled using Eq. (4.6) with the exponents: $\theta_s = 1\ 52$ and $\theta_d = 1\ 69$, determined minimizing the Euclidean distance between parametrically collapsed distributions. Units are mm or min to the corresponding powers appearing in the axes.

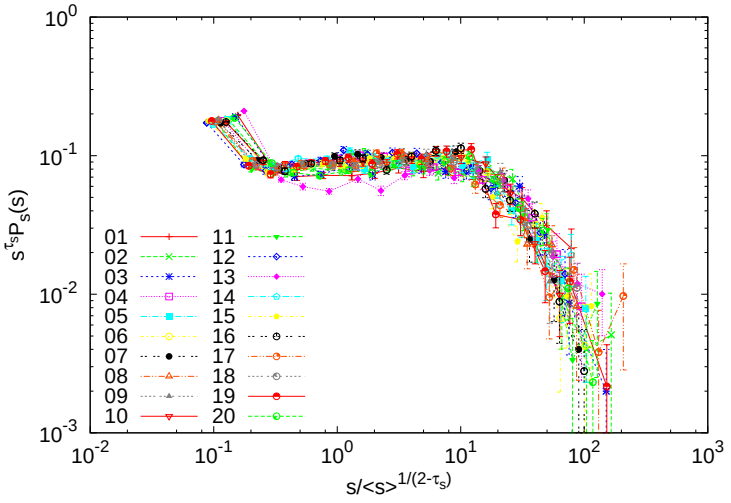

(a)

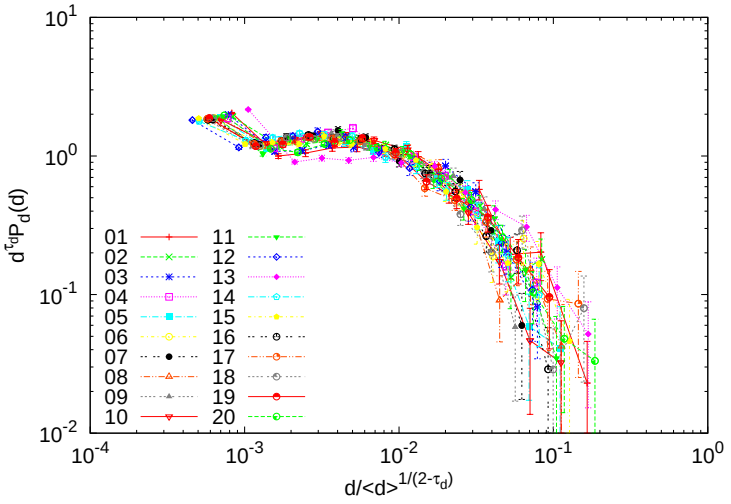

(b)

FIGURE 4.5: Inferred scaling functions $\mathcal{G}_s$ and $\mathcal{G}_d$ corresponding to the rescaled distributions of s and d in Figure 4.4, multiplied by s^{τ_s} and d^{τ_d}. Units in the abscissae are as in the previous plot, whereas in the ordinates these are mm^{τ_s-1} and min^{τ_d-1}.

Chapter 5

Testing Universality in Critical Exponents: the Case of Rainfall

This chapter corresponds to unpublished work, related to the non-peer-review publication that can be found in Appendix A.

Abstract One of the key clues to consider rainfall as a self-organized critical phenomenon is the existence of power-law distributions for rain-event sizes. We have studied the problem of universality in the exponents of these distributions by means of a suitable statistic whose distribution is inferred by several variations of a permutational test. In contrast to more common approaches, our procedure does not suffer from the difficulties of multiple testing and does not require the precise knowledge of the uncertainties associated to the exponents. When applied to seven sites monitored by the Atmospheric Radiation Measurement Program the tests lead to the rejection of the universality hypothesis, despite the fact that the exponents are rather close to each other.

5.1 Introduction

The concept of universality is one of the most striking features of the theory of critical phenomena (Yeomans, 1992), giving sense to the extended use of modelling in statistical physics. Strictly, it would mean that using a naive model one could derive all the critical exponents and scaling functions of any real system displaying a second order phase transition, no matter the complications of the interactions in the system, because critical exponents and scaling functions should be *universal*. In practice, the name universality is somewhat pretentious (Stanley, 1999), and what one instead obtains are several *universality classes*, which are sets of systems sharing the same behaviour

(in terms of critical exponents and scaling functions), depending only, in equilibrium and for systems with short-range interactions, on the dimensionality of space and the symmetry of the order parameter. This is in sharp contrast with the behaviour of other important properties, as for instance the critical temperature, justifying the perplexity for the universality phenomenon.

The classification of many disparate systems into a relatively reduced number of universality classes is therefore a fundamental problem (analogous somehow to the construction of the Mendeleev s periodic table (Stanley, 1999)), which relies on the accurate determination of critical exponents and scaling functions. A weaker form of universality considers only the coincidence of the critical exponents, disregarding the scaling functions. This is due, when dealing with experimental or numerical data, to the fact that critical exponents can be obtained directly as a single number each one, whereas scaling functions need to be parametrized (which introduces some degree of arbitrariness in the parametrization); otherwise, scaling functions need to be obtained from the analytical solution of a model.

Among all the different critical exponents, an important subset are those arising from probability distributions, such as cluster number densities, avalanche size distributions, etc. (Christensen and Moloney, 2005, Stauffer and Aharony, 1994). In this case, the probability mass function or the probability density $f(s)$ of the variable s can be written, at least for large s, as

$$f(s) = s^{-\tau} G(s \;\; s_c) \tag{5.1}$$

where s_c is a characteristic value of s and G is a scaling function that can be an exponential or any other function going to a constant for small s and decaying very fast for large s. Close to the critical point and in the infinite system-size limit, s_c diverges, G tends to a constant, $f(s)$ becomes a power law, and θ emerges as a genuine critical exponent.

Similar situations arise outside critical phenomena; for instance, in anomalous diffusion, the long-term behavior of a diffusion process (with short-range correlations) can be classified within a continuous of universality classes defined by the Lévy-stable laws, characterized by power-law tails (Bouchaud and Georges, 1990). Although the behavior of the system is not governed by a continuous phase transition, it is possible to understand it from the existence of a fixed point in some renormalization-group transformation equations. Other stochastic processes lead to analogous situations (Corral, 2009a, Gyorgyi et al., 2008).

The determination of critical exponents is not an easy task, even more difficult when they are the exponents of power-law distributions. Very recently, considerable attention

has been devoted to the proper fit of such distributions, together with the subsequent goodness-of-fit testing. White et al. and Clauset et al. (among others) (Clauset et al., 2009, White et al., 2008) mention the systematic errors that can arise from using the least-square linear regression method applied to $\ln f(s)$ as a function of $\ln s$, although the alternative recipe proposed by Clauset et al. to find the most suitable power-law range has been found to perform badly in some cases (Corral et al., 2011), so somewhat different methods have been suggested by other authors (Deluca and Corral, 2013b, Peters et al., 2010).

But determining the critical exponents as accurately and unbiasedly as possible, together with their associated uncertainties, is not the end of the story if one is looking for universality. The exponents need to be properly compared, in order to test if they are statistically compatible with each other or not. From a more practical point of view, if universality does not hold, one may monitor some process by the changes in the value of some power-law exponent, which can play the role of a precursor of catastrophic failure (see citations at Ref. (Baró et al., 2013)).

The subject of this paper is to develop a systematic procedure to compare critical exponents, applying it to study in detail a non-equilibrium problem: that of universality in rain-event size distributions, which is important to characterize rainfall as a self-organized critical phenomena (Bak, 1996, Christensen and Moloney, 2005). These distributions were first analyzed for one single location in the Baltic coast by Peters et al. (Peters and Christensen, 2002, Peters et al., 2002), who reported a power-law distribution with an exponent θ around 1.4. More recently, Ref. (Peters et al., 2010) widened the study to 10 sites around the globe; after discarding 3 of them due to different instrumentally induced biases and errors, not only the power-law hypothesis was confirmed but also the scaling form of the distribution, Eq. (5.1), with rather smaller exponents, ranging from $\theta = 1\,14$ to 1.19. However, a proper statistical test to decide if the exponents were compatible with a unique value or not was not attempted. This is what we undertake here, extending the study in order to include new data and new sites. In the following section we introduce the rain data, the definition of rain events, and the precise way of fitting the power-law exponents. Next, we explain some naive ways of compare the values of the exponents. Section IV is devoted to the development of a simple permutational test in order to test the universality of the exponents for the rain data of Ref. (Peters et al., 2010), whereas in Sec. V this test is improved.

5.2 Data, rain events, and power-law fitting

As in Ref. (Peters et al., 2010), we analyze rain data from the Atmospheric Radiation Measurement (ARM) Program (www.arm.gov). The ARM rain database presents the advantage of its homogeneity in the sense that all sites are equipped with the same type of pluviometer, an optical rain gauge from MiniOrg (Optical Scientific, Inc.), Model ORG-815-DA. Rain rate is recorded with a one-minute temporal resolution, with a minimum value of 0.001 mm/hour, but we disregard rain rates below 0.2 mm/hour (i.e., we treat them as zero), as recommended by the ARM Handbook. Other corrections were applied to the data using the ARM Data Quality Reports (dat).

In order to compare with the results of Ref. (Peters et al., 2010), we consider the same sites studied there, excepting the 3 sites that those authors found problematic (North Slope of Alaska, Point Reyes, and Southern Great Plains, all 3 in USA); this yields a remainder of M=7 sites, see Table 5.1. For some of these sites (Manus, Nauru, Darwin, and Graciosa) new data are available since the study of Ref. (Peters et al., 2010), so our database has been updated accordingly. The rest of the sites (Niamey, Heselbach, and Shouxian) remain essentially the same, except perhaps little operational errors reported since then.

TABLE 5.1: ARM observation sites with corresponding starting and ending times and location. I. stands for island.

Site	start time	end time	latitude	longitude
Manus I., Papua New Guinea	2005/02/15	2012/03/18	2.116°S	147.425°E
Nauru I., Nauru Republic	2005/02/15	2012/03/18	0.521°S	166.916°E
Darwin, Australia	2005/02/15	2012/03/18	12.425°S	130.892°E
Niamey, Niger	2005/12/26	2006/12/08	13.522°N	2.632°E
Heselbach, Germany	2007/04/01	2008/01/01	48.450°N	8.397°E
Shouxian, China	2008/05/09	2008/12/28	32.558°N	116.482°E
Graciosa I., Azores, Portugal	2009/04/14	2011/01/06	39.091°N	28.029°E

The fundamental concept in this kind of approaches is the rain event, which is defined as a sequence of rain-rate values all above a certain threshold (starting and ending below threshold) (Andrade et al., 1998, Peters and Christensen, 2002, Peters et al., 2002); in our study the threshold is set to 0.2 mm/hour (Peters et al., 2010). The size s of the event is the total amount of rain collected during the lifetime of the event, i.e., the time integral of the rain rate along event duration. A large record of rainfall contains enough events to estimate the probability density of the rain-event size, $f(s)$, and, independently, to test if this distribution follows a power law or not.

The key to fit properly power-law distributions to real-world data is to have an objective criterion to decide at which point the power law starts and (in the truncated case) at

which point it ends; these cut-offs define the fitting range. This is so because incompleteness of the data for very small sizes and finite-size effects for large sizes lead to considerable deviations from a power-law regime. As a fitting method we essentially use the improvement and extension of the Clauset et al. s method (Clauset et al., 2009) introduced in Ref. (Peters et al., 2010) and explained in much detail elsewhere (Deluca and Corral, 2013b). Summarizing, all fitting ranges are considered, and among those which yield acceptable fits (high enough $p-$values), the one containing more data points (i.e., more events) is selected.

Fitting is performed by maximum likelihood estimation, goodness of fit is tested by the Kolmogorov-Smirnov distance, and the $p-$value of the fit is computed from Monte Carlo simulations. To look for the fitting range we sweep 20 values per order of magnitude (equidistant in logscale) of the small-size and large-size cut-offs. We consider a fit as acceptable (or not rejectable) if $p > 0\,10$, which is computed with 300 Monte Carlo realizations. Provided that we find at least one non-rejectable fit, for each site i we end up with three optimized values: one is the estimated exponent θ_i and the other two, a_i and b_i (the small-size and large-size cut-offs), define the fitting range $a_i \leq s \leq b_i$ for which the power-law fit holds. The uncertainty in the exponent is quantified by the standard deviation of the maximum likelihood estimation, calculated using the jackknife procedure (the formula of Ref. (Aban et al., 2006) and our Monte Carlo simulations are in agreement with this method). Results of the fits for the rain-event size distributions are shown in Table 5.2.

As a first trial, in order to simplify the comparison between the different sites, we decide to consider the common range over which all distributions are power laws. We define then $a = \max_i a_i$ and $b = \min_i b_i$ (verifying that $a \ll b$); then, new exponents θ_i are recalculated for this common range by maximum likelihood estimation. The estimated power-law fittings will be given then by

$$f_i(s) \quad \frac{1}{s^{\tau_i}} \quad \text{for } a \leq s \leq b \tag{5.2}$$

The resulting exponents will be different but very close to the previous ones (within the expected fluctuations), see Table 5.2. Nevertheless, the $p-$value for the new fits may change, even being possible that some of them drop below the acceptance threshold. This is what naturally happens in goodness-of-fit testing (as the null hypothesis may be rejected even when it is true). We do not need to do anything in this regard, just the reader must be aware of it.

TABLE 5.2: Results of power-law fits for the 7 sites studied in Ref. (Peters et al., 2010) (with updated data). The total number of rain events (for $0 < s <$) is N_i. The resulting optimum cut-offs a_i and b_i are displayed, in mm, together with the resulting number of events in fitting range $\bar{n}_i$ and exponent θ_i. When the fits are restricted to the common range, $a = 0\,0071$ mm and $b = 0\,501$ mm, the new number of events and power-law exponents are n_i and θ_i. The quantity in parenthesis is the standard deviation of the exponents in units of the last significant digit of the exponent.

Site i	N_i	a_i	b_i	$b_i\ a_i$	$\bar{n}_i$	θ_i	n_i	θ_i
1. Manus	15725	0.0071	10.0	1413	11910	1.152(05)	8455	1.151(09)
2. Nauru	8404	0.0063	3.2	501	6350	1.120(07)	4831	1.122(12)
3. Darwin	5216	0.0063	3.5	562	3946	1.106(09)	2959	1.095(15)
4. Niamey	260	0.0040	56.2	14125	231	1.193(26)	135	1.231(72)
5. Heselbach	2437	0.0040	0.6	141	1844	1.132(16)	1569	1.149(21)
6. Shouxian	476	0.0040	1.3	316	372	1.165(32)	290	1.185(48)
7. Graciosa	4260	0.0071	0.5	71	2841	1.147(15)	2841	1.147(15)

5.3 Difficulties of multiple testing

Let us consider first the simple case in which one only has to decide if some exponent (or in general, some statistic) θ takes the same value or not in two different systems, 1 and 2. The null hypothesis is then $\theta_1 = \theta_2$. What one usually has is an estimation for each exponent, denoted as θ_i, with $i = 1\ 2$, together with an estimation of their standard deviations, which, if the number of data for each system is large, we can assume converges to the true standard deviation, σ_i.

Under the null hypothesis, the difference $d = \theta_1 - \theta_2$ will have zero mean, and, if datasets 1 and 2 are independent samples (which will be the common situation if the two systems are unrelated), the standard deviation of the difference of the estimators will be $\sigma_d = \sqrt{\sigma_1^2 + \sigma_2^2}$. As, asymptotically, θ_1 and θ_2 are normally distributed (Aban et al., 2006), so will be their difference, and therefore it is straightforward to obtain a confidence interval for it. If the interval, centered at zero, includes the observed value of the difference, the null hypothesis cannot be rejected and the exponents can be considered to take the same value in both systems (which can belong then to the same universality class, at least regarding the exponent θ).

Observe that, although the test for the differences is well known, it is not in agreement with the somewhat extended practice of verifying if the confidence intervals of θ_1 and θ_2 overlap, which yields a smaller significance level (and is, then, less rigorous , or more permissive [1]). For instance, if we compare the exponents of the Manus and Darwin sites, the difference between them is $d = \theta_{Manus} - \theta_{Darwin} = 0\,055$ with standard deviation

[1] For instance, at a significance level of 5 % the uncertainty of $\hat{\tau}_i$ is given by $\pm z_c \sigma_i$, with $z_c = 1.96$. If $\sigma_1 = \sigma_2 = \sigma$, the probability of $|\hat{\tau}_1 - \hat{\tau}_2| > \sqrt{2}\sigma z_c$ is indeed $p(|z| > z_c) = 0.05$, but testing if $|\hat{\tau}_1 - \hat{\tau}_2| > 2\sigma z_c$ reduces drastically the significance level to $p(|z| > \sqrt{2} z_c) = 0.0066$.

TABLE 5.3: Difference between power-law exponents for the common fitting range. Uncertanty is evaluated as $1\,96\sigma_d$, corresponding to 5% significance level. Significant differences are underlined.

	Nauru	Darwin	Niamey	Heselbach	Shouxian	Graciosa
Manus	0.03±0.03	0.06±0.03	0.08±0.14	0.00±0.04	0.03±0.10	0.00±0.03
Nauru	-	0.03±0.04	0.11±0.14	0.03±0.05	0.06±0.10	0.02±0.04
Darwin	-	-	0.14±0.14	0.05±0.05	0.09±0.10	0.05±0.04
Niamey	-	-	-	0.08±0.15	0.05±0.17	0.08±0.14
Heselbach	-	-	-	-	0.04±0.10	0.00±0.05
Shouxian	-	-	-	-	-	0.04±0.10

$\sigma_d = \sqrt{\sigma^2_{Manus} + \sigma^2_{Darwin}} = 0\,0175$. Considering the $1\,96\sigma_d$ interval, we should reject the hypothesis that both exponents are the same, with a 95 % confidence.

But the situation is not so simple when one needs to analyze 3 or more systems. Taking the naive approach of comparing the overlap of the confidence intervals, some systems may lay outside the overlap region of the rest just by chance, which will be more likely as the number of systems increases. So, the rejection in the previous example could be caused by an unavoidable "bad luck", as those sites are just a part of a much larger collection of sites. Also, it might be difficult to define which is the overlap region, as there can be several subsets, or a continuous of overlapping subsets.

If we take all pairs of systems, this leads to $M(M-1)\ 2$ pair tests if there are M different systems. In our case, $M = 7$ and $M(M-1)\ 2 = 21$. Comparing the M exponents by pairs one can see from Table 5.3 that the null hypothesis would be rejected in 3 out of the 21 cases, at the 5% significance level. Are these rejections really significant? In order to avoid the rejection of the null hypothesis for a given test "by accident", one can apply some correction of the significance level, as the Bonferroni correction or the Šidák correction (Abdi, 2007, Bland and Altman, 1995). With a confidence level of 95 % we have a probability of rejecting the null hypothesis when it is true of $\alpha \equiv 1 - 0\,95 = 0\,05$ (this is indeed the significance level); so, sooner or later we will get large enough differences in the exponents, due to statistical fluctuations, if the number of tests is large enough. Therefore, the probability of at least one rejection in 21 independent tests is $1 - (1-\alpha)^{21} = 0\,67$, and we can consider this number as the global (or familywise) significance level, which turns out to be rather high.

The idea of the Šidák correction is to select α in such a way that the resulting global significance level is more reasonable, say 0.05; then, in our case, $\alpha = 1 - \sqrt[21]{1 - 0\,05} = 0\,0024$. For the Bonferroni correction one approximates $1 - (1-\alpha)^{21}$ $1 - (1 - 21\alpha) = 0\,05$, which leads in this case to essentially the same $\alpha = 0\,0024$. This has the advantage of not requiring the independence of the tests, providing a lower bound for the significance level. To achieve a confidence level of 99 76% with the normal

distribution it is necessary to consider a bit more than 3 standard deviations, this is $3\,036\ \sqrt{\sigma_w^2 + \sigma_l^2}$. In this case, all pairs of exponents seem to be compatible except one, corresponding to sites 1 and 3. These sites yield a difference between their exponents equal to $0\,055 \pm 0\,053$, which we can consider in the limit of rejection and makes the decission about the universality on the value of exponents a very critical issue.

However, the Bonferroni and Šidák corrections seem too generous (in order to claim for universality, or too conservative in order to detect differences). They reduce the type I error (false positive) at the cost of an enormeous increase of the type II error (false negative). We could explore a different approach. When the null hypothesis is true, the number of rejections of the null hypothesis in independent tests will be binomially distributed, and the probability of having x rejections in 21 tests will be

$$g(x) = \binom{21}{x} \alpha^x (1-\alpha)^{21-x} \tag{5.3}$$

This leads to the fact that the probability of getting 3 or more rejections (which is what we got at the 95 % confidence level, $\alpha = 0\,05$) is $1 - (g(0) + g(1) + g(2)) = 0\,085$, which seems somewhat small, but not small enough to reject the hypothesis of equality of exponents for all pairs. (Notice that the Šidák correction arises imposing that the probability of one or more rejections is $1 - g(0) = 0\,05$.) Nevertheless, the reasoning based on the binomial distribution is problematic, as there cannot be 21 independent tests with 7 datasets. Rather, the number of independest tests would be just 3; for instance, the first test could be between datasets 1 and 2, the second between 3 and 4, and the third between 5 and 6 (but of course there are other combinations...). Let us note that the dependence of the tests was not taken into account in Ref. (Lippiello et al., 2012).

5.4 Restricted permutational test

The purpose of the previous examples was to illustrate the difficulty of dealing with multiple testing. An additional problem is the identification of the standard deviation of the maximum likelihood exponent for fixed a_i and b_i with the true error of the exponent for the whole optimization process. We expect this error to be larger, but its precise value is hard to quantify. Instead of multiple testing, we propose an alternative track, using a permutational test, which avoids these drawbacks.

The null hypothesis H_0 is now that for the common range $a \leq s \leq b$ all exponents are the same, i.e., $\theta_i = \theta_j$, for all i and j (note that before we had $M(M-1)$ 2 null

hypotheses, one for each pair). What we need first is a statistic that quantifies the divergence between all the exponents, in such a way that the largest the value of the statistic, the stronger the evidence against the null hypothesis. In order to construct this statistic we may take a weigthed sum of $(\theta_i - \theta_j)^2$, or of $\theta_i - \theta_j$, for all i and j, or rather, the maximum of all the differences, max $_{ij}(\theta_i - \theta_j)$. The first option gives more weight to the most extreme differences than the option of taking instead the sum of the absolute values of the differences, but lest weight than the option of the maximum difference. So, the second power of the differences constitutes a compromise between the importance given to the extremes and the importance given to the central values. Our particular selection for the statistic is

$$\Theta = \sum_{i=1}^{M-1} \sum_{j=i+1}^{M} \frac{n_i n_j}{n_i + n_j} (\theta_i - \theta_j)^2 \tag{5.4}$$

where n_i is the number of data of site i in the common power-law range, $a \leq s \leq b$. When this statistic refer to the empirical data (and not to simulations) we will call it Θ_{data}.

The prefactor depending on n_i and n_j can be easily justified. Under the null hypothesis, and for independent datasets, each $\theta_i - \theta_j$ has zero mean and variance $\sigma_i^2 + \sigma_j^2$. But $\sigma_i \quad 1 \quad \overline{n_i}$, where the proportionality constant depends on the value of the exponent and on the fitting range (Aban et al., 2006). Therefore, for identical exponents and for a common fitting range, the expected value $(\theta_i - \theta_j)^2$ is proportional to 1 $n_i + 1$ n_j, and so, $n_i n_j$ $(n_i + n_j)$ $(\theta_i - \theta_j)^2$ is the same for all i and j, independently of the number of data n_i and n_j. Then, every term in Θ has the same expected value and contributes the same to the sum (on average). If we did not include the prefactor we would be giving more weight to the smallest datasets. On the contrary, if, for some reason, we wanted to give more weight to the largest datasets we could have taken $[n_i n_j \ (n_i + n_j)]^2$ as a prefactor, for example.

The scale for Θ is provided by the *achieved significance level* or $P-$value of the test, which is defined as the probability that, under the null hypothesis H_0, the random variable Θ is larger than the value we obtained for the observed data Θ_{data}, i.e.,

$$P = \text{Prob} \ \Theta \geq \Theta_{\text{data}} \quad H_0 \text{ is true} \tag{5.5}$$

so, the smaller the $P-$value, the stronger the evidence against H_0 (we use capital P in order to distinguish this $P-$value from the $p-$value of the power-law fit). Although each term in the sum of Θ follows a gamma distribution, with the same parameters, there is no easy way to compute the distribution of the sum, due to the fact that the terms

are not independent. That is, even if all datasets i j k, etc., are independent, the terms $(\theta_i - \theta_j)^2$, $(\theta_j - \theta_k)^2$, etc., are not.

Fisher s permutation test (Efron and Tibshirani, 1993) (also called randomization test) is a clever way to compute the $P-$value in cases like these. It is based on the idea that, if the null hypothesis is correct, any data value could correspond to any dataset and the data values (the size of the rain events in our case) are therefore interchangeable. In order to proceed with the test, we combine the $n_1 + n_2 + \quad + n_M$ observations from all the datasets into a single meta-dataset and take M random samples of sizes n_1, n_2, ..., n_M without replacement (this is done just by a permutation or reshuffling of the meta-dataset, and then taking consecutive n_i values). This generates M new datasets with the same number of data than the initial ones. Next we fit the power-law exponents (in the common fitting range) for each permuted or reshuffled dataset and from their values we compute the new test statistic $\Theta_{\rm sh}$, in the same way as for $\Theta_{\rm data}$ (sh stands for shuffled now). As the fitting range, given by a and b is fixed, the fit of the exponent is simple, using just maximum likelihood estimation. The distribution of the test statistic, under the null hypothesis, is obtained repeating the process a large enough number of times, $N_{\rm sh}$. In our case, we always take $N_{\rm sh} = 100$. With that we can compute easily an approximation of the $P-$value by

$$P - \text{value} \approx \frac{\#\ \Theta_{\rm sh} \geq \Theta_{\rm data}}{N_{\rm sh}} \tag{5.6}$$

where $\#\ \Theta_{\rm sh} \geq \Theta_{\rm data}$ is the number of permutations for which $\Theta_{\rm sh} \geq \Theta_{\rm data}$. For our $M = 7$ rain datasets we obtain $\Theta_{\rm data} = 30\ 3$, which, after the permutational procedure, leads to $P = 0\ 03$. So, at the 5% significance level, we reject the hypothesis that all the exponents take the same value and we cannot give statistical support to universality in rainfall.

5.5 Complete permutational test

One can realize that the previous procedure has at least one drawback. The choice of a common fitting range seems somewhat artificial, due to the fact that this range is optimum for some empirical dataset but not necessarily for any of the permutations, a fact that can introduce a bias in the procedure. In other words, the fit can be better for the true datasets than for the reshuffled ones, and in this way we are not treating the latter in the same way as the former. This is something that needs to be avoided; simulated or permuted data have to be treated in exactly the same way as the real data to avoid biases and artifacts (Clauset et al., 2009, Malmgren et al., 2008).

In order to proceed in the same way with the permuted data, we have to look, for each reshuffled dataset, for the most appropriate fitting range, and then select the common power-law range. Thus, we introduce a modification of the test in which we do not reshuffle the common part of the data in which all distributions are power law, but we reshuffle the whole data. That is, we aggregate the $N_1 + N_2 + \cdots + N_M$ data, where N_i is the total size of dataset i, and take random samples, without replacement, of size N_1, N_2, , N_M, and, we insist, we perform with these datasets in the same way as with the true data. Notice that in the previous subsection the null hypothesis was that, over a common range given by a and b, all the distributions were power laws with the same exponent. Now the null hypothesis is different, rather, we test if there exist a common range over which all the distributions are power laws with the same exponent, but we do not specify which is that common range.

The procedure is summarized as follows, for every permutation (with from 1 to $N_{\rm sh}$):

1. For each reshuffled data set $i = 1$ M calculate the values of $a_i^{(\ )}$ and $b_i^{(\ )}$ which lead to the largest number of data in a power law fitted in that range, provided that $p \geq 0$ 10. This is done by maximum likelihood estimation of the exponent plus the Kolmogorov-Smirnov test plus Monte Carlo simulations of a power law in the range $a_i^{(\ )} \leq s \leq b_i^{(\ )}$.

2. Select the common fitting range for the M reshuffled datasets, as $a^{(\ )} = \max_{\ i} a_i^{(\ )}$ and $b^{(\ )} = \min_{\ i} b_i^{(\ )}$ (and verify that $a^{(\ )} \ll b^{(\ )}$). This yields $n_i^{(\ )}$ events in the common power-law range for dataset i.

3. Calculate new exponents in the common fitting range, by maximum likelihood estimation. We call these exponents $\theta_i^{(\ )}$.

4. Calculate the test statistic $\Theta_{\rm sh}^{(\ )}$ (with a new definition, see Eq. (5.8) below).

And the same is repeated for every permutation. Then, the $P-$ value is calculated as in the previous case, Eq. (5.6).

Note that step 1, the most time consuming (due to the Monte Carlo simulations), was removed in the method of the previous section, as the common fitting range was the same in all permutations (obviously, step 2 was also unnecessary). This meant that only data inside the common fitting range had to be permuted. Now, we release such a restriction, and as a result, each collection of reshuffled datasets will lead to a different common fitting range. In this case, one has to take care in order to compare the test statistic Θ corresponding to the real data and the reshuffled data, as our previous definition did not take into account that different fitting ranges correspond to different variances of

$\theta_i - \theta_j$. Indeed, from Ref. (Aban et al., 2006) we know that the standard deviation of the estimation of the power-law exponent θ_i for the empirical data will be

$$\sigma_i = \frac{1}{\overline{n_i}} \left[\frac{1}{(\theta_i - 1)^2} - \frac{r^{\tau_i - 1} \ln^2 r}{(1 - r^{\tau_i - 1})^2} \right]^{-1\ 2} \tag{5.7}$$

with $r = a\ \ b$ and analogously for the reshuffled data, replacing θ_i by $\theta_i^{(\ )}$, r by $r^{(\ )} = a^{(\ )}\ \ b^{(\ )}$, and n_i by $n_i^{(\ )}$. Note that for the empirical data, the exponents of both methods, θ_i and θ_i, are the same, but not necessarily for the reshuffled data. The same happens for the number of events in the power-law regime and the resulting standard deviations, i.e., $n_i = n_i$ and $\sigma_i = \sigma_i$ (for the empirical data), but we need to distinguish $n_i^{(\ )}$ from $n_i^{(\ )}$ and $\sigma_i^{(\ )}$ from $\sigma_i^{(\ )}$ (for the permuted data).

In general, the larger the fitting range, the smaller r, and the smaller also σ_i (even if the number of data keeps constant). In order to compensate this fact, we define the test statistic as

$$\Theta = \sum_{i=1}^{M-1} \sum_{j=i+1}^{M} \frac{(\theta_i - \theta_j)^2}{(\sigma_i^2 + \sigma_j^2)} \tag{5.8}$$

where σ_i is the standard deviation of the exponent, calculated either from Eq. (5.7), from Monte Carlo simulations, or from the jackknife method (our particular choice). By dividing by the sum of the variances we do not only ensure that each pair of datasets contributes the same to the statistic (on average) but also that the statistic has the same average value for each permutation (under the null hypothesis). When the fitting range is fixed for all permutations, this statistic is essentially the same (except for a constant factor) as the one employed in the previous section, Eq. (5.4). Note nevertheless that, in contrast with the multiple testing explained before, the outcome of this test is not influenced by the size of the error bars associated to the exponents, i.e., we could duplicate the value of σ_i and the $P-$value of the test would not change. In other words, we just use the standard deviation as a scaling factor of the differences between the exponents. The results of this generalized test for the $M = 7$ data yield $\Theta_{\text{data}} = 44\ 8$ and $P = 0\ 04$; again, the null hypothesis of universality can be rejected at the 5% significance level.

5.6 Conclusions

We have developed permutational tests to deal with the universality or not of the critical exponents arising from power-law probability distributions. More common methods require the precise estimation of the uncertainty of the exponents, which is difficult for our sophisticated fitting and testing procedure of the value of the exponents Deluca and

Corral (2013b). Moreover, those common methods suffer from the difficulties of multiple testing, as for instance the artificially high values of the family-wise significance level and the non-independence of the tests.

Our alternative permutational tests give clear and unambiguous results: despite the fact that the differences between the exponents are rather small, the universality hypothesis is rejected, both for a extremely simple version of the permutational test and for a more complete implementation that avoids artificial biases in the procedure. It is worth mentioning also that for the original data analyzed in Ref. Peters et al. (2010) (which contains less events due to the shorter time span covered), the tests are not able to find deviations from universality. So, it is only when a critical amount of data is available that these deviations show up. This issue needs to be further investigated, but we can speculate that the deviations could arise from a lack of stationarity, due to long-term slight variations associated for instance with El Nino phenomenon or to seasonal fluctuations. At present, the number of data available is still small to shed light on this point. Finally, the fact that the universality hypothesis is rejected in the tests does not mean that one has to rule out the existence of a universal mechanism for atmospheric convection, as uncontrolled systematic errors can be present in the collection of data.

Chapter 6

Probabilistic Forecasting and The Effect of Thresholding

Many atmospheric processes related to precipitation have large scale correlations in time and space, which are the result of the coupling between several non-linear mechanisms with different temporal and spatial characteristic scales. Despite the diversity of individual rain events, a recent array of statistical measures presents surprising statistical regularities giving support to the hypothesis that atmospheric convection and precipitation may be a real-world example of Self-Organised Criticality (SOC) (Bak et al., 1987, Tang and Bak, 1988). The usual approach consists of looking at the occurrence of rain by days or months. For episodic rain events, similar to avalanches in cellular-automaton models, scale-free rain event distributions are found (Peters et al., 2002). However, a power-law distribution (i.e. scale-free) of the observable is not sufficient evidence for SOC dynamics, as there are many alternative mechanisms that give rise to such behaviour (see, for example, Dickman (2003), Mitzenmacher (2004)).

Further support for the SOC hypothesis was given by Peters and Neelin (2006), who found a relation between satellite estimates of rain rate and water vapour over the tropical oceans compatible with a phase transition, in which large parts of the troposphere would be in a convectively active phase. In addition, it was shown that the system was close to the transition point. They also related it to the concept of atmospheric quasi-equilibrium (Arakawa and Schubert, 1974), which argues that, since driven processes are generally slow compared to convection, the system should typically be in a far-from equilibrium statistically stationary state, where driving and dissipation are in balance. In addition, recent works have shown that local event size distributions present signs of universality in the system, as was expected in the SOC framework (Deluca and Corral, 2013a, Deluca et al., 2013, Peters et al., 2010). The resulting rain event size

distributions were found to be well approximated by power laws of similar exponents over broad ranges, with differences in the large-scale cutoffs of the distributions. The possible consequences of this framework for the prediction of atmospheric phenomena still remain unclear.

6.1 Data and Methods

In this contribution we use high-resolution (1 minute) local rain intensities across different climates described in Peters et al. (2010), stochastic convective models (Stechmann and Neelin, 2011) and SOC models such as the BTW model and the Manna model, for investigating how predictable the time series of rain activity and rain event sizes are (Bak et al., 1987, Manna, 1991).

We use the hazard function H_q as a decision variable, which is sensitive to clustering or repulsion between events in the time series. The conventional precursor pattern technique requires a large amount of data, does not capture long memory and has been found to perform worse than the hazard function in similar analysis (Bogachev et al., 2009). H_q is defined as the probability that a threshold-crossing event will occur in the next Δt, conditional on no previous event within the past t_w

$$H_q(t_w; \Delta t) = \frac{\int_{t_w}^{t_w+\Delta t} P_q(\tau)\mathrm{d}\tau}{\int_{t_w}^{\infty} P_q(\tau)\mathrm{d}\tau}, \tag{6.1}$$

where q corresponds to the different thresholds on sizes and Δt is set to 1 *min* for the rain data and one parallel update for the SOC models. The various quantities are illustrated in Figure 6.1.

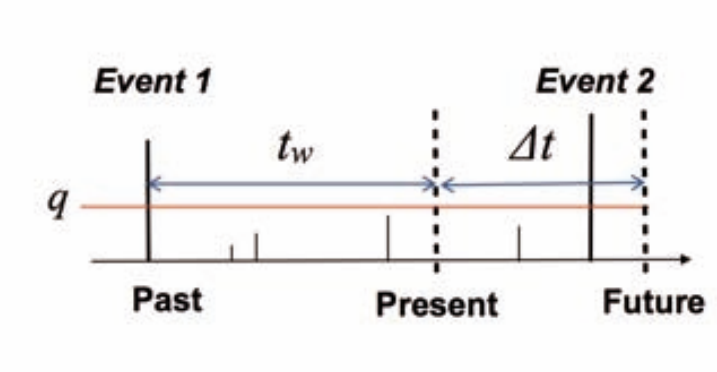

FIGURE 6.1: Sketch of the hazard function variables

Note that the hazard function gives us a probabilistic forecast and in order to perform a deterministic prediction we will need to consider a discrimination threshold.

We also evaluate the quality of the prediction with the receiver operating characteristics method (ROC) (Egan, 1975). For any binary prediction (occurrence or non-occurrence of an event) four possible outcomes can occur: true positive (TP), false positive (FP), true negative (TN) and false negative (FN), see Figure 6.2.

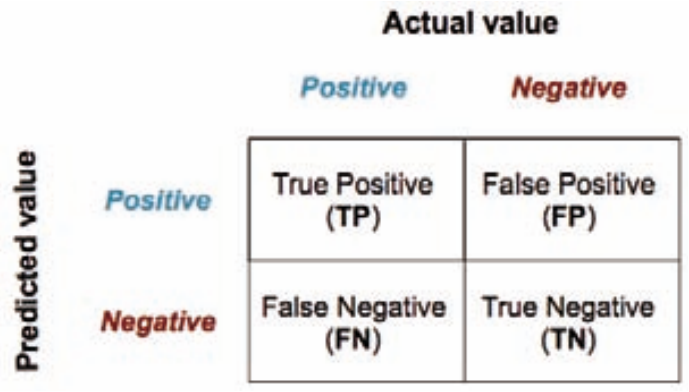

FIGURE 6.2: Four possible outcomes of a binary prediction in a contingency table.

ROC curves compare sensitivity and specificity. The sensitivity is defined as the number of correctly predicted occurrences divided by the total number of actual occurrences, and the specificity as the number of correctly predicted non-occurrences divided by the total number of actual non-occurrences,

$$\text{sensitivity} = \frac{\text{TP}}{\text{TP} + \text{FN}} \qquad \text{specificity} = \frac{\text{TN}}{\text{FP} + \text{TN}}. \tag{6.2}$$

Each threshold on the decision variable will give a different point on the ROC curve. If we consider the minimum possible threshold we will always predict the occurrence of an event, for which the sensitivity is one and the specificity zero. The diagonal in Figure 6.3 corresponds to random prediction. Points above the diagonal represent good predictions (better than random) and points below poor predictions.

6.2 Results

We find that on the events scale (slow time scale), rain data renormalise to a trivial Poisson point process for large thresholds, while for small thresholds events cluster. This is in contrast to the anti-clustering of high-threshold events in the 2D BTW model as a result of finite-size effects and the building up of correlations, seen previously by Garber et al. (2009) (see Figure 6.3(a) and Figure 6.3(b)).

However, rain data has an unavoidable threshold on intensity due to the device resolution that blurs the interpretation of the results on the event scale. At the level of intensities (slow time scale), we find that prediction is insensitive to all but very high thresholds.

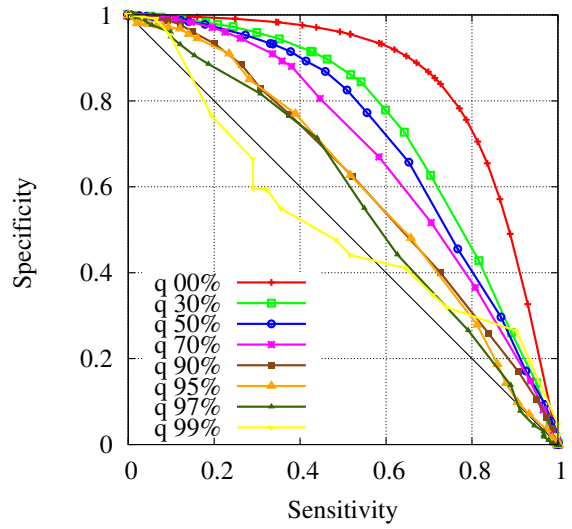

(a)

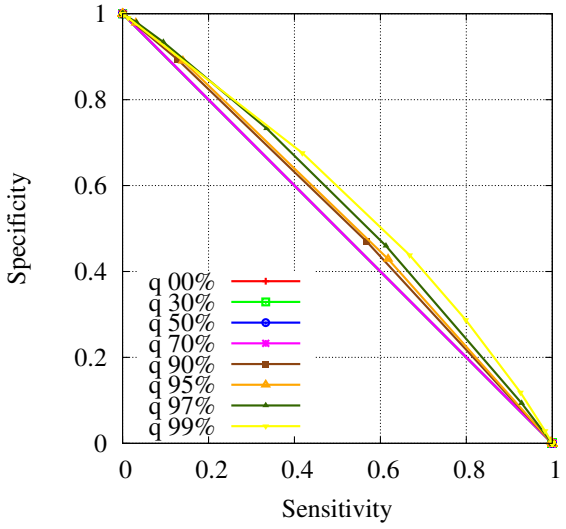

(b)

FIGURE 6.3: Example of ROC curves data on the slow time scale for rainfall data (a) and for the 2D BTW SOC Model simulated data (b).

Chapter 7

Summary, Conclusions and Expectations

The debate about the reliability of the big number of power-law claims found in the literature can only come to an end by advancing not only the current statistical methods for testing such hypothesis, but also by refining, improving and extending the theoretical framework that should support the mechanisms from which they emerge. These improved tests can also help to distinguish between different possible underlying mechanisms and to explore if the real-world data fulfil their particular expectations. This final chapter summarizes the results that this investigation has reached and outlines the perspectives of future work.

The focus of this thesis has been to investigate geophysical phenomena with a wide range of spatial and temporal scales, which present an emergent behaviour that manifests as scale-invariant distributions for the coarse-grained observables of the system. These phenomena occur in out-of-equilibrium slowly driven systems with fast dissipation mechanisms and a dynamical evolution controlled by local threshold-interactions.

First, in Chapters 2 and 3, statistical techniques have been developed for making accurate estimations of the parameters of power-law distributions, based on maximum likelihood methods, the Kolmogorov-Smirnov test and Monte Carlo simulations of the distributions. We have corrected important flaws of the work presented by Clauset et al. (2009), which has become already a standard reference with more than 600 cites up to now by indexed publications in the ISI web of Knowledge. We have also generalized the procedure for the case in which the power-law distribution has both a lower and an upper cutoff, case in which Clauset *et al.* s method is not applicable. The applicability of this new method is broad, including many types of truncated distributions.

In Chapter 2 (Deluca and Corral (2013b)) the fitting procedure has been explained in detail. Its performance has been checked using synthetic power-law datasets and previously reported power laws for different geophysical systems such as seismic moments (worldwide and in Southern California), energy dissipated by tropical cyclones, waiting times between earthquakes in different subdivisions of Southern California and half-lives of radionuclides, confirming previous positive results that were previously obtained by dubious methods. In addition, it has been tested for a negative case also giving the expected results: forest fires in Italy do not follow a power-law distribution.

In Chapter 3 (Peters et al. (2010)) the method has been applied for investigating the reproducibility of the observation of scale-free rain event avalanche distributions using data from different locations and looking for signs of universality in the associated fitted exponents. The rain event size distributions, measured with identical instruments in climatically different locations, have been found consistent with a single value of the exponent $\theta_s = 1\ 17(3)$. However, universality cannot be clearly verified from this analysis, because the statistical error in this estimate is too small. It does not take into account the whole procedure of the test, but just gives the error assuming that the range of the fit was previously known, and then we believe that the true systematic errors are larger. Although the exponents does not seem significantly different, climatological variations are reflected in the greater large-scale cut-off of the distributions for tropical measurements. Dry-spells durations have been found also to follow another power law with $\theta_s = 1\ 2(1)$, with regional differences also observed in the cutoff. Event durations present a broad distribution, but which is clearly no a power law.

After this, in Chapter 4 we have analysed data from Catalonia (NE Spain). In this case the temporal resolution was lower than in the study reported in Chapter 3, leading to higher uncertainties at the initial part of the distribution and then, to smaller power-law ranges. In addition, the data also presented a higher minimum rate measurement, which is found to have a non-trivial effect on the exponents values that are consistent with a single value of $\theta_s = 1\ 50(5)$, compatible with the values obtained in Peters et al. (2002). Dry-spells are found to follow power-law distribution with $\theta_d = 1\ 50(5)$ (called θ_q in this chapter), in some cases for more than 2 decades. Scaling techniques are applied in order to see the collapse of the distributions and also used for determining collective exponents, which are found consistent with the fitting method.

Determining the critical exponents and their uncertainties in an accurate and unbiased way is not enough for checking universality. Therefore, in Chapter 6, a method based on a permutation test has been developed in order to determine if the estimated exponents for the global database of rain (Chapter 3) are statistically compatible. Updating the available datasets the method is capable to see differences between the exponents.

Even so, the exponents that have been obtained are very similar, and although the test clearly rejects universality, this does not rule out the existence of an underlying common universal mechanism for deep convection. Further investigation is needed in order to determine the origin of the small discrepancies.

Finally, in Chapter 6 we have studied the effect of thresholding on SOC models, rain models and actual rain data. The predictability of extreme events and extreme intensities is studied by means of a decision variable sensitive to the tendency to cluster or repulse between them and its quality evaluated by the receiver operating characteristics method. On the events scale (large scale), times between events for rainfall data and models renormalise to a trivial point process, and then the predictability decreases when the threshold increases. Moreover, for small thresholds there is clustering between events. The opposite behaviour (anti-clustering) arises in simple SOC models due to finite-size effects and building up correlations as the threshold raises, which makes our results intriguing. However, these results are challenged by the fact that rain data has an unavoidable threshold on intensity due to the measuring device resolution. In the intensity picture (short scale), the prediction is not affected by the threshold, as the process remains mostly unchanged (also their critical corresponding exponents) until very high thresholds are reached.

7.1 Future work and perspectives

This thesis raises perspectives in three interrelated research lines: generalization of the current fitting methods for mixtures of power laws with other distributions; the development of a new theoretical framework for convection modelling able to reproduce the observed behaviour, as well as increasing empirical evidence supporting the connection between SOC and deep convection; and studies on consequences on the predictability of events in SOC-like systems.

7.1.1 Fitting and testing

A complete investigation about the reasons of when and why Clauset *et al.* s method (2009) fails is needed. This analysis may answer if alternatives to the KS-distance could be useful in order to the deal with the limitations of their approach.

Our method can be very easily extended to fit other long-tailed distributions, which are usually alternatives to the power-law distribution, such as the log-normal distribution. Likelihood-ratio tests can be used to determine the best statistical model for each

particular case. A nice alternative to that is to use a more general distribution that depending on their parameters can be one or the other, such as the Full-Tails Gamma distribution (del Castillo et al., 2012).

On the other hand, there is a clear limitation of our approach that should be taken into account. Why just fit the power law range of the distribution? Truncated power laws are justified in some contexts, but not in general. Many geophysical data sets used in this thesis present finite size effects at the tail of the distribution and lack of data for small values. But this is not the case in general, and then, the development of methods for proper and accurate fitting of mixtures of power laws with other distributions is an important task for the future.

Also, it would be interesting to develop of a statistical framework for detection of changes on the statistical behaviour of key variables of a given system, for example detecting universality classes shifts. The potential applicability of this is very broad, including detection of climate change, identification of different kind of convection, or for detecting the onset of financial crises.

7.1.2 Rainfall and convection

In particular, this thesis has contributed to recent observational studies that have shown strong, although not definitive, evidence in support of criticality in the transition to active deep convection. However, the number of studies is still limited and alternative non-critical mechanisms may also explain the observations. A new theoretical framework for convection modelling able to reproduce the observed behaviour is sorely needed. However, although the SOC hypothesis is fully compatible with observational analyses conducted so far, alternative explanations for the observed behaviours are also possible, as commented in Section 1.5.3. Thus, there remains a need to delve further into the observations.

The observation of scale-free rainfall event sizes suggests the presence of long-range correlations in the system. Direct measurements of the behaviour of the correlation function for the precipitation field under changes of the (much more slowly varying) background fields of water vapour and temperature are desirable to clarify whether the long range correlation is a consequence of the flow field, of the proximity to a critical point, or of a combination of both.

Moreover, there has been little work to date in assessing whether observational features consistent with criticality can be reproduced using cloud-resolving models (CRMs), in which convection is modelled explicitly rather than being parametrized. If so, this could

offer valuable insights by allowing a systematic investigation into the key dynamical mechanisms responsible for such behaviour. If not, this would raise important questions about the interpretation of observations, and also about the possibility of important missing processes in the cloud models.

The construction of simple models can help to elucidate important underlying mechanisms. Different alternatives can be discriminated by comparing them with observational results. Thus, for the near future, it is very important to build a critical stochastic model with extended interaction of convective plumes, able to reproduce the observed patterns, controlled by local threshold-interactions between plumes (SOC-like), see Figure 7.1. This would be a simplified model which could be tested in an idealized setting, with a view towards understanding how to build the essential critical mechanisms into future parametrizations of convection.

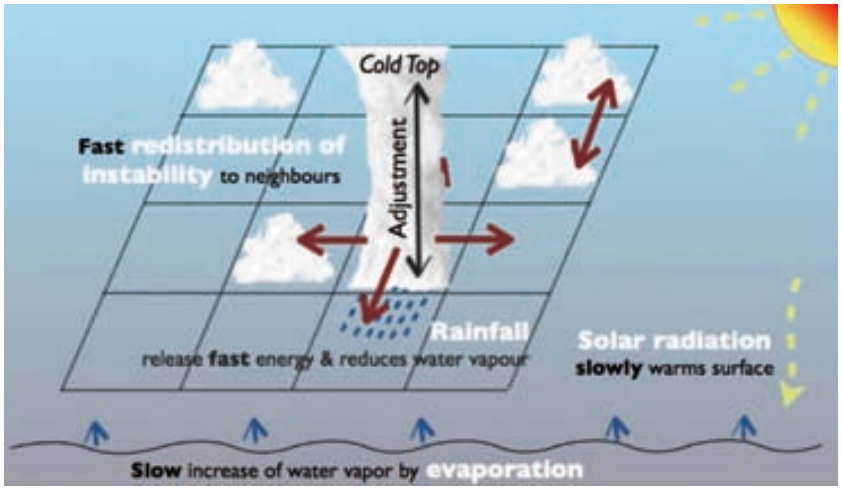

FIGURE 7.1: Simplified sketch of a hypothetical cellular automaton model controlled by local-threshold spatial interactions between convective plumes.

The development of a fundamental critical model that can lead to the observed critical behaviour is a difficult challenge that holds much promise for both Critical Phenomena and Atmospheric Sciences. Very little has been done along these lines. To the best of our knowledge, there have not been any published attempts. A Master's thesis from the University of Reading represents an interesting but preliminary attempt at addressing this problem (Jordan, 2008). Moreover, a simple stochastic model has been designed by Stechmann and Neelin (2011), which was able to reproduce various statistical empirical measures. However, the authors make clear that the criticality was introduced ad-hoc into their model, and it therefore cannot answer how and why the criticality arises.

This representation aims to develop the fundamental statistical theory. Significantly, such an approach can be interfaced with stochastic convective parametrizations that will have an impact on more complicated and realistic parametrizations suitable for

Global Circulation or Numerical Weather Prediction models (Bengtsson et al., 2013, Plant, 2012, Ragone et al., 2013). Some prototype models based on cellular automaton ideas have been recently developed but none of them have been suitably developed to reproduce the temporal and spatial critical patterns observed (e.g. Khouider et al., 2003, 2010, Plant, 2012).

7.1.3 Thesholding, predictability and SOC

Indirect thresholding given by the measurement resolutions is present almost in any real-world data set and the effects of it should not be underestimated. Moreover, applying thresholds is needed for studying large events, which are crucial for the modelling of man geophysical processes, as they are the events that have the largest impact in societies (floods, high-magnitude earthquakes, solar flares, *etc.*).

From a theoretical point of view, it has been seen that thresholding, on the intensity scale or on the event scale, has a non-trivial effect in SOC models time series. A deep study of this effects on mean-field limit of SOC models can help to have a better understanding of the thresholding process. This is connected to the study of correlations in time and space and has been seen to have a big impact in the possibilities of using them in order to make stochastic forecasting of the time series.

Chapter 8

Main Publications

The next list of peer-review accepted publications that constitute the main part of this thesis.

[A] O. Peters, A. Deluca, A. Corral, J. D. Neelin and C. E. Holloway, ***Universality of rain event size distributions***, Journal of Statistical Mechanics: Theory and Experiment. P11030, (2010).

[B] A. Deluca and A. Corral, ***Fitting and goodness-of-fit test of non-truncated and truncated power-law distributions***, Acta Geophys., (2013).

VERSITA

Acta Geophysica
vol. 61, no. 6, Dec. 2013, pp. 1351-1394
DOI: 10.2478/s11600-013-0154-9

Fitting and Goodness-of-Fit Test of Non-Truncated and Truncated Power-Law Distributions

Anna DELUCA and Álvaro CORRAL

Centre de Recerca Matemàtica, Edifici C, Bellaterra, Barcelona, Spain

Departament de Matemàtiques, Universitat Autònoma de Barcelona, Cerdanyola, Spain
e-mails: ADeluca@crm.cat, ACorral@crm.cat

Abstract

Recently, Clauset, Shalizi, and Newman have proposed a systematic method to find over which range (if any) a certain distribution behaves as a power law. However, their method has been found to fail, in the sense that true (simulated) power-law tails are not recognized as such in some instances, and then the power-law hypothesis is rejected. Moreover, the method does not work well when extended to power-law distributions with an upper truncation. We explain in detail a similar but alternative procedure, valid for truncated as well as for non-truncated power-law distributions, based in maximum likelihood estimation, the Kolmogorov–Smirnov goodness-of-fit test, and Monte Carlo simulations. An overview of the main concepts as well as a recipe for their practical implementation is provided. The performance of our method is put to test on several empirical data which were previously analyzed with less systematic approaches. We find the functioning of the method very satisfactory.

Key words: power-law distribution estimation, goodness-of-fit tests, binning, seismic-moment distribution, waiting-time distribution, tropical-cyclone energy.

1. INTRODUCTION

Over the last decades, the importance of power-law distributions has continuously increased, not only in geoscience but also elsewhere (Johnson *et al.* 1994). These are probability distributions defined by a probability density (for a continuous variable x) or by a probability mass function (for a discrete variable x) given by

$$f(x) \propto \frac{1}{x^{\alpha}} , \tag{1}$$

for $x \geq a$ and $a > 0$, with a normalization factor (hidden in the proportionality symbol $\propto$) which depends on whether x is continuous or discrete. In any case, normalization implies $\alpha > 1$. Sometimes power-law distributions are also called Pareto distributions (Evans *et al.* 2000, Johnson *et al.* 1994) or Riemann zeta distributions in the discrete case (Johnson *et al.* 2005), although in other contexts the name Pareto is associated to a slightly different distribution (Johnson *et al.* 1994). So we stick to the clearer term of power-law distribution.

These have remarkable, non-usual statistical properties, as are scale invariance and divergence of moments. The first one means that power-law functions (defined between 0 and ∞) are invariant under (properly performed) linear rescaling of axes (both x and f) and therefore have no characteristic scale, and hence cannot be used to define a prototype of the observable represented by x (Christensen and Moloney 2005, Corral 2008, Newman 2005, Takayasu 1990). For example, no unit of distance can be defined from the gravitational field of a point mass (a power law), whereas a time unit can be defined for radioactive decay (an exponential function). However, as power-law distributions cannot be defined for all $x > 0$ but for $x \geq a > 0$, their scale invariance is not "complete" or strict.

A second uncommon property is the non-existence of finite moments; for instance, if $\alpha \leq 2$ not a single finite moment exists (no mean, no variance, *etc.*). This has important consequences, as the law of large numbers does not hold (Kolmogorov 1956, p. 65), *i.e.*, the mean of a sample does not converge to a finite value as the size of the sample increases; rather, the sample mean tends to infinite (Shiryaev 1996, p. 393). If $2 < \alpha \leq 3$ the mean exists and is finite, but higher moments are infinite, which means, for instance, that the central limit theorem, in its classic formulation, does not apply (the mean of a sample is not normally distributed and has infinite standard deviation) (Bouchaud and Georges 1990). Higher α's yield higher-order moments infinite, but then the situation is not so "critical". Newman reviews other peculiar properties of power-law distributions, such as the 80|20 rule (Newman 2005).

Although the normal (or Gaussian) distribution gives a non-zero probability that a human being is 10 m or 10 km tall, the definition of the probability density up to infinity is not questionable at all, and the same happens

with an exponential distribution and most "standard" distributions in probability theory. However, one already sees that the power-law distribution is problematic, in particular for $\alpha \leq 2$, as it predicts an infinite mean, and for $2 \leq \alpha < 3$, as the variability of the sample mean is infinite. Of course, there can be variables having an infinite mean (one can easily simulate in a computer processes in which the time between events has an infinite mean), but in other cases, for physical reasons, the mean should be finite. In such situations a simple generalization is the truncation of the tail (Aban *et al.* 2006, Burroughs and Tebbens 2001, Carrillo-Menéndez and Suárez 2012, Johnson *et al.* 1994), yielding the truncated power-law distribution, defined in the same way as before by $f(x) \propto 1/x^{\alpha}$ but with $a \leq x \leq b$, with b finite, and with normalizing factor depending now on a and b (in some cases it is possible to have $a = 0$, see next section). Obviously, the existence of a finite upper cutoff b automatically leads to well-behaved moments, if the statistics is enough to "see" the cutoff; on the other hand, a range of scale invariance can persist, if $b \gg a$. What one finds in some practical problems is that the statistics is not enough to decide which is the sample mean and one cannot easily conclude if a pure power law or a truncated power law is the right model for the data.

A well known example of (truncated or not) power-law distribution is the Gutenberg–Richter law for earthquake "size" (Kagan 2002, Kanamori and Brodsky 2004, Utsu 1999). If by size we understand radiated energy, the Gutenberg–Richter law implies that, in any seismically active region of the world, the sizes of earthquakes follow a power-law distribution, with an exponent $\alpha = 1 + 2B/3$ and B close to 1. In this case, scale invariance means that if one asks how big (in terms of radiated energy) earthquakes are in a certain region, such a simple question has no possible answer. The non-convergence of the mean energy can easily be checked from data: catastrophic events such as the Sumatra–Andaman mega-earthquake of 2004 contribute to the mean much more than the previous recorded history (Corral and Font-Clos 2013). Note that for the most common formulation of the Gutenberg–Richter law, in terms of the magnitude, earthquakes are not power-law distributed, but this is due to the fact that magnitude is an (increasing) exponential function of radiated energy, and therefore magnitude turns out to be exponentially distributed. In terms of magnitude, the statistical properties of earthquakes are trivial (well behaved mean, existence of a characteristic magnitude, *etc.*), but we insist that this is not the case in terms of radiated energy.

Malamud (2004) lists several other natural hazards following power-law distributions in some (physical) measure of size, such as rockfalls, landslides (Hergarten 2002), volcanic eruptions (Lahaie and Grasso 1998, McClelland *et al.* 1989), and forest fires (Malamud *et al.* 2005), and we can add rainfall (Peters *et al.* 2001, 2010), tropical cyclones (roughly speaking, hurricanes)

(Corral *et al.* 2010), auroras (Freeman and Watkins 2002), tsunamis (Burroughs and Tebbens 2005), *etc.* In some cases this broad range of responses is triggered simply by a small driving or perturbation (the slow motion of tectonic plates for earthquakes, the continuous pumping of solar radiation in hurricanes, *etc.*); then, this highly nonlinear relation between input and output can be labeled as crackling noise (Sethna *et al.* 2001). Notice that this does not apply for tsunamis, for instance, as they are not slowly driven (or at least not directly slowly driven).

Aschwanden (2013) reviews disparate astrophysical phenomena which are distributed according to power laws, some of them related to geoscience: sizes of asteroids, craters in the Moon, solar flares, and energy of cosmic rays. In the field of ecology and close areas, the applicability of power-law distributions has been overviewed by White *et al.* (2008), mentioning also island and lake sizes. Aban *et al.* (2006) provides bibliography for power-law and other heavy-tailed distributions in diverse disciplines, including hydrology, and Burroughs and Tebbens (2001) provide interesting geological examples.

A theoretical framework for power-law distributed sizes (and durations) of catastrophic phenomena not only in geoscience but also in condensed matter physics, astrophysics, biological evolution, neuroscience, and even the economy, is provided by the concept of self-organized criticality, and summarized by the sandpile paradigm (Bak 1996, Christensen and Moloney 2005, Jensen 1998, Pruessner 2012, Sornette 2004). However, although the ideas of self-organization and criticality are very reasonable in the context of most of the geosystems mentioned above (Corral 2010, Peters and Christensen 2006, Peters and Neelin 2006), one cannot rule out other mechanisms for the emergence of power-law distributions (Czechowski 2003, Dickman 2003, Mitzenmacher 2004, Newman 2005, Sornette 2004).

On the other hand, it is interesting to mention that, in addition to sizes and durations, power-law distributions have also been extensively reported in time between the occurrences of natural hazards (waiting times), as for instance in solar flares (Baiesi *et al.* 2006, Boffetta *et al.* 1999), earthquakes (Bak *et al.* 2002, Corral 2003, 2004b), or solar wind (Wanliss and Weygand 2007); in other cases the distributions contain a power-law part mixed with other factors (Corral 2004a, 2009b, Geist and Parsons 2008, Saichev and Sornette 2006). Nevertheless, the possible relation with critical phenomena is not direct (Corral 2005, Paczuski *et al.* 2005). The distance between events, or jumps, has received relatively less attention (Corral 2006, Davidsen and Paczuski 2005, Felzer and Brodsky 2006).

The importance of power-law distributions in geoscience is apparent; however, some of the evidence gathered in favor of this paradigm can be considered as "anecdotic" or tentative, as it is based on rather poor data analysis.

A common practice is to find some (naive or not) estimation of the probability density or mass function $f(x)$ and plot $\ln f(x)$ *versus* $\ln x$ and look for a linear dependence between both variables. Obviously, a power-law distribution should behave in that way, but the opposite is not true: an apparent straight line in a log-log plot of $f(x)$ should not be considered a guarantee of an underlying power-law distribution, or perhaps the exponent obtained from there is clearly biased (Bauke 2007, Clauset *et al.* 2009, Goldstein *et al.* 2004, White *et al.* 2008). But in order to discriminate between several competing theories or models, as well as in order to extrapolate the available statistics to the most extreme events, it is very important to properly fit power laws and to find the right power-law exponent (if any) (White *et al.* 2008).

The subject of this paper is a discussion on the most appropriate fitting, testing of the goodness-of-fit, and representation of power-law distributions, both non-truncated and truncated. A consistent and robust method will be checked on several examples in geoscience, including earthquakes, tropical cyclones, and forest fires. The procedure is in some points analogous to that of Clauset *et al.* (2009), although there are variations is some key steps, in order to correct several drawbacks of the original method (Corral *et al.* 2011, Peters *et al.* 2010). The most important difference is in the criterion to select the range over which the power law holds. As the case of most interest in geoscience is that of a continuous random variable, the more involving discrete case will be postponed to a separate publication (Corral *et al.* 2012).

2. POWER-LAW FITS AND GOODNESS-OF-FIT TESTS

2.1 Non-truncated and truncated power-law distributions

Let us consider a continuous power-law distribution, defined in the range $a \leq x \leq b$, where b can be finite or infinite and $a \geq 0$. The probability density of x is given by

$$f(x) = \frac{\alpha - 1}{a^{1-\alpha} - 1/b^{\alpha-1}} \left(\frac{1}{x}\right)^{\alpha}, \tag{2}$$

the limit $b \to \infty$ with $\alpha > 1$ and $a > 0$ provides the non-truncated power-law distribution, also called here pure power law; otherwise, for finite b one has the truncated power law, for which no restriction exists on α if $a > 0$, but $\alpha < 1$ if $a = 0$ (which is sometimes referred to as the power-function distribution (Evans *et al.* 2000)); the case $\alpha = 1$ needs a separate treatment, with

$$f(x) = \frac{1}{x \ln(b/a)}\,. \tag{3}$$

We will consider in principle that the distribution has a unique parameter, α, and that a and b are fixed and known values. Remember that, at point x, the probability density function of a random variable is defined as the probability per unit of the variable that the random variable lies in a infinitesimal interval around x, that is,

$$f(x) = \lim_{\Delta x \to 0} \frac{\text{Prob}[x \leq \text{random variable} < x + \Delta x]}{\Delta x} , \tag{4}$$

and has to verify $f(x) \geq 0$ and $\int_{-\infty}^{\infty} f(x)dx = 1$; see for instance Ross (2002).

Equivalently, the distribution can be also characterized by its (complementary) cumulative distribution function,

$$S(x) = \text{Prob}[\text{random variable} \geq x] = \int_x^{\infty} f(x')dx'. \tag{5}$$

For a truncated or non-truncated power law this leads to

$$S(x) = \frac{1/x^{\alpha-1} - 1/b^{\alpha-1}}{a^{1-\alpha} - 1/b^{\alpha-1}} , \tag{6}$$

if $\alpha \neq 1$ and

$$S(x) = \frac{\ln(b/x)}{\ln(b/a)} , \tag{7}$$

if $\alpha = 1$. Note that although $f(x)$ always has a power-law shape, $S(x)$ only has it in the non-truncated case ($b \to \infty$ and $\alpha > 1$); nevertheless, even not being a power law in the truncated case, the distribution is a power law, as it is $f(x)$ and not $S(x)$ which gives the name to the distribution.

2.2 Problematic fitting methods

Given a set of data, there are many methods to fit a probability distribution. Goldstein *et al.* (2004), Bauke (2007), White *et al.* (2008), and Clauset *et al.* (2009) check several methods based in the fitting of the estimated probability densities or cumulative distributions in the power-law case. As mentioned in the first section, $\ln f(x)$ is then a linear function of $\ln x$, both for non-truncated and truncated power laws. The same holds for $\ln S(x)$, but only in the non-truncated case. So, one can either estimate $f(x)$ from data, using some binning procedure, or estimate $S(x)$, for which no binning is necessary, and then fit a straight line by the least-squares method. As we find White *et al.*'s (2008) study the most complete, we summarize their results below, although those of the other authors are not very different.

For non-truncated power-law distributions, White *et al.* (2008) find that the results of the least-squares method using the cumulative distribution are reasonable, although the points in $S(x)$ are not independent and linear regression should yield problems in this case. We stress that this procedure only can work for non-truncated distributions (*i.e.*, with $b \to \infty$); truncated ones yield bad results (Burroughs and Tebbens 2001).

The least-squares method applied to the probability density $f(x)$ has several variations, depending on the way of estimating $f(x)$. Using linear binning one obtains a simple histogram, for which the fitting results are catastrophic (Pueyo and Jovani 2006, Bauke 2007, Goldstein *et al.* 2004, White *et al.* 2008). This is not unexpected, as linear binning of a heavy-tailed distribution can be considered as a very naive approach. If instead of linear binning one uses logarithmic binning the results improve (when done "correctly"), and are reasonable in some cases, but they still show some bias, high variance, and bin-size dependence. A fundamental point is to avoid having empty bins, as they are disregarded in logscale, introducing an important bias.

In summary, methods of estimation of probability-distribution parameters based on least-squares fitting can have many problems, and usually the results are biased. Moreover, these methods do not take into account that the quantity to be fitted is a probability distribution (*i.e.*, once the distributions are estimated, the method is the same as for any other kind of function). We are going to see that the method of maximum likelihood is precisely designed for dealing with probability distributions, presenting considerable advantages in front of the other methods just mentioned.

2.3 Maximum likelihood estimation

Let us denote a sample of the random variable x with N elements as x_1, x_2, ..., x_N, and let us consider a probability distribution $f(x)$ parameterized by α. The likelihood function $L(\alpha)$ is defined as the joint probability density (or the joint probability mass function if the variable were discrete) evaluated at x_1, x_2, ..., x_N in the case in which the variables were independent, *i.e.*,

$$L(\alpha) = \prod_{i=1}^{N} f(x_i) \, . \tag{8}$$

Note that the sample is considered fixed, and it is the parameter α what is allowed to vary. In practice it is more convenient to work with the log-likelihood, the natural logarithm of the likelihood (dividing by N also, in our definition),

$$\ell(\alpha) = \frac{1}{N} \ln L(\alpha) = \frac{1}{N} \sum_{i=1}^{N} \ln f(x_i) \, . \tag{9}$$

The maximum likelihood (ML) estimator of the parameter α based on the sample is just the value of α that yields the maximum of $\ell(\alpha)$ (which coincides with the maximum of $L(\alpha)$, obviously). For a given sample, we will denote the ML estimator as α_e (e is from empirical), but it is important to realize that the ML estimator is indeed a statistic (a quantity calculated from a random sample) and therefore can be considered as a random variable; in this case it is denoted as $\hat{\alpha}$. In a formula,

$$\alpha_e = \arg\max_{\forall\alpha} \ell(\alpha) \,, \tag{10}$$

where argmax refers to the argument of the function ℓ that makes it maximum.

For the truncated or the non-truncated continuous power-law distribution we have, substituting $f(x)$ from Eqs. (2)-(3) and introducing $r = a/b$, disregarding the case $a = 0$,

$$\ell(\alpha) = \ln \frac{\alpha - 1}{1 - r^{\alpha-1}} - \alpha \ln \frac{g}{a} - \ln a \,, \quad \text{if } \alpha \neq 1, \tag{11}$$

$$\ell(\alpha) = -\ln \ln \frac{1}{r} - \ln g \,, \quad \text{if } \alpha = 1 \,; \tag{12}$$

where g is the geometric mean of the data, $\ln g = N^{-1} \sum_1^N \ln x_i$, and the last term in each expression is irrelevant for the maximization of $\ell(\alpha)$. The equation for $\alpha = 1$ is necessary in order to avoid overflows in the numerical implementation of Eq. (11). Remember that the distribution is only parameterized by α, whereas a and b (and r) are constant parameters; therefore, $\ell(\alpha)$ is not a function of a and b, but of α.

In order to find the maximum of $\ell(\alpha)$ one can derive with respect α and set the result equal to zero (Aban *et al.* 2006, Johnson *et al.* 1994),

$$\left.\frac{d\ell(\alpha)}{d\alpha}\right|_{\alpha=\alpha_e} = \frac{1}{\alpha_e - 1} + \frac{r^{\alpha_e - 1} \ln r}{1 - r^{\alpha_e - 1}} - \ln \frac{g}{a} = 0 \,, \tag{13}$$

which constitutes the so-called likelihood equation for this problem. For a non-truncated distribution, $r = 0$, and it is clear that there is one and only one solution,

$$\alpha_e = 1 + \frac{1}{\ln(g/a)} \,, \tag{14}$$

which corresponds to a maximum, as

$$L(\alpha) = e^{N\ell(\alpha)} = \frac{1}{a^N} (\alpha - 1)^N e^{-N\alpha \ln(g/a)} \,, \tag{15}$$

has indeed a maximum (resembling a gamma probability density, see next subsection). Figure 1 illustrates the log-likelihood function and its derivative, for simulated power-law data.

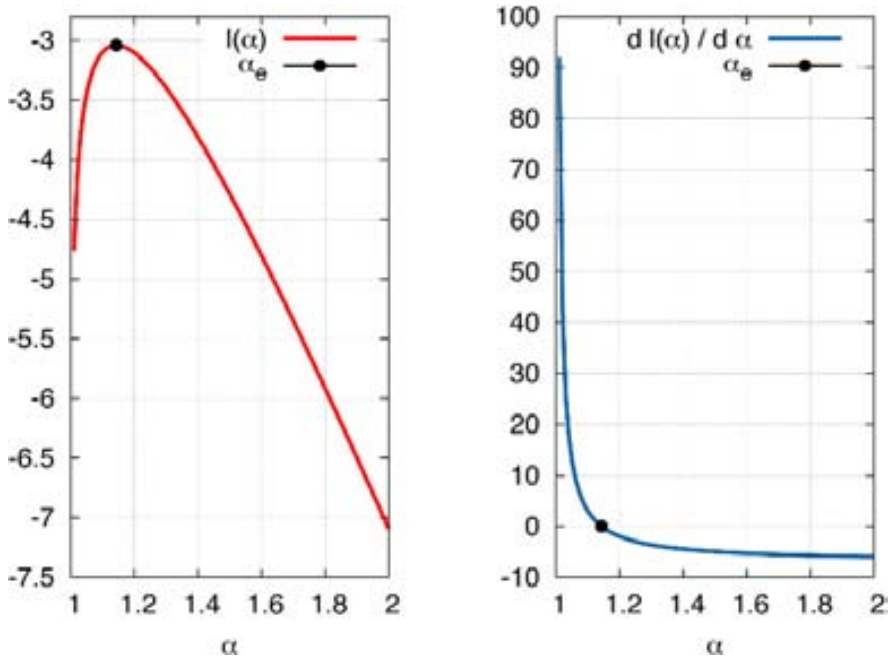

Fig. 1. Log-likelihood $\ell(\alpha)$ and its derivative, for simulated non-truncated power-law data with exponent $\alpha = 1.15$ and $a = 0.001$. The total number of data is $N_{\rm tot} = 1000$. The resulting estimation yields $\alpha_e = 1.143$, which will lead to a confidence interval $\alpha \pm \sigma = 1.143 \pm 0.005$.

In the truncated case it is not obvious that there is a solution to the likelihood equation (Aban *et al.* 2006); however, one can take advantage of the fact that the power-law distribution, for fixed a and b, can be viewed as belonging to the regular exponential family, for which it is known that the maximum likelihood estimator exists and is unique; see Barndorff-Nielsen (1978, p. 151) or del Castillo (2013). Indeed, in the single-parameter case, the exponential family can be written in the form

$$f(x) = C^{-1}(\alpha) H(x) e^{\theta(\alpha)\cdot T(x)} \,, \tag{16}$$

where both $\theta(\alpha)$ and $T(x)$ can be vectors, the former containing the parameter α of the family. Then, for $\theta(\alpha) = -\alpha$, $T(x) = \ln x$, and $H(x) = 1$ we obtain the (truncated or not) power-law distribution, which therefore belongs to the regular exponential family, which guarantees the existence of a unique ML solution.

In order to find the ML estimator of the exponent in the truncated case, we proceed by maximizing directly the log-likelihood $\ell(\alpha)$ (rather than by solving the likelihood equation). The reason is a practical one, as our procedure is part of a more general method, valid for arbitrary distributions $f(x)$, for which the derivative of $\ell(\alpha)$ can be difficult to evaluate. We will use the downhill simplex method, through the routine "amoeba" of Press *et al.* (1992), although any other simpler maximization procedure should work, as the problem is one-dimensional, in this case. One needs to take care when the value of α gets very

close to one in the maximization algorithm, and then replace $\ell(\alpha)$ by its limit at $\alpha = 1$,

$$\ell(\alpha) \to_{\alpha\to 1} -\ln\ln\frac{1}{r} - \alpha\ln\frac{g}{a} - \ln a\,, \tag{17}$$

which is in agreement with the likelihood function for a (truncated) power-law distribution with $\alpha = 1$.

An important property of ML estimators, not present in other fitting methods, is their invariance under re-parameterization. If instead of working with parameter α we use $\nu = h(\alpha)$, then the ML estimator of ν is "in agreement" with that of α, *i.e.*, $\hat{\nu} = h(\hat{\alpha})$. Indeed,

$$\frac{d\ell}{d\nu} = \frac{d\ell}{d\alpha}\frac{d\alpha}{d\nu}\,, \tag{18}$$

so, the maximum of ℓ as a function of ν is attained at the point $h(\hat{\alpha})$, provided that the function h is "one-to-one". Note that the parameters could be multidimensional as well. Casella and Berger (2002) study this invariance with much more care.

In their comparative study, White *et al.* (2008) conclude that maximum likelihood estimation outperforms the other fitting methods, as always yields the lowest variance and bias of the estimator. This is not unexpected, as the ML estimator is, mathematically, the one with minimum variance among all asymptotically unbiased estimators. This property is called asymptotical efficiency (Bauke 2007, White *et al.* 2008).

2.4 Standard deviation of the ML estimator

The main result of this subsection is the value of the uncertainty σ of $\hat{\alpha}$, represented by the standard deviation of $\hat{\alpha}$ and given by

$$\sigma = \frac{1}{\sqrt{N}}\left[\frac{1}{(\alpha_e-1)^2} - \frac{r^{\alpha_e-1}\ln^2 r}{(1-r^{\alpha_e-1})^2}\right]^{-1/2}, \tag{19}$$

(Aban *et al.* 2006). This formula can be used directly, although σ can be computed as well from Monte Carlo simulations, as explained in another subsection. A third option is the use of the jackknife procedure, as done by Peters *et al.* (2010). The three methods lead to essentially the same results. The rest of this subsection is devoted to the particular derivation of σ for a non-truncated power-law distribution, and therefore can be skipped by readers interested mainly in the practical use of ML estimation.

For the calculation of $\hat{\alpha}$ (the ML estimator of α) one needs to realize that this is indeed a statistic (a quantity calculated from a random sample) and therefore it can be considered as a random variable. Note that α denotes the

true value of the parameter, which is unknown. It is more convenient to work with $\alpha - 1$ (the exponent of the cumulative distribution function); in the non-truncated case ($r = 0$ with $\alpha > 1$) we can easily derive its distribution. First let us consider the geometric mean of the sample, g, rescaled by the minimum value a,

$$\ln \frac{g}{a} = \frac{1}{N} \sum_{i=1}^{N} \ln \frac{x_i}{a} \, . \tag{20}$$

As each x_i is power-law distributed (by hypothesis), a simple change of variables shows that $\ln(x_i/a)$ turns out to be exponentially distributed, with scale parameter $1/(\alpha - 1)$; then, the sum will be gamma distributed with the same scale parameter and with shape parameter given by N (this is the key property of the gamma distribution (Durrett 2010)). Therefore, $\ln(g/a)$ will follow the same gamma distribution but with scale parameter $N^{-1}(\alpha - 1)^{-1}$.

At this point it is useful to introduce the generalized gamma distribution (Evans *et al.* 2000, Johnson *et al.* 1994, Kalbfleisch and Prentice 2002), with density, for a random variable $y \geq 0$,

$$D(y) = \frac{|\delta|}{c\Gamma(\gamma/\delta)} \left(\frac{y}{c}\right)^{\gamma-1} e^{-(y/c)^{\delta}} \, , \tag{21}$$

where $c > 0$ is the scale parameter and γ and δ are the shape parameters, which have to verify $0 < \gamma/\delta < \infty$ (so, the only restriction is that they have the same sign, although the previous references only consider $\gamma > 0$ and $\delta > 0$); the case $\delta = 1$ yields the usual gamma distribution and $\delta = \gamma = 1$ is the exponential one. Again, changing variables one can show that the inverse $z = 1/y$ of a generalized gamma variable is also a generalized gamma variable, but with transformed parameters,

$$\gamma, \delta, c \to -\gamma, -\delta, \frac{1}{c} \, . \tag{22}$$

So, $\hat{\alpha} - 1 = z = 1/\ln(g/a)$ will have a generalized gamma distribution, with parameters $-N$, -1, and $N(\alpha - 1)$ (keeping the same order as above). Introducing the moments of this distribution (Evans *et al.* 2000),

$$\langle y^m \rangle = c^m \frac{\Gamma\left(\frac{\gamma+m}{\delta}\right)}{\Gamma\left(\gamma/\delta\right)} \tag{23}$$

(valid for $m > -\gamma$ if $\gamma > 0$ and for $m < |\gamma|$ if $\gamma < 0$, and $\langle y^m \rangle$ infinite otherwise), we obtain the expected value of $\hat{\alpha} - 1$,

$$\langle \hat{\alpha} - 1 \rangle = \frac{N(\alpha - 1)}{N - 1} \, . \tag{24}$$

Note that the ML estimator, $\hat{\alpha}$, is biased, as its expected value does not coincide with the right value, α; however, asymptotically, the right value is recovered. An unbiased estimator of α can be obtained for a small sample as $(1-1/N)\alpha_e + 1/N$, although this will not be of interest to us.

In the same way, the standard deviation of $\hat{\alpha}-1$ (and of $\hat{\alpha}$) turns out to be

$$\sigma = \sqrt{\langle(\hat{\alpha}-1)^2\rangle - \langle\hat{\alpha}-1\rangle^2} = \frac{\alpha-1}{(1-1/N)\sqrt{N-2}}\,, \tag{25}$$

which leads asymptotically to $(\alpha-1)/\sqrt{N}$. In practice, we need to replace α by the estimated value α_e; then, this is nothing else than the limit $r=0$ $(b\to\infty)$ of the general formula stated above for σ (Aban *et al.* 2006). The fact that the standard deviation tends to zero asymptotically (together with the fact that the estimator is asymptotically unbiased) implies that any single estimation converges (in probability) to the true value, and therefore the estimator is said to be consistent.

2.5 Goodness-of-fit test

One can realize that the maximum likelihood method always yields a ML estimator for α, no matter which data one is using. In the case of power laws, as the data only enters in the likelihood function through its geometric mean, any sample with a given geometric mean yields the same value for the estimation, although the sample can come from a true power law or from any other distribution. So, no quality of the fit is guaranteed and thus, maximum likelihood estimation should be rather called minimum unlikelihood estimation. For this reason a goodness-of-fit test is necessary (although recent works do not take into account this fact (Baró and Vives 2012, Kagan 2002, White *et al.* 2008)).

Following Goldstein *et al.* (2004) and Clauset *et al.* (2009) we use the Kolmogorov–Smirnov (KS) test (Chicheportiche and Bouchaud 2012, Press *et al.* 1992), based on the calculation of the KS statistic or KS distance d_e between the theoretical probability distribution, represented by $S(x)$, and the empirical one, $S_e(x)$. The latter, which is an unbiased estimator of the cumulative distribution (Chicheportiche and Bouchaud 2012), is given by the stepwise function

$$S_e(x) = n_e(x)/N\,, \tag{26}$$

where $n_e(x)$ is the number of data in the sample taking a value of the variable larger than or equal to x. The KS statistic is just the maximum difference, in absolute value, between $S(x)$ and $n_e(x)/N$, that is,

$$d_e = \max_{a\le x\le b}|S(x)-S_e(x)| = \max_{a\le x\le b}\left|\frac{1}{1-r^{\alpha_e-1}}\left[\left(\frac{a}{x}\right)^{\alpha_e-1} - r^{\alpha_e-1}\right] - \frac{n_e(x)}{N}\right|, \tag{27}$$

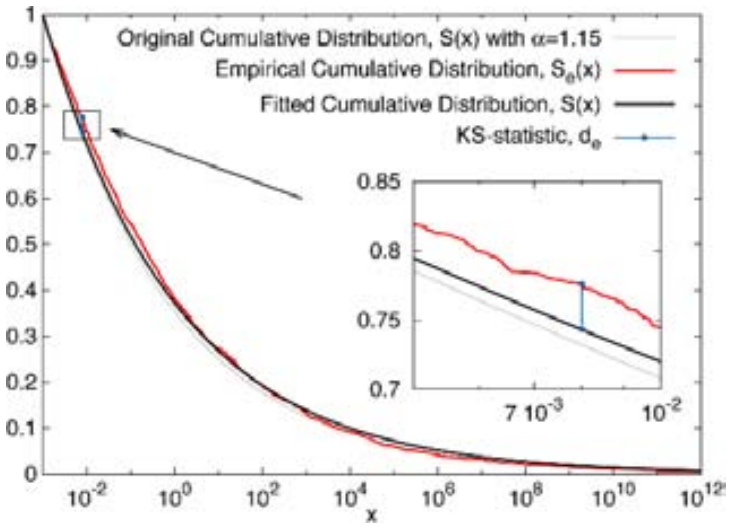

Fig. 2. Empirical (complementary) cumulative distribution for a simulated non-truncated power-law distribution with $\alpha = 1.15$, $a = 0.001$, and $N_{\rm tot} = 1000$, together with its corresponding fit, which yields $\alpha_e = 1.143$. The maximum difference between both curves, $d_e = 0.033$, is marked as an illustration of the calculation of the KS statistic. The original theoretical distribution, unknown in practice, is also plotted. Colour version of this figure is available in electronic edition only.

where the bars denote absolute value. Note that the theoretical cumulative distribution $S(x)$ is parameterized by the value of α obtained from ML, α_e. In practice, the difference only needs to be evaluated around the points x_i of the sample (as the routine "ksone" of Press *et al.* (1992) does) and not for all x. A more strict mathematical definition uses the supremum instead of the maximum, but in practice the maximum works perfectly. We illustrate the procedure in Fig. 2, with a simulation of a non-truncated power law.

Intuitively, if d_e is large the fit is bad, whereas if d_e is small the fit can be considered as good. But the relative scale of d_e is provided by its own probability distribution, through the calculation of a p-value. Under the hypothesis that the data follow indeed the theoretical distribution, with the parameter α obtained from our previous estimation (this is the null hypothesis), the p-value provides the probability that the KS statistic takes a value larger than the one obtained empirically, *i.e.*,

$$p = \text{Prob}[\text{KS statistic for power-law data (with } \alpha_e) \text{ is} > d_e] \; ; \tag{28}$$

then, bad fits will have rather small p-values.

It turns out that, in principle, the distribution of the KS statistic is known, at least asymptotically, independently of the underlying form of the distribution, so

$$\begin{aligned} p_Q &= Q(d_e\sqrt{N} + 0.12d_e + 0.11d_e/\sqrt{N}) \\ &= 2\sum_{j=1}^{\infty}(-1)^{j-1}\exp[-2j^2(d_e\sqrt{N} + 0.12d_e + 0.11d_e/\sqrt{N})^2] \; , \end{aligned} \tag{29}$$

for which one can use the routine "probks" of Press *et al.* (1992) (but note their Eq. (14.3.9) is not right). Nevertheless, this formula will not be accurate in our case, and for this reason we use the symbol p_Q instead of p. The reason is that we are "optimizing" the value of α using the same sample to which we apply the KS test, which yields a bias in the test, *i.e.*, the formula would work for the true value of α, but not for one obtained by ML, which would yield in general a smaller KS statistic and too large p-values (because the fit for α_e is better than for the true value α) (Clauset *et al.* 2009, Goldstein *et al.* 2004). However, for this very same reason the formula can be useful to reject the goodness of a given fit, *i.e.*, if p_Q obtained in this way is already below 0.05, the true p will be even smaller and the fit is certainly bad. But the opposite is not true. In a formula

$$\text{if } p_Q < 0.05 \Rightarrow \text{ reject power law }, \tag{30}$$

otherwise, no decision can be taken yet. Of course, the significance level 0.05 is arbitrary and can be changed to another value, as usual in statistical tests. As a final comment, perhaps a more powerful test would be to use, instead of the KS statistic, the Kuiper's statistic (Press *et al.* 1992), which is a refinement of the former one. It is stated by Clauset *et al.* (2009) that both tests lead to very similar fits. In most cases, we have also found no significant differences between both tests.

2.6 The Clauset *et al.*'s recipe

Now we are in condition to explain the genuine Clauset *et al.*'s (2009) method. This is done in this subsection for completeness, and for the information of the reader, as we are not going to apply this method. The key to fitting a power law is neither the ML estimation of the exponent nor the goodness-of-fit test, but the selection of the interval $[a, b]$ over which the power law holds. Initially, we have taken a and b as fixed parameters, but in practice this is not the case, and one has to decide where the power law starts and where ends, independently of the total range of the data. In any case, N will be the number of data in the power-law range (and not the total number of data).

The recipe of Clauset *et al.* (2009) applies to non-truncated power-law distributions $(b \to \infty)$, and considers that a is a variable which needs to be fit from the sample (values of x below a are outside the power-law range). The recipe simply consists in the search of the value of a which yields a minimum of the KS statistic, using as a parameter of the theoretical distribution the one obtained by maximum likelihood, α_e, for the corresponding a (no calculation of a p-value is required for each fixed a). In other words,

$$a = \text{the one that yields minimum } d_e. \tag{31}$$

Next, a global p-value is computed by generating synthetic samples by a mixture of parametric bootstrap (similarly to what is explained in the next subsection) and non-parametric bootstrap. Then, the same procedure applied to the empirical data (minimization of the KS distance using ML for fitting) is applied to the syntetic samples in order to fit a and α.

These authors do not provide any explanation of why this should work, although one can argue that, if the data is indeed a power law with the desired exponent, the larger the number of data (the smaller the a-value), the smaller the value of d_e, as d_e goes as $1/\sqrt{N}$ (for large N, see previous subsection). On the other hand, if for a smaller a the data departs from the power law, this deviation should compensate and overcome the reduction in d_e due to the increase of N, yielding a larger d_e. But there is no reason to justify this overcoming.

Nevertheless, we will not use the Clauset *et al.*'s (2009) procedure for two other reasons. First, its extension to truncated power laws, although obvious, and justifiable with the same arguments, yields bad results, as the resulting values of the upper truncation cutoff, b, are highly unstable. Second, even for non-truncated distributions, it has been shown that the method fails to detect the existence of a power law for data simulated with a power-law tail (Corral *et al.* 2011): the method yields an a-value well below the true power-law region, and therefore the resulting p is too small for the power law to become acceptable. We will explain an alternative method that avoids these problems, but first let us come back to the case with a and b fixed.

2.7 Monte Carlo simulations

Remember that we are considering a power-law distribution, defined in $a \leq x \leq b$. We already have fit the distribution, by ML, and we are testing the goodness of the fit by means of the KS statistic. In order to obtain a reliable p-value for this test we will perform Monte Carlo simulations of the whole process. A synthetic sample power-law distributed and with N elements can be obtained in a straightforward way, from the inversion or transformation method (Devroye 1986, Press *et al.* 1992, Ross 2002)

$$x_i = \frac{a}{[1-(1-r^{\alpha_e-1})u_i]^{1/(\alpha_e-1)}}, \tag{32}$$

where u_i represents a uniform random number in $[0,1)$. One can use any random number generator for it. Our results arise from "ran3" of Press *et al.* (1992).

2.8 Application of the complete procedure to many syntetic samples and calculation of p-value

The previous fitting and testing procedure is applied in exactly the same way to the synthetic sample, yielding a ML exponent α_s (where the subindex s stands from synthetic or simulated), and then a KS statistic d_s, computed as the difference between the theoretical cumulative distribution, with parameter α_s, and the simulated one, $n_s(x)/N$ (obtained from simulations with α_e, as described in the previous subsection), *i.e.*,

$$d_s = \max_{a \leq x \leq b} \left| \frac{1}{1 - r^{\alpha_s - 1}} \left[\left(\frac{a}{x} \right)^{\alpha_s - 1} - r^{\alpha_s - 1} \right] - \frac{n_s(x)}{N} \right| . \tag{33}$$

Both values of the exponent, α_e and α_s, should be close to each other, but they will not be necessarily the same. Note that we are not parameterizing $S(x)$ by the empirical value α_e, but with a new fitted value α_s. This is in order to avoid biases, as a parameterization with α_e would lead to worse fits (as the best one would be with α_s) and therefore to larger values of the resulting KS statistic and to artificially larger p-values. So, although the null hypothesis of the test is that the exponent of the power law is α_e, and synthetic samples are obtained with this value, no further knowledge of this value is used in the test. This is the procedure used by Clauset *et al.* (2009) and Malmgren *et al.* (2008), but it is not clear if it is the one of Goldstein *et al.* (2004).

In fact, one single synthetic sample is not enough to do a proper comparison with the empirical sample, and we repeat the simulation many times. The most important outcome is the set of values of the KS statistic, d_s, which allows to estimate its distribution. The p-value is simply calculated as

$$p = \frac{\text{number of simulations with } d_s \geq d_e}{N_s} , \tag{34}$$

where N_s is the number of simulations. Figure 3 shows an example of the distribution of the KS statistic for simulated data, which can be used as a table of critical values when the number of data and the exponent are the same as in the example (Goldstein *et al.* 2004).

The standard deviation of the p-value can be calculated just using that the number of simulations with $d_s \geq d_e$ is binomially distributed, with standard deviation $\sqrt{N_s p(1-p)}$ and therefore the standard deviation of p is the same divided by N_s,

$$\sigma_p = \sqrt{\frac{p(1-p)}{N_s}} . \tag{35}$$

In fact, the p-value in this formula should be the ideal one (the one of the whole population) but we need to replace it by the estimated value; further, when doing

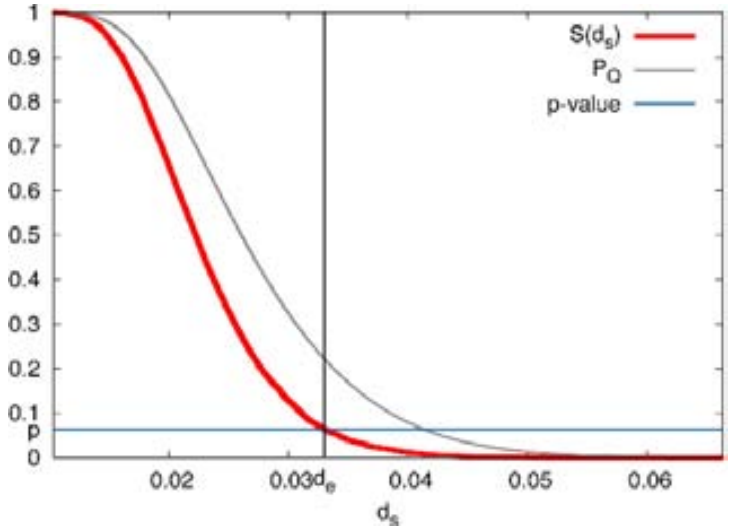

Fig. 3. Cumulative (complementary) distribution of the Kolmogorov–Smirnov statistic for simulated non-truncated power-law distributions with $\alpha = \alpha_e = 1.143$, $a = 0.001$, and $N_{\rm tot} = 1000$. The original "empirical" value $d_e = 0.033$ is also shown. The resulting p-value turns our to be $p = 0.060 \pm 0.008$. The "false" p-value, p_Q, arising from the KS formula, leads to higher values for the same d_e, in concrete, $p_Q = 0.22$. Colour version of this figure is available in electronic edition only.

estimation from data, N_s should be $N_s - 1$, but we have disregarded this bias correction. It will be also useful to consider the relative uncertainty of p, which is the same as the relative uncertainty of the number of simulations with $d_s \geq d_e$ (as both are proportional). Dividing the standard deviation of p by its mean (which is p) , we obtain

$$CV_p = \sqrt{\frac{1-p}{pN_s}} \simeq \sqrt{\frac{1-p}{\text{number of simulations with } d_s \geq d_e}} \tag{36}$$

(we will recover this formula for the error of the estimation of the probability density).

In this way, small p-values are associated to large values of d_e, and therefore to bad fits. However, note that if we put the threshold of rejection in, let us say, $p \leq 0.05$, even true power-law distributed data, with exponent α_e, yield "bad fits" in one out of 20 samples (on average). So we are rejecting true power laws in 5% of the cases (type I error). On the other hand, lowering the threshold of rejection would reduce this problem, but would increase the probability of accepting false power laws (type II error). In this type of tests a compromise between both types of errors is always necessary, and depends on the relative costs of rejecting a true hypothesis or accepting a false one.

In addition, we can obtain from the Monte Carlo simulations the uncertainty of the ML estimator, just computing $\bar{\alpha}_s$, the average value of α_s, and from here its standard deviation,

$$\sigma = \sqrt{\overline{(\alpha_s - \bar{\alpha}_s)^2}}\,, \tag{37}$$

where the bars indicate average over the N_s Monte Carlo simulations. This procedure yields good agreement with the analytical formula of Aban *et al.* (2006), but can be much more useful in the discrete power-law case.

2.9 Alternative method to the one by Clauset *et al.*

At this point, for given values of the truncation points, a and b, we are able to obtain the corresponding ML estimation of the power-law exponent as well as the goodness of the fit, by means of the p-value. Now we face the same problem Clauset *et al.* (2009) tried to solve: how to select the fitting range? In our case, how to find not only the value of a but also of b? We adopt the simple method proposed by Peters *et al.* (2010): sweeping many different values of a and b we should find, if the null hypothesis is true (*i.e.*, if the sample is power-law distributed), that many sets of intervals yield acceptable fits (high enough p-values), so we need to find the "best" of such intervals. And which one is the best? For a non-truncated power law the answer is easy, we select the largest interval, *i.e.*, the one with the smaller a, provided that the p-value is above some fixed significance level p_c. All the other acceptable intervals will be inside this one.

But if the power law is truncated, the situation is not so clear, as there can be several non-overlapping intervals. In fact, many true truncated power laws can be contained in the data, at least there are well know examples of stochastic processes with double power-law distributions (Boguñá and Corral 1997, Corral 2003, 2009a, Klafter *et al.* 1996). At this point any selection can be reasonable, but if one insists in having an automatic, blind procedure, a possibility is to select either the interval which contains the larger number of data, N (Peters *et al.* 2010), or the one which has the larger log-range, b/a. For double power-law distributions, in which the exponent for small x is smaller than the one for large x, the former recipe has a tendency to select the first (small x) power-law regime, whereas the second procedure changes this tendency in some cases.

In summary, the final step of the method for truncated power-law distributions is contained in the formula

$$[a,b] = \text{the one that yields higher} \left\{ \begin{array}{c} N \\ \text{or} \\ b/a \end{array} \right\} \text{provided that } p > p_c \,, \qquad (38)$$

which contains in fact two procedures, one maximizing N and the other maximizing b/a. We will test both in this paper. For non-truncated power-law distributions the two procedures are equivalent.

One might be tempted to choose $p_c = 0.05$; however, it is safer to consider a larger value, as for instance $p_c = 0.20$. Note that the p-value we are using is

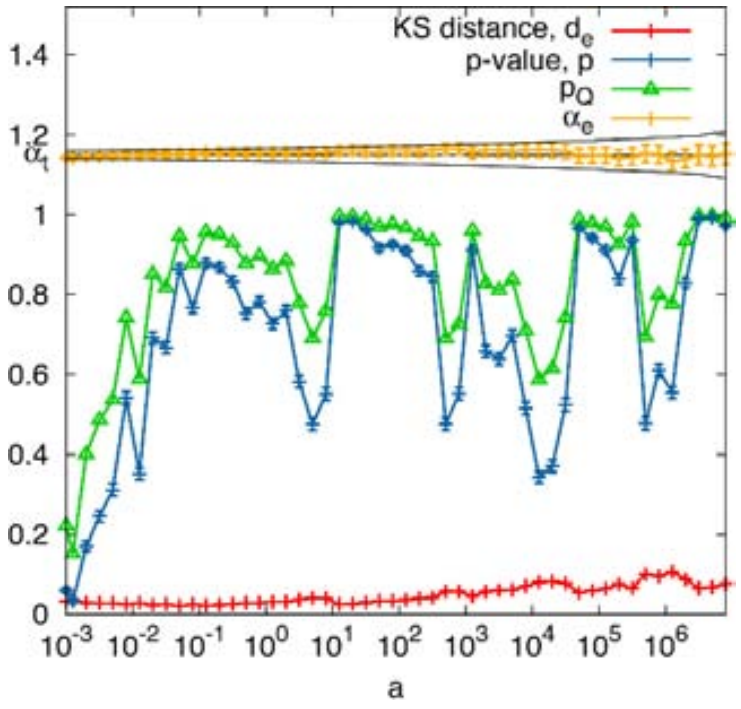

Fig. 4. Evolution as a function of a of the KS statistic, the false p-value p_Q, the true p-value (for fixed a), and the estimated exponent. The true exponent, here called α_t and equal to 1.15, is displayed as a thin black line, together with a 2σ interval. Colour version of this figure is available in electronic edition only.

the one for fixed a and b, and then the p-value of the whole procedure should be different, but at this point it is not necessary to obtain such a p-value, as we should have already come out with a reasonable fit. Figure 4 shows the results of the method for true power-law data.

2.10 Truncated or non-truncated power-law distribution?

For broadly distributed data, the simplest choice is to try to fit first a non-truncated power-law distribution. If an acceptable fit is found, it is expected that a truncated power law, with $b \geq x_{\max}$ (where $x_{\max}$ is the largest value of x) would yield also a good fit. In fact, if b is not considered as a fixed value but as a parameter to fit, its maximum likelihood estimator when the number of data is fixed, *i.e.*, when b is in the range $b \geq x_{\max}$, is $b_e = x_{\max}$. This is easy to see (Aban *et al.* 2006), just looking at the Eqs. (11) and (12) for $\ell(\alpha)$, which show that $\ell(\alpha)$ increases as b approaches $x_{\max}$. (In the same way, the ML estimator of a, for fixed number of data, would be $a_e = x_{\min}$, but we are not interested in such a case now.) On the other hand, it is reasonable that a truncated power law yields a better fit than a non-truncated one, as the former has two parameters and the latter only one (assuming that a is fixed, in any case).

In order to do a proper comparison, in such situations the so-called Akaike information criterion (AIC) can be used. This is defined simply as the difference

between twice the number of parameters and twice the maximum of the log-likelihood multiplied by the number of data, *i.e.*,

$$\mathrm{AIC} = 2 \times (\text{number of parameters}) - 2N\ell(\alpha_e) \; . \tag{39}$$

In general, having more parameters leads to better fits, and to higher likelihood, so, the first term compensates this fact. Therefore, given two models, the one with smaller AIC is preferred. Note that, in order that the comparison based on the AIC makes sense, the fits that are compared have to be performed exactly over the same data. So, in our case this can only be done for non-truncated power laws and for truncated power laws with $b \geq x_{\max}$. Nevertheless, due to the limitations of this paper we have not performed the comparison.

3. ESTIMATION OF PROBABILITY DENSITIES AND CUMULATIVE DISTRIBUTION FUNCTIONS

The method of maximum likelihood does not rely on the estimation of the probability distributions, in contrast to other methods. Nevertheless, in order to present the results, it is useful to display some representation of the distribution, together with its fit. This procedure has no statistical value (it cannot provide a substitution of a goodness-of-fit test) but is very helpful as a visual guide, specially in order to detect bugs in the algorithms.

3.1 Estimation of the probability density

In the definition of the probability density,

$$f(x) = \lim_{\Delta x \to 0} \frac{\text{Prob}[x \leq \text{random variable} < x + \Delta x]}{\Delta x} \; , \tag{40}$$

a fundamental issue is that the width of the interval Δx has to tend to zero. In practice Δx cannot tend to zero (there would be no statistics in such case), and one has to take a non-zero value of the width. The most usual procedure is to draw a histogram using linear binning (bins of constant width); however, there is no reason why the width of the distribution should be fixed (some authors even take $\Delta x = 1$ as the only possible choice). In fact, Δx should be chosen in order to balance the necessity of having enough statistics (large Δx) with that of having a good sampling of the function (small Δx). For power-law distributions and other fat-tailed distributions, which take values across many different scales, the right choice depends of the scale of x. In these cases it is very convenient to use the so-called logarithmic binning (Hergarten 2002, Pruessner 2012). This uses bins that appear as constant in logarithmic scale, but that in fact grow exponentially (for which the method is sometimes called

exponential binning instead). Curiously, this useful method is not considered by classic texts on density estimation (Silverman 1986).

Let us consider the semi-open intervals $[a_0, b_0), [a_1, b_1), \ldots, [a_k, b_k), \ldots$, also called bins, with $a_{k+1} = b_k$ and $b_k = Ba_k$ (this constant B has nothing to do with the one in the Gutenberg–Richter law, Section 1). For instance, if $B = \sqrt[5]{10}$ this yields 5 intervals for each order of magnitude. Notice that the width of every bin grows linearly with a_k, but exponentially with k, as $b_k - a_k = (B-1)a_k = a_0(B-1)B^k$. The value of B should be chosen in order to avoid low populated bins; otherwise, a spurious exponent equal to one appears (Pruessner 2012).

We simply will count the number of occurrences of the variable in each bin. For each value of the random variable x_i, the corresponding bin is found as

$$k = \text{int}\left(\frac{\ln(x_i/a_0)}{\ln B}\right), \tag{41}$$

where the function int denotes the integer part of its argument. Of course, a_0 has to be smaller than any possible value of x. For a continuous variable the concrete value of a_0 should be irrelevant (if it is small enough), but in practice one has to avoid that the resulting values of a_k coincide with round values of the variable (Corral *et al.* 2011).

So, with this logarithmic binning, the probability density can be estimated (following its definition) as the relative frequency of occurrences in a given bin divided by its width, *i.e.*,

$$f_e(x_k^*) = \frac{\text{number of occurrences in bin } k}{(b_k - a_k) \times \text{number of occurrences}}\,, \tag{42}$$

where the estimation of the density is associated to a value of x represented by x_k^*. The most practical solution is to take it in the middle of the interval in logscale, so $x_k^* = \sqrt{a_k b_k}$. However, for sparse data covering many orders of magnitude it is necessary to be more careful. In fact, what we are looking for is the point x_k^* whose value of the density coincides with the probability of being between a_k and b_k divided by the width of the interval. This is the solution of

$$f(x_k^*) = \frac{1}{b_k - a_k}\int_{a_k}^{b_k} f(x)dx = \frac{S(a_k) - S(b_k)}{b_k - a_k}\,, \tag{43}$$

where f and S are the theoretical distributions. When the distribution and its parameters are known, the equation can be solved either analytically or numerically. It is easy to see that for a power-law distribution (truncated or not) the solution can be written

$$x_k^* = \sqrt{a_k b_k}\left[(\alpha-1)\frac{B^{\alpha/2-1}(B-1)}{B^{\alpha-1}-1}\right]^{1/\alpha}\,, \tag{44}$$

where we have used that $B = b_k/a_k$ (if we were not using logarithmic binning we would have to write a bin-dependent B_k). Note that for constant (bin-independent) B, *i.e.*, for logarithmic binning, the solution is proportional but not equal to the geometric mean of the extremes of the bin. Nevertheless, the omission of the proportionality factor does not alter the power-law behavior, just shifts (in logarithmic scale) the curve. But for a different binning procedure this is no longer true. Moreover, for usual values of B the factor is very close to one (Hergarten 2002), although large values of B (Corral *et al.* 2011) yield noticeable deviations if the factor in brackets is not included; see also our treatment of the radionuclide half-lives in Section 3, with $B = 10$. Once the value of B is fixed (usually in this paper to $\sqrt[5]{10}$) , in order to avoid empty bins we merge consecutive bins until the resulting merged bins are not empty. This leads to a change in the effective value of B for merged bins, but the method is still perfectly valid.

The uncertainty of $f_e(x)$ can be obtained from its standard deviation (the standard deviation of the estimation of the density, f_e, not of the original random variable x). Indeed, assuming independence in the sample (which is already implicit in order to apply maximum likelihood estimation), the number of occurrences of the variable in bin k is a binomial random variable (in the same way as for the p-value). As the number of occurrences is proportional to $f_e(x)$, the ratio between the standard deviation and the mean for the number of occurrences will be the same as for $f_e(x)$, which is,

$$\frac{\sigma_f(x)}{f_e(x)} = \sqrt{\frac{q}{\text{mean number of occurrences in } k}} \simeq \frac{1}{\sqrt{\text{occurrences in } k}} , \qquad (45)$$

where we replace the mean number of occurrences in bin k (not available from a finite sample) by the actual value, and q, the probability that the occurrences are not in bin k, by one. This estimation of $\sigma_f(x)$ fails when the number of counts in the bin is too low, in particular if it is one.

One final consideration is that the fitted distributions are normalized between a and b, with N number of data, whereas the empirical distributions include all data, with N_{tot} of them, $N_{\text{tot}} \geq N$. Therefore, in order to compare the fits with the empirical distributions, we will plot $Nf(x)/N_{\text{tot}}$ together with $f_e(x_k^*)$.

3.2 Estimation of the cumulative distribution

The estimation of the (complementary) cumulative distribution is much simpler, as bins are not involved. One just needs to sort the data, in ascending order, $x_{(1)} \leq x_{(2)} \leq \cdots \leq x_{(N_{\text{tot}}-1)} \leq x_{(N_{\text{tot}})}$; then, the estimated cumulative distribution is

$$S_e(x_{(i)}) = \frac{n_e(x_{(i)})}{N_{\text{tot}}} = \frac{N_{\text{tot}} - i + 1}{N_{\text{tot}}} , \qquad (46)$$

for the data points, $S_e(x) =$ constant below these data points, and $S_e(x) = 0$ for $x > x_{(N_{\rm tot})}$; $n_e(x_{(i)})$ is the number of data with $x \geq x_{(i)}$ in the empirical sample. The formula relating $n_e(x_{(i)})$ with i assumes that repeated values of the variable are not possible, so it would not be valid for a discrete x. We use the case of empirical data as an example, but it is of course the same for simulated data. For the comparison of the empirical distribution with the theoretical fit we need to correct the different number of data in both cases. So, we plot both $[NS(x) + n_e(b)]/N_{\rm tot}$ and $S_e(x)$, in order to check the accuracy of the fit.

4. DATA ANALYZED AND RESULTS

We have explained how, in order to certify that a dataset is compatible with a simple power-law distribution, many mathematical formulas are required, leading to an astonishingly large number of calculations. Now we check the performance of our method with diverse geophysical data, which were previously analyzed with different, less rigorous or worse-functioning methods. For the peculiarities and challenges of the dataset, we also include the half-lives of unstable nuclides. The parameters of the method are fixed to $N_s = 1000$ Monte Carlo simulations and the values of a and b are found sweeping a fixed number of points per order of magnitude, equally spaced in logarithmic scale. This number is 10 for non-truncated power laws (in which b is fixed to infinity) and 5 for truncated power laws. Three values of p_c are considered: 0.1, 0.2, and 0.5, in order to compare the dependence of the results on this parameter. The results are reported using the Kolmogorov–Smirnov test for goodness-of-fit. If, instead, the Kuiper's test is used, the outcome is not significantly different in most of the cases. In a few cases the fitting range, and therefore the exponent, changes, but without a clear trend, *i.e.*, the fitting range can become smaller or increase. These cases deserve a more in-depth investigation.

4.1 Half-lives of the radioactive elements

Corral *et al.* (2011) studied the statistics of the half-lives of radionuclides (comprising both nuclei in the fundamental and in excited states). Any radionuclide has a constant probability of disintegration per unit time, the decay constant, let us call it λ (Krane 1988). If M is the total amount of radioactive material at time t, this means that

$$-\frac{1}{M}\frac{dM}{dt} = \lambda \, . \tag{47}$$

This leads to an exponential decay, for which a half-life $t_{1/2}$ or a lifetime τ can be defined, as

$$t_{1/2} = \tau \ln 2 = \frac{\ln 2}{\lambda} \, . \tag{48}$$

It is well known that the half-lives take disparate values, for example, that of ^{238}U is 4.47 (American) billions of years, whereas for other nuclides it is a very tiny fraction of a second.

It has been recently claimed that these half-lives are power-law distributed (Corral *et al.* 2011). In fact, three power-law regions were identified in the probability density of $t_{1/2}$, roughly,

$$f(t_{1/2}) \propto \begin{cases} 1/t_{1/2}^{0.65} & \text{for } 10^{-6}\,\text{s} \leq t_{1/2} \leq 0.1\,\text{s} \\ 1/t_{1/2}^{1.19} & \text{for } 100\,\text{s} \leq t_{1/2} \leq 10^{10}\,\text{s} \\ 1/t_{1/2}^{1.09} & \text{for } t_{1/2} \geq 10^{8}\,\text{s}. \end{cases} \tag{49}$$

Notice that there is some overlap between two of the intervals, as reported in the original reference, due to problems in delimiting the transition region. The study used variations of the Clauset *et al.*'s (2009) method of minimization of the KS statistic, introducing and upper cutoff and additional conditions to escape from the global minimum of the KS statistic, which yielded the rejection ($p = 0.000$) of the power-law hypothesis. These additional conditions were of the type of taking either a or b/a greater than a fixed amount.

For comparison, we will apply the method explained in the previous section to this problem. Obviously, our random variable will be $x = t_{1/2}$. The data is exactly the same as in the original reference, coming from the Lund/LBNL Nuclear Data Search web page (Chu *et al.* 1999). Elements whose half-life is only either bounded from below or from above are discarded for the study, which leads to 3002 radionuclides with well-defined half-lives; 2279 of them are in their ground state and the remaining 723 in an exited state. The minimum and maximum half-lives in the dataset are 3×10^{-22} s and 7×10^{31} s, respectively, yielding more than 53 orders of magnitude of logarithmic range. Further details are in Corral *et al.* (2011).

The results of our fitting and testing method are shown in Table 1 and in Fig. 5. The fitting of a non-truncated power law yields results in agreement with Corral *et al.* (2011), with $\alpha = 1.09 \pm 0.01$ and $a = 3 \times 10^7$ s, for the three values of p_c analyzed (0.1, 0.2, and 0.5). When fitting a truncated power law, the maximization of the log-range, b/a, yields essentially the same results as for a non-truncated power law, with slightly smaller exponents α due to the finiteness of b (results not shown). In contrast, the maximization of the number of data N yields an exponent $\alpha \simeq 0.95$ between $a \simeq 0.1\,\text{s}$ and $b \simeq 400\,\text{s}$ (with some variations depending on p_c). This result is in disagreement with Corral *et al.* (2011), which yielded a smaller exponent for smaller values of a and b. In fact, as the intervals do not overlap both results are compatible, but it is also likely that a different function would lead to a better fit; for instance, a lognormal between 0.01 s and 10^5 s was proposed by Corral *et al.* (2011),

Table 1

Results of the fits for the $N_{\rm tot} = 3002$ nuclide half-lives data, for different values of p_c

N	a [s]	b [s]	b/a	$\alpha \pm \sigma$	p_c
143	0.316×10^8	∞	∞	1.089 ± 0.007	0.10
143	0.316×10^8	∞	∞	1.089 ± 0.007	0.20
143	0.316×10^8	∞	∞	1.089 ± 0.008	0.50
1596	0.0794	501	6310	0.952 ± 0.010	0.10
1539	0.1259	501	3981	0.959 ± 0.011	0.20
1458	0.1259	316	2512	0.950 ± 0.011	0.50
1311	125.9	0.501×10^{23}	0.398×10^{21}	1.172 ± 0.005	0.10
1309	125.9	0.316×10^{22}	0.251×10^{20}	1.175 ± 0.005	0.20
1303	125.9	0.794×10^{18}	0.631×10^{16}	1.177 ± 0.005	0.50

Notes: We show the cases of a pure or non-truncated power law (with $b = \infty$, fixed) and truncated power law (with b finite, estimated from data), maximizing N. The latter is split into two subcases: exploring the whole range of a (rows 4, 5, and 6) and restricting a to $a > 100$ s (rows 7, 8, and 9).

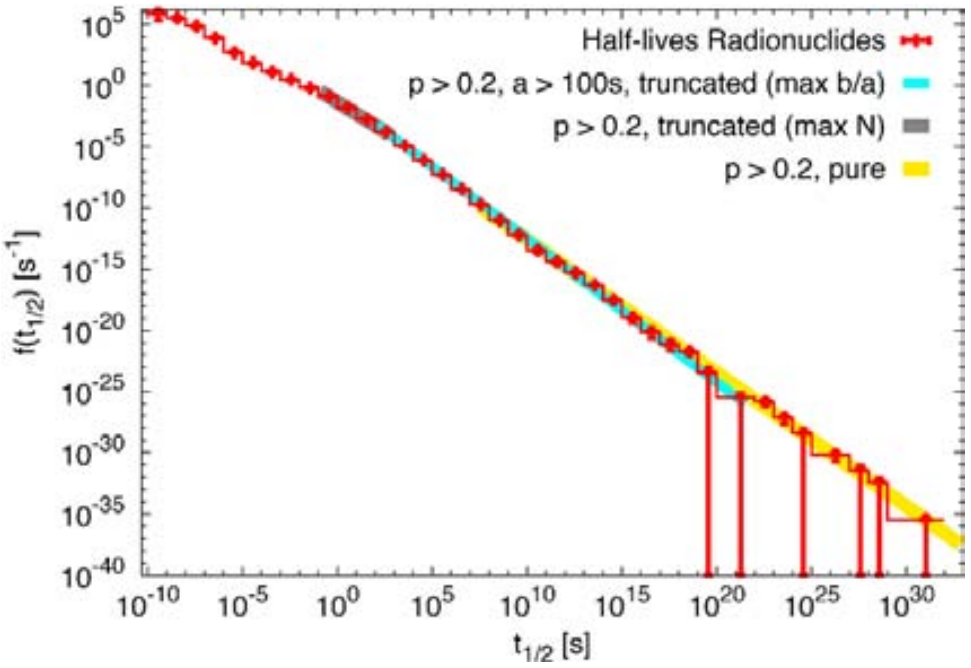

Fig. 5. Estimated probability density of the half-lives of the radionuclides, together with the power-law fits explained in the text. The number of log-bins per order of magnitude is one, which poses a challenge in the correct estimation of the density, as explained in Section 3. Data below 10^{-10} s are not shown. Colour version of this figure is available in electronic edition only.

although the fitting procedure there was not totally reliable. Finally, the intermediate power-law range reported in the original paper (the one with $\alpha = 1.19$) is not found by any of our algorithms working on the entire dataset. It is necessary to cut the dataset, removing data below, for instance, 100 s (which is equivalent to impose $a > 100$ s), in order that the algorithm converges to that solution. So, caution must be taken when applying the algorithm blindly, as important power-law regimes may be hidden by others having either larger N or larger log-range.

4.2 Seismic moment of earthquakes

The statistics of the sizes of earthquakes (Gutenberg and Richter 1944) has been investigated not only since the introduction of the first magnitude scale, by Richter, but even before, in the 1930's, by Wadati (Utsu 1999). From a modern perspective, the most reliable measure of earthquake size is given by the (scalar) seismic moment M, which is the product of the mean final slip, the rupture area, and the rigidity of the fault material (Ben-Zion 2008). It is usually assumed that the energy radiated by an earthquake is proportional to the seismic moment (Kanamori and Brodsky 2004), so, a power-law distribution of the seismic moment implies a power-law distribution of energies, with the same exponent.

The most relevant results for the distribution of seismic moment are those of Kagan for worldwide seismicity (Kagan 2002), who showed that its probability density has a power-law body, with a universal exponent in agreement with $\alpha = 1.63 \simeq 5/3$, but with an extra, non-universal exponential decay (at least in terms of the complementary cumulative distribution). However, Kagan's (2002) analysis, ending in 2000, refers to a period of global seismic "quiescence"; in particular, the large Sumatra–Andaman earthquake of 2004 and the subsequent global increase of seismic activity are not included. Much recently, Main *et al.* (2008) have shown, using a Bayesian information criterion, that the inclusion of the new events leads to the preference of the non-truncated power-law distribution in front of models with a faster large- M decay.

We take the Centroid Moment Tensor (CMT) worldwide catalog analyzed by Kagan (2002) and by Main *et al.* (2008), including now data from January 1977 to December 2010, and apply our statistical method to it. Although the statistical analysis of Kagan is rather complete, his procedure is different to ours. Note also that the dataset does not comprise the recent (2011) Tohoku earthquake in Japan; nevertheless, the qualitative change in the data with respect to Kagan's period of analysis is very remarkable. Following this author, we separate the events by their depth: shallow for depth ≤ 70 km, intermediate for 70 km $<$ depth ≤ 300 km, and deep for depth > 300 km. The number of earthquakes in each category is 26824, 5281, and 1659, respectively.

Second, we also consider the Southern California's Waveform Relocated Earthquake Catalog, from 1 January 1981 to 30 June 2011, covering a rectangular box of coordinates $(122^\circ\,\mathrm{W}, 30^\circ\,\mathrm{N})$, $(113^\circ\,\mathrm{W}, 37.5^\circ\,\mathrm{N})$ (Hauksson *et al.* 2012, Shearer *et al.* 2005). This catalog contains 111981 events with $m \geq 2$. As, in contrast with the CMT catalog, this one does not report the seismic moment M, the magnitudes m there are converted into seismic moments, using the formula

$$\log_{10} M = \frac{3}{2}(m + 6.07)\,, \tag{50}$$

where M comes in units of Nm (Newtons times meters); however, this formula is a very rough estimation of seismic moment, as it is only accurate (and exact) when m is the so-called moment magnitude (Kanamori and Brodsky 2004), whereas the magnitudes recorded in the catalog are not moment magnitudes. In any case, our procedure here is equivalent to fit an exponential distribution to the magnitudes reported in the catalog.

Tables 2 and 3 and Fig. 6 summarize the results of analyzing these data with our method, taking $x = M$ as the random variable. Starting with the non-truncated power-law distribution, we always obtain an acceptable (in the sense of non-rejectable) power-law fit, valid for several orders of magnitude. In all cases the exponent α is between 1.61 and 1.71, but for Southern California it is always very close to 1.66. For the worldwide CMT data the largest value of a is $3 \times 10^{18}\,\mathrm{Nm}$, corresponding to a magnitude $m = 6.25$ (for shallow depth), and the smallest is $a = 8 \times 10^{16}\,\mathrm{Nm}$, corresponding to $m = 5.2$ (intermediate depth). If the events are not separated in terms of their depth (not shown), the results are dominated by the shallow case, except for $p_c = 0.5$, which leads to very large values of a and α $(a = 5 \times 10^{20}\,\mathrm{Nm}$ and $\alpha \simeq 2)$. The reason is probably the mixture of the different populations, in terms of depth, which is not recommended by Kagan (2002). This is an indication that the inclusion of an upper limit b to the power law may be appropriate, with each depth corresponding to different b's. For Southern California, the largest a found (for $p_c = 0.5)$ is $1.6 \times 10^{15}\,\mathrm{Nm}$, giving $m = 4$. This value is somewhat higher, in comparison with the completeness magnitude of the catalog; perhaps the reason that the power-law fit is rejected for smaller magnitudes is due to the fact that these magnitudes are not true moment magnitudes, but come from a mixture of different magnitude definitions. If the value of a is increased, the number of data N is decreased and the power-law hypothesis is more difficult to reject, due simply to poorer statistics. When a truncated power law is fitted, using the method of maximizing the number of data leads to similar values of the exponents, although the range of the fit is in some cases moved to smaller values (smaller a, and b smaller than the maximum M on the dataset). The method of maximizing b/a leads to results that are very close to the non-truncated power law.

Table 2

Results of the non-truncated power-law fit $(b = \infty)$ applied to the seismic moment of earthquakes in CMT worldwide catalog (separating by depth) and to the Southern California catalog, for different p_c

Catalog	N	a [Nm]	$\alpha \pm \sigma$	p_c
CMT deep	1216	0.1259×10^{18}	1.622 ± 0.019	0.10
intermediate	3701	0.7943×10^{17}	1.654 ± 0.011	0.10
shallow	5799	0.5012×10^{18}	1.681 ± 0.009	0.10
CMT deep	898	0.1995×10^{18}	1.608 ± 0.020	0.20
intermediate	3701	0.7943×10^{17}	1.654 ± 0.011	0.20
shallow	5799	0.5012×10^{18}	1.681 ± 0.009	0.20
CMT deep	898	0.1995×10^{18}	1.608 ± 0.021	0.50
intermediate	3701	0.7943×10^{17}	1.654 ± 0.011	0.50
shallow	1689	0.3162×10^{19}	1.706 ± 0.018	0.50
S. California	1327	0.1000×10^{16}	1.660 ± 0.018	0.10
S. California	1327	0.1000×10^{16}	1.660 ± 0.018	0.20
S. California	972	0.1585×10^{16}	1.654 ± 0.021	0.50

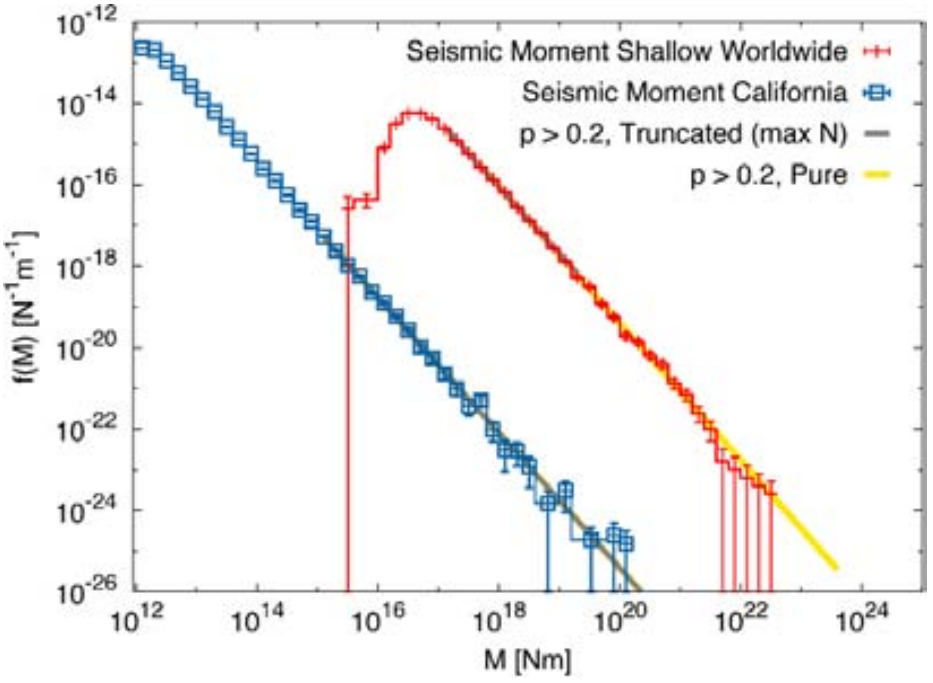

Fig. 6. Estimated probability densities and corresponding power-law fits of the seismic moment M of shallow earthquakes in the worldwide CMT catalog and of the estimated M in the Southern California catalog. Colour version of this figure is available in electronic edition only.

Table 3

Results of the truncated power-law fit, by maximizing the number of data, applied to the seismic moment of earthquakes in CMT worldwide catalog (separating by depth) and to the Southern California catalog, for the different p_c

Catalog	N	a [Nm]	b [Nm]	b/a	$\alpha \pm \sigma$	p_c
CMT deep	1216	0.1259×10^{18}	0.3162×10^{23}	0.2512×10^{6}	1.621 ± 0.019	0.10
intermediate	3701	0.7943×10^{17}	0.7943×10^{22}	0.1000×10^{6}	1.655 ± 0.011	0.10
shallow	13740	0.1259×10^{18}	0.5012×10^{20}	0.3981×10^{3}	1.642 ± 0.007	0.10
CMT deep	1076	0.1259×10^{18}	0.5012×10^{19}	0.3981×10^{2}	1.674 ± 0.033	0.20
intermediate	3701	0.7943×10^{17}	0.7943×10^{22}	0.1000×10^{6}	1.655 ± 0.011	0.20
shallow	13518	0.1259×10^{18}	0.1995×10^{20}	0.1585×10^{3}	1.636 ± 0.008	0.20
CMT deep	898	0.1995×10^{18}	0.3162×10^{23}	0.1585×10^{6}	1.604 ± 0.021	0.50
intermediate	3701	0.7943×10^{17}	0.7943×10^{22}	0.1000×10^{6}	1.655 ± 0.011	0.50
shallow	11727	0.1259×10^{18}	0.1995×10^{19}	0.1585×10^{2}	1.608 ± 0.012	0.50
S. California	1146	0.1259×10^{16}	0.1259×10^{22}	0.1000×10^{7}	1.663 ± 0.020	0.10
S. California	1146	0.1259×10^{16}	0.1259×10^{22}	0.1000×10^{7}	1.663 ± 0.020	0.20
S. California	344	0.7943×10^{16}	0.1259×10^{22}	0.1585×10^{6}	1.664 ± 0.036	0.50

Note: Except for global shallow seismicity (and for the global deep case with $p_c = 0.20$) the selected b is larger than the maximum value of the variable.

4.3 Energy of tropical cyclones

Tropical cyclones are devastating atmospheric-oceanic phenomena comprising tropical depressions, tropical storms, and hurricanes or typhoons (Emanuel 2005a). Although the counts of events every year have been monitored for a long time, and other measurements to evaluate annual activity have been introduced (see Corral and Turiel (2012) for an overview), little attention has been paid to the statistics of individual tropical cyclones.

In 2005, Emanuel introduced the power-dissipation index (PDI) as a simple way to obtain a rough estimation of the total energy dissipated by all tropical cyclones in a given season and some ocean basin (Emanuel 2005b). But the PDI can also be used to characterize individual events as well, as it was done later by Corral *et al.* (2010). Indeed, the PDI is defined as the sum for all the discrete times t (that comprise the lifetime of a tropical cyclone) of the cube of the maximum sustained wind speed multiplied by the time interval of sampling, Δt. In a formula,

$$\mathrm{PDI} = \sum_{\forall t} v_t^3 \Delta t \,, \tag{51}$$

where v_t is the maximum sustained wind speed. In the so-called best-track records, $\Delta t = 6$ hours; this factor would only be necessary in order to compare

with other data with different Δt (but caution should be present in this case for the possible fractal nature of the speed signal). Although the speeds are reported in knots, they are converted to m/s (using that 1 knot $= 0.514$ m/s), and then we report the PDI in $\mathrm{m}^3/\mathrm{s}^2$.

Corral *et al.* (2010) studied the statistics of the PDI (defined for individual events, in contrast to Emanuel's (2005b) work) in 4 different ocean basins for several time periods. The results showed a rapid, perhaps exponential, decay at the tail, but a body of the distribution compatible with a power law, for 1 or 2 orders of magnitude, with exponents close to one. The connection with SOC phenomena was discussed by Corral (2010). The method used was again a variation of the Clauset *et al.*'s (2009) one, introducing an upper cutoff and additional restrictions to the variations of the parameters. Here we revisit this problem, trying to use updated data (whenever it has been possible), and applying the method which is the subject of this paper to $x = \mathrm{PDI}$.

The data has been downloaded from the National Hurricane Center (NHC) of NOAA, for the North Atlantic and the Northeastern Pacific (Jarvinen *et al.* 1988, NHC 2012) and from the Joint Typhoon Warning Center (JTWC) of the US Navy (Chu *et al.* 2002, JTWC Annual Tropical Cyclone Reports 2012) for the Northwestern Pacific, the Southern Hemisphere (comprising the Southern Indian and the Southwestern Pacific), and the Northern Indian Ocean. The abbreviation, time span, and number of events for each basin are: NAtl, 1966-2011, 532; EPac, 1966-2011, 728; WPac, 1986-2011, 690; SHem, 1986-2007 (up to May), 523; NInd, 1986-2007, 110. The latter case was not studied in any of the previous works.

The results for a truncated power law maximizing N, shown in Table 4 and Fig. 7, are in agreement with those of Corral *et al.* (2010). In general, exponents are close but above 1, except for the Northwestern Pacific, where $\alpha \simeq 0.96$, and for the North Indian Ocean, where α is substantially higher than one. We consider that this method performs rather well. It would be interesting to test if universality can nevertheless hold (the high value for the North Indian Ocean is based in much less data than for the rest of basins), or if there is some systematic bias in the value of the exponents (the protocols of the NHC and the JTWC are different, and the satellite coverage of each basin is also different).

If a non-truncated power law is fit to the data, the fits turn out to be rather short, with a high exponent (up to 6) describing the tail of the distribution (except for the Southern Hemisphere, where no such tail is apparent). We do not give any relevance to these results, as other alternatives, as for instance a simple exponential tail, have to be considered (Corral and Turiel 2012, del Castillo *et al.* 2012). Coming back to a truncated power law, but maximizing the log-range, the algorithm sometimes fits the power law in the body of the distribution (with exponent close to 1) and for some other times the algorithm goes to the fast-decaying tail. So the method of maximizing b/a is not useful for this data.

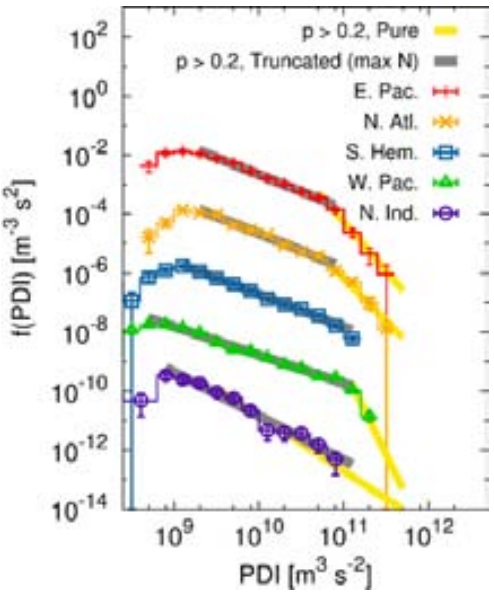

Fig. 7. Estimated probability densities of the PDI of tropical cyclones in 5 ocean basins, together with their power-law fits. The values of the densities are multiplied by 1, 10^2, 10^4, 10^6, and 10^8, for clarity sake. The fits for the non-truncated case are also displayed, although they are not tabulated. Colour version of this figure is available in electronic edition only.

Table 4

Results of the truncated power-law fits, maximizing N, for the PDI in the 5 ocean basins with tropical-cyclone activity, for different values of p_c

Basin	N	a [m^3/s^2]	b [m^3/s^2]	b/a	$\alpha \pm \sigma$	p_c
EPac	637	0.1259×10^{10}	0.7943×10^{11}	63	1.094 ± 0.033	0.10
NAtl	417	0.1995×10^{10}	0.7943×10^{11}	40	1.168 ± 0.047	0.10
SHem	523	0.1259×10^{10}	0.1259×10^{12}	100	1.108 ± 0.034	0.10
WPac	637	0.5012×10^{9}	0.1259×10^{12}	251	0.957 ± 0.025	0.10
NInd	102	0.7943×10^{9}	0.1995×10^{12}	251	1.520 ± 0.077	0.10
EPac	571	0.1995×10^{10}	0.7943×10^{11}	40	1.149 ± 0.039	0.20
NAtl	417	0.1995×10^{10}	0.7943×10^{11}	40	1.168 ± 0.047	0.20
SHem	523	0.1259×10^{10}	0.1259×10^{12}	100	1.108 ± 0.033	0.20
WPac	637	0.5012×10^{9}	0.1259×10^{12}	251	0.957 ± 0.025	0.20
NInd	102	0.7943×10^{9}	0.1259×10^{12}	158	1.490 ± 0.077	0.20
EPac	571	0.1995×10^{10}	0.7943×10^{11}	40	1.149 ± 0.040	0.50
NAtl	417	0.1995×10^{10}	0.7943×10^{11}	40	1.168 ± 0.045	0.50
SHem	465	0.1995×10^{10}	0.1259×10^{12}	63	1.132 ± 0.040	0.50
WPac	637	0.5012×10^{9}	0.1259×10^{12}	251	0.957 ± 0.024	0.50
NInd	86	0.7943×10^{9}	0.1259×10^{11}	16	1.323 ± 0.139	0.50

4.4 Area of forest fires

The statistics of the size of forest fires was an intense topic of research since the introduction of the concept of SOC, at the end of the 1980's, but only from the point of view of cellular-automaton models. Real data analysis had to wait several years (Malamud *et al.* 1998, 2005), leading to power-law distributions, more or less in agreement with the models. Here we are particularly interested in a dataset from Italy, for which a power-law distribution of sizes was ruled out (Corral *et al.* 2008). Instead, a lognormal tail was proposed for the fire-size probability density.

The data considered by Corral *et al.* (2008), and reanalyzed in this study, comes from the Archivio Incendi Boschivi (AIB) fire catalog compiled by the (Italian) Corpo Forestale dello Stato (2012). The subcatalog to which we restrict covers all Italy and spans the 5-year period 1998-2002, containing 36 748 fires. The size of each fire is measured by the burned area A, in hectares, with $1\ \mathrm{ha} = 10^4\ \mathrm{m}^2$. In this subsection we analyze the case of $x = A$.

The results in Table 5 and Fig. 8 show that a pure (non-truncated) power law is only acceptable (in the sense of non-rejectable) for the rightmost part of the tail of the distribution, comprising less than one order of magnitude. It is very indicative that only 51 data are in the possible power-law tail. Therefore, we disregard this power-law behavior as spurious and expect that other distributions can yield a much better fit (not in order of the quality of the fit but regarding the number of data it spans). This seems in agreement with other analyses of forest-fire data (Clauset *et al.* 2009, Newman 2005). If a truncated power-law is considered, fitted by maximizing the number of data, the results are not clearly

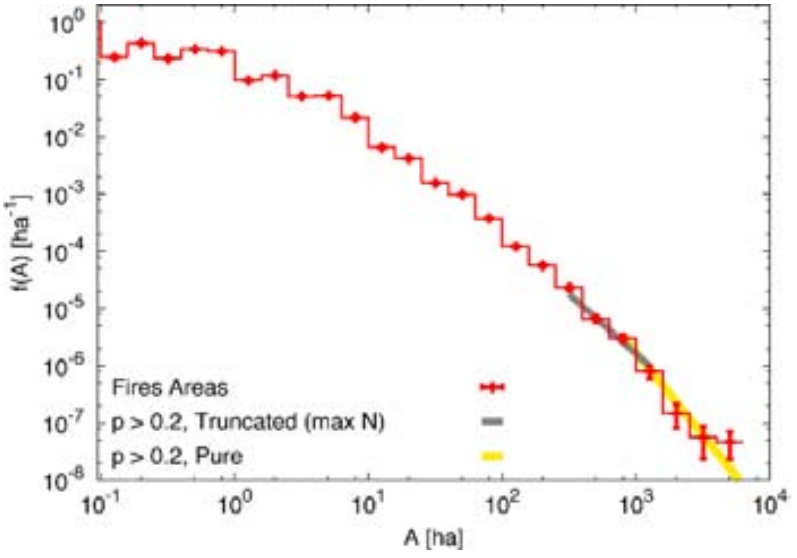

Fig. 8. Estimated probability density of the area of fires in the Italian catalog, together with the power-law fits. In contrast to the previous datasets analyzed, we consider these power-law fits as irrelevant. Colour version of this figure is available in electronic edition only.

Table 5

Results of the fits for the burned area of the $N_{\rm tot} = 36\,748$ fires recorded in the Italian catalog, for different p_c

N	a [ha]	b [ha]	b/a	$\alpha \pm \sigma$	p_c
51	794	∞	∞	2.880 ± 0.276	0.10
51	794	∞	∞	2.880 ± 0.277	0.20
51	794	∞	∞	2.880 ± 0.277	0.50
168	316	7943	25	2.353 ± 0.117	0.10
148	316	1259	4	2.075 ± 0.213	0.20
51	794	79430	100	2.870 ± 0.281	0.50

Note: The cases of a non-truncated power law and a truncated power law, maximizing N, are shown. In the latter case, for $p_c = 0.10$ and 0.50 the value of b is larger than the maximun value of the variable.

better, as seen in the table. Moreover, there is considerable variation with the value of p_c. So, we do not give any relevance to such power-law fits. Finally, the method of maximizing b/a yields the same results as for the non-truncated power law (except by the fact that the exponents are slightly smaller, not shown). In order to provide some evidence for the better adequacy of the lognormal tail in front of the power-law tail for these data, it would be interesting to apply an adaptation of the test explained by del Castillo and Puig (1999).

4.5 Waiting time between earthquakes

The temporal properties of earthquakes have been a subject relatively little studied (at least in comparison with the size of earthquakes). It is true that the Omori law has been known for more than 100 years (Utsu 2002, Utsu *et al.* 1995), and that this is a law extremely important in order to assess the hazard of aftershocks after a big event, but the Omori law looks at time properties in a very coarse-grained way, as it only provides the number of events in relatively large time windows. Thus, no information on the fine time structure of seismicity is provided, at least directly.

The situation has changed in the last decade, since the seminal study of Bak *et al.* (2002), who found a unified scaling law for earthquake waiting-time distributions. They took Southern California and divided it in different areas, and computed the time between consecutive earthquakes for each area. So, if t_i^j denotes the time of occurrence of the i-th earthquake in area j, the corresponding waiting time τ_i^j is

$$\tau_i^j = t_i^j - t_{i-1}^j \,. \tag{52}$$

The key point is that all the resulting waiting times were added to the same distribution (and not to a different distribution j for each area). Subsequently, the unified scaling law was found to be valid for other regions of the world (Corral 2004b). The shape of the resulting probability density corresponds to a double power law, one for small waiting times, associated to a mixture of scales of waiting times due to the Omori law, and another for large waiting times, due to spatial heterogeneity arising from the mixture of different areas with different seismic rates (Bak *et al.* 2002, Corral 2003, 2004b, Corral and Christensen 2006). The first exponent was found to be close to 1, whereas the second one was about 2.2; the fits were done by means of the nonlinear least-squares Marquardt–Levenberg algorithm from "gnuplot", applied to the logarithm of the log-binned empirical density. Here we apply our more sophisticated method to updated data for Southern California seismicity, with $x = \tau$.

We use again the relocated Southern California catalog of Hauksson *et al.* (2012), see also Shearer *et al.* (2005), but starting in 1984 and ending in 30 June 2011. This is to avoid some holes in the catalog for the preceding years. As for earthquake sizes, the occurrence takes place in a rectangle of coordinates $(122^\circ\,\mathrm{W}, 30^\circ\mathrm{N})$, $(113^\circ\,\mathrm{W}, 37.5^\circ\mathrm{N})$. This rectangle is divided into equal parts both in the West-East axis and in the South-North axis, in such a way that we consider a number of subdivisions of $4\times4,\ 8\times8,\ 16\times16,$ and 32×32. The waiting times for events of magnitude $m \geq 2$ in each of these subdivisions are computed as explained above, resulting in a number of data between 103 000 and 104 000 in all cases.

For a non-truncated power law, the results are only coherent with the previous reported ones (exponent around 2.2) for the intermediate cases, *i.e.*, 8×8 and $16 \times 16,$ see Table 6 and Fig. 9. The disagreement for the other cases can easily be explained. For $4 \times 4,$ the number of resulting subdivisions, 16, seems rather small. As mentioned, in Corral and Christensen (2006) the power-law tail was explained in terms of a power-law mixture of exponentials; so, with only 16 regions it is possible that the asymptotic behavior is still not reached. On the other hand, the effect of the finite duration of the catalog is visible in the 32×32 data. Due to the scaling behavior of the distributions (Corral 2003, 2004b), the possible power-law tail in this case is displaced to larger waiting times; but the time span of the catalog, about $10^{10}\ \mathrm{s},$ clearly alters this power law, which starts to bend at about $10^9\ \mathrm{s}$. Thus, we conclude that a power-law exponent of about $\alpha \simeq 2.2$ or 2.3 indeed exists, provided that the number of spatial subdivisions is high enough and the temporal extension of the catalog is large enough.

When a truncated power-law is fitted, using the method of maximizing the number of data $N,$ the other power law emerges, but for a range shorter than what the plot of the densities suggests. The exponent is in a range from 0.95 to 1.04 (except for the 4×4 cases, in which it is a bit smaller). The largest

Table 6

Results of the fits with a non-truncated power law and a truncated power law, maximizing N, for earthquake waiting times calculated for different subdivisions of Southern California

Subdivisions	N	a [s]	b [s]	b/a	$\alpha \pm \sigma$	p_c
4×4	124	0.5012×10^7	∞	∞	1.921 ± 0.085	0.10
8×8	1671	0.3162×10^7	∞	∞	2.198 ± 0.031	0.10
16×16	542	0.3162×10^8	∞	∞	2.324 ± 0.056	0.10
32×32	67	0.3162×10^9	∞	∞	4.404 ± 0.405	0.10
4×4	124	0.5012×10^7	∞	∞	1.921 ± 0.085	0.20
8×8	1671	0.3162×10^7	∞	∞	2.198 ± 0.031	0.20
16×16	542	0.3162×10^8	∞	∞	2.324 ± 0.056	0.20
32×32	67	0.3162×10^9	∞	∞	4.404 ± 0.403	0.20
4×4	77	0.7943×10^7	∞	∞	1.856 ± 0.098	0.50
8×8	322	0.1259×10^8	∞	∞	2.231 ± 0.070	0.50
16×16	24	0.3162×10^9	∞	∞	4.106 ± 0.703	0.50
32×32	67	0.3162×10^9	∞	∞	4.404 ± 0.449	0.50
4×4	38765	1995	0.5012×10^5	25	0.867 ± 0.006	0.10
8×8	39851	316	0.1995×10^5	63	0.987 ± 0.004	0.10
16×16	44178	7943	0.7943×10^6	100	0.956 ± 0.004	0.10
32×32	43512	1259	0.1995×10^6	158	1.029 ± 0.003	0.10
4×4	38765	1995	0.5012×10^5	25	0.867 ± 0.006	0.20
8×8	39851	316	0.1995×10^5	63	0.987 ± 0.004	0.20
16×16	39481	7943	0.5012×10^6	63	0.950 ± 0.005	0.20
32×32	39654	1259	0.1259×10^6	100	1.033 ± 0.004	0.20
4×4	34113	3162	0.5012×10^5	16	0.864 ± 0.007	0.50
8×8	39851	316	0.1995×10^5	63	0.987 ± 0.004	0.50
16×16	39481	7943	0.5012×10^6	63	0.950 ± 0.005	0.50
32×32	39654	1259	0.1259×10^6	100	1.033 ± 0.004	0.50

Note: Different minimum p-values are shown. The total number of data is above 103 000 in any case.

log-range is 100, *i.e.*, two decades. The graphical representation of the density seems to indicate that the possible power law is influenced by the effect of two crossovers, one for large waiting times, associated to a change in exponent, and

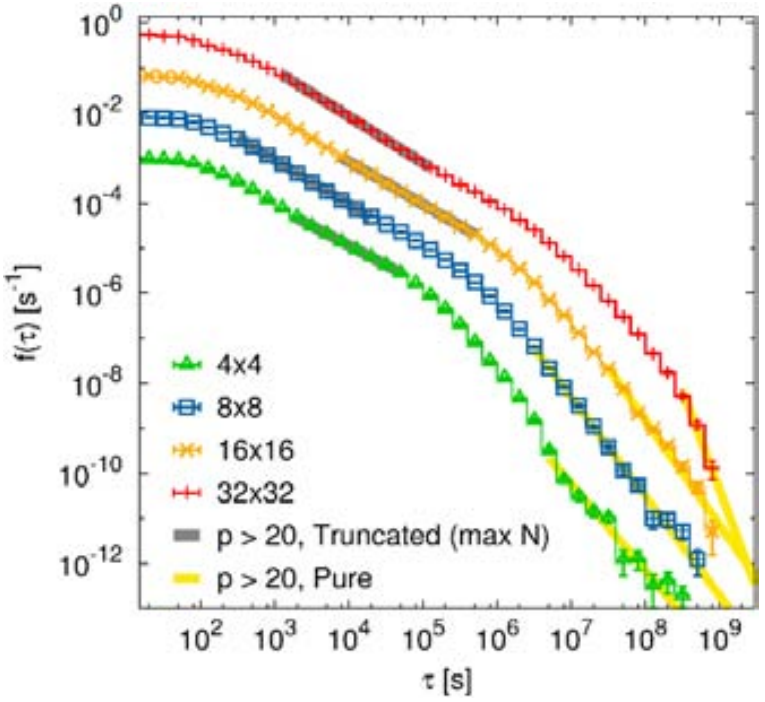

Fig. 9. Estimated probability densities and corresponding power-law fits for the waiting times of $m \geq 2$ in the Southern California catalog, for different spatial subdivisions. The values of the density are multiplied by factors 1, 10, 100, and 1000, for clarity sake. Colour version of this figure is available in electronic edition only.

another one for smaller times, where the distribution becomes flat. Finally, the method of fitting which maximizes the log-range leads to results that are similar to the non-truncated power-law case, although sometimes intervals corresponding to very small times are selected. The latter results have no physical meaning, as correspond to times below 1 s, *i.e.*, below the error in the determination of the occurrence time.

5. CONCLUSIONS

For power-law distributions, the fitting and the testing of the goodness of the fit is a difficult but very relevant problem in complex-systems science, in general, and in geoscience in particular. The most critical step is to select, automatically (without introducing any subjective bias), where the power-law regime starts and where it ends. We have explained in detail a conceptually simple but somewhat laborious procedure in order to overcome some difficulties previously found in the method introduced by Clauset *et al.* (2009); see Corral *et al.* (2011). Our method is summarized in fitting by maximum likelihood estimation and testing the goodness of fit by the Kolmogorov–Smirnov statistic, using Monte Carlo simulations. Although these steps are in common with the Clauset *et al.*'s (2009) recipe, the key difference is in the criterion of selection of the

power-law range. Despite the many steps of these procedures, ours can be easily implemented, and the resulting algorithms run very fast in current computers. We also have explained how to estimate properly the probability density of a random variable which has a power law or a fat-tail distribution. This is important to draw graphical representations of the results of the fitting (specially in Fig. 5) but it is not required to perform neither the fits nor the goodness-of-fit tests.

The performance of the method is quite good, as checked in synthetic power-law datasets, and the results of the analysis of previously reported power laws are very consistent. We confirm a very broad power-law tail in the distribution of the half-lives of the radionuclides, with exponent $\alpha = 1.09,$ as well as other power-law regimes in the body of the distribution. The results for the power-law exponent of the distribution of seismic moments worldwide and in Southern California are in agreement with previous estimates, but in addition our method provides a reliable way to determining the minimum seismic-moment value for which the Gutenberg–Richter law holds. This can be useful to check systematically for the completeness thresholds of seismic catalogs. For the energy dissipated by tropical cyclones, measured roughly through the PDI, we confirm the power-law behavior in the body of the distribution previously reported, with exponents close to one. We also survey new results for the Southern Indian Ocean, but with a higher power-law exponent. In contrast, for the case of the area affected by forest fires in an Italian catalog, we obtain power-law-distributed behavior only for rather small windows of the burnt area, containing a very few number of fires. Finally, for the waiting times between earthquakes in different subdivisions of Southern California we conclude that the power-law behavior of the tail is very delicate, affected either by a small number of subdivisions, when the size of those is large, or by the finite duration of the record, which introduces a sharp decay of the distribution when the number of subdivisions is high. For the body of the distribution another power law is found, but the range is limited by crossovers below and above it. We conclude that, in general, the method for truncated power laws works better when the number of data in the power-law range is maximized. When the quantity that is maximized is the logarithmic range $(b/a),$ the fitting range can jump between different regimes. Also, the selection of a p-value above 0.50 seems too strict sometimes, and values about 0.10 or 0.20 are more useful. Naturally, the methods studied in this paper can be directly applied to the overwhelming number of fat-tailed distributions reported during the last decades in geoscience.

A c k n o w l e d g m e n t s. Our development of the fitting and goodness-of-fit testing method presented here was originated from a collaboration with O. Peters, and was influenced by comments from L.A.N. Amaral and R.D. Malmgren. Research in hurricanes and half-lives started jointly with

A. Ossó and F. Font, respectively. We got the references for the law of large numbers from J.L. Solé. L. Telesca and R. Lasaponara provided permission to use their fire catalog. We are particularly indebted to I. Serra and J. del Castillo, and to P. Bak, who is the ultimate ancestor of all this. Research projects providing some money to us were FIS2009-09508, from the disappeared MICINN, FIS2012-31324, from MINECO, and 2009SGR-164, from Generalitat de Catalunya.

References

Aban, I.B., M.M. Meerschaert, and A.K. Panorska (2006), Parameter estimation for the truncated Pareto distribution, *J. Am. Stat. Assoc.* **101**, 473, 270-277, DOI: 10.1198/016214505000000411.

Aschwanden, M.J. (2013), SOC systems in astrophysics. **In**: M.J. Aschwanden (ed.), *Self-Organized Criticality Systems*, Open Academic Press, Berlin, 439-478.

Baiesi, M., M. Paczuski, and A.L. Stella (2006), Intensity thresholds and the statistics of the temporal occurrence of solar flares, *Phys. Rev. Lett.* **96**, 5, 051103, DOI: 10.1103/PhysRevLett.96.051103.

Bak, P. (1996), *How Nature Works: The Science of Self-Organized Criticality*, Copernicus, New York.

Bak, P., K. Christensen, L. Danon, and T. Scanlon (2002), Unified scaling law for earthquakes, *Phys. Rev. Lett.* **88**, 17, 178501, DOI: 10.1103/PhysRevLett.88.178501.

Barndorff-Nielsen, O. (1978), *Information and Exponential Families in Statistical Theory*, John Wiley & Sons Inc., New York, 238 pp.

Baró, J., and E. Vives (2012), Analysis of power-law exponents by maximum-likelihood maps, *Phys. Rev. E* **85**, 6, 066121, DOI: 10.1103/PhysRevE.85.066121.

Bauke, H. (2007), Parameter estimation for power-law distributions by maximum likelihood methods, *Eur. Phys. J. B* **58**, 2, 167-173, DOI: 10.1140/epjb/e2007-00219-y.

Ben-Zion, Y. (2008), Collective behavior of earthquakes and faults: continuum-discrete transitions, progressive evolutionary changes, and different dynamic regimes, *Rev. Geophys.* **46**, 4, RG4006, DOI: 10.1029/2008RG000260.

Boffetta, G., V. Carbone, P. Giuliani, P. Veltri, and A. Vulpiani (1999), Power laws in solar flares: Self-organized criticality or turbulence? *Phys. Rev. Lett.* **83**, 22, 4662-4665, DOI: 10.1103/PhysRevLett.83.4662.

Boguñá, M., and A. Corral (1997), Long-tailed trapping times and Lévy flights in a self-organized critical granular system, *Phys. Rev. Lett.* **78**, 26, 4950-4953, DOI: 10.1103/PhysRevLett.78.4950.

Bouchaud, J.-P., and A. Georges (1990), Anomalous diffusion in disordered media: statistical mechanisms, models and physical applications, *Phys. Rep.* **195**, 4-5, 127-293, DOI: 10.1016/0370-1573(90)90099-N.

Burroughs, S.M., and S.F. Tebbens (2001), Upper-truncated power laws in natural systems, *Pure Appl. Geophys.* **158**, 4, 741-757, DOI: 10.1007/PL00001202.

Burroughs, S.M., and S.F. Tebbens (2005), Power-law scaling and probabilistic forecasting of tsunami runup heights, *Pure Appl. Geophys.* **162**, 2, 331-342, DOI: 10.1007/s00024-004-2603-5.

Carrillo-Menéndez, S., and A. Suárez (2012), Robust quantification of the exposure to operational risk: Bringing economic sense to economic capital, *Comput. Oper. Res.* **39**, 4, 792-804, DOI: 10.1016/j.cor.2010.10.001.

Casella, G., and R.L. Berger (2002), *Statistical Inference*, 2nd ed., Duxbury Advanced Series, Duxbury Thomson Learning, Pacific Grove, 660 pp.

Chicheportiche, R., and J.-P. Bouchaud (2012), Weighted Kolmogorov–Smirnov test: Accounting for the tails, *Phys. Rev. E* **86**, 4, 041115, DOI: 10.1103/PhysRevE.86.041115.

Christensen, K., and N.R. Moloney (2005), *Complexity and Criticality*, Imperial College Press Advanced Physics Texts, Vol. 1, Imperial College Press, London.

Chu, J.-H., C.R. Sampson, A.S. Levine, and E. Fukada (2002), The Joint Typhoon Warning Center tropical cyclone best-tracks, 1945-2000, Naval Research Laboratory, Tech. Rep. NRL/MR/7540-02-16.

Chu, S.Y.F., L.P. Ekström, and R.B. Firestone (1999), The Lund/LBNL Nuclear Data Search, Version 2.

Clauset, A., C.R. Shalizi, and M.E.J. Newman (2009), Power-law distributions in empirical data, *SIAM Rev.* **51**, 4, 661-703, DOI: 10.1137/070710111.

Corpo Forestale dello Stato (2012), http://www.corpoforestale.it.

Corral, A. (2003), Local distributions and rate fluctuations in a unified scaling law for earthquakes, *Phys. Rev. E* **68**, 3, 035102, DOI: 10.1103/PhysRevE.68.035102.

Corral, A. (2004a), Long-term clustering, scaling, and universality in the temporal occurrence of earthquakes, *Phys. Rev. Lett.* **92**, 10, 108501, DOI: 10.1103/PhysRevLett.92.108501.

Corral, A. (2004b), Universal local versus unified global scaling laws in the statistics of seismicity, *Physica A* **340**, 4, 590-597, DOI: 10.1016/j.physa.2004.05.010.

Corral, A. (2005), Comment on "Do earthquakes exhibit self-organized criticality?", *Phys. Rev. Lett.* **95**, 15, 159801, DOI: 10.1103/PhysRevLett.95.159801.

Corral, A. (2006), Universal earthquake-occurrence jumps, correlations with time, and anomalous diffusion, *Phys. Rev. Lett.* **97**, 17, 178501, DOI: 10.1103/PhysRevLett.97.178501.

Corral, A. (2008), Scaling and universality in the dynamics of seismic occurrence and beyond. **In**: A. Carpinteri and G. Lacidogna (eds.), *Acoustic Emission and Critical Phenomena*, Taylor and Francis, London, 225-244.

Corral, A. (2009a), Point-occurrence self-similarity in crackling-noise systems and in other complex systems, *J. Stat. Mech.* P01022, DOI: 10.1088/1742-5468/2009/01/P01022 .

Corral, A. (2009b), Statistical tests for scaling in the inter-event times of earthquakes in California, *Int. J. Mod. Phys. B* **23**, 28-29, 5570-5582, DOI: 10.1142/S0217979209063869.

Corral, A. (2010), Tropical cyclones as a critical phenomenon. **In**: J.B. Elsner, R.E. Hodges, J.C. Malmstadt, and K.N. Scheitlin (eds.), *Hurricanes and Climate Change*, Vol. 2, Springer, Heidelberg, 81-99, DOI: 10.1007/978-90-481-9510-7_5.

Corral, A., and K. Christensen (2006), Comment on "Earthquakes descaled: On waiting time distributions and scaling laws", *Phys. Rev. Lett.* **96**, 10, 109801, DOI: 10.1103/PhysRevLett.96.109801.

Corral, A., and F. Font-Clos (2013), Criticality and self-organization in branching processes: application to natural hazards. **In**: M. Aschwanden (ed.), *Self-Organized Criticality Systems*, Open Academic Press, Berlin, 183-228.

Corral, A., and A. Turiel (2012), Variability of North Atlantic hurricanes: seasonal versus individual-event features. **In**: A.S. Sharma, A. Bunde, V.P. Dimri, and D.N. Baker (eds.), *Extreme Events and Natural Hazards: the Complexity Perspective*, Geopress, Washington, 111-125, DOI: 10.1029/2011GM001069.

Corral, A., L. Telesca, and R. Lasaponara (2008), Scaling and correlations in the dynamics of forest-fire occurrence, *Phys. Rev. E* **77**, 1 016101, DOI: 10.1103/PhysRevE.77.016101.

Corral, A., A. Ossó, and J.E. Llebot (2010), Scaling of tropical-cyclone dissipation, *Nature Phys.* **6**, 693-696, DOI: 10.1038/nphys1725.

Corral, A., F. Font, and J. Camacho (2011), Noncharacteristic half-lives in radioactive decay, *Phys. Rev. E* **83**, 6, 066103, DOI: 10.1103/PhysRevE.83.066103.

Corral, A., A. Deluca, and R. Ferrer-i-Cancho (2012), A practical recipe to fit discrete power-law distributions, arXiv:1209.1270.

Czechowski, Z. (2003), The privilege as the cause of power distributions in geophysics, *Geophys. J. Int.* **154**, 3, 754-766, DOI: 10.1046/j.1365-246X.2003.01994.x.

Davidsen, J., and M. Paczuski (2005), Analysis of the spatial distribution between successive earthquakes, *Phys. Rev. Lett.* **94**, 4, 048501, DOI: 10.1103/PhysRevLett.94.048501.

del Castillo, J. (2013), Exponential models, Lecture notes (unpublished).

del Castillo, J., and P. Puig (1999), The best test of exponentiality against singly truncated normal alternatives, *J. Am. Stat. Assoc.* **94**, 446, 529-532, DOI: 10.1080/01621459.1999.10474147 .

del Castillo, J., J. Daoudi, and I. Serra (2012), The full-tails gamma distribution applied to model extreme values, arXiv:1211.0130.

Devroye, L. (1986), *Non-Uniform Random Variate Generation*, Springer-Verlag, New York.

Dickman, R. (2003), Rain, power laws, and advection, *Phys. Rev. Lett.* **90**, 10, 108701, DOI: 10.1103/PhysRevLett.90.108701 .

Durrett, R. (2010), *Probability: Theory and Examples*, 4th ed., Cambridge University Press, Cambridge.

Emanuel, K. (2005a), *Divine Wind: the History and Science of Hurricanes*, Oxford University Press, New York.

Emanuel, K. (2005b), Increasing destructiveness of tropical cyclones over the past 30 years, *Nature* **436**, 7051, 686-688, DOI: 10.1038/nature03906.

Evans, M., N. Hastings, and B. Peacock (2000), *Statistical Distributions*, 3rd ed., John Wiley & Sons Inc., New York.

Felzer, K.R., and E.E. Brodsky (2006), Decay of aftershock density with distance indicates triggering by dynamic stress, *Nature* **441**, 7094, 735-738, DOI: 10.1038/nature04799 .

Freeman, M.P., and N.W. Watkins (2002), The heavens in a pile of sand, *Science* **298**, 5595, 979-980, DOI: 10.1126/science.1075555.

Geist, E.L., and T. Parsons (2008), Distribution of tsunami interevent times, *Geophys. Res. Lett.* **35**, 2, L02612, DOI: 10.1029/2007GL032690.

Goldstein, M.L., S.A. Morris, and G.G. Yen (2004), Problems with fitting to the power-law distribution, *Eur. Phys. J. B* **41**, 2, 255-258, DOI: 10.1140 /epjb/e2004-00316-5.

Gutenberg, B., and C.F. Richter (1944), Frequency of earthquakes in California, *Bull. Seismol. Soc. Am.* **34**, 4, 185-188.

Hauksson, E., W. Yang, and P. Shearer (2012), Waveform relocated earthquake catalog for southern California (1981 to June 2011), *Bull. Seismol. Soc. Am.* **102**, 5, 2239-2244, DOI: 10.1785/0120120010.

Hergarten, S. (2002), *Self-Organized Criticality in Earth Systems*, Springer, Berlin.

Jarvinen, B.R., C.J. Neumann, and M.A.S. Davis (1988), A tropical cyclone data tape for the North Atlantic basin, 1886-1983: contents, limitations, and uses, NOAA Technical Memorandum NWS NHC 22, National Hurricane Center, Miami, USA, http://www.nhc.noaa.gov/pdf/NWS-NHC-1988-22.pdf.

Jensen, H.J. (1998), *Self-Organized Criticality. Emergent Complex Behavior in Physical and Biological Systems*, Cambridge University Press, Cambridge.

Johnson, N.L., S. Kotz, and N. Balakrishnan (1994), *Continuous Univariate Distributions*. Vol. 1, 2nd ed., John Wiley & Sons Inc., New York.

Johnson, N.L., A.W. Kemp, and S. Kotz (2005), *Univariate Discrete Distributions*, 3rd ed., John Wiley & Sons Inc., Hoboken.

JTWC (2012), Annual tropical cyclone report, Joint Typhoon Warning Center, http://www.usno.navy.mil/NOOC/nmfc-ph/RSS/jtwc/best_tracks.

Kagan, Y.Y. (2002), Seismic moment distribution revisited: I. Statistical results, *Geophys. J. Int.* **148**, 3, 520-541, DOI: 10.1046/j.1365-246x.2002.01594.x.

Kalbfleisch, J.D., and R.L. Prentice (2002), *The Statistical Analysis of Failure Time Data*, 2nd ed., John Wiley & Sons Inc., Hoboken.

Kanamori, H., and E.E. Brodsky (2004), The physics of earthquakes, *Rep. Prog. Phys.* **67**, 8, 1429-1496, DOI: 10.1088/0034-4885/67/8/R03.

Klafter, J., M.F. Shlesinger, and G. Zumofen (1996), Beyond Brownian motion, *Phys. Today* **49**, 2, 33-39, DOI: 10.1063/1.881487.

Kolmogorov, A.N. (1956), *Foundations of the Theory of Probability*, 2nd ed., Chelsea Pub. Co., New York.

Krane, K.S. (1988), *Introductory Nuclear Physics*, John Wiley & Sons Inc., New York.

Lahaie, F., and J.R. Grasso (1998), A fluid-rock interaction cellular automaton of volcano mechanics: Application to the Piton de la Fournaise, *J. Geophys. Res.* **103**, B5, 9637-9650, DOI: 10.1029/98JB00202.

Main, I.G., L. Li, J. McCloskey, and M. Naylor (2008), Effect of the Sumatran mega-earthquake on the global magnitude cut-off and event rate, *Nature Geosci.* **1**, 3, 142, DOI: 10.1038/ngeo141.

Malamud, B.D. (2004), Tails of natural hazards, *Phys. World* **17** , 8, 31-35.

Malamud, B.D., G. Morein, and D.L. Turcotte (1998), Forest fires: An example of self-organized critical behavior, *Science* **281**, 5384, 1840-1842, DOI: 10.1126/science.281.5384.1840.

Malamud, B.D., J.D.A. Millington, and G.L.W. Perry (2005), Characterizing wildfire regimes in the United States, *Proc. Natl. Acad. Sci. USA* **102**, 13, 4694-4699, DOI: 10.1073/pnas.0500880102.

Malmgren, R.D., D.B. Stouffer, A.E. Motter, and L.A.N. Amaral (2008), A Poissonian explanation for heavy tails in e-mail communication, *Proc. Natl. Acad. Sci. USA* **105**, 47, 18153-18158, DOI: 10.1073/pnas.0800332105.

McClelland, L., T. Simkin, M. Summers, E. Nielsen, and T.C. Stein (eds.) (1989), *Global Volcanism 1975-1985*, Prentice Hall, Englewood Cliffs.

Mitzenmacher, M. (2004), A brief history of generative models for power law and lognormal distributions, *Internet Math.* **1**, 2, 226-251, DOI: 10.1080/15427951.2004.10129088.

Newman, M.E.J. (2005), Power laws, Pareto distributions and Zipf's law, *Contemp. Phys.* **46**, 5, 323 -351, DOI: 10.1080/00107510500052444.

NHC (2012), National Hurricane Center, http://www.nhc.noaa.gov/pastall.shtml# hurdat.

Paczuski, M., S. Boettcher, and M. Baiesi (2005), Interoccurrence times in the Bak-Tang-Wiesenfeld sandpile model: A comparison with the observed statistics of solar flares, *Phys. Rev. Lett.* **95**, 18, 181102, DOI: 10.1103/PhysRevLett.95.181102.

Peters, O., and K. Christensen (2006), Rain viewed as relaxational events, *J. Hydrol.* **328**, 1-2, 46-55, DOI: 10.1016/j.hydrol.2005.11.045.

Peters, O., and J.D. Neelin (2006), Critical phenomena in atmospheric precipitation, *Nat. Phys.* **2**, 393-396, DOI: 10.1038/nphys314.

Peters, O., C. Hertlein, and K. Christensen (2001), A complexity view of rainfall, *Phys. Rev. Lett.* **88**, 1, 018701, DOI: 10.1103/PhysRevLett.88.018701.

Peters, O., A. Deluca, A. Corral, J.D. Neelin, and C.E. Holloway (2010), Universality of rain event size distributions, *J. Stat. Mech.* **2010**, P11030, DOI: 10.1088/1742-5468/2010/11/P11030.

Press, W.H., S.A. Teukolsky, W.T. Vetterling, and B.P. Flannery (1992), *Numerical Recipes in FORTRAN: The Art of Scientific Computing*, 2nd ed., Cambridge University Press, Cambridge.

Pruessner, G. (2012), *Self-Organised Criticality: Theory, Models and Characterisation*, Cambridge University Press, Cambridge.

Pueyo, S., and R. Jovani (2006), Comment on "A keystone mutualism drives pattern in a power function", Science **313**, 5794, 1739c–1740c, DOI: 10.1126/science.1129595.

Ross, S. (2002), *A First Course in Probability*, 6th ed., Pearson Education, 528 pp.

Saichev, A., and D. Sornette (2006), "Universal" distribution of interearthquake times explained, *Phys. Rev. Lett.* **97**, 7, 078501, DOI: 10.1103/PhysRevLett.97.078501.

Sethna, J.P., K.A. Dahmen, and C.R. Myers (2001), Crackling noise, *Nature* **410**, 6825, 242-250, DOI: 10.1038/35065675.

Shearer, P., E. Hauksson, and G. Lin (2005), Southern California hypocenter relocation with waveform cross-correlation. Part 2: Results using source-specific station terms and cluster analysis, *Bull. Seismol. Soc. Am.* **95**, 3, 904-915, DOI: 10.1785/0120040168.

Shiryaev, A.N. (1996), *Probability*, 2nd ed., Graduate Texts in Mathematics, Springer, New York.

Silverman, B.W. (1986), *Density Estimation for Statistics and Data Analysis*, Chapman and Hall, New York.

Sornette, D. (2004), *Critical Phenomena in Natural Sciences. Chaos, Fractals, Selforganization and Disorder: Concepts and Tools*, 2nd ed., Springer, Berlin.

Takayasu, H. (1990), *Fractals in the Physical Sciences*, Manchester University Press, Manchester.

Utsu, T. (1999), Representation and analysis of the earthquake size distribution: a historical review and some new approaches, *Pure Appl. Geophys.* **155**, 2-4, 509-535, DOI: 10.1007/s000240050276.

Utsu, T. (2002), Statistical features of seismicity. **In**: W.H.K. Lee, H. Kanamori, P.C. Jennings, and C. Kisslinger (eds.), *International Handbook of Earthquake and Engineering Seismology, Part A*, Vol. 81, Academic Press, Amsterdam, 719-732, DOI: 10.1016/S0074-6142(02)80246-7.

Utsu, T., Y. Ogata, and R. Matsu'ura (1995), The centenary of the Omori formula for a decay law of aftershock activity, *J. Phys. Earth* **43**, 1, 1-33, DOI: 10.4294/jpe1952.43.1.

Wanliss, J.A., and J.M. Weygand (2007), Power law burst lifetime distribution of the SYM-H index, *Geophys. Res. Lett.* **34**, 4, L04107, DOI: 10.1029/2006GL028235.

White, E.P., B.J. Enquist, and J.L. Green (2008), On estimating the exponent of power-law frequency distributions, *Ecology* **89**, 4, 905-912, DOI: 10.1890/07-1288.1.

Received 1 December 2012
Received in revised form 1 March 2013
Accepted 18 March 2013

Journal of Statistical Mechanics: Theory and Experiment
An IOP and SISSA journal

Universality of rain event size distributions

Ole Peters[1,2], A Deluca[3], A Corral[3], J D Neelin[2] and C E Holloway[4]

[1] Department of Mathematics and Grantham Institute for Climate Change, Imperial College London, 180 Queen's Gate, London SW7 2AZ, UK
[2] Department of Atmospheric and Oceanic Sciences and Institute for Geophysics and Planetary Physics, University of California, Los Angeles, 405 Hilgard Avenue, Los Angeles, CA 90095-1565, USA
[3] Centre de Recerca Matemàtica, Campus de Bellaterra, Edifici C, 08193 Bellaterra (Barcelona), Spain
[4] Department of Meteorology, University of Reading, Earley Gate, PO Box 243, Reading RG6 6BB, UK
E-mail: ole@santafe.edu, adeluca@crm.cat, acorral@crm.cat, neelin@atmos.ucla.edu and c.e.holloway@reading.ac.uk

Received 5 October 2010
Accepted 28 October 2010
Published 19 November 2010

Online at stacks.iop.org/JSTAT/2010/P11030
doi:10.1088/1742-5468/2010/11/P11030

Abstract. We compare rain event size distributions derived from measurements in climatically different regions, which we find to be well approximated by power laws of similar exponents over broad ranges. Differences can be seen in the large-scale cutoffs of the distributions. Event duration distributions suggest that the scale-free aspects are related to the absence of characteristic scales in the meteorological mesoscale.

Keywords: finite-size scaling, self-organized criticality (experiment), heat transfer and convection

1742-5468/10/P11030+15$30.00

Contents

1. Introduction

Atmospheric convection and precipitation have been hypothesized to be a real-world realization of self-organized criticality (SOC). This idea is supported by observations of avalanche-like rainfall events [1, 2] and by the nature of the transition to convection in the atmosphere [3, 4]. Many questions remain open, however, as summarized below. Here we ask whether the observation of scale-free avalanche size distributions is reproducible using data from different locations and whether the associated fitted exponents show any sign of universality.

Many atmospheric processes are characterized by long-range spatial and temporal correlation, and by corresponding structure on a wide range of scales. There are two complementary explanations why this is so, and both are valid in their respective regimes: structure on many scales can be the result of different processes producing *many* characteristic scales [5, 6]; it can also be the result of an *absence* of characteristic scales over some range, such that all intermediate scales are equally significant [7]. The latter perspective is relevant, for instance, in critical phenomena and in the inertial subrange of fully developed turbulence.

Processes relevant for precipitation are associated with many different characteristic time and spatial scales, see e.g. [6]. The list of these scales has a gap, however, from a few kilometers (a few minutes) to 1000 km (a few days), spanning the so-called mesoscale, and it is in this gap that the following arguments are most likely to be relevant.

The atmosphere is slowly driven by incident solar radiation, about half of which is absorbed by the planet's surface, heating and moistening the atmospheric boundary layer;

J. Stat. Mech. (2010) P11030

combined with radiative cooling at the top of the troposphere this creates an instability. This instability drives convection, which in the simplest case is dry. More frequently, however, moisture and precipitation play a key role. Water condenses in moist rising air, heating the environment and reinforcing the rising motion, and often, the result of this process is rainfall. The statistics of rainfall thus contain information about the process of convection and the decay towards stability in the troposphere. A common situation is conditional instability, where saturated air is convectively unstable, whereas dry air is stable. Under-saturated air masses then become unstable to convection if lifted by a certain amount, meaning that relatively small perturbations can trigger large responses.

Since driving processes are generally slow compared to convection, it has been argued that the system as a whole should typically be in a far-from equilibrium statistically stationary state close to the onset of instability. In the parlance of the field, this idealized state, where drive and dissipation are in balance, is referred to as 'quasi-equilibrium' (QE) [8]. In [3], using satellite data over tropical oceans, it was found that departures from the point of QE into the unstable regime can be described as triggering a phase transition whereby large parts of the troposphere enter into a convectively active phase. Assuming that the phase transition is continuous, the attractive QE state would be a case of SOC—a critical point of a continuous phase transition acting as an attractor in the phase space of a system [9, 10].

The link between SOC and precipitation processes has also been made by investigating event size distributions in a study using data from a mid-latitude location [2]. Both the tropical data in [3] and the mid-latitude data in [2] support some notion of SOC in precipitation processes, but the climatologies in these regions are very different. Rainfall in the mid-latitudes is often generated in frontal systems, whereas in the tropics, much of the precipitation is convective, supporting high rain rates. It is not *a priori* clear whether these differences are relevant to the SOC analogy, or whether they are outweighed by the robust similarities between the systems. For instance, drive and dissipation timescales are well separated also in the mid-latitudes. In time series from Sweden the average duration of precipitation events was found to be three orders of magnitude smaller than the average duration of dry spells [11]. It is therefore desirable to compare identical observables from different locations.

Scale-free event size distributions suggest long-range correlation in the system, which in turn hints at a continuous transition to precipitation. Similar effects, however, can also result directly from a complex flow field, as was shown in simulations using randomized vortices and passive tracers [12]. Since the fluid dynamics is complex enough to generate apparent long-range correlation, and it is difficult from direct observation to judge whether the transition is continuous, we cannot rule out a discontinuous jump.

This uncertainty is mirrored in parameterizations of convection. The spatial resolution of general circulation models is limited by constraints in computing power to about 100 km in the horizontal. Dynamically there is nothing special about this scale, and the approach in climate modeling for representing physical processes whose relevant spatial scales are smaller is to describe their phenomenology in parameterizations. Parameterizations of convection and precipitation processes often contain both continuous and discontinuous elements. For instance, the intensity of convection and precipitation typically depends continuously on a measure of convective plume buoyancy (such as convective available potential energy) and water vapor content [8, 13], but sometimes

J. Stat. Mech. (2010) P11030

Table 1. Observation sites with corresponding time periods, number of observed precipitation events N, estimated annual precipitation in millimeters, and location.

Site	From	Until	N	Precip./yr	Location
Manus Island, Papua New Guinea	02/15/2005	08/27/2009	11 981	5 883.29	2.116°S, 147.425°E
Nauru Island, Republic of Nauru	02/15/2005	08/27/2009	5 134	1 860.87	0.521°S, 166.916°E
Darwin, Australia	02/15/2005	08/27/2009	2 883	1 517.09	12.425°S, 130.892°E
Niamey, Niger	12/26/2005	12/08/2006	262	608.37	13.522°N, 2.632°E
Heselbach, Germany	04/01/2007	01/01/2008	2 439	2 187.85	48.450°N, 8.397°E
Shouxian, China	05/09/2008	12/28/2008	480	1 221.20	32.558°N, 116.482°E
Graciosa Island, Azores	04/14/2009	07/10/2010	3 066	702.35	39.091°N, 28.029°E
NSA, USA	04/01/2001	10/13/2003	9 097	23 516.16	71.323°N, 156.616°E
Point Reyes, USA	02/01/2005	09/15/2005	579	797.85	38.091°N, 122.957°E
SGP, USA	11/06/2007	08/24/2009	1 624	968.95	36.605°N, 97.485°E

a discontinuous threshold condition is introduced to decide whether convection occurs at all [14].

2. Data sets

We study rain data from all ten available sites of the Atmospheric Radiation Measurement (ARM) Program, see www.arm.gov, over periods from about eight months to four years, see table 1. Precipitation rates were recorded at 1 min resolution, with an optical rain gauge, Model ORG-815-DA MiniOrg (Optical Scientific, Inc.) [15]. Data were corrected using the ARM Data Quality Reports [16], and rates below 0.2 mm h^{-1} were treated as zero measurements, as recommended by the ARM Handbook [15], see figure 1.

The measurements are from climatically different regions using a standardized technique, making them ideal for our purpose. Three sites are located in the Tropical Western Pacific (Manus, Nauru and Darwin), known for strong convective activity. Niamey is subject to strong monsoons, with a pronounced dry season. Heselbach is a mid-latitude site with an anomalously large amount of rainfall due to orographic effects. Rainfall in Shouxian is mostly convective in the summer months, which constitute most of the data set. Graciosa Island in the Azores archipelago is a sub-tropical site, chosen for the ARM program to study precipitation in low clouds of the marine boundary layer.

Three data are less straightforward: the Point Reyes measurements specifically target Marine Stratus clouds, which dominate the measurement period and are known to produce drizzle in warm-cloud conditions (without ice phase). Unfortunately the measurements only cover six months, and it is unclear whether observed differences are due to the different physics or to the small sample size. The Southern Great Plains (SGP) measurements suffer from a malfunction that led to apparent rain rates of about 0.1 mm h^{-1} over much of the observation period. The problem seems to be present in most other data sets but is far less pronounced there, see figure 1. Measurements at temperatures below 3 °C were discarded as these can contain snow from which it is difficult

J. Stat. Mech. (2010) P11030

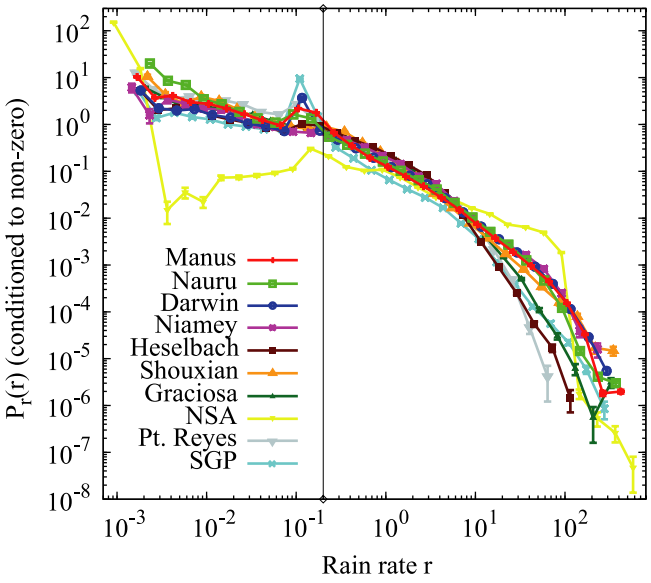

Figure 1. Probability (relative frequency) density of precipitation rate, r in mm h^{-1}. The vertical line indicates the lower intensity cutoΘ at 0.2 mm h^{-1}. Smaller rain rates are treated as zero. The peak around 0.1 mm h^{-1}, most pronounced in the Southern Great Plains data, is due to a malfunction of the instrument. The Alaska data set contains mostly snow and is included only for completeness.

to infer equivalent rates of liquid water precipitation. The North Slope of Alaska (NSA) data set contains mostly snow; it is included only for completeness.

None of the data sets showed significant seasonal variations in the scaling exponents. In the Point Reyes, SGP and NSA data we found slight variations but could not convince ourselves that these were significant. Data from all seasons are used.

3. Event sizes

The data used here are (0+1)-dimensional time series, whereas the atmosphere is a (3+1)-dimensional system. We leave the question unanswered as to which spatial dimensions are most relevant—the system becomes vertically unstable, but it also communicates in the two horizontal dimensions through various processes [4].

Following [2], we define an event as a sequence of non-zero measurements of the rain rate, see inset in figure 2. The event size s is the rain rate, $r(t)$, integrated over the event, $s = \int_{\text{event}} \mathrm{d}t\, r(t)$. The dimension of this object is $[s] = \text{mm}$, specifying the depth of the layer of water left on the ground during the event. 1 mm corresponds to an energy density of some 2500 kJ m^{-2} released latent heat of condensation. If the rain rate were known over the area covered by the event, then the event size could be defined precisely as the energy released during one event. Since spatial information is not available, it is ignored in our study.

For each data set, the probability density function $P_s(s)$ in a particular size interval $[s, s+\Delta s)$ is estimated as $P_s(s) \approx n(s)/(N\Delta s)$, where $n(s)$ is the number of events in the

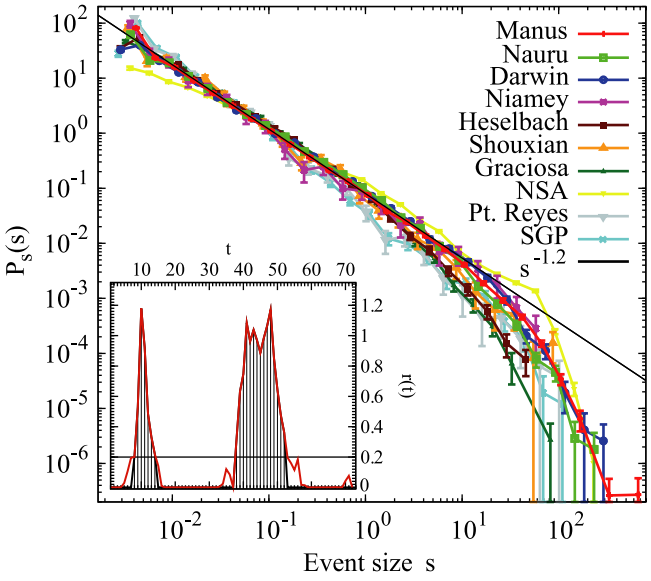

Figure 2. Probability densities of event sizes, s in mm, and a power-law "t (black straight line). Inset: precipitation rates from Niamey, including two rain events lasting 7 and 15 min respectively. Interpreting reported rain rates of less than 0.2 mm h^{-1} as zero, the shaded areas are the corresponding event sizes.

interval and N the total number of events. We use $(s + \Delta s)/s = 10^{1/5} \approx 1.58$, i.e. 5 bins per order of magnitude in s. Standard errors are shown, for $P_s(s)$: assuming Poissonian arrivals of events in any given bin, the error in $n(s)$ is approximated by $\sqrt{n(s)}$.

4. SOC scaling

Studies of simple SOC models that approach the critical point of a continuous phase transition focus on Avalanche size distributions, which we liken to rain event sizes. Critical exponents are derived from finite-size scaling, that is, the scaling of observables with system size (as opposed to critical scaling, the scaling of observables with the distance from criticality). In SOC models, moments of the avalanche size distribution scale with system size L like

$$\langle s^k \rangle \propto L^{D(1+k-\tau_s)} \qquad \text{for } k > \tau_s - 1, \tag{1}$$

defining the exponent D, sometimes called the avalanche dimension, and the exponent τ_s, which we call the avalanche size exponent. Equation (1) is consistent with probability density functions $P_s(s)$ of the form

$$P_s(s) = s^{-\tau_s} \mathcal{G}_s(s/s_\xi) \qquad \text{for } s > s_l \tag{2}$$

where $s_\xi = L^D$, and the scaling function $\mathcal{G}_s(s/s_\xi)$ falls off very fast for large arguments, $s/s_\xi > 1$, and is constant for small arguments, $s/s_\xi \ll 1$, down to a lower cutoff, $s = s_l$, where non-universal microscopic effects (e.g. discreteness of the system) become important.

J. Stat. Mech. (2010) P11030

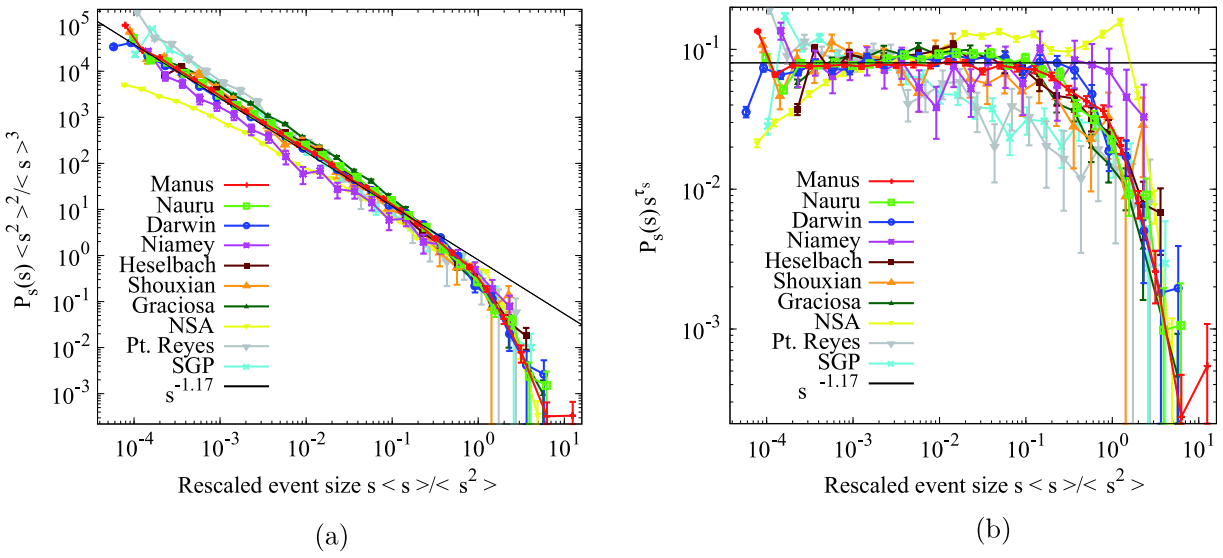

Figure 3. (a) Event size distributions shifted along the supposed power laws to collapse the loci of the cutoffs. (b) Inferred scaling function $\mathcal{G}_s$, using $\tau_s = 1.17$ for all data sets. By far the largest deviations from a common scaling function are observed for the unreliable data sets, Alaska (NSA) and Southern Great Plains (SGP).

Assuming that we have observations from an SOC system, and that a significant part of the observed avalanche sizes are in the region $s_l < s \ll s_\xi$, we expect to find a range of scales where the power law

$$P_s(s) = \mathcal{G}_s(0) s^{-\tau_s} \tag{3}$$

holds. Under sufficiently slow drive the exponent τ_s is believed to be robust in SOC models [17, 18]. We infer event size distributions as in [2] from measurements in different locations and compare values for the apparent avalanche size exponent τ_s. As a first step to assess the validity of (3) we produce log–log plots of $P_s(s)$ versus s and look for a linear regime, figure 2. Since the study of critical phenomena is a study of limits that cannot be reached in physical systems, the field is notorious for debates regarding the significance of experimental work, which is especially true for SOC. While an element of interpretation necessarily remains, we devise methods to maximize the objectivity of our analysis.

In our data sets, time series of rain rates from different locations, we interpret the upper limit s_ξ of the scale-free range as an effective system size. We cannot control this size; nonetheless the scaling hypothesis, (2), can be tested using appropriate moment ratios [19]. For instance, $s_\xi \propto \langle s^2 \rangle / \langle s \rangle$, provided $s_l \ll s_\xi$. Hence, to account for changes in effective system sizes the s-axis in figure 2 can be rescaled to $s\langle s \rangle / \langle s^2 \rangle$, see figure 3(a). This collapses the loci of the large-scale cutoffs. The $P_s(s)$-axis is rescaled by $\langle s^2 \rangle^2 / \langle s \rangle^3 \propto s_\xi^\tau$, so that figure 3(a) shows the curves of figure 2 shifted along their supposed power laws, without having to estimate any parameters. The curves are neither normalized nor do they collapse vertically—the degree of vertical collapse is comparable to that in figure 2. Plotting $P_s(s) s^{\tau_s}$ against the rescaled variable $s\langle s \rangle / \langle s^2 \rangle$ produces figure 3(b) of the scaling function $\mathcal{G}_s(s/(a s_\xi))$, where a is the proportionality constant relating s_ξ to the moment ratio. This has the advantage of reducing the logarithmic vertical range, which makes it

Table 2. Avalanche size exponent $_s$ for all sites (last column). Lower and upper end of "tting range (in mm), logarithmic range s_{max}/s_{min}, number of events N, number of events in the "tting range, $\bar{N}$, and a moment ratio proportional to the cutoΘ s_ξ are shown. Brackets ( ) denote errors in the last digit, determined by jackknife [22].

Site	s_{min}	s_{max}	s_{max}/s_{min}	N	$\bar{N}$	$\langle s^2\rangle/\langle s\rangle$(er)	$_s$(er)
Manus	0.0069	18.7	2 719	11 981	9320	53(1)	1.19(1)
Nauru	0.0066	4.7	704	5 134	3996	37(1)	1.14(1)
Darwin	0.0067	21.6	3 230	2 883	2410	50(1)	1.16(1)
Niamey	0.0041	55.0	13 500	262	232	25(2)	1.19(3)
Heselbach	0.0072	1.4	195	2 439	1764	13(1)	1.18(2)
Shouxian	0.0037	2.5	677	480	406	39(2)	1.19(3)
Graciosa	0.0069	1.0	148	3 066	2260	14.4(3)	1.16(1)
NSA	0.0205	5.9	288	9 097	6030	47(1)	1.01(1)
Pt. Reyes	0.0062	66.7	10 796	579	427	37(2)	1.40(2)
SGP	0.0062	58.8	9 463	1 624	1196	27(1)	1.40(2)

possible to see differences in the distributions that would otherwise be concealed visually. Figure 3(a) covers nine orders of magnitude vertically, whereas figure 3(b) covers little more than two.

5. Exponent estimation and goodness of t

For a detailed discussion, see appendix A. We apply a form of Kolmogorov–Smirnov (KS) test [20] similar to that in [21]. First, a fitting range $[s_{min}, s_{max}]$ is selected. In this range the maximum-likelihood value for τ_s in (3) is found. Next, the maximum difference between the empirical cumulative distribution in this range and the cumulative distribution corresponding to the best-fit power law is found. The same measure is applied to synthetic samples of data (each with the same number of instances), generated from the best-fit power-law distribution. This yields the 'p'-value, i.e. the fraction of samples generated from the tested model (the best-fit power law) where at least such a difference is observed. We stress that each synthetic data set is compared to its own maximum-likelihood power-law distribution, i.e. an exponent has to be fitted for each sample, so that no bias be introduced.

We keep a record of the triplet $(s_{min}, s_{max}, \tau_s)$ if the p-value is greater than 10% (our arbitrarily chosen threshold). After trying all possible fitting ranges with s_{min} and s_{max} increasing by factors of $10^{0.01}$, we select the triplet which maximizes the number $\bar{N}$ of data between s_{min} and s_{max}.

The distributions in figure 2 are visually compatible with a power law (black straight line) over most of their ranges. The procedure consisting of maximum-likelihood estimation plus a goodness-of-fit test confirms this result: over ranges between 2 and 4 orders of magnitude, all data sets are consistent with a power-law distribution and the estimates of the apparent exponents are in agreement with the hypothesis of a single exponent $\tau_s = 1.17(3)$, brackets indicating the uncertainty in the last digit, except for the three problematic data sets from Point Reyes, the Southern Great Plains and Alaska. The complete results are collected in table 2. While the best-fit exponents in

J. Stat. Mech. (2010) P11030

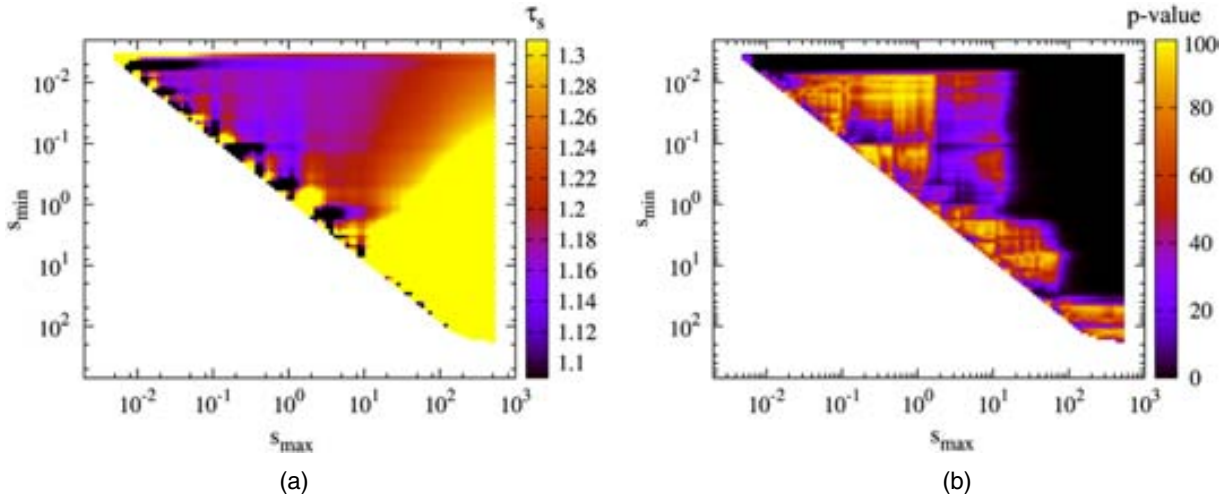

Figure 4. (a) Color map showing the best-"t value for the exponent $_{s}$ for all pairs of $s_{\min}$ and $s_{\max}$, (lower and upper ends of the chosen "tting range in mm) for the Manus dataset. The large plateau corresponds to $_{s} \approx 1.17$. (b) Analogous plot for the p-value.

this table are surprisingly similar (given the climatic differences between the measuring sites), the error estimates are unrealistically small. Taking the statistical results literally, we would have to conclude that the exponents are very similar but mutually incompatible (e.g. $\tau_{\rm s}^{\rm Manus} = 1.18(1)$ and $\tau_{\rm s}^{\rm Nauru} = 1.14(1)$) suggesting that $\tau_{\rm s}$ is not universal. On physical grounds we do not believe this conclusion because systematic errors arising from the measurement process, the introduction of the sensitivity threshold, binning during data recording etc, are likely to be much larger than the purely statistical errors quoted here. For example, [2] used a different type of measurement with a smaller sensitivity threshold and led to a best estimate for the exponent of 1.36. Furthermore, the apparent exponent can only be seen as a rough estimate of any true underlying exponent. We tested that, fixing $\tau_{\rm s} = 1.17$, all data sets yield $p > 10\%$ over a range larger than two and a half orders of magnitude, except for the three problematic data sets. A two-sample Kolmogorov–Smirnov test for all pairs of datasets further confirms the similarity of the distributions for the different sites, appendix B.

In figure 4(a) we show a color plot of all triplets $(s_{\min}, s_{\max}, \tau_{\rm s})$, corresponding to the Manus dataset. There is a large plateau where $\tau_{\rm s} \approx 1.17$, indicating that this value is the best estimate for many intervals. Figure 4(b) is an analogous plot for the p-value, showing that the goodness of the fit is best in the region of the plateau.

Climatic differences between regions are scarcely detectable in event size distributions, which may be surprising on the grounds of climatological considerations. However, the cutoff s_{ξ}, representing the capacity of the climatic region around a measuring site to generate rain events, changes significantly from region to region, confirming meteorological intuition. This is difficult to see in the logarithmic scales of figure 2 but is easily extracted from the moments of the distributions, table 2. Thus, the smallest cutoff (and likely maximum event size) in the ARM data is found in Heselbach (mid-latitudes), whereas the largest is in Manus (Western Pacific warm pool). We note that $\langle s^2 \rangle / \langle s \rangle$ is only

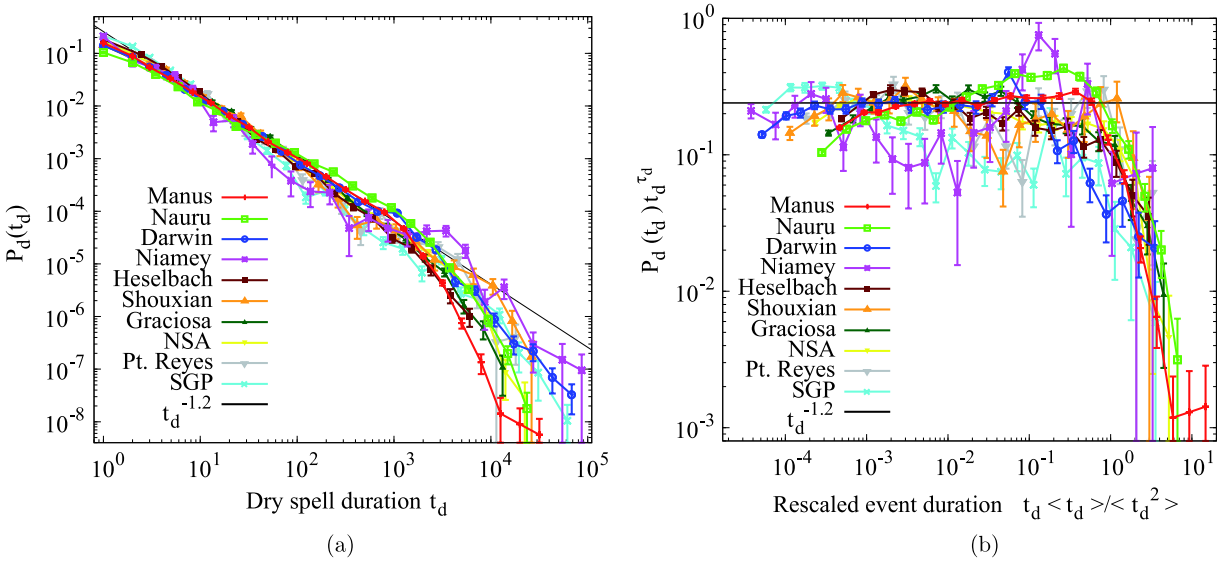

Figure 5. (a) Probability densities for dry spell durations (in min). The diurnal cycle is most pronounced in Niamey, otherwise the distributions are similar. (b) Distributions collapsed onto their scaling function, similar to "gure 3(b).

proportional to the actual cutoff s_ξ. Assuming a box function for the scaling function and using the value $\tau_s = 1.17$, we can estimate the proportionality constant and find $s_\xi \approx 2.2\langle s^2\rangle/\langle s\rangle$. With this estimate, none of the fitting ranges extends beyond the cutoff.

6. Dry spells

The durations of precipitation-free intervals have also been reported to follow an approximate power law [23, 2]. We therefore repeat for dry spell durations the same analysis as for the event sizes. Figure 5(a) shows the distributions, with a collapse corresponding to figure 3(b) in figure 5(b). We notice the different strengths of the diurnal cycle, here visible as a relative peak near one day dry spell duration. Exponents fitted to the distributions are similar, see table 3. They also agree with the analyses in [23], where a double-power-law fit was performed. For dry spell durations between a few seconds and a few hours the authors found an exponent value of 1.35. The second, smaller, exponent for longer dry spells found in that study may reflect the signal from the diurnal cycle. This signal is strong in [2], where a single-power-law fit yielded an exponent estimate of 1.42.

7. Event durations

Precipitation event duration distributions are broad for all locations. Durations provide a link to studies of geometric properties of precipitation fields. Numerous studies of tropical deep convective rain fields [24], shallow convection fields [25], clouds [26]–[29], and model data from large eddy simulations [30] have reported the distributions of ground covered by events (in radar snap shots etc) to be well approximated by power laws. We note that

Table 3. Dry spell exponent (last column). Lower and upper end of "tting range (in min), logarithmic range $t_{d\max}/t_{d\min}$, number of dry spells in data set, N, and number of dry spells in the "tting range, $\bar{N}$, and a moment ratio proportional to the cutoΘ are shown. Brackets ( ) denote errors in the last digit, determined by jackknife. The number of dry spells need not be within ±1 of the number of events, as our de"nition of an event (and a dry spell) implies that it can be split in two if it contains an erroneous measurement. Note the magnitude of this eΘect in the NSA data set.

Site	$t_{d\min}$	$t_{d\max}$	$t_{d\max}/t_{d\min}$	N	$\overline{N}$	$\langle {t_d}^2\rangle/\langle t_d\rangle$(er)	$_d$(er)
Manus	24.4	1 363.1	55.8	11 992	4505	2 149(20)	1.16(2)
Nauru	7.5	1 027.5	137.7	5 126	2912	3 557(50)	0.99(2)
Darwin	8.5	3 660.6	432.6	2 892	1595	19 477(368)	1.17(1)
Niamey	2.4	1 774.0	726.1	262	135	26 386(1699)	1.33(5)
Heselbach	9.5	5 748.0	605.4	2 441	1035	2 043(34)	1.37(2)
Shouxian	2.7	13 488.5	4957.1	478	365	8 776(404)	1.27(3)
Graciosa	14.6	415.2	28.5	3 068	1185	2 943(49)	1.28(3)
NSA	12.2	9 033.2	739.7	3 440	1531	4 293(73)	1.3(2)
Pt. Reyes	3.6	17 141.0	4826.3	579	379	5 513(233)	1.27(2)
SGP	8.4	2 248.7	268.5	1 625	523	17 243(463)	1.46(3)

Table 4. Duration exponent (last column). Lower and upper end of "tting range (in min), logarithmic range $t_{w\max}/t_{w\min}$, number of events in data set, N, and number of events in the "tting range, $\bar{N}$, are shown. Brackets ( ) denote errors in the last digit, determined by jackknife.

Site	$t_{w\min}$	$t_{w\max}$	$t_{w\max}/t_{w\min}$	N	$\bar{N}$	$\langle {t_w}^2\rangle/\langle t_w\rangle$	$_w$(er)
Manus	34.4	641.9	18.7	11 981	1200	122(1)	2.12(4)
Nauru	25.4	437.5	17.2	5 134	540	106(1)	2.09(6)
Darwin	17.87	89.30	5.00	2 883	554	109(2)	2.0(1)
Niamey	2.7	211.8	78.4	262	157	79(5)	1.39(7)
Heselbach	18.2	1005.0	55.1	2 439	388	261(5)	1.97(6)
Shouxian	7.7	197.5	25.5	480	172	84(4)	1.73(9)
Graciosa	12.7	424.0	33.4	3 066	512	60(1)	2.12(6)
NSA	75.2	103.3	1.4	9 097	16	49(1)	6(3)
Pt. Reyes	5.7	784.0	138.6	579	178	272(1)	1.71(7)
SGP	9.4	278.2	29.7	1 624	303	143(4)	1.74(7)

in the clustering null model of critical two-dimensional percolation, clusters defined in one-dimensional cuts, akin to durations, do not scale, whereas two-dimensional clusters, akin to cloud-projections, do.

Applying to the durations the methods we used for the event sizes, we find comparatively short power-law ranges, see table 4. The scaling range, if it exists, is expected to be smaller than for event sizes, as the size distribution is a complicated convolution of the event duration and precipitation rate distributions, figure 1, whose product covers a broader range than either of the distributions alone. The event size distribution is broader than the duration distribution also because long events tend to be more intense (not shown).

J. Stat. Mech. (2010) P11030

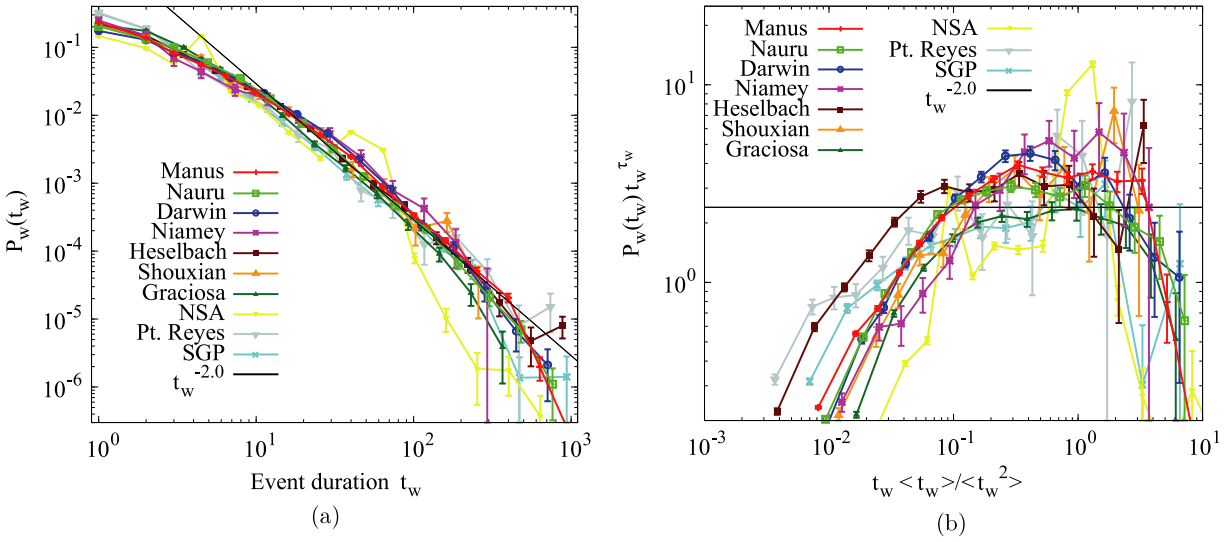

Figure 6. (a) Probability densities for event durations (in min) are broad for all data sets. From a few min up to a few hundred min a power law with an exponent $_m \approx 2.0$ roughly describes the data. (b) Collapsed distributions, similar to "gure 3(b).

8. Conclusions

We find that the apparent avalanche size exponents, measured with identical instruments in different locations, are consistent with a single value of $\tau_s = 1.17(3)$ for all reliable data sets. We note that the data sets from Point Reyes and from the Southern Great Plains are similar in many respects, despite the different reasons for treating them with suspicion.

The statistical error in this estimate is surprisingly small, but neither the value itself nor the error change much using different fitting techniques or introducing different sensitivity thresholds (not shown). Nonetheless we believe systematic errors to be larger. Thus, the analysis gives an impression of the universality of the result but not necessarily the physical 'true' value of the exponent. This does not contradict the climatological situation—tropical regions, for instance, are expected to support larger events than mid-latitude locations, which could be realized as a smaller exponent value τ_s. While the exponents are not significantly different, the larger tropical events are reflected in the greater large-scale cutoff of the tropical distributions. Similarly, the dry spell durations seem to follow another power law with $\tau_d = 1.2(1)$, and regional differences can be seen in the strength of the diurnal cycle and the cutoff dry spell duration. The broad range of event durations, figure 6, suggests a link to the lack of characteristic scales in the mesoscale regime, where approximately scale-free distributions of clusters of convective activity, for example cloud or precipitation, have been observed to span areas between $\mathcal{O}(1\ \mathrm{km}^2)$ and $\mathcal{O}(10^6\ \mathrm{km}^2)$ [25, 24, 30, 28, 26]. The observation of scale-free rainfall event sizes suggests long-range correlation in the pertinent fields, a possible indication of critical behavior near the transition to convective activity. Direct measurements of the behavior of the correlation function for the precipitation field under changes of the (much more slowly varying) background fields of water vapor and temperature are desirable to clarify

J. Stat. Mech. (2010) P11030

whether the long-range correlation is a consequence of the flow field, of the proximity to a critical point, or of a combination of both.

Acknowledgments

This work was supported in part by the National Oceanic and Atmospheric Administration Grant NA08OAR4310882 and the National Science Foundation Grant ATM-0645200. Data were obtained from the Atmospheric Radiation Measurement (ARM) Program sponsored by the US Department of Energy, Office of Science, Office of Biological and Environmental Research, Environmental Sciences Division. AD would like to thank the Spanish Ministerio de Educación for travel support and Imperial College London for hospitality. Initial research by AD was supported by a grant from the Explora-Ingenio 2010 project FIS2007-29088-E. Other grants: FIS2009-09508, and 2009SGR-164. AC is a participant of the CONSOLIDER i-MATH project.

Appendix A. Fitting procedure

In order to obtain reliable values of, for example, the exponent τ_s, independent of the binning procedure used for the plots of $P_s(s)$, we use maximum-likelihood estimation. We assume a power-law distribution $P_s(s) = a_{\tau_s} s^{-\tau_s}$, with support $[s_{\min}, s_{\max}]$. Normalization yields $a_{\tau_s} = (1-\tau_s)/(s_{\max}^{1-\tau_s} - s_{\min}^{1-\tau_s})$ for a given value of τ_s.

We compute the log-likelihood function,

$$\mathcal{L} := \ln \prod_{i=1}^{\bar{N}} P_s(s_i) = \sum_{i=1}^{\bar{N}} \ln \left(a_{\tau_s} {s_i}^{-\tau_s} \right) \tag{A.1}$$

where the index i runs over all $\bar{N}$ events whose size s_i is between $s_{\min}$ and $s_{\max}$. Holding $s_{\min}$ and $s_{\max}$ fixed, the value of τ_s which maximizes $\mathcal{L}$ is the maximum-likelihood estimate of the exponent. Uncertainties in τ_s are determined using the jackknife method.

The goodness of the fit is assessed by a Kolmogorov–Smirnov (KS) test [20]. The KS statistic, or KS distance, d, is defined as

$$d := \max_{s_{\min} \le s \le s_{\max}} |S_{\bar{N}}(s) - F_s(s)| \tag{A.2}$$

where $S_{\bar{N}}(s)$ denotes the empirical cumulative distribution, defined as the fraction of observed events with a size smaller than s, in the interval $[s_{\min}, s_{\max}]$. Thus, ordering the observed values by size, $s_1 \le \cdots \le s_i \le s_{i+1} \cdots \le s_{\bar{N}}$, we have $S_{\bar{N}}(s) = i/\bar{N}$ if $s_i < s \le s_{i+1}$; F_s denotes the cumulative distribution of the maximum-likelihood distribution, $F_s(s) := \int_{s_{\min}}^{s} P_s(t)\, \mathrm{d}t$.

The KS distance translates into the p-value. The p-value is the probability that synthetic data, here drawn from a power-law distribution with exponent τ_s, result in a KS distance of at least d. For instance, $p = 10\%$ means that for power-law-distributed data with exponent τ_s there is a probability of 0.90 that the KS distance takes a value smaller than d. Thus, if the data really are generated by a power law and we decide to reject the power law as a model if $p < 10\%$, we will reject the correct model in 10% of our tests. Conversely, decreasing the limit of rejection in the p-value implies that we accept more false models.

J. Stat. Mech. (2010) P11030

In our implementation of the KS test the distribution to be tested, $P_s(s)$, is not independent of the empirical data. This is because the exponent τ_s is obtained from the data that are later used to test the distribution. We therefore cannot use the standard analytic expression for $p(d)$, see [20], chapter 15. Instead, we determine the distribution of the KS distance and therefore the p-value by means of Monte Carlo simulations: we generate synthetic power-law-distributed data sets between $s_{\min}$ and $s_{\max}$ with exponent τ_s and number of data $\bar{N}$ (see table 2), and proceed exactly in the same way as for the empirical data, first obtaining a maximum-likelihood estimate of the exponent τ_s and then computing the KS distance between the empirical distribution of the simulated data and the fitted distribution containing the estimated value of τ_s. The p-value is obtained as the fraction of synthetic data sets for which the KS statistic is larger than the value obtained for the empirical data.

The final step is to compare results for different ranges $[s_{\min}, s_{\max}]$. We try all possible fitting ranges with $s_{\min}$ and $s_{\max}$ increasing by factors of $10^{0.01} \approx 1.023$. We choose to report those intervals $[s_{\min}, s_{\max}]$ that contain the largest number of events $\bar{N}$ with a corresponding p-value larger than 10%.

Appendix B. Two-sample Kolmogorov Smirnov tests

A two-sample Kolmogorov–Smirnov test was performed for each pair of data sets, i, j to test whether the two underlying event size probability distributions differ. This test does not assume any functional form for the probability distributions [20]. As in the fitting of the exponent, we vary the testing ranges $[s_{\min}, s_{\max}]$, keeping those which yield $p > 10\%$. We report the range with the maximum effective number of data, $\bar{N}_e \equiv \bar{N}_i \bar{N}_j / (\bar{N}_i + \bar{N}_j)$. The results, shown in table B.1, confirm that the pairs of distributions from the reliable data sets are similar over broad ranges.

Table B.1. Maximum range $s_{\max}/s_{\min}$ over which the p-value of a two-sample KS test is greater than 10%.

	Nauru	Darwin	Niamey	Heselbach	Shouxian	Graciosa	NSA	Pt. Reyes	SGP
Manus	5386	16 257	16 386	679	6 355	638	14	32	8
Nauru		6 753	13 495	236	221	342	27	19	7
Darwin			12 247	236	271	575	27	16	5
Niamey				3466	16 420	2 358	1599	668	253
Heselbach					14 600	13 265	18	20	5
Shouxian						26 440	13	65	39
Graciosa							11	17	589
NSA								10	3
Pt. Reyes									19 916

References

[1] Andrade R F S, Schellnhuber H J and Claussen M, *Analysis of rainfall records: possible relation to self-organized criticality*, 1998 *Physica* A **254** 557

[2] Peters O, Hertlein C and Christensen K, *A complexity view of rainfall*, 2002 *Phys. Rev. Lett.* **88** 018701

J. Stat. Mech. (2010) P11030

[3] Peters O and Neelin J D, *Critical phenomena in atmospheric precipitation*, 2006 *Nat. Phys.* **2** 393
[4] Neelin J D, Peters O and Hales K, *The transition to strong convection*, 2009 *J. Atmos. Sci.* **66** 2367
[5] Klein R, *Scale-dependent models for atmospheric flows*, 2010 *Annu. Rev. Fluid Mech.* **42** 249
[6] Bodenschatz E, Malinowski S P, Shaw R A and Stratmann F, *Can we understand clouds without turbulence?*, 2010 *Science* **327** 970
[7] Barenblatt G I, 1996 *Scaling, Self-similarity and Intermediate Asymtotics* (Cambridge: Cambridge University Press)
[8] Arakawa A and Schubert W H, *Interaction of a cumulus cloud ensemble with large-scale environment*, 1974 *J. Atmos. Sci.* **31** 674
[9] Tang C and Bak P, *Critical exponents and scaling relations for self-organized critical phenomena*, 1988 *Phys. Rev. Lett.* **60** 2347
[10] Dickman R, Vespignani A and Zapperi S, *Self-organized criticality as an absorbing-state phase transition*, 1998 *Phys. Rev.* E **57** 5095
[11] Olsson J, Niemczynowicz J and Berndtsson R, *Fractal analysis of high-resolution rainfall time-series*, 1993 *J. Geophys. Res.* **98** 23265
[12] Dickman R, *Rain, power laws, and advection*, 2003 *Phys. Rev. Lett.* **90** 108701
[13] Betts A K and Miller M J, *A new convective adjustment scheme. Part II: single column tests using GATE wave, BOMEX, ATEX and arctic air-mass data sets*, 1986 *Q. J. R. Meteorol. Soc.* **112** 693
[14] Neelin J D, Peters O, Lin J W B, Hales K and Holloway C E, *Rethinking convective quasi-equilibrium: observational constraints for stochastic convective schemes in climate models*, 2008 *Phil. Trans. R. Soc.* A **366** 2581
[15] Ritsche M T, *ARM surface meteorology systems handbook and surface meteorology (smet) handbook*, http://www.arm.gov/publications/handbooks
[16] ARM data quality program http://www.arm.gov/data/data_quality.stm
[17] Alava M J, Laurson L, Vespignani A and Zapperi S, *Comment on self-organized criticality and absorbing states: lessons from the Ising model*, 2008 *Phys. Rev.* E **77** 048101
[18] Pruessner G and Peters O, *Reply to comment on 'Self-organized criticality and absorbing states: lessons from the Ising model'*, 2008 *Phys. Rev.* E **77** 048102
[19] Rosso A, Le Doussal P and Wiese K J, *Avalanche-size distribution at the depinning transition: a numerical test of the theory*, 2009 *Phys. Rev.* B **80** 144204
[20] Press W H, Teukolsky S A, Vetterling W T and Flannery B P, 2002 *Numerical Recipes* 3rd edn (Cambridge: Cambridge University Press)
[21] Clauset A, Shalizi C R and Newman M E J, *Power-law distributions in empirical data*, 2009 *SIAM Rev.* **51** 661
[22] Efron B, *The jackknife, the bootstrap and other resampling plans*, 1982 *CBMS-NSF Regional Conf. Series in Applied Mathematics* (*Monograph* vol 38) (Philadelphia: SIAM)
[23] Lavergnat J and Golé P, *A stochastic raindrop time distribution model*, 1998 *J. Appl. Meteor.* **37** 805
[24] Peters O, Neelin J D and Nesbitt S W, *Mesoscale convective systems and critical clusters*, 2009 *J. Atmos. Sci.* **66** 2913
[25] Trivej P and Stevens B, *The echo size distribution of precipitating shallow cumuli*, 2010 *J. Atmos. Sci.* **67** 788
[26] Cahalan R F and Joseph J H, *Fractal statistics of cloud fields*, 1989 *Mon. Weather Rev.* **117** 261
[27] Mapes B E and Houze R A Jr, *Cloud clusters and superclusters over the Oceanic Warm Pool*, 1993 *Mon. Weather Rev.* **121** 1398
[28] Benner T C and Curry J A, *Characteristics of small tropical cumulus clouds and their impact on the environment*, 1998 *J. Geophys. Res.* **103** 28753
[29] Schertzer D and Lovejoy S, *The dimension and intermittency of atmospheric dynamics*, 1985 *Turbulent Shear Flows* vol 4, ed B Launder (New York: Springer) pp 7–33
[30] Neggers R A J, Jonker H J J and Siebesma A P, *Size statistics of cumulus cloud populations in large-Eddy simulations*, 2003 *J. Atmos. Sci.* **60** 1060

J. Stat. Mech. (2010) P11030

Journal of Statistical Mechanics: Theory and Experiment
An IOP and SISSA journal

Addendum: Universality of rain event size distributions

Ole Peters[1,2], A Deluca[3], A Corral[3], J D Neelin[2] and C E Holloway[4]

[1] Department of Mathematics and Grantham Institute for Climate Change, Imperial College London, 180 Queen's Gate, London SW7 2AZ, UK
[2] Department of Atmospheric and Oceanic Sciences and Institute for Geophysics and Planetary Physics, University of California, Los Angeles, 405 Hilgard Avenue, Los Angeles, CA 90095-1565, USA
[3] Centre de Recerca Matemàtica, Campus de Bellaterra, Edifici C, E-08193 Bellaterra (Barcelona), Spain
[4] Department of Meteorology, University of Reading, Earley Gate, PO Box 243, Reading RG6 6BB, UK
E-mail: ole@santafe.edu, adeluca@crm.cat, acorral@crm.cat, neelin@atmos.ucla.edu and c.e.holloway@reading.ac.uk

Received 2 June 2013
Accepted 5 June 2013
Published 27 June 2013

Online at stacks.iop.org/JSTAT/2013/P06019
doi:10.1088/1742-5468/2013/06/P06019

The author AD would like to clarify that she was, when this paper was published, a member of the PhD in Mathematics Program at the Universitat Autònoma de Barcelona (UAB) and of the Esfera UAB.

J. Stat. Mech. (2013) P06019

1742-5468/13/P06019+01$33.00

Appendix A

Appendix A: Other Publications

The next list of non-peer-review accepted publications, submitted peer-review publications and preprints related with the contents of this thesis.

Submitted

[C] A. Deluca and A. Corral, ***Scale Invariant Events and Dry Spells for Medium Resolution Local Rain Data***, submitted to *Nonlinear Processes in Geophysics*, (2012).

To be submitted

[D] A. Deluca, P. Puig and A. Corral, ***Testing Universality in Critical Exponents: the Case of Rainfall***, *In preparation*, (2013).

[E] A. Deluca N. R. Moloney and A. Corral, ***Analysis of the predictability of local rain records across different climates***, *In preparation*, (2013).

Non-peer-reviewed Publications

[F] A. Corral, A. Deluca and R. Ferrer-i-Cancho, ***A practical recipe to fit discrete power-law distributions***, , (2012) . *http://arxiv.org/abs/1209.1270*

[G] A. Deluca, P. Puig and A. Corral, ***Testing universality and goodness-of-fit test of power-law distribution***, Extended Conference Abstracts, CRM Documents Spring 2013 , *Accepted,* (2013).

[H] A. Deluca N. R. Moloney and A. Corral, ***Criticality on Rainfall: Statistical Observational Constrains for the Onset of Strong Convection Modelling***, Extended Conference Abstracts, CRM Documents Spring 2013 , *Accepted,* (2013).

Testing universality and goodness-of-fit test of power-law distributions

Anna Deluca[1,2], Pere Puig[2], and Álvaro Corral[1]

[1] Centre de Recerca Matemàtica, Edifici C, Campus de Bellaterra, E-08193, Cerdanyola, Barcelona, Spain
[2] Departament de Matemàtiques, Universitat Autònoma de Barcelona, E-08193, Cerdanyola, Barcelona, Spain

Power-law distributions contain precious information about a large variety of physical processes [**1**]. Although there are sound theoretical grounds for these distributions, the empirical evidence giving support to power laws has been traditionally weak.

Here, we present an alternative procedure, valid for truncated as well as for non-truncated power-law distributions, based in maximum likelihood estimation of the exponent, the Kolmogorov-Smirnov goodness-of-fit test, and Monte Carlo simulations [**2, 3, 4**]. In addition, we also present procedures for testing the existence of a single universal exponent in a collection of different datasets, based on the definition of a statistic that contains the weighted sum of the differences of the values of the exponents for all pairs of datasets.

Power-Law Fitting

A continuous variable x, where $a \leq x \leq b$ with b finite or infinite and $a > 0$, is power-law distributed if its probability density is given by,

$$f(x) = \frac{\alpha - 1}{a^{1-\alpha} - 1/b^{\alpha-1}} \left(\frac{1}{x}\right)^{\alpha}. \tag{1}$$

If $b \to \infty$ and $\alpha > 1$ the distribution is called a non-truncated power-law distribution; while for finite b the distribution is called a truncated power law, for which no restriction exists on α.

The key to fit properly power-law distributions to real-world data is to have an objective criteria to decide at which point the power law starts (and, in the truncated case, at which point it ends); this is the fitting range.

The Method

Given a sample of the random variable x with N elements as $x_1, x_2, \ldots, x_N$, we want to estimate the parameter α and determine the interval defined by a and b where the power-law holds.

In order to obtain a reliable estimate of the exponent α we use maximum likelihood estimation. For that, we assume a and b as known. We compute the log-likelihood function for our particular case,

$$\ell(\alpha) = \ln \frac{\alpha - 1}{1 - r^{\alpha-1}} - \alpha \ln \frac{g}{a} - \ln a, \text{ if } \alpha \neq 1, \tag{2}$$

where $r = a/b$ and g is the geometric mean. Holding a and b fixed, the value of α which maximizes $\ell(\alpha)$ is the maximum likelihood of the exponent.

Then, the quality of the fit is assessed by a Kolmogorov-Smirnov (KS) test [**5**]. The KS statistic, or KS distance, d_e, is defined as the maximum difference in absolute value between the theoretical cumulative distribution and the empirical cumulative distribution, which is estimated by $\frac{n_e(x)}{N}$[**6**].

The KS distance allows us to calculate the p-value, the probability that, under the null hypothesis, the KS statistic takes a value larger than the one obtained empirically. As the exponent α is obtained from the data, we need to determine the distribution of the KS distance using Monte Carlo simulations. Next, we apply the same procedure for all possible ranges $[a, b]$ and compare the results. We keep the fits, *i.e.* , the triplets $\{a, b, \alpha\}$, such that the corresponding p-values are larger than a certain p_c.

Finally, we need to select objectively one fitting range among all the listed triplets. For a non-truncated power law ($b = \infty$) we select the largest interval, *i.e.* , the smaller a. If the power law is truncated we consider two different criteria for choosing the range: select the interval that maximizes the number of data in it or select the larger log-range b/a. In fact, many true truncated power laws can be contained in the data [**7**]. Maximizing N tends to select power laws in the initial range on values, while maximizing the log-range tends to select power laws nearer to the tail of the distribution.

Application for the seismic moment of earthquakes

In Fig. 1 one can see an illustration of the method performance results for the seismic moment (M) of earthquakes worldwide and in Southern California. Starting with the non-truncated power-law distribution, we always obtain significant power-law fit, valid for several orders of magnitude. In both cases the exponent α is between 1.61 and 1.71, but for Southern California is more stable. For the worldwide CMT catalog restricted to shallow earthquakes the largest value of a is 3×10^{18} Nm, corresponding to a magnitude $m = 6.25$. For Southern California, the largest a found (for $p_c = 0.5$) is 1.6×10^{15} Nm, giving $m = 4$. This value is somewhat higher, in comparison with the completeness magnitude of the catalog; this can be attributed to this catalog specific characteristics [**3**]. When a truncated power law is fitted, using the method of maximizing the number of data leads to similar values of the exponents, although the range of the fit is in some cases moved to smaller values (smaller a, and b smaller than the maximum M on the dataset). The method of maximizing b/a leads to results that are very close to the non-truncated power law.

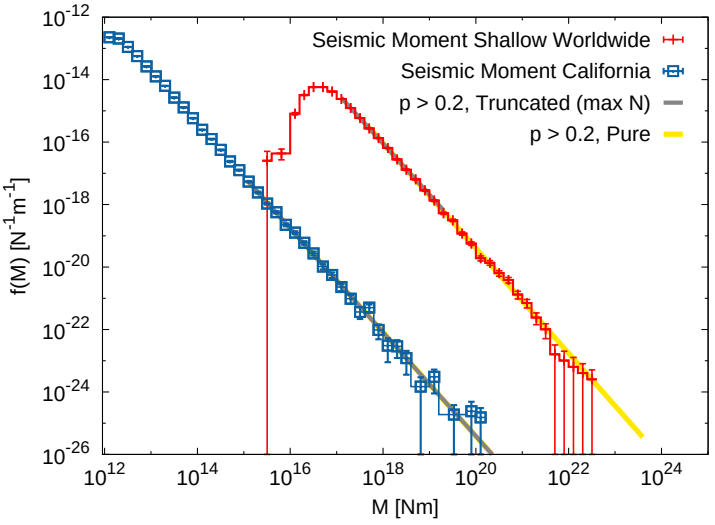

FIGURE 1. Estimated probability densities and corresponding power-law fits of the seismic moment M of shallow earthquakes in the worldwide CMT catalog and of the estimated M in the Southern California catalog.

Universality Verification

As we have just seen, the determination of the exponents of power-law distributions is not a straightforward task. However, determining the critical exponents as accurately and unbiasedly as possible, together with their associated uncertainties, is not enough for verifying universality. The exponents need to be properly compared, in order to test if they are statistically compatible.

Confidence intervals for exponent differences

In the case in which one only has two different datasets with estimated exponents α_{e1} and α_{e2}, the difference $\alpha_{e1} - \alpha_{e2}$ will have zero mean, under the null hypothesis. Also if datasets are independent, the standard deviation of the difference of the estimators will be $\sqrt{\sigma_{e1}^2 + \sigma_{e2}^2}$.

As, asymptotically, power-law MLE exponents are normally distributed [**8**], so will be their difference. Then, it is straightforward to obtain a confidence interval for the difference. If the interval includes the observed difference value, the null hypothesis cannot be rejected and the exponents can be considered to take the same value.

Nevertheless, the situation is not so simple when one needs to analyse 3 or more systems. In order to avoid the rejection of the null hypothesis by chance, corrections of the significance level, as the Bonferroni correction or the Šidák correction [**9**], need to be applied. However, these corrections are too generous in order to claim for universality.

The Permutation Test

For multiple testing we propose a permutation test [**10**]. We define a *test statistic* such that the larger its value, the stronger the evidence against the null hypothesis H_0. The null hypothesis will be that for the common range $a \leq x_j \leq b$ all exponents are the same, i.e., $\alpha_{ei} = \alpha_{ej}$, for all i and j.

We choose for example,

$$\widehat{\Theta} = \sum_{i=1}^{M-1} \sum_{j=i+1}^{M} (\alpha_{ei} - \alpha_{ej})^2, \tag{3}$$

where M is the number of datasets. More complex and powerful alternatives are considered in [**11**].

The scale for $\widehat{\Theta}$ is provided by the *achieved significance level* or $p-$value of the test, which is defined as the probability that, under the null hypothesis H_0, the random variable $\widehat{\Theta}$ is larger than the value we obtained for the observed data $\widehat{\Theta}_{\rm data}$, i.e.,

$$p = \text{Prob}\{\widehat{\Theta} \geq \widehat{\Theta}_{\rm data} \mid H_0 \text{ is true}\}, \tag{4}$$

so, the smaller the $p-$value, the stronger the evidence against H_0.

We will use a permutation test as a way to compute the $p-$value. It is based on the idea that, if the null hypothesis is correct, any data value could correspond to any dataset and the data values (the size of the events in our case) are therefore interchangeable. First, we combine the $n_1+n_2+...+n_M$ observations from all the datasets into a single meta-dataset (n_i the number of data $a \leq x_j \leq b$ for each dataset) and take M random samples of sizes n_1, n_2, ..., n_M without replacement. This generates M new datasets with the same number of data than the initial ones. Next, we fit the power-law exponents (in the common fitting range) for each permuted or reshuffled dataset and from their values we compute the new test statistic $\widehat{\Theta}_{\rm sh}$ (where sh stands for shuffled).

The distribution of the test statistic, under the null hypothesis, is obtained repeating the process a large enough number of times. With that we can compute easily an approximation of

the $p-$value by

$$p - \text{value} \approx \frac{\#\{\widehat{\Theta}_{\text{sh}} \geq \widehat{\Theta}_{\text{data}}\}}{N_{\text{sh}}} \tag{5}$$

where $\#\{\widehat{\Theta}_{\text{sh}} \geq \widehat{\Theta}_{\text{data}}\}$ is the number of permutations for which $\widehat{\Theta}_{\text{sh}} \geq \widehat{\Theta}_{\text{data}}$.

Application for rainfall data

We apply the method to rain data from the Atmospheric Radiation Measurement (ARM) Program (www.arm.gov) used in Ref. [**2**], excluding the 3 sites that were found problematic there. For the rain event sizes, defined as in Ref. [**2**], we obtain $\widehat{\Theta}_{\text{data}} = 0.051$ which leads to $p = 0.26$. So we cannot rule out the universality of the exponents.

Conclusions

For power-law distributions, the fitting and testing the goodness-of-fit is a difficult but very relevant problem in complex-systems science, in particular in geoscience. The most critical step is to select, automatically (without introducing any subjective bias), where the power-law regime starts and where it ends. We present a procedure that overcomes some problems found in the method introduced by Clauset et al. (2009), see [**12**].

We tested the performance of the method with synthetic power-law datasets and real-world data. The results for the power-law exponent of the distribution of seismic moments worldwide and in Southern California are in agreement with previous estimates, but in addition our method provides a reliable way to determining the minimum seismic-moment value for which the Gutenberg-Richter law holds.

Moreover, we present procedures for comparing the estimated critical exponents in order to test the existence of a single universal exponent [**11**]. The results for the rainfall data are consistent with theoretical expectations [**2**].

References

[1] B. D. Malamud. Tails of natural hazards. *Phys. World*, 17 (8):31–35, 2004.
[2] O. Peters, A. Deluca, A. Corral, J. D. Neelin, and C. E. Holloway. Universality of rain event size distributions. *J. Stat. Mech.*, P11030, 2010.
[3] A. Corral and A. Deluca. Fitting and goodness-of-fit test of non-truncated and truncated power-law distributions. *Acta Geophys.*, 2013. Accepted for publication.
[4] A. Corral, A. Deluca, and R. Ferrer i Cancho. A practical recipe to fit discrete power-law distributions. *ArXiv*, 1209:1270, 2012.
[5] W. H. Press, S. A. Teukolsky, W. T. Vetterling, and B. P. Flannery. *Numerical Recipes in FORTRAN*. Cambridge University Press, Cambridge, 2nd edition, 1992.
[6] R. Chicheportiche and J.-P. Bouchaud. Weighted Kolmogorov-Smirnov test: Accounting for the tails. *Phys. Rev. E*, 86:041115, 2012.
[7] A. Corral. Point-occurrence self-similarity in crackling-noise systems and in other complex systems. *J. Stat. Mech.*, P01022, 2009.
[8] I. B. Aban, M. M. Meerschaert, and A. K. Panorska. Parameter estimation for the truncated Pareto distribution. *J. Am. Stat. Assoc.*, 101:270–277, 2006.
[9] J. M. Bland and D. G. Altman. Multiple significance tests: the Bonferroni method. *Brit. Med. J.*, 310:170–170, 1995.
[10] Efron B and Tibshirani R J. *An Introduction to the Bootstrap*. Chapman & Hall/CRC, 1st edition, 1993.
[11] A. Deluca, P. Puig, and A. Corral. Testing universality of critical exponents: the case of rainfall. page In preparation, 2013.
[12] A. Corral, F. Font, and J. Camacho. Non-characteristic half-lives in radioactive decay. *Phys. Rev. E*, 83:066103, 2011.

Criticality on Rainfall: Statistical Observational Constraints for the Onset of Strong Convection Modelling

Anna Deluca[1 2], **Álvaro Corral**[1], **and Nicholas R. Moloney**[3]

[1] Centre de Recerca Matemàtica, Edifici C, Campus de Bellaterra, E-08193, Cerdanyola, Barcelona, Spain

[2] Departament de Matemàtiques, Universitat Autònoma de Barcelona, E-08193, Cerdanyola, Barcelona, Spain

[3] London Mathematical Laboratory, 14 Buckingham Street, WC2N 6DF London, United Kingdom

1 Introduction

A better understanding of convection is crucial for reducing the intrinsic errors present in climate models [**1**]. Many atmospheric processes related to precipitation have large scale correlations in time and space, which are the result of the coupling between several non-linear mechanisms with different temporal and spatial characteristic scales. Despite the diversity of individual rain events, a recent array of statistical measures presents surprising statistical regularities giving support to the hypothesis that atmospheric convection and precipitation may be a real-world example of Self-Organised Criticality (SOC) [**3, 4**]. The usual approach consists of looking at the occurrence of rain by days or months. For episodic rain events, similar to avalanches in cellular-automaton models, scale-free rain event distributions are found [**6**]. However, a power-law distribution (i.e. scale-free) of the observable is not sufficient evidence for SOC dynamics, as there are many alternative mechanisms that give rise to such behaviour (see, for example, [**7, 8**]).

Further support for the SOC hypothesis was given by Peters and Neelin [**9**], who found a relation between satellite estimates of rain rate and water vapour over the tropical oceans compatible with a phase transition, in which large parts of the troposphere would be in a convectively active phase. In addition, it was shown that the system was close to the transition point. They also related it to the concept of atmospheric quasi-equilibrium [**10**], which argues that, since driven processes are generally slow compared to convection, the system should typically be in a far-from equilibrium statistically stationary state, where driving and dissipation are in balance. In addition, recent works have shown that local event size distributions present signs of universality in the system, as was expected in the SOC framework [**11, 12, 13**]. The resulting rain event size distributions were found to be well approximated by power laws of similar exponents over broad ranges, with differences in the large-scale cutoffs of the distributions. The possible consequences of this framework for the prediction of atmospheric phenomena still remain unclear.

2 Data and Methods

In this contribution we use very high-resolution (1 minute) local rain intensities across different climates described in [**11**], stochastic convective models [**14**] and SOC models

Extended Conference Abstracts, Spring 2013, CRM Documents, vol. ??
Centre de Recerca Matemàtica, Bellaterra (Barcelona)

such as the BTW model and the Manna model, for investigating how predictable the time series of rain activity and rain event sizes are [**2, 3**].

We use the hazard function H_q as a decision variable, which is sensitive to clustering or repulsion between events in the time series. The conventional precursor pattern technique requires a large amount of data, does not capture long memory and has been found to perform worse than the hazard function in similar analysis [**15**]. H_q is defined as the probability that a threshold-crossing event will occur in the next Δt, conditional on no previous event within the past t_w

$$H_q(t_w;\Delta t) = \frac{\int_{t_w}^{t_w+\Delta t} P_q(\tau)\mathrm{d}\tau}{\int_{t_w}^{\infty} P_q(\tau)\mathrm{d}\tau}, \tag{1}$$

where q corresponds to the different thresholds on sizes and Δt is set to 1 *min* for the rain data and one parallel update for the SOC models. The various quantities are illustrated in Fig. 1.

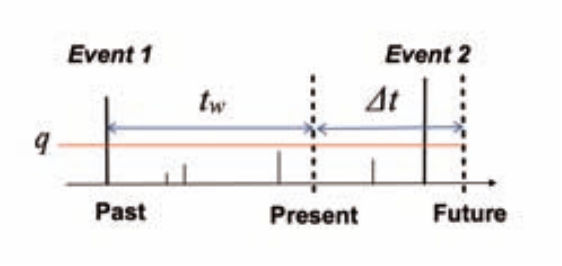

FIGURE 1. Sketch of the hazard function variables

Note that the hazard function gives us a probabilistic forecast and in order to perform a deterministic prediction we will need to consider a discrimination threshold.

We also evaluate the quality of the prediction with the receiver operating characteristics method (ROC) [**16**]. For any binary prediction (occurrence or non-occurrence of an event) four possible outcomes can occur: true positive (TP), false positive (FP), true negative (TN) and false negative (FN), see Fig. 2.

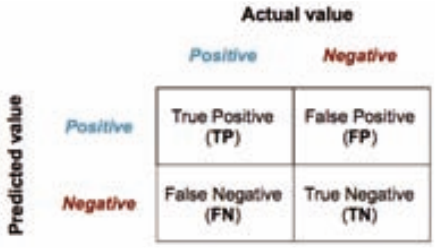

FIGURE 2. Four possible outcomes of a binary prediction in a contingency table.

ROC curves compare *sensitivity* and *specificity*. The *sensitivity* is defined as the number of correctly predicted occurrences divided by the total number of actual occurrences,

and the *specificity* as the number of correctly predicted non-occurrences divided by the total number of actual non-occurrences,

$$sensitivity = \frac{TP}{TP + FN} \qquad specificity = \frac{TN}{FP + TN} \tag{2}$$

Each threshold on the decision variable will give a different point on the ROC curve. If we consider the minimum possible threshold we will always predict the occurrence of an event, for which the *sensitivity* is one and the *specificity* zero. The diagonal in Fig. 3 corresponds to random prediction. Points above the diagonal represent good predictions (better than random) and points below poor predictions.

3 Results

We find that on the events scale (slow time scale), rain data renormalise to a trivial Poisson point process for large thresholds, while for small thresholds events cluster. This is in contrast to the anti-clustering of high-threshold events in the 2D BTW model as a result of finite-size effects and the building up of correlations, seen previously by Garber *et al.* [**17**] (see Fig. 3(a) and Fig. 3(b)).

However, rain data has an unavoidable threshold on intensity due to the device resolution that blurs the interpretation of the results on the event scale. At the level of intensities (slow time scale), we find that prediction is insensitive to all but very high thresholds.

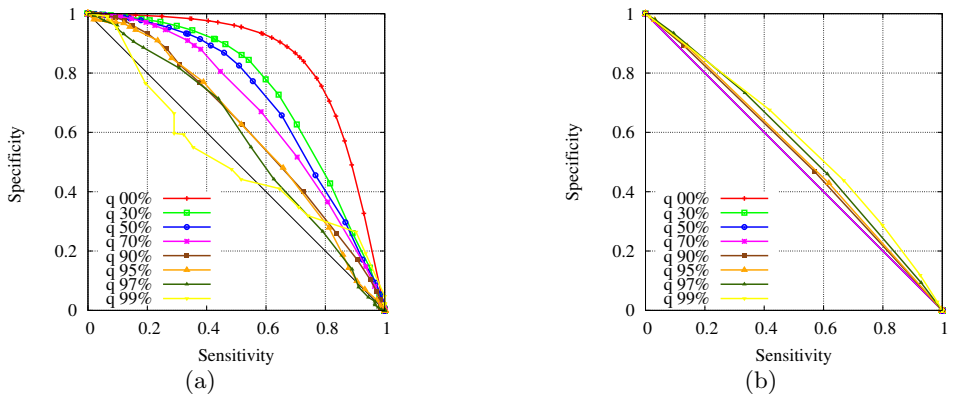

FIGURE 3. Example of ROC curves data on the slow time scale for rainfall data (a) and for the 2D BTW SOC Model simulated data (b).

References

[1] Core Writing Team, Pachauri, R.K. and Reisinger, A. (Eds.) Fourth Assessment Report of the Intergovernmental Panel on Climate Change IPCC, Geneva, Switzerland. pp 104
[2] Manna S S. *J. Phys. A: Math Gen.*, 24(8):363 369, 1991.
[3] Bak P, Tang C and Wiesenfeld K. *Phys. Rev. Lett.*, 59(23):2347 2350, 1988.
[4] Tang C and Bak P. *Phys. Rev. Lett.*, 60(23):2347 2350, 1988.
[5] Andrade R F S, Schellnhuber H J, and Claussen M. *Physica A*, 254(3-4):557 568, 1998.
[6] Peters O, Hertlein C, and Christensen K. *Phys. Rev. Lett.*, 88(1):018701(1 4), 2002.

[7] Dickman R. *Phys. Rev. Lett.*, 90(10):108701(1 4), 2003.
[8] Mitzenmacher M *Internet Math.*, 1(2):226 251, 2014.
[9] Peters O and Neelin J D. *Nature Phys.*, 2(6):393 396, 2006.
[10] Arakawa A and Schubert W H. *J. Atmos. Sci.*, 31(3):674 701, 1974.
[11] Peters O, Deluca A, Corral A, Neelin J D and Holloway C E *J. Stat. Mech.*, P11030, 2010.
[12] Deluca A and Corral A. Scale Invariant Events and Dry Spells for Medium Resolution Local Rain Data. *Submitted to Non. Proc. Geophys.*
[13] Deluca A, Puig P, and Corral A. Testing Universality in Critical Exponents: the Case of Rainfall *In preparation.*
[14] Stechmann S and Neelin J D. A stochastic model for the transition to strong convection. *J. Clim.*, 68:2955 2970), 2011.
[15] Bogachev M I, Kireenkov I S, Nifontov E M, and Bunde A. Statistics of return intervals between long heartbeat intervals and their usability for online prediction of disorders. *New J. Phys.*, 11(063036):1 19, 2009.
[16] Egan J P. *Signal Detection Theory and ROC analysis.* Academic Press, New York, 1975.
[17] Garber A, Hallerberg S, and Kantz H. Predicting extreme avalanches in self-organized critical sandpiles. *Phys. Rev. E*, 80:026124(1 5), 2009.
[18] Deluca A, Moloney N R, and Corral A. Analysis of the predictability of local rain records across different climates *In preparation.*

Bibliography

ARM data quality program. `http://www.arm.gov/data/data_quality.stm`. [p. 106]

I. B. Aban, M. M. Meerschaert, and A. K. Panorska. Parameter estimation for the truncated Pareto distribution. *J. Am. Stat. Assoc.*, 101:270 277, 2006. [p. 23, 24, 28, 29, 30, 32, 38, 40, 107, 108, 111, 114]

H. Abdi. Bonferroni and šidák corrections for multiple comparisons. In N. J. Salkind, editor, *Encyclopedia of Measurement and Statistics*, pages 103 107. Sage, Thousand Oaks, 2007. [p. 109]

M. J. Alava, L. Laurson, A. Vespignani, and S. Zapperi. Comment on Self-organized criticality and absorbing states: Lessons from the Ising model . *Phys. Rev. E*, 77(4): 048101(1 2), 2008. [p. 68]

R. F. S. Andrade, H. J. Schellnhuber, and M. Claussen. Analysis of rainfall records: possible relation to self-organized criticality. *Physica A*, 254:557 568, 1998. [p. 16, 61, 80, 85, 106]

A. Arakawa and W. H. Schubert. Interaction of a cumulus cloud ensemble with the large-scale environment, part I. *J. Atmos. Sci.*, 31:674 701, 1974. [p. 15, 62, 63, 82, 117]

M. Aschwanden. *Self-Organized Criticality in Astrophysics: The Statistics of Nonlinear Processes in the Universe*. Springer Praxis Books, 2011. [p. 24]

M. Baiesi, M. Paczuski, and A. L. Stella. Intensity thresholds and the statistics of the temporal occurrence of solar flares. *Phys. Rev. Lett.*, 96:051103, 2006. [p. 24]

P. Bak. *How Nature Works: The Science of Self-Organized Criticality*. Copernicus, New York, 1996. [p. 16, 24, 80, 105]

P. Bak, C. Tang, and K. Wiesenfeld. Self-organized criticality: an explanation of 1 f noise. *Phys. Rev. Lett.*, 59:381 384, 1987. [p. 8, 12, 13, 117, 118]

P. Bak, K. Christensen, L. Danon, and T. Scanlon. Unified scaling law for earthquakes. *Phys. Rev. Lett.*, 88:178501, 2002. [p. 24, 55, 56]

M. A. Ball and R. S. Plant. Comparison of stochastic parameterization approaches in a single-column model. *Phil. Trans. Roy. Soc. A*, 366:2605 2623, 2008. [p. 15]

G. I. Barenblatt. *Scaling, Self-similarity and Intermediate Asymtotics.* Cambridge University Press, Cambridge, 1996. [p. 62]

O. Barndorff-Nielsen. *Information and exponential families in statistical theory.* John Wiley & Sons, Chichester, 1978. [p. 29]

J. Baró and E. Vives. Analysis of power-law exponents by maximum-likelihood maps. *Phys. Rev. E*, 85:066121, 2012. [p. 32]

J. Baró, A. Corral, X. Illa, A. Planes, E. K. H. Salje, W. Schranz, D. E. Soto-Parra, and E. Vives. Statistical similarity between the compression of a porous material and earthquakes. *Phys. Rev. Lett.*, 110(8):088702, 2013. [p. 105]

H. Bauke. Parameter estimation for power-law distributions by maximum likelihood methods. *Eur. Phys. J. B*, 58:167 173, 2007. [p. 25, 26, 27, 30, 98]

Y. Ben-Zion. Collective behavior of earthquakes and faults: continuum-discrete transitions, progressive evolutionary changes, and different dynamic regimes. *Rev. Geophys.*, 46:RG4006, 2008. [p. 46]

L. Bengtsson, M. Steinheimer, P. Bechtold, and J. Geleyn. A stochastic parameterization for deep convection using cellular automata. *Q. J. R. Meteorol. Soc.*, DOI: 10.1002/qj.2108, 2013. [p. 126]

T. C. Benner and J. A. Curry. Characteristics of small tropical cumulus clouds and their impact on the environment. *J. Geophys. Res.*, 103(D22):28753 28767, 1998. [p. 73, 75]

A. K. Betts and M. J. Miller. A new convective adjustment scheme. Part II: Single column tests using GATE wave, BOMEX, ATEX and Arctic air-mass data sets. *Q. J. R. Meteorol. Soc.*, 112(473):693 709, 1986. [p. 63]

J. M. Bland and D. G. Altman. Multiple significance tests: the Bonferroni method. *Brit. Med. J.*, 310:170 170, 1995. [p. 109]

E. Bodenschatz, S. P. Malinowski, R. A. Shaw, and F. Stratmann. Can we understand clouds without turbulence? *Science*, 327(5968):970 971, 2010. [p. 14, 62, 80]

G. Boffetta, V. Carbone, P. Giuliani, P. Veltri, and A. Vulpiani. Power laws in solar flares: Self-organized criticality or turbulence? *Phys. Rev. Lett.*, 83:4662 4665, 1999. [p. 24]

M. I. Bogachev, I. S. Kirrenkov, E. M. Nifotov, and A. Bunde. Statistics of return intervals between long heartbeat intervals and their usability for online prediction of disorders. *New J. Phys.*, 11(063036):1 19, 2009. [p. 118]

M. Boguná and A. Corral. Long-tailed trapping times and Lévy flights in a self-organized critical granular system. *Phys. Rev. Lett.*, 78:4950 4953, 1997. [p. 38]

S. Bornholdt and T. Rohl. Self-organized critical neural networks. *Phys. Rev. E*, 67(6): 066118, 2003. [p. 13]

J. P. Bouchaud and A. Georges. Anomalous diffusion in disordered media: statistical mechanisms, models and physical applications. *Phys. Rep.*, 195:127 293, 1990. [p. 8, 22, 104]

S. M. Burroughs and S. F. Tebbens. Upper-truncated power laws in natural systems. *Pure Appl. Geophys.*, 158:741 757, 2001. [p. 23, 24, 27]

S. M. Burroughs and S. F. Tebbens. Power-law scaling and probabilistic forecasting of tsunami runup heights. *Pure Appl. Geophys.*, 162:331 342, 2005. [p. 24]

R. F. Cahalan and J. H. Joseph. Fractal statistics of cloud fields. *Mon. Wea. Rev.*, 117 (2):261 272, 1989. [p. 14, 73, 75, 80]

S. Carrillo-Menéndez and A. Suárez. Robust quantification of the exposure to operational risk: Bringing economic sense to economic capital. *Comput. Oper. Res.*, 39(4): 792 804, 2012. [p. 23]

G. Casella and R. L. Berger. *Statistical Inference*. Duxbury, Pacific Grove CA, 2nd edition, 2002. [p. 30]

R. Chicheportiche and J.-P. Bouchaud. Weighted Kolmogorov-Smirnov test: Accounting for the tails. *Phys. Rev. E*, 86:041115, 2012. [p. 32]

K. Christensen and N. R. Moloney. *Complexity and Criticality*. Imperial College Press, London, 2005. [p. 4, 12, 22, 24, 80, 89, 90, 104, 105]

J.-H. Chu, C. R. Sampson, A. S. Levine, and E. Fukada. The Joint Typhoon Warning Center tropical cyclone best-tracks, 1945-2000. *https://metocph.nmci.navy.mil/jtwc/best_tracks/TC_bt_report.html*, 2002. [p. 51]

S. Y. F. Chu, L. P. Ekstrom, and R. B. Firestone. Lund/LBNL Nuclear Data Search webpage. `http://nucleardata.nuclear.lu.se/nucleardata/toi`, version 2.0, February 1999. [p. 45]

A. Clauset, C. R. Shalizi, and M. E. J. Newman. Power-law distributions in empirical data. *SIAM Rev.*, 51(4):661 703, 2009. [p. 6, 7, 25, 26, 32, 34, 36, 54, 69, 87, 88, 105, 107, 112, 121]

A. Corral. Local distributions and rate fluctuations in a unified scaling law for earthquakes. *Phys. Rev. E*, 68:035102, 2003. [p. 24, 38, 56]

A. Corral. Universal local versus unified global scaling laws in the statistics of seismicity. *Physica A*, 340:590 597, 2004a. [p. 24, 56]

A. Corral. Long-term clustering, scaling, and universality in the temporal occurrence of earthquakes. *Phys. Rev. Lett.*, 92:108501, 2004b. [p. 24]

A. Corral. Comment on Do earthquakes exhibit self-organized criticality? . *Phys. Rev. Lett.*, 95:159801, 2005. [p. 24, 94]

A. Corral. Universal earthquake-occurrence jumps, correlations with time, and anomalous diffusion. *Phys. Rev. Lett.*, 97:178501, 2006. [p. 25]

A. Corral. Scaling and universality in the dynamics of seismic occurrence and beyond. In A. Carpinteri and G. Lacidogna, editors, *Acoustic Emission and Critical Phenomena*, pages 225 244. Taylor and Francis, London, 2008. [p. 22]

A. Corral. Point-occurrence self-similarity in crackling-noise systems and in other complex systems. *J. Stat. Mech.*, P01022, 2009a. [p. 38, 104]

A. Corral. Statistical tests for scaling in the inter-event times of earthquakes in California. *Int. J. Mod. Phys. B*, 23(28-29):5570 5582, 2009b. [p. 24]

A. Corral. Tropical cyclones as a critical phenomenon. In J. B. Elsner, R. E. Hodges, J. C. Malmstadt, and K. N. Scheitlin, editors, *Hurricanes and Climate Change: Volume 2*, pages 81 99. Springer, Heidelberg, 2010. [p. 24, 51]

A. Corral and K. Christensen. Comment on Earthquakes descaled: On waiting time distributions and scaling laws . *Phys. Rev. Lett.*, 96:109801, 2006. [p. 56]

A. Corral and F. Font-Clos. Criticality and self-organization in branching processes: application to natural hazards. In M. Aschwanden, editor, *Self-Organized Critical Phenomena*, pages 183 228. Open Academic Press, Berlin, 2013. [p. 11, 23]

A. Corral and A. Turiel. Variability of North Atlantic hurricanes: seasonal versus individual-event features. In A. S. Sharma, A. Bunde, V. P. Dimri, and D. N. Baker, editors, *Extreme Events and Natural Hazards: the Complexity Perspective*, pages 111 125. Geopress, Washington, 2012. [p. 50, 52]

A. Corral, L. Telesca, and R. Lasaponara. Scaling and correlations in the dynamics of forest-fire occurrence. *Phys. Rev. E*, 77:016101, 2008. [p. 54]

A. Corral, A. Ossó, and J. E. Llebot. Scaling of tropical-cyclone dissipation. *Nature Phys.*, 6:693 696, 2010. [p. 24, 50, 51, 52]

A. Corral, F. Font, and J. Camacho. Non-characteristic half-lives in radioactive decay. *Phys. Rev. E*, 83:066103, 2011. [p. 7, 25, 35, 41, 42, 44, 45, 58, 87, 105]

A. Corral, A. Deluca, and R. Ferrer i Cancho. A practical recipe to fit discrete power-law distributions. *ArXiv*, 1209:1270, 2012. [p. 25]

Z. Czechowski. The privilege as the cause of power distributions in geophysics. *Geophys. J. Int.*, 154:754 766, 2003. [p. 24]

J. Davidsen and M. Paczuski. Analysis of the spatial distribution between successive earthquakes. *Phys. Rev. Lett.*, 94:048501, 2005. [p. 25]

R. Deidda et al. Rainfall downscaling in a space-time multifractal framework. *Water Resour. Res.*, 36(7):1779 1794, 2000. [p. 81]

J. del Castillo. Exponential models. Lecture Notes, unpublished, 2013. [p. 29]

J. del Castillo and P. Puig. The best test of exponentiality against singly truncated normal alternatives. *J. Am. Stat. Assoc.*, 94:529 532, 1999. [p. 54]

J. del Castillo, J. Daoudi, and I Serra. The full-tails gamma distribution applied to model extreme values. *ArXiv*, 1211:0130, 2012. [p. 52, 124]

A. Deluca and A. Corral. Scale invariant events and dry spells for medium resolution local rain data. *Submitted to Non. Proc. Geophys*, 2013a. [p. 117]

A. Deluca and A. Corral. Fitting and goodness-of-fit test of non-truncated and truncated power-law distributions. *Acta Geophys.*, 61(6):1351 1394, 2013b. [p. 105, 107, 114, 122]

A. Deluca, P. Puig, and A. Corral. Testing universality in critical exponents: the case of rainfall. *In progress*, 2013. [p. 117]

B. R. Dennis. Solar flare hard X-ray observations. *Solar Phys.*, 118(1-2):49 94, 1988. [p. 13]

L. Devroye. *Non-Uniform Random Variate Generation*. Springer-Verlag, New York, 1986. [p. 36]

R. Dickman. Rain, power laws, and advection. *Phys. Rev. Lett.*, 90(10):108701(1 4), 2003. [p. 18, 24, 63, 81, 117]

R. Dickman, A. Vespignani, and S. Zapperi. Self-organized criticality as an absorbing-state phase transition. *Phys. Rev. E*, 57(5):5095 5105, 1998. [p. 63, 80]

R. Dickman, M. A. Munoz, A. Vespignani, and S. Zapperi. Paths to self-organized criticality. *Braz. J. Phys.*, 30:27 41, 2000. [p. 80]

P. Diodati, F. Marchesoni, and S. Piazza. Acoustic emission from volcanic rocks: An example of self-organized criticality. *Phys. Rev. Lett.*, 67(17):2239 2243, 1991. [p. 13]

R. Durrett. *Probability: Theory and Examples*. Cambridge University Press, Cambridge, 4th edition, 2010. [p. 31]

B. Efron. The jackknife, the bootstrap and other resampling plans. *CBMS-NSF Regional Conference Series in Applied Mathematics, Monograph 38, SIAM, Philadelphia.*, 1982. [p. 71]

B. Efron and R. J. Tibshirani. *An Introduction to the Bootstrap*. Chapman and Hall, New York, 1993. An Introduction to the Bootstrap. [p. 112]

J. P. Egan. *Signal Detection Theory and ROC analysis*. Academic Press, New York, 1975. [p. 119]

K. Emanuel. *Divine Wind: the History and Science of Hurricanes*. Oxford University Press, New York, 2005a. [p. 50]

K. Emanuel. Increasing destructiveness of tropical cyclones over the past 30 years. *Nature*, 436:686 688, 2005b. [p. 50]

M. Evans, N. Hastings, and B. Peacock. *Statistical Distributions*. Wiley-Interscience, New York, 3rd edition, 2000. [p. 7, 22, 26, 31]

D. Farmer and J. Geanakoplos. Power laws in economics and elsewhere. Preprint, 2008. [p. 8]

K. R. Felzer and E. E. Brodsky. Decay of aftershock density with distance indicates triggering by dynamic stress. *Nature*, 441:735 738, 2006. [p. 25]

M. P. Freeman and N. W. Watkins. The heavens in a pile of sand. *Science*, 298:979 980, 2002. [p. 24]

A. Garber, S. Hallerberg, and H. Kantz. Predicting extreme avalanches in self-organized critical sandpiles. *Phys. Rev. E*, 80:026124, 2009. [p. 94, 119]

E. L. Geist and T. Parsons. Distribution of tsunami interevent times. *Geophys. Res. Lett.*, 35:L02612, 2008. [p. 24]

M. L. Goldstein, S. A. Morris, and G. G. Yen. Problems with fitting to the power-law distribution. *Eur. Phys. J. B*, 41:255 258, 2004. [p. 25, 26, 27, 32, 34, 36]

G. W. Grabowski. An improved framework for superparameterization. *J. Atmos. Sci.*, 61:1940 1952, 2004. [p. 15]

S. Grauwin, G. Beslon, E. Fleury, S. Franceschelli, C. Robardet, J. Rouquier, and P. Jensen. Complex systems science: dreams of universality, interdisciplinary reality. *J. Assn. Inf. Sci. Technol.*, 63(7):1327 1338, 2012. [p. 3]

B. Gutenberg and C. F. Richter. Frequency of earthquakes in California. *Bull. Seismol. Soc. Am.*, 34:185 188, 1944. [p. 12, 45]

G. Gyorgyi, N. R. Moloney, K. Ozogány, and Z. Rácz. Finite-size scaling in extreme statistics. *Phys. Rev. Lett.*, 100(21):210601, 2008. [p. 104]

T. E. Harris. *The Theory of Branching Processes*. Dover, New York, 1989. [p. 11]

E. Hauksson, W. Yang, and P. Shearer. Waveform Relocated Earthquake Catalog for Southern California. [p. 47, 56]

S. Hergarten. *Self-Organized Criticality in Earth Systems*. Springer, Berlin, 2002. [p. 24, 41, 42, 95]

C. E. Holloway and J. D. Neelin. Temporal relations of column water vapor and tropical precipitation. *J. Atmos. Sci.*, 67(4):1091 1105, 2010. [p. 82]

C. Hooge, S. Lovejoy, D. Schertzer, S. Pecknold, J.F. Malouin, F. Schmitt, et al. Mulifractal phase transitions: the origin of self-organized criticality in earthquakes. *Nonlinear Proc. Geophys.*, 1(2/3):191 197, 1994. [p. 82]

http://www.corpoforestale.it. [p. 54]

IPCC4. Contribution of working groups i ii and ii to the fourth assesment report of the intergovernmental panel on climate change. Technical report, IPCC, Geneva, Switzerland, 2007. [p. 15]

N. Jan, L. Moseley, T. Ray, and D. Stauffer. Is the fossil record indicative of a critical system? *Advances in Complex Systems*, 2(02):137 141, 1999. [p. 9]

B. R. Jarvinen, C. J. Neumann, and M. A. S. David. A tropical cyclone data tape for the North Atlantic basin, 1886-1983: contents, limitations, and uses. *http://www.nhc.noaa.gov/pdf/NWS-NHC-1988-22.pdf*, 1988. [p. 51]

H. J. Jensen. *Self-Organized Criticality, Emergent Complex Behavior in Physical and Biological Systems*. Cambridge University Press, Cambridge, 1998. [p. 12, 24, 80]

N. L. Johnson, S. Kotz, and N. Balakrishnan. *Continuous Univariate Distributions*, volume 1. Wiley-Interscience, New Jersey, 2nd edition, 1994. [p. 7, 22, 23, 28, 31]

N. L. Johnson, A. W. Kemp, and S. Kotz. *Univariate Discrete Distributions*. Wiley-Interscience, New Jersey, 3rd edition, 2005. [p. 7, 22]

Joint Typhoon Warning Center, Annual Tropical Cyclone Reports. http://www.usno.navy.mil/nooc/nmfc-ph/rss/jtwc/best_tracks. [p. 51]

T. Jordan. Does self-organised criticality occur in the tropical convective system? Master s thesis, School of Mathematics, Meteorology and Physics, University of Reading, August 2008. [p. 16, 125]

Y. Y. Kagan. Seismic moment distribution revisited: I. statistical results. *Geophys. J. Int.*, 148:520 541, 2002. [p. 23, 32, 46]

J. D. Kalbfleisch and R. L. Prentice. *The Statistical Analysis of Failure Time Data*. Wiley, Hoboken, NJ, 2nd edition, 2002. [p. 31]

H. Kanamori and E. E. Brodsky. The physics of earthquakes. *Rep. Prog. Phys.*, 67: 1429 1496, 2004. [p. 23, 46, 47]

B. Khouider, A. J. Majda, and M. A. Katsoulakis. Coarse-grained stochastic models for tropical convection and climate. *Proc. Natl. Acad. Sci. USA*, 100(21):11941 11946, 2003. [p. 126]

B. Khouider, J. Biello, and A. J. Majda. A stochastic multicloud model for tropical convection. *Commun. Math. Sci.*, 8(1):187 216, 2010. [p. 126]

J. Klafter, M. F. Shlesinger, and G. Zumofen. Beyond Brownian motion. *Phys. Today*, 49(2):33 39, 1996. [p. 38]

R. Klein. Scale-dependent models for atmospheric flows. *Anu. Rev. Fluid Mech.*, 42: 249 274, 2010. [p. 62]

A. N. Kolmogorov. *Foundations of the theory of probability*. Chelsea Pub. Co., New York, 2nd edition, 1956. [p. 7, 22]

K. S. Krane. *Introductory Nuclear Physics*. Wiley, New York, 1988. [p. 44]

F. Lahaie and J. R. Grasso. A fluid-rock interaction cellular automaton of volcano mechanics: Application to the Piton de la Fournaise. *J. Geophys. Res.*, 103 B:9637 9650, 1998. [p. 24]

J. Lavergnat and P. Golé. A stochastic raindrop time distribution model. *Journal of Applied Meteorology*, 37(8):805 818, 1998. [p. 72]

J. Lavergnat and P. Golé. A stochastic model of raindrop release: Application to the simulation of point rain observations. *J. Hidrol.*, 328(1):8 19, 2006. [p. 80]

E. Lippiello, A. Corral, M. Bottiglieri, C. Godano, and L. de Arcangelis. Scaling behavior of the earthquake intertime distribution: Influence of large shocks and time scales in the omori law. *Phys. Rev. E*, 86(6):066119, 2012. [p. 110]

S. Lovejoy. Area-perimeter relation for rain and cloud areas. *Science*, 216:185 187, 1982. [p. 14, 80]

S. Lovejoy and D. Schertzer. Multifractals and rain. In Z. W. Kundzewicz, editor, *New Uncertainty Concepts in Hydrology and Water Resources*, pages 61 103. Cambridge University Press Cambridge, UK, 1995. [p. 81]

I. G. Main, L. Li, J. McCloskey, and M. Naylor. Effect of the Sumatran mega-earthquake on the global magnitude cut-off and event rate. *Nature Geosci.*, 1:142, 2008. [p. 47]

A. J. Majda and B. Khouider. Stochastic and mesoscopic models for tropical convection. *Proc. Natl. Acad. Sci. USA*, 99:1123 1128, 2002. [p. 15]

B. D. Malamud. Tails of natural hazards. *Phys. World*, 17 (8):31 35, 2004. [p. 23, 80]

B. D. Malamud, G. Morein, and D. L. Turcotte. Forest fires: An example of self-organized critical behavior. *Science*, 281:1840 1842, 1998. [p. 13, 54, 80]

B. D. Malamud, J. D. A. Millington, and G. L. W. Perry. Characterizing wildfire regimes in the United States. *Proc. Natl. Acad. Sci. USA*, 102:4694 4699, 2005. [p. 24, 54]

R. D. Malmgren, D. B. Stouffer, A. E. Motter, and L. A. N. Amaral. A Poissonian explanation for heavy tails in e-mail communication. *Proc. Natl. Acad. Sci. USA*, 105:18153 18158, 2008. [p. 36, 112]

S. S. Manna. Two-state model of self-organized criticality. *J. Phys. A: Math Gen.*, 24: L363 L369, 1991. [p. 118]

B. E. Mapes. Equilibrium vs. activation control of large-scale variations of tropical deep convection. In R. K. Smith, editor, *The Physics and Parameterization of Moist Atmospheric Convection*, pages 321 358. Kluwer Academic Publishers, 1997. [p. 15]

B. E. Mapes and R. A. Houze Jr. Cloud clusters and superclusters over the Oceanic Warm Pool. *Mon. Wea. Rev.*, 121:1398 1415, 1993. [p. 73]

E. Martin, A. Shreim, and M. Paczuski. Activity-dependent branching ratios in stocks, solar X-ray flux, and the Bak-Tang-Wiesenfeld sandpile model. *Phys. Rev. E*, 81: 016109, 2010. [p. 94]

L. McClelland, T. Simkin, M. Summers, E. Nielsen, and T. C. Stein, editors. *Global volcanism 1975-1985*. Prentice Hall, Englewood Cliffs, 1989. [p. 24]

M. Mitzenmacher. A brief history of generative models for power law and lognormal distributions. *Internet Math.*, 1 (2):226 251, 2004. [p. 8, 24, 117]

L. Molini, A. Parodi, N. Rebora, and G. C. Craig. Classifying severe rainfall events over Italy by hydrometeorological and dynamical criteria. *Q. J. R. Meteorol. Soc.*, 137: 148 154, 2011. [p. 85, 94]

C. J. Muller, L. E. Back, P. A. O Gorman, and K. A. Emanuel. A model for the relationship between tropical precipitation and column water vapor. *Geophys. Res. Lett.*, 36(16), 2009. [p. 18]

National Hurricane Center. http://www.nhc.noaa.gov/pastall.shtml# hurdat. [p. 51]

J. D. Neelin, O. Peters, J. W.-B. Lin, K. Hales, and C. E. Holloway. Rethinking convective quasi-equilibrium: observational constraints for stochastic convective schemes in climate models. *Phil. Trans. R. Soc. A*, 366:2581 2604, 2008. [p. 17, 18, 63]

J. D. Neelin, O. Peters, and K. Hales. The transition to strong convection. *J. Atmos. Sci.*, 66(8):2367 2384, 2009. [p. 62, 67]

R. A. J. Neggers, H. J. J. Jonker, and A. P. Siesbesma. Size statistics of cumulus cloud populations in large-eddy simulations. *J. Atmos. Sci.*, 60(8):1060 1074, 2003. [p. 73, 75]

M. E. J. Newman. Power laws, Pareto distributions and Zipf s law. *Cont. Phys.*, 46: 323 351, 2005. [p. 6, 8, 22, 23, 24, 54]

M. E. J. Newman. Resource letter CS-1: Complex systems. *Am. J. Phys.*, 79:800 810, 2011. [p. 3]

Z. Olami and K. Christensen. Temporal correlations, universality, and multifractality in a spring-block model of earthquakes. *Phys. Rev. E*, 46(4):1720 1723, 1992. [p. 82]

J. Olsson, J. Niemczynowicz, and R. Berndtsson. Fractal analysis of high-resolution rainfall time-series. *J. Geophys. Res.*, 98(D12):23265 23274, 1993. [p. 63, 80]

M. Paczuski, S. Boettcher, and M. Baiesi. Interoccurrence times in the Bak-Tang-Wiesenfeld sandpile model: A comparison with the observed statistics of solar flares. *Phys. Rev. Lett.*, 95:181102, 2005. [p. 24, 94]

O. Peters and K. Christensen. Rain: Relaxations in the sky. *Phys. Rev. E*, 66(3):036120, 2002. 2A. [p. 13, 86, 105, 106]

O. Peters and K. Christensen. Rain viewed as relaxational events. *J. Hidrol.*, 328:46 55, 2006. [p. 24, 86]

O. Peters and J. D. Neelin. Critical phenomena in atmospheric precipitation. *Nature Phys.*, 2(6):393 396, 2006. [p. ix, 17, 24, 62, 63, 82, 117]

O. Peters, C. Hertlein, and K. Christensen. A complexity view of rainfall. *Phys. Rev. Lett.*, 88(1):018701(1 4), 2002. [p. 16, 24, 61, 63, 67, 68, 70, 72, 82, 85, 86, 93, 105, 106, 117, 122]

O. Peters, J. D. Neelin, and S. W. Nesbitt. Mesoscale convective systems and critical clusters. *J. Atmos. Sci.*, 66(9):2913 2924, 2009. [p. 14, 18, 72, 75, 80]

O. Peters, A. Deluca, A. Corral, J. D. Neelin, and C. E. Holloway. Universality of rain event size distributions. *J. Stat. Mech.*, 11:P11030, 2010. [p. 13, 19, 24, 25, 30, 38, 81, 82, 87, 88, 89, 93, 105, 106, 107, 108, 115, 117, 118, 122]

R. S. Plant. A new modelling framework for statistical cumulus dynamics. *Philosophical Transactions of the Royal Society A: Mathematical, Physical and Engineering Sciences*, 370(1962):1041 1060, 2012. [p. 126]

R. S. Plant and G. C. Craig. A stochastic parameterization for deep convection based on equilibrium statistics. *J. Atmos. Sci.*, 65(1):87 105, 2008. [p. 15]

W. H. Press, S. A. Teukolsky, W. T. Vetterling, and B. P. Flannery. *Numerical Recipes in Fortran, Third Edition.* Cambridge University Press, Cambridge, 3rd edition, 2002. [p. 30, 32, 33, 34, 36, 69, 75, 76, 87, 91]

ARM Data Quality Program. *http://www.arm.gov/data/data_quality.stm.* [p. 64]

G. Pruessner. *Self-Organised Criticality: Theory, Models and Characterisation.* Cambridge University Press, Cambridge, 2012. [p. 11, 13, 24, 41]

G. Pruessner and O. Peters. Reply to Comment on Self-organized criticality and absorbing states: Lessons from the Ising model . *Phys. Rev. E*, 77(4):048102(1 2), 2008. [p. 68]

S. Pueyo and R. Jovani. Comment on a keystone mutualism drives pattern in a power function . *Science*, 313:1739c 1740c, 2006. [p. 27]

F. Ragone, K. Fraedrich, H. Borth, and F. Lunkeit. Coupling a minimal stochastic lattice-gas model of a cloud system to an agcm. *Q. J. R. Meteorol. Soc.*, Submitted, 2013. [p. 126]

D. M. Raup. Biological extinction in Earth history. *Science*, 231:1528 1533, 1986. [p. 13]

S. Redner. *A guide to first-passage processes.* Cambridge University Press, 2001. [p. 10]

M. T. Ritsche. ARM Surface Meteorology Systems Handbook and Surface Meteorology (SMET) Handbook. *http://www.arm.gov/publications/handbooks.* [p. 64]

S. M. Ross. *A First Course in Probability.* Prentice Hall, Englewood Cliffs, 2002. [p. 26, 36]

A. Rosso, P. Le Doussal, and K. J. Wiese. Avalanche-size distribution at the depinning transition: A numerical test of the theory. *Phys. Rev. B*, 80(14):144204(1 10), 2009. [p. 69, 90]

A. Saichev and D. Sornette. Universal distribution of interearthquake times explained. *Phys. Rev. Lett.*, 97:078501, 2006. [p. 24]

A. Saichev, A. Helmstetter, and D. Sornette. Power-law distributions of offspring and generation number in branching models of earthquake triggering. *Pure Appl. Geophys.*, 162:1113 1134, 2005. [p. 11]

D. Schertzer and S. Lovejoy. Multifractal generation of self-organized criticality. In *Fractals in the Natural and Applied Sciences*, Proceedings of the Second IFIP Working Conference on Fractals in the Natural and Applied Sciences, pages 325 339. Elsevier, North-Holland: Amsterdam, 1994. [p. 82]

J. P. Sethna, K. A. Dahmen, and C. R. Myers. Crackling noise. *Nature*, 418:242 250, 2001. [p. 24]

P. Shearer, E. Hauksson, and G. Lin. Southern California hypocenter relocation with waveform cross- correlation, part 2: Results using source-specific station terms and cluster analysis. *Bull. Seismol. Soc. Am.*, 95:904 915, 2005. `http://www.data.scec.org/ftp/catalogs/SHLK/`, file `SHLK_1_02.txt`. [p. 47, 56]

A. N. Shiryaev. *Probability.* Springer-Verlag, New York, 2nd edition, 1996. [p. 8, 22]

B. W. Silverman. *Density Estimation for Statistics and Data Analysis.* Chapman and Hall, New York, 1986. [p. 41]

S. Smirnov. Critical percolation in the plane: Conformal invariance, Cardy s formula, scaling limits. *Comptes Rendus de l Académie des Sciences-Series I-Mathematics*, 333 (239 244), 2001. [p. 3]

K. Sneppen, P. Bak, H. Flyvbjerg, and M. H. Jensen. Evolution as a self-organized critical phenomenon. *Proc. Natl. Acad. Sci. USA*, 92:5209 5213, 1995. [p. 13]

R. V. Solé and S. C. Manrubia. *Orden y caos en sistemas complejos. Fundamentos*, volume 5, chapter 18. Edicions UPC, Barcelona, 2001. [p. 13]

A. Sornette and D. Sornette. Self-organized criticality and earthquakes. *Europhys. Lett.*, 9:197 202, 1989. [p. 16, 80]

D. Sornette. Sweeping of an instability: an alternative to self-organized criticality to get powerlaws without parameter tuning. *J. de Physique I*, 4(2):209 221, 1994. [p. 13, 18]

D. Sornette. *Critical Phenomena in Natural Sciences*. Springer, Berlin, 2nd edition, 2004. [p. 8, 24, 80, 81]

H. E. Stanley. Scaling, universality, and renormalization: Three pillars of modern critical phenomena. *Rev. Mod. Phys.*, 71:S358 S366, 1999. [p. 4, 5, 103, 104]

D. Stauffer and A. Aharony. *Introduction To Percolation Theory*. CRC Press, 2 edition, July 1994. ISBN 0748402535. URL `http://www.worldcat.org/isbn/0748402535`. [p. 104]

S. Stechmann and J. D. Neelin. A stochastic model for the transition to strong convection. *J. Clim.*, 68:2955 2970, 2011. [p. 82, 118, 125]

M. P. H. Stumpf and M. A. Porter. Critical truths about power laws. *Science*, 335 (6069):665 666, 2012. [p. 6]

H. Takayasu. *Fractals in the Physical Sciences*. Manchester University Press, Manchester, 1989. [p. 22]

C. Tang and P. Bak. Critical exponents and scaling relations for self-organized critical phenomena. *Phys. Rev. Lett.*, 60(23):2347 2350, 1988. [p. 63, 80, 117]

L. Telesca, V. Lapenna, E. Scalcione, and D. Summa. Searching for time-scaling features in rainfall sequences. *Chaos, Solitons and Fractals*, 32:35 41, 2007. [p. 86]

P. Trivej and B. Stevens. The echo size distribution of precipitating shallow cumuli. *J. Atmos. Sci.*, 67(3):788 804, 2010. [p. 72, 75]

T. Utsu. Representation and analysis of earthquake size distribution: a historical review and some new approaches. *Pure Appl. Geophys.*, 155:509 535, 1999. [p. 23, 45]

T. Utsu. Statistical features of seismicity. In W. H. K. Lee, H. Kanamori, P. C. Jennings, and C. Kisslinger, editors, *International Handbook of Earthquake and Engineering Seismology, Part A*, pages 719 732. Academic Press, Amsterdam, 2002. [p. 54]

T. Utsu, Y. Ogata, and R.S. Matsu ura. The centenary of the Omori formula for a decay law of aftershock activity. *J. Phys. Earth*, 43:1 33, 1995. [p. 54]

G. Vattay and A. Harnos. Scaling behavior in daily air humidity fluctuations. *Phys. Rev. Lett.*, 73:768 771, 1994. [p. 14]

D. Veneziano and C. Lepore. The scaling of temporal rainfall. *Water Resources Research*, 48(8):W08516, 2012. [p. 81]

R. von Mises. *Mathematical Theory of Probability and Statistics*. Academic Press, New York, 1964. [p. 95]

J. A. Wanliss and J. M. Weygand. Power law burst lifetime distribution of the SYM-H index. *Geophys. Res. Lett.*, 34:L04107, 2007. [p. 24]

E. P. White, B. J. Enquist, and J. L. Green. On estimating the exponent of power-law frequency distributions. *Ecol.*, 89:905 912, 2008. [p. 24, 25, 26, 27, 30, 32, 105]

K. G. Wilson. Renormalization Group and Critical Phenomena. I. Renormalization Group and the Kadanoff Scaling Picture. *Phys. Rev. B*, 4(9):3174 3183, 1971. [p. 6]

R. Wood and P. R. Field. The distribution of cloud horizontal sizes. *J. Clim.*, 24(18): 4800 4816, 2011. [p. 14, 18, 80]

J. I. Yano and R. S. Plant. Convective quasi-equilibrium. *Rev. Geophys.*, 50(4), 2012. [p. 18]

J. I. Yano, R. Blender, C. Zhang, and K. Fraedrich. 1/f noise and pulse-like events in the tropical atmospheric surface variabilities. *Q. J. R. Meteorol. Soc.*, 130:1697 1721, 2003. [p. 14]

J. I. Yano, L. Changhai, and M. W. Moncrieff. Self-organized criticality and homeostasis in atmospheric convective organization. *J. Atmos. Sci.*, 69(12):3449 3462, 2012. [p. 18]

J.M. Yeomans. *Statistical Mechanics of Phase Transitions*. Oxford University Press, New York, 1992. [p. 5, 103]

S. Zapperi, K. B. Lauritsen, and H. E. Stanley. Self-organized branching processes: Mean-field theory for avalanches. *Phys. Rev. Lett.*, 75:4071 4074, 1995. [p. 11]